

# Experiments and theory in cold and ultracold collisions

John Weiner

*Laboratory for Atomic, Molecular, and Optical Science and Engineering,  
University of Maryland, College Park, Maryland 20742*

Vanderlei S. Bagnato and Sergio Zilio

*Instituto de Física de São Carlos Universidade de São Paulo, São Carlos,  
São Paulo 13560, Brazil*

Paul S. Julienne

*Atomic Physics Division, National Institute of Standards and Technology,  
Gaithersburg, Maryland 20899*

The authors review progress in understanding the nature of atomic collisions occurring at temperatures ranging from the millidegrees Kelvin to the nanodegrees Kelvin regime. The review includes advances in experiments with atom beams, light traps, and purely magnetic traps. Semiclassical and fully quantal theories are described and their appropriate applicability assessed. The review divides the subject into two principal categories: collisions in the presence of one or more light fields and ground-state collisions in the dark. [S0034-6861(99)00101-4]

## CONTENTS

I. Foreword	2	f. Sodium-potassium mixed-species trap loss	37
II. General Introduction	2	g. Rare-gas metastable loss in MOTs and optical lattices	38
III. Introduction to Cold Collision Theory	5	B. Ground-state trap-loss collisions	39
A. Basic concepts of scattering theory	5	1. Hyperfine-changing collisions	39
B. Quantum properties as $E \rightarrow 0$	8	a. Cesium and rubidium	39
C. Collisions in a light field	10	b. Sodium	40
IV. Experimental Methods for the Study of Cold Collisions	12	2. Summary comparison of trap-loss rate constants	40
A. Atom traps	12	VI. Photoassociation Spectroscopy	41
1. Light forces	12	A. Introduction	41
2. The magneto-optical trap (MOT)	14	B. Photoassociation at ambient and cold temperatures	42
a. Basic notions	14	C. Associative and photoassociative ionization	43
b. Densities in a MOT	15	1. Photoassociative ionization at small detuning	46
3. Dark SPOT MOT	15	2. PAI and molecular hyperfine structure	47
4. The far-off resonance trap (FORT)	15	3. Two-color PAI	47
5. Magnetic traps	16	D. Photoassociation spectroscopy in MOTs and FORTs	50
B. Atom beams	17	1. Sodium	50
V. Inelastic Exoergic Collisions in MOTs	18	2. Rubidium	52
A. Excited-state trap-loss collisions	18	3. Lithium	53
1. Early quasistatic models	18	4. Potassium	54
a. Gallagher-Pritchard model	18	E. Atomic lifetimes from photoassociation spectroscopy	55
b. Julienne-Vigué model	20	F. Precision measurement of scattering length by photoassociative spectroscopy	57
2. Theoretical approaches to excited-state trap loss	21	1. Lithium	58
a. Quasistatic theories	21	2. Sodium	59
b. Method of complex potentials	21	3. Rubidium	59
c. Two-photon distorted wave theory	22	VII. Optical Shielding and Suppression	59
d. Optical Bloch equations	23	A. Introduction	59
e. Quantum Monte Carlo methods	23	B. Optical suppression of trap loss	61
3. Assessment of theoretical approaches	24	C. Optical shielding and suppression in photoassociative ionization	62
a. Quasistatic vs dynamical	24	D. Optical shielding in xenon and krypton collisional ionization	64
b. Small vs large detuning	24	E. Optical shielding in Rb collisions	65
4. Excited-state trap-loss measurements	26	F. Theories of optical shielding	66
a. Sodium trap loss	28	VIII. Ground—State Collisions	69
b. Cesium trap loss	30	A. Early work	69
c. Rubidium trap loss	30		
d. Lithium trap loss	34		
e. Potassium trap loss	36		

B. Bose-Einstein condensation	70
IX. Future Directions	75
Acknowledgments	76
References	76

## I. FOREWORD

Cold and ultracold collisions occupy a strategic position at the intersection of several powerful themes of current research in chemical physics, in atomic, molecular, and optical physics, and even in condensed matter. The nature of these collisions bears critically on optical manipulation of inelastic and reactive processes, precision measurement of molecular and atomic properties, matter-wave coherences and quantum-statistical condensates of dilute, weakly interacting atoms. This crucial position explains the wide interest and explosive growth of the field since its inception in 1987, but presents the authors of a review with both a blessing and curse. The blessing is self-evident. Exciting physics speaks for itself and will capture the reader's attention in spite of errors and flaws in the presentation. The curse is unfortunately just as self-evident. Any review attempting to encompass the breadth of scientific developments engendered by such wide appeal runs the risk of discouraging all but the most determined from reading it serially from start to finish. We have, therefore, tried to minimize this risk by organizing the review so subsets of it might conform to readers' more focused interests. For example, readers interested in broadening their general culture of physics in this area could read Secs. II, III, IV, VI.A,B, VII.A, and VIII.B. Readers interested primarily in experimental developments could concentrate on Secs. II, IV, V.A.4, V.B, VI, VII.A–VII.E, VIII, and IX. Theoretical work is concentrated in Secs. III, V.A.1–V.A.3, VII.F, and VIII. Ground-state collisions, of primary importance to Bose-Einstein condensates, are discussed in Sec. VIII. Control of collisional processes by optical fields is concentrated in Secs. VI and VII. We have also reluctantly decided to omit many very important advances in the determination of molecular potentials, and their calculation and experimental determination, because it would render an already large review completely unmanageable. For the same reason we have omitted review of the exciting advances in Bose-Einstein condensation except where they touch explicitly on collisions. Within this more modest scope we have attempted to be comprehensive; but of course we take responsibility for all errors and omissions and would like to hear from readers who detect them.

## II. GENERAL INTRODUCTION

Just over a decade ago the first successful experiments and theory<sup>1</sup> demonstrating that light could be used to

<sup>1</sup>A good introduction to the early physics of laser cooling and trapping can be found in two special issues of the Journal of the Optical Society of America B: "The Mechanical Effects of Light," J. Opt. Soc. Am. B **2**, No. 11, November 1985 and

cool and confine atoms to submillikelvin temperatures (Phillips *et al.*, 1985; Dalibard and Cohen-Tannoudji, 1985) opened several exciting new chapters in atomic, molecular, and optical physics. Atom interferometry (Adams, Carnal, and Mlynek, 1994; Adams, Sigel, and Mlynek, 1994), matter-wave holography (Morinaga *et al.*, 1996), optical lattices (Jessen and Deutsch, 1996), and Bose-Einstein condensation in dilute gases<sup>2</sup> all exemplify startling new physics where collisions between atoms cooled with light play a pivotal role. These collisions have become the subject of intensive study not only because of their importance to these new areas of atomic, molecular, and optical physics but also because their investigation has led to new insights into how cold collision spectroscopy can lead to precision measurements of atomic and molecular parameters and how radiation fields can manipulate the outcome of a collision itself. As a general orientation Fig. 1 shows how a typical atomic de Broglie wavelength varies with temperature and where various physical phenomena situate along the scale. With de Broglie wavelengths on the order of a few thousandths of a nanometer, conventional gas-phase chemistry can usually be interpreted as the interaction of classical nuclear point particles moving along potential surfaces defined by their associated electronic charge distribution. At one time liquid helium was thought to define a regime of cryogenic physics, but it is clear from Fig. 1 that optical and evaporative cooling have created cryogenic environments many orders of magnitude below the temperature of liquid helium. At the level of Doppler cooling and optical molasses<sup>1</sup> the de Broglie wavelength becomes comparable to or longer than the chemical bond, approaching the length of the cooling optical light wave. Here we can expect wave and relativistic effects such as resonances, interferences, and interaction retardation to become important. Following Suominen (1996), we will term the Doppler cooling and optical molasses temperature range, roughly between 1 mK and 1  $\mu$ K, the regime of cold collisions. Most collision phenomena at this level are studied in the presence of one or more light fields used to confine the atoms and to probe their interactions. Excited quasimolecular states often play an important role. Below about 1  $\mu$ K, where evaporative cooling and Bose-Einstein condensation (see footnote 2) become the focus of attention, the de Broglie wavelength grows to a scale comparable to the mean distance separating atoms at the critical condensation density; quantum degenerate states of the

"Laser Cooling and Trapping of Atoms," J. Opt. Soc. Am. B **6**, No. 11, November 1989. Two more recent reviews (Metcalf and van der Straten, 1994; Adams and Riis, 1997) update a decade of developments since the early work recounted in the J. Opt. Soc. Am. B special issues.

<sup>2</sup>For an introduction to current research in alkali-atom Bose-Einstein condensation see the special issue on Bose-Einstein condensation in the Journal of Research of the National Institute of Standards and Technology **101**, No. 4, July-August 1996.

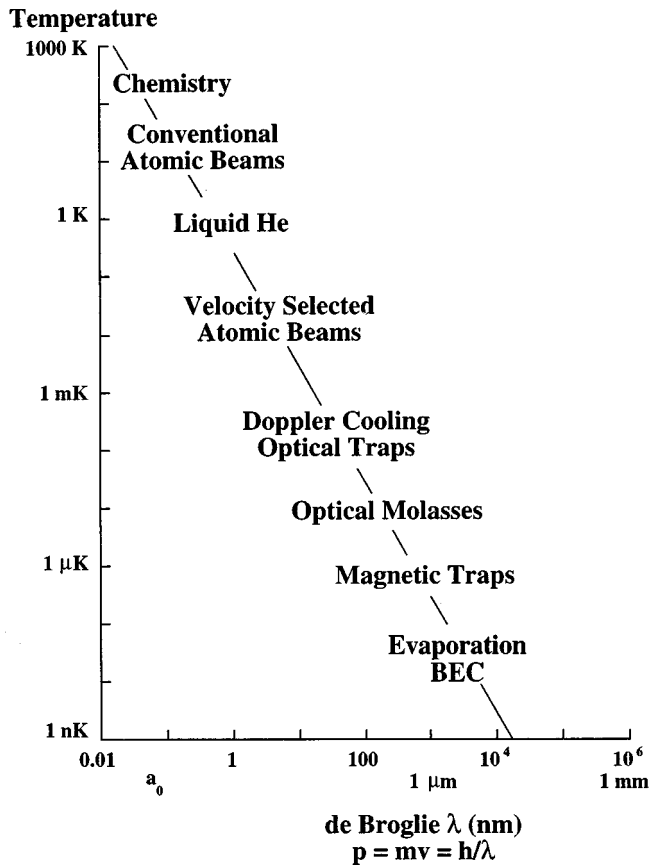


FIG. 1. Illustrative plot of various physical phenomena along a scale of temperature (energy divided by Boltzmann's constant  $k_B$ ) plotted against the de Broglie wavelength for atomic sodium. The term  $a_0$  represents the Bohr radius of the H atom.

atomic ensemble begin to appear. In this regime ground state collisions only take place through radial (not angular) motion and are characterized by a phase shift, or scattering length, of the ground-state wave function. Since the atomic translational energy now lies below the kinetic energy transferred to an atom by recoil from a scattered photon, light can play no further role in atom cooling, and collisions in a temperature range from  $1 \mu\text{K} \rightarrow 0$  must occur in the dark. These collisions are termed ultracold. We and others have used the terms “cold” and “ultracold” in various ways in the past but now prefer to use the terminology of Suominen (1996) in distinguishing between the two. This review will recount progress in understanding collision processes in both the cold and ultracold domains.

We start with cold collisions because many experiments carried out in optical traps and optically slowed atomic beams take place in this temperature range. Soon after the first successful experiments reported optical cooling and trapping in alkali gases, Vigué (1986) and Pritchard (1986) discussed the possible consequences of binary collisions in a cold or ultracold gaseous medium. Figure 2 shows schematically the general features of a cold binary collision. Two  $S$  ground-state atoms interact at long range through electrostatic dispersion forces, and approach along an attractive  $C_6/R^6$  potential. The first

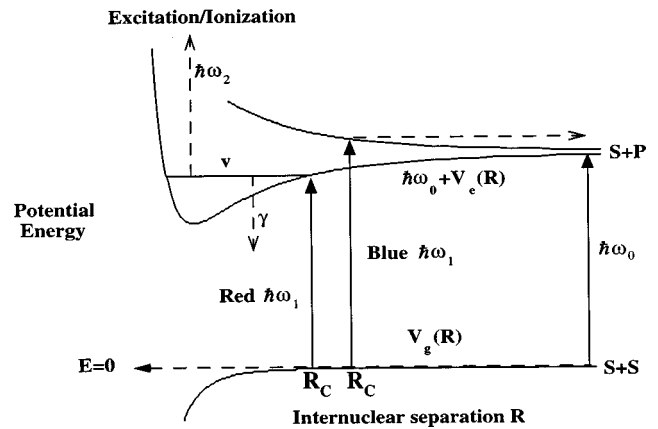


FIG. 2. Schematic of a cold collision. Light field  $\hbar\omega_1$ , red detuned with respect to the  $S+P$  asymptote, excites the quasimolecule in a free-bound transition around the Condon point  $R_C$  and can lead to excitation or ionization with the absorption of a second photon  $\hbar\omega_2$ . Light field  $\hbar\omega_1$ , blue detuned with respect to the  $S+P$  asymptote, prevents atoms from approaching significantly beyond the Condon point. Blue-detuned excitation leads to optical shielding and suppression of inelastic and reactive collision rates.

excited states, correlating to an  $S+P$  asymptote and separated from the ground state by the atomic excitation energy  $\hbar\omega_0$ , interact by resonance dipole-dipole forces and approach either along an attractive or repulsive  $C_3/R^3$  curve. If the colliding atoms on the ground state potential encounter a *red-detuned* optical field  $\hbar\omega_1$ , the probability of a free-bound transition to some vibration-rotation level  $v$  of the attractive excited state will maximize around the Condon point  $R_C$  where  $\hbar\omega_1$  matches the potential difference. The quasimolecule finds itself photoassociated and vibrating within the attractive well. A second field  $\hbar\omega_2$  can then further excite or even ionize the photoassociated quasimolecule, or it can relax back to some distribution of the continuum and bound levels of the ground state with a spontaneous emission rate  $\gamma$ . Photoassociation and subsequent inelastic processes comprise the discussion of Secs. V and VI. If the atoms colliding on the ground state potential interact with a *blue-detuned* optical field  $\hbar\omega_1$ , the probability of transition to some continuum level of the repulsive excited state will maximize around the Condon point  $R_C$ , which will also be quite close to the turning point of the nuclear motion on the repulsive excited state. The atoms approach no further and begin to separate along the repulsive curve leading to the  $S+P$  asymptote. The blue-detuned field “shields” the atoms from further interaction at more intimate internuclear separation and “suppresses” the rate of various inelastic and reactive processes. Optical shielding and suppression is the topic of Sec. VII. Cold collisions in the presence of optical fields or in the ground state reveal new physics in domains where atomic scales of length, time, and spectral line width are reversed from their conventional relations. In addition to the atomic de Broglie wave increasing to a length several hundred times that of the chemical bond, the collisional interaction time grows to

several times the spontaneous emission lifetime, and the inhomogeneous Doppler line width at cold and ultracold temperatures narrows to less than the natural width of an atomic dipole transition. The narrow, near-threshold continuum state distribution means that at most a few partial waves will contribute to a scattering event. Averaging therefore does not obscure matter wave effects such as resonances, nodes, and antinodes in scattering wave function amplitudes, and channel-opening threshold laws. In the cold collision regime, Doppler broadening is narrow compared to the radiative natural width, therefore permitting ultrahigh precision, free-bound molecular spectroscopy, and efficient participation of the entire atom ensemble in the excitation process. Long collision duration ensures interacting partners sufficient time to exchange multiple photons with modes of an externally applied radiation field. The frequency, intensity, and polarization of the optical field can in turn modify effective interaction potentials and control the probability of inelastic, reactive, and elastic final product channels.

Three questions have motivated significant developments in cold collisions: (1) How do collisions lead to loss of atom confinement in traps? (2) How can photoassociation spectroscopy yield precision measurements of atomic properties and insight into the quantum nature of the scattering process itself? (3) How can optical fields be used to control the outcome of a collisional encounter?

This third question has had an enduring appeal to chemical physicists, and we review here some of the early history to put in perspective current developments and to emphasize the importance of the ultracold regime. In the decade of the seventies, after the development of the CO<sub>2</sub> laser, researchers in atomic and chemical physics immediately thought to use it to influence or control inelastic processes and chemical reactions. However, early attempts to induce reactivity by exciting well-defined, localized molecular sites such as double bonds or functional groups failed because the initial optical excitation diffused rapidly into the rotations, vibrations, and torsional bending motions of the molecular nuclei. The unfortunate result was that the infrared light of the CO<sub>2</sub> laser essentially heated the molecules much as the familiar and venerable Bunsen burner. Enthusiasm for laser-controlled chemistry cooled when researchers realized that this rapid energy diffusion throughout the molecular skeleton blocked significant advance along the road to optical control of reactivity. In the early eighties the development of the pulsed dye laser, tunable in the visible region of the spectrum, together with new proposals for “radiative collisions,” in which the electrons of the molecule interact with the light rather than the nuclei, revived interest. A second round of experiments achieved some success in optically transforming reactants to products; in general, however, the high peak powers necessary to enhance reactivity significantly interfered with the desired effects by inducing nonlinear, multiphoton excitation and ionization in the molecule itself. The necessity for high peak power in turn arose

from two crucial factors: (1) Doppler broadening at ambient temperature permits only a few percent of all molecular collisions to interact with an applied optical field mode so the product “yield” is low, and (2) the optical field had to influence the strong chemical binding interaction in order to affect atomic behavior during the collisional encounter. This requirement implied the need for power densities greater than a few megawatts per square centimeter. Power densities of this order are well above the threshold for multiphoton absorption and ionization, and these processes quickly convert atoms or molecules from a neutral gas into an ionized plasma. It appeared depressingly difficult to control collisions with light without first optically destroying them.

However, atomic deceleration and optical cooling brightened this discouraging picture, by narrowing the inhomogeneous Doppler broadening to less than a natural line width of an atomic transition and transferring the optical-particle interaction from the “chemical” zone of strong wave-function overlap to an outer region where weak electrostatic terms characterize the collision. In this weakly interacting outer zone only hundreds of milliwatts per square centimeter of optical power density suffice to profoundly alter the inelastic and reactive collision rate constant. Furthermore, although a conventional atomic collision lasts only a few hundred femtoseconds, very short compared to the tens of nanoseconds required before excited molecules or atoms spontaneously emit light, in the ultracold regime particles move much more slowly, taking up to hundreds of nanoseconds to complete a collisional encounter. The long collision duration leaves plenty of time for the two interacting partners to absorb energy from an external radiation field or emit energy by spontaneous or stimulated processes.

To the three earlier questions motivating studies of cold collisions may now be added a fourth relevant to the ultracold regime: What role do collisions play in the attainment and behavior of boson and fermion gases in the quantum degenerate regime? Quantum statistical effects have been observed and studied in the superfluidity of liquid helium and in the phenomena of metallic and high-temperature superconductivity. These dramatic and significant manifestations of quantum collective effects are nevertheless difficult to study at the atomic level because the particles are condensed and strongly interacting. Observation and measurement of weakly interacting dilute gases, however, relate much more directly to the simplest, microscopic models of this behavior. The differences between model ideal quantum gases and real quantum gases begin with binary interactions between the particles, and therefore the study of ultracold collisions is a natural point of departure for investigation. Collisions determine two crucial aspects of Bose-Einstein condensation experiments: (1) the evaporative cooling rate necessary for the attainment of Bose-Einstein condensation depends on the elastic scattering cross section, proportional to the square of the *s*-wave scattering length, and (2) the sign of the scattering length indicates the stability of the condensate: positive

scattering lengths lead to large, stable condensates while negative scattering lengths do not. The ability to produce condensates by sympathetic cooling also depends critically on the elastic and inelastic (loss and heating) rate constants among different states of the colliding partners. Although a confined Bose atom condensate bears some analogy to an optical cavity (photons are bosons), the atoms interact through collisions; these collisions limit the coherence length of any atom laser coupled out of the confining cavity or Bose-Einstein condensation trap. Another important point, relating back to optical control, is that the amplitude and sign of the scattering length depends sensitively on the fine details of the ground potentials. The possibility of manipulating these potentials and consequently collision rates with external means, using optical, magnetic, or radio frequency fields, holds the promise of tailoring the properties of the quantum gas to enhance stability and coherence. Finally it now appears that the limiting loss process for dilute gaseous Bose-Einstein condensations are three-body collisions that also measure the third-order coherence, thus providing a critical signature of true quantum statistical behavior. Understanding the quantum statistical collective behavior of ultracold dilute gases will drive research in ultracold collisions for years to come.

### III. INTRODUCTION TO COLD COLLISION THEORY

#### A. Basic concepts of scattering theory

Let us first consider some of the basic concepts that are needed to describe the collision of two ground state atoms. We initially consider the collision of two distinguishable, structureless particles  $a$  and  $b$  with interaction potential  $V_g(R)$  moving with relative momentum  $\mathbf{k}$ , where  $\mathbf{R}$  is the vector connecting  $a$  and  $b$ . We will generalize below to the cases of identical particles and particles with internal structure. The collision energy is  $E = \hbar^2 k^2 / 2\mu$ , where  $\mu$  is the reduced mass of the two particles. If there is no interaction between the particles,  $V_g = 0$ , the wave function describing the relative motion of the two particles in internal states  $|0_a\rangle$  and  $|0_b\rangle$  is

$$\Psi_g^+(\mathbf{R}) = e^{i\mathbf{k}\cdot\mathbf{R}} |0_a 0_b\rangle. \quad (1)$$

If the interaction potential is nonzero, the collision between the particles results in a scattered wave, and at large  $R$  beyond the range of the potential the wave function is represented as

$$\Psi_g^+(\mathbf{R}) \sim \left\{ e^{i\mathbf{k}\cdot\mathbf{R}} + \frac{e^{ikR}}{R} f(E, \hat{\mathbf{k}}, \hat{\mathbf{k}}_s) \right\} |0_a 0_b\rangle, \quad (2)$$

where  $\hat{\mathbf{k}}$  is a unit vector indicating the direction of  $\mathbf{k}$  and  $\hat{\mathbf{k}}_s$  is a unit vector indicating the direction of the scattered wave with amplitude  $f(E, \hat{\mathbf{k}}, \hat{\mathbf{k}}_s)$ . The overall effect of the collision is described by a cross section  $\sigma(E)$ . In a gas cell, for which all directions  $\hat{\mathbf{k}}$  are possible,  $\sigma(E)$  is determined by integrating over all scattered directions and averaging over all values of initial  $\hat{\mathbf{k}}$ :

$$\sigma(E) = \int_{4\pi} \frac{d\hat{\mathbf{k}}}{4\pi} \int_{4\pi} d\hat{\mathbf{k}}_s |f(E, \hat{\mathbf{k}}, \hat{\mathbf{k}}_s)|^2. \quad (3)$$

Since  $f$  has units of length, the cross section has units of  $\text{length}^2 = \text{area}$ . Equation (3) simplifies for a spherically symmetric potential, for which  $f$  depends only on the angle  $\theta$  between  $\hat{\mathbf{k}}$  and  $\hat{\mathbf{k}}_s$ :

$$\sigma(E) = 2\pi \int_0^\pi d\theta \sin(\theta) |f(E, \theta)|^2 \quad (4)$$

The object of scattering theory is to calculate the scattering amplitude and cross section, given the interaction potentials between the two atoms. The first step in reducing the problem to practical computation is to introduce the partial wave expansion of the plane wave:

$$e^{i\mathbf{k}\cdot\mathbf{R}} = 4\pi \sum_{l=0}^{\infty} \sum_{m=-l}^l i^l Y_{lm}^*(\hat{\mathbf{k}}) Y_{lm}(\hat{\mathbf{k}}_s) j_l(kR), \quad (5)$$

where  $Y_{lm}$  is a spherical harmonic and the function  $j_l$  has the following form as  $R \rightarrow \infty$ :

$$j_l(kR) \sim \frac{\sin[kR - (\pi/2)l]}{kR}. \quad (6)$$

The complete wave function at all  $R$  is also expanded in a partial wave series:

$$\Psi_g^+(\mathbf{R}) = 4\pi \sum_{l=0}^{\infty} \sum_{m=-l}^l i^l Y_{lm}^*(\hat{\mathbf{k}}) Y_{lm}(\hat{\mathbf{k}}_s) \times \frac{F_l^+(E, R)}{R} |0_a 0_b\rangle, \quad (7)$$

where  $F_l^+(E, R)$  is determined from the Schrödinger equation,

$$\frac{d^2 F_l^+(E, R)}{dR^2} + \frac{2\mu}{\hbar^2} \left( E - V_g(R) + \frac{\hbar^2 l(l+1)}{2\mu R^2} \right) F_l^+(E, R) = 0. \quad (8)$$

By imposing the following boundary condition on  $F_l^+(E, R)$  as  $R \rightarrow \infty$ , the asymptotic wave function has the desired form, Eq. (2), representing an incident plane wave plus scattered wave:

$$\frac{F_l^+(E, R)}{R} \sim \sin\left(kR - \frac{\pi}{2}l + \eta_l\right) \frac{e^{i\eta_l}}{kR} \sim j_l(kR) + \frac{i}{2} \frac{e^{i[kR - (\pi/2)l]}}{kR} T_l(E). \quad (9)$$

Here  $\eta_l$  is the phase shift induced by the interaction potential  $V_g(R)$ , and  $T_l(E) = 1 - e^{2i\eta_l}$  is the  $T$ -matrix element from which the amplitude of the scattered wave is determined,

$$f(E, \hat{\mathbf{k}}, \hat{\mathbf{k}}_s) = \frac{2\pi i}{k} \sum_{l=0}^{\infty} \sum_{m=-l}^l i^l Y_{lm}^*(\hat{\mathbf{k}}) Y_{lm}(\hat{\mathbf{k}}_s) T_l(E) \quad (11)$$

Using the simpler form of Eq. (4), the cross section becomes

$$\sigma(E) = \frac{\pi}{k^2} \sum_{l=0}^{\infty} (2l+1) |T_l(E)|^2 \quad (12)$$

$$= \frac{4\pi}{k^2} \sum_{l=0}^{\infty} (2l+1) \sin^2 \eta_l. \quad (13)$$

The cross section has a familiar semiclassical interpretation. If the interaction potential  $V_g(R)$  vanishes, the particle trajectory is a straight line with relative angular momentum  $\mathbf{R} \times \mathbf{p} = b\mathbf{p}$ , where  $p$  is linear momentum and  $b$  is the distance of closest approach. If we take the angular momentum to be  $b\mathbf{p} = \hbar \sqrt{l(l+1)} \approx \hbar(l + \frac{1}{2})$ , where the ‘‘classical’’  $l$  here is nonquantized, then  $b$  is the classical turning point of the repulsive centrifugal potential  $\hbar^2 l(l+1)/2\mu R^2$  in Eq. (8). The semiclassical expression for the cross section, analogous to Eq. (12), has the form of an area,

$$\sigma(E, \text{semiclassical}) = 2\pi \int_0^{\infty} b P(b, E) db \quad (14)$$

weighted by  $P(b, E) = |T_l(E)|^2$ . An important feature of cold collisions is that only a very few values of  $l$  can contribute to the cross section, because the classical turning points of the repulsive centrifugal potential are at large values of  $R$ . Only collisions with the very lowest  $l$  values allow the atoms to get close enough to one another to experience the interatomic interaction potential. We will discuss below the specific quantum properties associated with discrete values of  $l$ . Semiclassical theory is useful for certain types of trap loss collisions in relatively warm traps where light is absorbed by atom pairs at very large  $R$ , but a quantum treatment always becomes necessary at sufficiently low collision energy.

In the simple introduction above, the cross section in Eq. (13) represents elastic scattering, for which the internal states of the particles do not change, and their relative kinetic energy  $E$  is the same before and after the collision. In general, the atoms will have nonzero internal angular momentum due to hyperfine structure in the case of alkali atoms or due to electronic structure in the case of rare gas metastable atoms. In a field-free region, these internal states are characterized by total angular momentum  $F$  and projection  $M$  on a space-fixed quantization axis. Often an external field, either a magnetic or an optical or radio frequency electromagnetic field, is present in cold collision experiments, and these  $FM$  states are modified by the external field. Species like hydrogen and alkali atoms, which have  $^2S$  ground states and nonvanishing nuclear spin  $I$ , have two hyperfine components with  $F = I + \frac{1}{2}$  and  $F = I - \frac{1}{2}$ . Figure 3 shows the Zeeman splitting of the two  $F=1$  and  $F=2$  hyperfine components of ground state  $^{87}\text{Rb}$  atoms, and Fig. 4 shows the ground-state interaction potentials for two interacting Rb atoms. If the atomic field-modified states, commonly called field-dressed states, are represented by  $|\alpha_i\rangle$  for atom  $i=a, b$ , then the general collision process represents a transition from the state  $|\alpha_a\rangle|\alpha_b\rangle$  to the state  $|\alpha'_a\rangle|\alpha'_b\rangle$ , represented by the general transition amplitude  $f(E, \hat{\mathbf{k}}, \hat{\mathbf{k}}_s, \alpha_a \alpha_b \rightarrow \alpha'_a \alpha'_b)$  and the  $T$ -matrix ele-

ment  $T(E, \alpha_a \alpha_b \rightarrow \alpha'_a \alpha'_b)$ . These are the most complete transition amplitudes that describe an observable transition, specified in terms of quantities that can be selected experimentally. The most complete  $T$ -matrix elements that can be calculated from the multicomponent version of Eq. (8) are also specified by the initial and final partial waves:  $T(E, \alpha_a \alpha_b l m \rightarrow \alpha'_a \alpha'_b l' m')$ . There are three distinct physical axes which define these amplitudes: a space-fixed axis which defines the space projection quantum numbers  $M_a$  and  $M_b$ , the asymptotic direction of approach  $\hat{\mathbf{k}}$ , and the asymptotic direction of separation  $\hat{\mathbf{k}}_s$ . In beam experiments all three axes can be different. Most all the work on cold atom collisions is carried out in a homogeneous gas, where neither  $\hat{\mathbf{k}}$  nor  $\hat{\mathbf{k}}_s$  are selected or measured, and a cell average cross section defined as in Eq. (12) for the general  $\sigma(E, \alpha_a \alpha_b \rightarrow \alpha'_a \alpha'_b)$  is appropriate. Some experiments, especially in the context of Bose-Einstein condensation, have a well-defined local space-fixed axis, and select particular values of  $M_a$  and  $M_b$ , but most of the work we will describe is for unpolarized gases involving an average over  $M_a$  and  $M_b$ .

Instead of cross sections, it is usually preferable to give a rate coefficient for a collision process. The rate coefficient is directly related to the number of collision events occurring in a unit time in a unit volume. Consider the reaction



where the quantum numbers are all assumed to be different. If the density of species  $\alpha_i$  in a cell is  $n_{\alpha_i}$ , the rate of change of the density of the various species due to collision events is

$$\begin{aligned} \frac{n_{\alpha_a}}{dt} + \frac{n_{\alpha_b}}{dt} &= -\frac{n_{\alpha'_a}}{dt} - \frac{n_{\alpha'_b}}{dt} \\ &= K(T, \alpha_a \alpha_b \rightarrow \alpha'_a \alpha'_b) n_{\alpha_a} n_{\alpha_b}. \end{aligned} \quad (16)$$

The rate coefficient  $K(T, \alpha_a \alpha_b \rightarrow \alpha'_a \alpha'_b)$  is related to the cross section through

$$K(T, \alpha_a \alpha_b \rightarrow \alpha'_a \alpha'_b) = \langle \sigma(E, \alpha_a \alpha_b \rightarrow \alpha'_a \alpha'_b) v \rangle, \quad (17)$$

where the brackets imply an average over the distribution of relative collision velocities  $v$ .

The general theory of collisions of degenerate species is well understood. The basic multichannel theory can be found, for example, in Mies (1973a, 1973b) or Baylis *et al.* (1987). There is a considerable body of work on the theory of collisions of cold spin-polarized hydrogen atoms, as a consequence of the still unfulfilled quest to achieve Bose-Einstein condensation in such a system. This will be discussed in Sec. VIII. The Eindhoven group led by B. Verhaar has been especially active in developing the theory. Stoof, Koelman, and Verhaar (1988) give an excellent introduction to the subject. The theory of cold collisions in external magnetic fields and optical or radiofrequency electromagnetic fields has also been developed, as we will describe in more detail in the later sections of this review.

It is important to distinguish between two different kinds of collisions: elastic and inelastic. As mentioned above, an elastic collision is one in which the quantum states  $\alpha_a, \alpha_b$  of each atom remain unchanged by the collision. These collisions exchange momentum, thereby aiding the thermalizing of the atomic sample. These are “good” collisions that do not destroy the trapped states, and they are necessary for the process of evaporative cooling we will describe later. An inelastic collision is one in which one (or more) of these two quantum numbers changes in the collision. Most cold collision studies have dealt with inelastic events instead of elastic ones, that is, the collision results in hot atoms or untrapped species or even ionic species. As we will see in the next section, the quantum threshold properties of elastic and inelastic collisions are very different.

The basic difference between collisions of different atomic species and identical atomic species is the need to symmetrize the wave function with respect to exchange of identical particles in the latter case. Other than this symmetrization requirement, the theory is the same for the two cases. Symmetrization has two effects: the introduction of factors of two at various points in the theory, and the exclusion of certain states since they violate the exchange symmetry requirement. Such symmetry restrictions are well known in the context of diatomic molecular spectroscopy, leading to, for example, orthospecies and paraspecies of molecular hydrogen and to every other line being missing in the absorption spectrum of molecular oxygen, due to the zero nuclear spin of the oxygen atom (Herzberg, 1950). In the case of atomic collisions of identical species, if the two quantum numbers are identical,  $\alpha_a = \alpha_b$ , only even partial waves  $l$  are possible if the particles are composite bosons, and only odd partial waves are possible if the particles are composite fermions. If the two quantum numbers are not identical,  $\alpha_a \neq \alpha_b$ , both even and odd partial waves can contribute to collision rates. The effect of this symmetry is manifestly present in photoassociation spectra, where for example, half the number of lines appear in a doubly spin polarized gas (where all atoms are in the same quantum state) as contrasted to an unpolarized gas (where there is a distribution of quantum states). These spectra will be described in Section VI below.

Stoof, Koelman, and Verhaar (1988) give a good discussion of how to modify the theory to account for exchange symmetry of identical particles. Essentially, they set up the states describing the separated atoms, the so-called channel states of scattering theory, as fully symmetrized states with respect to particle exchange.  $T$ -matrix elements and event rate coefficients, defined as in Eq. (17), are calculated conventionally for transitions between such symmetrized states. The event rate coefficients are given by

$$K(\{\gamma\delta\} \rightarrow \{\alpha\beta\}) = \left\langle \frac{\pi\hbar}{\mu k} \sum_{l'm'} \sum_{lm} |T(E, \{\gamma\delta\} l' m', \{\alpha\beta\} lm)|^2 \right\rangle \quad (18)$$

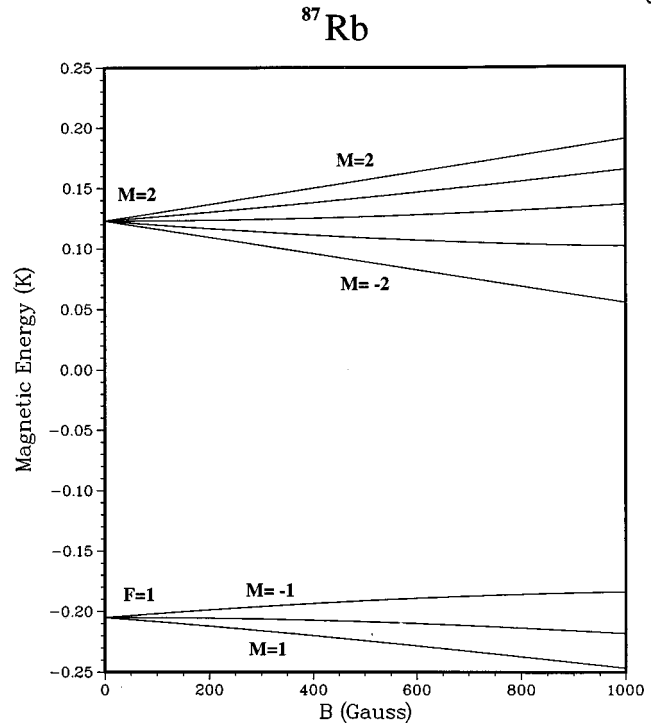


FIG. 3. Ground hyperfine levels of the  $^{87}\text{Rb}$  atom versus magnetic field strength. The Zeeman splitting of each manifold is evident. The energy has been divided by the Boltzmann constant in order to express it in temperature units.

where the braces  $\{\cdot\cdot\}$  signify symmetrized states, and the  $T$  matrix as defined in this review is related to the unitary  $S$  matrix by  $\mathbf{T} = \mathbf{1} - \mathbf{S}$ . Then collision rates are unambiguously given by

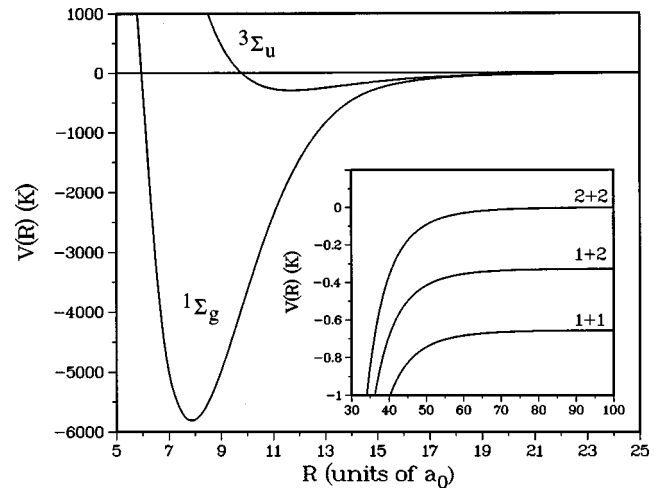


FIG. 4. The ground-state potential energy curves of the  $\text{Rb}_2$  molecule. The potentials have been divided by the Boltzmann constant in order to express them in units of temperature. The full figure shows the short range potentials on the scale of chemical bonding. The inset shows an enlargement at long range, showing the separated atom hyperfine levels  $F_a + F_b = 1+1, 1+2,$  and  $2+2$ . The upper two potentials in the inset correlate adiabatically with the  $^3\Sigma_u$ .

$$\frac{dn_\alpha}{dt} = \sum_\beta \sum_{\{\gamma\delta\}} (1 + \delta_{\alpha\beta}) \times [K(\gamma\delta \rightarrow \alpha\beta)n_\gamma n_\delta - K(\alpha\beta \rightarrow \gamma\delta)n_\alpha n_\beta]. \quad (19)$$

This also works for the case of elastic scattering of identical particles in identical quantum states:  $K(\alpha\alpha \rightarrow \alpha\alpha)$  must be multiplied by a factor of 2 to get the rate of momentum transfer  $\hat{\mathbf{k}}$  scatters to  $(\hat{\mathbf{k}}_s \neq \hat{\mathbf{k}})$  since two atoms scatter per collision event. Gao (1997) has also described the formal theory for collisions of cold atoms taking into account identical particle symmetry.

## B. Quantum properties as $E \rightarrow 0$

Cold and ultracold collisions have special properties that make them quite different from conventional room temperature collisions. This is because of the different scales of time and distance involved. The effect of the long collision time will be discussed in Sec. V. Here we will examine the consequence of the long de Broglie wavelength of the colliding atoms. The basic modification to collision cross sections when the de Broglie wavelength becomes longer than the range of the potential was described by Bethe (1935) in the context of cold neutron scattering, and has been widely discussed in the nuclear physics literature (Wigner, 1948; Delves, 1958). Such quantum threshold effects only manifest themselves in neutral atom collisions at very low temperature, typically  $\ll 1$  K (Julienne and Mies, 1989; Julienne, Smith, and Burnett, 1993), but they play a very important role in the regime of laser cooling and evaporative cooling that has been achieved.

Figure 1, in the Introduction, gave a qualitative indication of the range of  $\lambda$  as temperature is changed. Even at the high temperature end of the range of laser cooling,  $\lambda$  on the order of  $100a_0$  is possible, and at the lower end of evaporative cooling,  $\lambda > 1 \mu\text{m}$  ( $20\,000a_0$ ). These distances are much larger than the typical lengths associated with chemical bonds, and the delocalization of the collision wave function leads to characteristic behavior where collision properties scale as some power of the collision momentum  $k = \sqrt{2\mu E} = 2\pi/\lambda$  as  $k \rightarrow 0$ , depending on the inverse power  $n$  of the long range potential, which varies as  $R^{-n}$ .

In the case of elastic scattering, the phase shift  $\eta_l$  in Eqs. (9) and (13) has the following property as  $k \rightarrow 0$  (Mott and Massey, 1965): if  $2l < n - 3$ ,

$$\lim_{k \rightarrow 0} k^{2l+1} \cot \eta_l = -\frac{1}{A_l}, \quad (20)$$

where  $A_l$  is a constant, whereas, if  $2l > n - 3$ ,

$$\lim_{k \rightarrow 0} k^{n-2} \cot \eta_l = \text{const.} \quad (21)$$

For neutral ground state atoms, this ensures that the phase shift vanishes at least as fast as  $k^3$  for all  $l \geq 1$ . Thus all contributions to the cross section vanish when  $k$  becomes sufficiently small, except the contribution from the  $s$  wave,  $l=0$ . Since the  $s$ -wave phase shift varies as

$-kA_0$  as  $k \rightarrow 0$ , we see from Eq. (13) that the elastic scattering cross section for identical particles approaches

$$\sigma(E) \rightarrow 8\pi A_0^2, \quad (22)$$

where the factor of 8 instead of 4 occurs due to identical particle symmetry (two particles scatter per collision). Thus, the cross section for elastic scattering becomes constant in the low energy limit. The quantity  $A_0$  is the  $s$ -wave scattering length, an important parameter in the context of Bose-Einstein condensation. Note that the rate coefficient for elastic scattering vanishes as  $T^{1/2}$  in the limit of low temperature, since  $K = \langle \sigma v \rangle$ .

Figure 5 illustrates the properties of a very low collision energy wave function, taken for a model potential with a van der Waals coefficient  $C_6$  and mass characteristic of Na atom collisions. The upper panel illustrates the wave function at long range, on the scale of  $1 \mu\text{m}$ . The lower panel shows an enlargement of the short-range wave function for the case of three different potentials, with three different scattering lengths, negative, zero, and positive. The figure shows the physical interpretation of the scattering length, as the effective point of origin of the long wavelength asymptotic sine wave at  $R = A_0$ , since the long range wave function is proportional to  $\sin[k(R - A_0)]$ .

Inelastic collisions have very different threshold properties than elastic ones. As long as the internal energy of the separated atoms in the exit channel is lower than for the entrance channel, so that energy is released in the collision, the transition matrix element varies as (Bethe, 1935; Wigner, 1948; Julienne and Mies, 1989)

$$T(E) \propto k^{l+1/2}, \quad (23)$$

where  $l$  is the entrance channel partial wave index. Using this form in Eq. (12) shows that the cross section vanishes at least as fast as  $k$  for all  $l > 0$ , but it varies as  $1/k$  for the  $s$  wave. This variation (sometimes called the  $1/v$  law) was given by Bethe (1935) and is well known in nuclear physics. Although the cross section for an inelastic, energy-releasing, collision becomes arbitrarily large as  $k \rightarrow 0$ , the rate coefficient  $K$  remains finite, and approaches a nonvanishing constant. Although Côté *et al.* (1996) speak of a quantum suppression of cold inelastic collisions, the ‘‘suppression’’ is only relative to a semiclassical process, and actual rate constants can be surprisingly large near zero temperature, as will be discussed in Sec. VIII B.

The range of  $k$  where these limiting threshold laws become valid depends strongly on the particular species, and even on the specific quantum numbers of the separated atoms. Knowledge of the long range potential alone does not provide a sufficient condition to determine the range of  $k$  in which they apply. This range, as well as the scattering length itself, depends on the actual phase shift induced by the whole potential, and is very sensitive to uncertainties in the short range part of the potential in the chemical bonding region (Gribakin and Flambaum, 1993). On the other hand, a necessary condition for threshold law behavior can be given based solely on the long-range potential (Julienne and Mies,

1989; Julienne, Smith, and Burnett, 1993). This condition is based on determining where a semiclassical, WKB connection breaks down between the long-range asymptotic  $s$  wave and the short-range wave function that experiences the acceleration of the potential. Consider the ground-state potential  $V_g(R)$  as a function of  $R$ . The long-range potential is

$$V_g(R) = -\frac{C_n}{R^n}, \quad (24)$$

where  $n$  is assumed to be  $\geq 3$ . Let us first define

$$E_Q = \frac{\hbar^2}{\mu} \left[ \left( 2 \frac{n+1}{3} \right)^{2n} \left( \frac{n-2}{6n} \right)^n \left( \frac{2n+2}{n-2} \cdot \frac{\hbar^2}{\mu C_n} \right)^2 \right]^{(1/n-2)} \quad (25)$$

$$R_Q = \left( \frac{n-2}{2n+2} \cdot \frac{C_n}{E_Q} \right)^{1/n}. \quad (26)$$

The properties of the wave function  $\Psi(E, R)$  depend on the values of  $E$  and  $R$  relative to  $E_Q$  and  $R_Q$ . When  $E \gg E_Q$ , the energy is high enough that it is always possible to make a semiclassical Wentzel-Kramers-Brillouin (WKB) connection between the wave function in the long-range zone,  $R \gg R_Q$ , and the wave function in the short-range zone,  $R \ll R_Q$ . In this case, the WKB representation of the  $s$ -wave wave function is a good approximation at all  $R$ , and there are no special threshold effects. On the other hand,  $E \ll E_Q$  satisfies the condition that there is some range of distance near  $R \approx R_Q$  where the WKB approximation fails, so that no semiclassical connection is possible between long- and short-range wave functions. This is the regime where a quantum connection, with its characteristic threshold laws, is necessary. When  $E \ll E_Q$  the wave function for  $R \gg R_Q$  is basically the asymptotic wave with the asymptotic phase shift (Julienne, 1996), whereas the wave function for  $R \ll R_Q$  is attenuated in amplitude, relative to the normal WKB amplitude, by a factor proportional to  $k^{l+1/2}$  (Julienne and Mies, 1989).

Julienne, Smith, and Burnett (1993) calculated the values of  $E_Q$  and  $R_Q$  for a number of alkali and rare gas metastable species that can be laser cooled. These are shown in Table I. The alkali values were based on known values of  $C_6$  for the  $n=6$  van der Waals potentials, and estimates were made for the metastable rare gas  $C_6$  coefficients, for which the weak  $C_5/R^5$  quadrupole-quadrupole contribution to the potential for metastable rare gases was ignored in comparison to the  $C_6$  contribution. The value of  $R_Q$  is small enough that relativistic retardation corrections to the ground state potential are insignificant. The  $R_Q, E_Q$  parameters for each rare gas are similar to those of the neighboring alkali species in the periodic table. Figure 6 shows a plot of the ground-state potential expressed in units of  $R_Q$  and  $E_Q$ . The position of the maximum in the barrier due to the centrifugal potential for  $l \neq 0$ , as well as the maximum binding energy and minimum outer classical turning point of the last bound state in the van der Waals potential, scale with  $C_6$  and mass as  $R_Q$  and  $E_Q$  do, scaling as  $(\mu C_6)^{1/4}$  and  $\mu^{-3/2} C_6^{-1/2}$ , respectively.

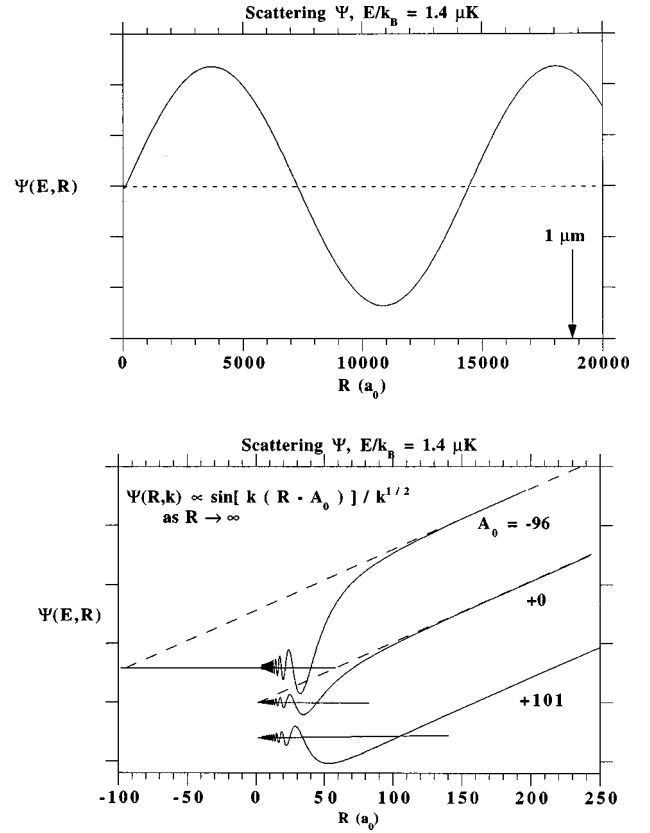


FIG. 5. The upper panel illustrates the long de Broglie wave at long range, on the scale of  $1 \mu\text{m}$ . The lower panel shows an enlargement of the short range wave function for the case of three different potentials, with three different scattering lengths, negative, zero, and positive.

These other scalable parameters are also indicated on Fig. 6, which gives a universal plot for any of the species in Table I. Figure 6 also shows  $\lambda_Q/2\pi = 0.857R_Q$  for  $E = E_Q$ . The centrifugal barriers for the lowest few partial waves are lower than  $E_Q$ , but lie outside  $R_Q$ . The positions  $R_C(l)$  and heights  $E_C(l)$  of the centrifugal barriers are  $R_C(l) = 2.67R_Q/[l(l+1)]^{1/4}$  and  $E_C(l) = 0.0193E_Q[l(l+1)]^{3/2}$  respectively. The  $p$ - and  $d$ -wave barriers have heights of  $0.055E_Q$  and  $0.28E_Q$ , respectively.  $E_Q$  is small enough that several partial waves typically contribute to ground-state collisions of the heavier species at typical magneto-optical trap temperatures of  $100 \mu\text{K}$  to  $1 \text{mK}$ .

The distance  $R_Q$ , closely related to the mean scattering length  $\bar{a} = 0.967R_Q$  defined by Gribakin and Flambaum (1993), is solely a property of the long-range potential and atomic mass. On the other hand, the approach to the quantum threshold laws is in a range  $0 < E \ll E_Q$ , where the actual range depends on the effect of the whole potential, as measured by the threshold phase shift proportional to the actual  $s$ -wave scattering length  $A_0$ . Let  $A_b$  be defined by  $E_b = \hbar^2/2\mu A_b^2$ , where  $E_b$  is the position of the last bound state of the potential just below threshold ( $A_b > 0$ ) or the position of a virtual bound state just above threshold ( $A_b < 0$ ). When  $E_b < E_Q$ , the range over which the threshold laws apply can be estimated from  $0 < k \ll |A_b|^{-1}$ , or  $0 < E \ll E_b$ .

Thus, the threshold laws apply only over a range comparable to the lesser of  $E_Q$  and  $E_b$ . In the limit where the last bound state is very near threshold, Gribakin and Flambaum (1993) find that  $A_0 = \bar{a} + A_b$ ; this reduces to the result of Mies *et al.* (1996),  $A_0 \approx A_b$ , when  $|A_0| \gg \bar{a}$ . The special threshold properties of the last bound state in the potential has recently been described by Boisseau, Audouard, and Vigué (1998) and Trost *et al.* (1998). The usual quantization rules in a long-range potential (LeRoy and Bernstein, 1970) do not adequately characterize the threshold limit of the last bound state.

Since the scattering length can be arbitrarily large, corresponding to the case where the last bound state is arbitrarily close to threshold,  $E_b$  can be arbitrarily small. Therefore, the actual range over which the threshold law expressions in Eqs. (22) and (23) apply can in principle be less than the actual temperature range in cold or even ultracold experiments. In fact, the Cs atom in its doubly spin polarized hyperfine level seems not yet to be in the threshold limit even at a few  $\mu\text{K}$  (Arndt *et al.*, 1997; Leo *et al.*, 1998).

To show how the interatomic potential affects the scattering length, we can imagine artificially modifying the ground-state potential by adding some small correction term  $\lambda V_{\text{corr}}(R)$  to it which has a short range compared to  $R_Q$ . Figure 7 shows that we can make  $A_0$  vary between  $-\infty$  and  $+\infty$  by making relatively small changes in the potential. The two singularities correspond to the case where the potential just supports another bound state. Thus, when  $\lambda V_{\text{corr}}$  changes across a singularity, the number of bound states in the potential changes by exactly one. The scattering length is negative when a new bound state is just about to appear, and positive when a new bound state has just appeared. Scattering lengths are sufficiently sensitive to potentials that, with rare exceptions, it is impossible to predict them accurately from first principles, and therefore they must be measured. How this can be done accurately will be described in the section on photoassociation spectroscopy.

### C. Collisions in a light field

Much of the work on collisions of cooled and trapped atoms has involved collisions in a light field. This is the subject of Secs. V, VI, and VII of this review and has been the subject of two earlier reviews. (Walker and Feng, 1994; Weiner, 1995). Therefore, it is useful to provide an overview of some of the concepts that are used in understanding cold collisions in a light field. Figure 2 gives a schematic description of the key features of these collisions, showing ground and excited state potentials,  $V_g(R)$  and  $V_e(R)$ , and indicating the optical coupling between ground and excited states induced by a light field at frequency  $\omega_1$ , which is detuned by  $\Delta = \omega_1 - \omega_0$  from the frequency of atomic resonance  $\omega_0$ . Detuning can be to the red or blue of resonance, corresponding to negative or positive  $\Delta$  respectively. The figure illustrates that the excited state potential, having a resonant-dipole form that varies as  $C_3/R^3$ , which can be attractive or repulsive, is of much longer range than the ground-state

TABLE I. Characteristic threshold parameters  $R_Q$  and  $E_Q$ .

Species	$R_Q$ (Bohr)	$E_Q$ (mK)	Species	$R_Q$ (Bohr)	$E_Q$ (mK)
Li	32	120	He*	34	180
Na	44	19	Ne*	40	26
K	64	5.3	Ar*	60	5.7
Rb	82	1.5	Kr*	79	1.6
Cs	101	0.6	Xe*	96	0.6

van der Waals potential. Figure 2 also indicates the Condon point  $R_C$  for the optical transition. This is the point at which the quasimolecule comprised of the two atoms is in optical resonance with the light field, i.e.,

$$V_e(R_C) - V_g(R_C) = \hbar \omega_1. \quad (27)$$

The Condon point is significant because in a semiclassical picture of the collision, it is the point at which the transition from the ground state to the excited state is considered to occur. The laser frequency  $\omega_1$  can be readily varied in the laboratory, over a wide range of red and blue detuning. Thus, the experimentalist has at his disposal a way of selecting the Condon point and the upper state which is excited by the light. By varying the detuning from very close to atomic resonance to very far from resonance, the Condon point can be selected to range from very large  $R$  to very small  $R$ .

Although the semiclassical picture implied by using the concept of a Condon point is very useful, a proper theory of cold collisions should be quantum mechanical, accounting for the delocalization of the wave function. If the light is not too intense, the probability of a transition,  $P_{ge}(E, \omega_1)$ , is proportional to a Franck-Condon overlap matrix element between ground- and excited-state wave functions:

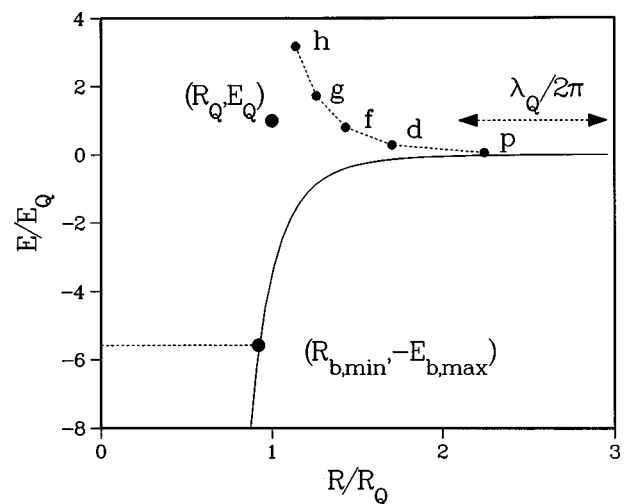


FIG. 6. The position of the maximum in the barrier due to the centrifugal potential for  $l \neq 0$ , as well as the maximum binding energy and minimum outer classical turning point of the last bound state in the van der Waals potential, all have identical scalings with  $C_6$  and mass as  $R_Q$  and  $E_Q$ , with scaling as  $(\mu C_6)^{1/4}$  and  $\mu^{3/2} C_6^{1/2}$ , respectively.

$$P_{ge}(E, \omega_1) \propto |\langle \Psi_e(R) | \Omega_{eg}(R) | \Psi_g(E, R) \rangle|^2 \quad (28)$$

$$\approx |\Omega_{eg}(R_C)|^2 |\langle \Psi_e(R) | \Psi_g(E, R) \rangle|^2, \quad (29)$$

where the optical Rabi matrix element  $\Omega_{eg}(R)$  measures the strength of the optical coupling. Julienne (1996) showed that a remarkably simple reflection approximation to the Franck-Condon factor, based on expanding the integrand of the Franck-Condon factor about the Condon point, applies over a wide range of ultracold collision energies and red or blue detunings. This approximation, closely related to the usual stationary phase approximation of line broadening theory, shows that the Franck-Condon factor (in the cases where there is only one Condon point for a given state) is proportional to the ground-state wave function at the Condon point:

$$F_{ge}(E, \Delta) = |\langle \Psi_e(R) | \Psi_g(E, R) \rangle|^2 \quad (30)$$

$$= \frac{1}{D_C} |\Psi_g(E, R_C)|^2 \quad \text{blue detuning} \quad (31)$$

$$= h\nu_v \frac{1}{D_C} |\Psi_g(E, R_C)|^2 \quad \text{red detuning.} \quad (32)$$

Here  $D_C = |d(V_e - V_g)/dR|_{R_C}$  is the slope of the difference potential, and the wave functions have been assumed to be energy normalized, that is, the wave functions in Eqs. (7) to (9) are multiplied by  $\sqrt{2\mu k/\pi\hbar^2}$  so that

$$|\langle \Psi_g(E, R) | \Psi_g(E', R) \rangle|^2 = \delta(E - E'). \quad (33)$$

The formulas for red and blue detuning differ because they represent free-bound and free-free transitions respectively; here  $\nu_v$  is the vibrational frequency of the bound vibrational level excited in the case of red detuning. Figure 8 shows the validity of this approximation over a range of Condon points and collision energies for a typical case. We thus see that it is legitimate to use the semiclassical concept of excitation at a Condon point in discussing cold collisions in a light field.

The excited-state potential can be written at long range as (Meath, 1968)

$$V_e(R) = f\hbar\Gamma_A \left( \frac{\lambda_A}{2\pi R} \right)^3, \quad (34)$$

where  $\lambda_A$  and  $\Gamma_A$  are the respective transition wavelength and spontaneous decay width of the atomic resonance transition, and where  $f$  is a dimensionless factor on the order of unity. Thus, in a magneto-optical trap, where  $|\Delta|$  is on the order of  $\Gamma_A$ , the Condon point will have a magnitude on the order of  $\lambda_A/2\pi$ , that is, on the order of  $1000a_0$  for typical laser cooling transitions. This is the regime of the trap loss experiments described in Sec. V. Optical shielding experiments are typically done with detuning up to several hundred  $\Gamma_A$ , corresponding to much smaller Condon points, on the order of a few hundred  $a_0$ . Photoassociation spectroscopy experiments use quite large detunings, and typically sample Condon points over a range from short range chemical bonding out to a few hundred  $a_0$ .

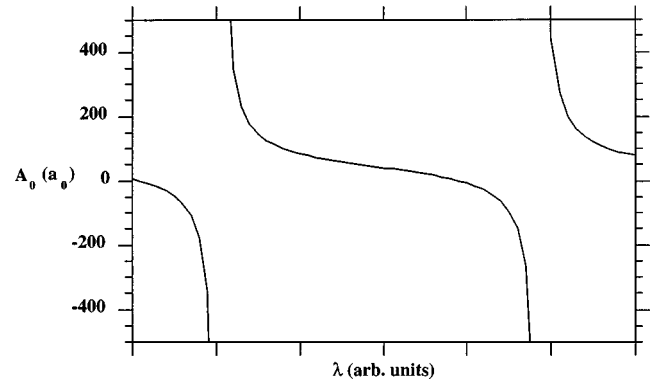


FIG. 7. The scattering length  $A_0$  varies between  $-\infty$  and  $+\infty$  by making relatively small changes ( $\lambda V_{corr}$ ) in the ground-state potential. The two singularities correspond to the case where the potential just supports another bound state.

Because of the very different ranges of  $\Delta$  and  $R_C$  in the various kinds of cold collisions in a light field, a number of different kinds of theories and ways of thinking about the phenomena have been developed to treat the various cold collision processes. Since  $R_C$  for magneto-optical trap-loss collisions is typically much larger than the centrifugal barriers illustrated in Fig. 6, many partial waves contribute to the collision, the quantum threshold properties are not evident at all, and semiclassical descriptions of the collision have been very fruitful in describing trap loss. The main difficulty in describing such collisions is in treating the strong excited-state spontaneous decay on the long time scale of the collision. We will see that a good, simple quantum mechanical description of such collisions is given by extending the above Condon point excitation picture to include excited state decay during the collision. Quantitative theory is still made difficult by the presence of complex molecular hyperfine structure, except in certain special cases. Since the Condon points are at much smaller  $R$  in the case of optical shielding, excited state decay during the collision is not a major factor in the dynamics, and the primary challenge to theory in the case of optical shielding is how to treat the effect of a strong radiation field, which does strongly modify the collision dynamics. Simple semiclassical pictures seem not to work very well in accounting for the details of shielding, and a quantum description is needed. The theory of photoassociation is the most quantitative and well developed of all. Since the Condon point is typically inside the centrifugal barriers and  $R_Q$ , only the lowest few partial waves contribute to the spectrum. Although the line shapes of the free-bound transitions exhibit the strong influence of the quantum threshold laws, they can be quantitatively described by Franck-Condon theory, which can include ground and excited state hyperfine structure. We will show how photoassociation spectroscopy has become a valuable tool for precision spectroscopy and determination of ground state scattering lengths.

#### IV. EXPERIMENTAL METHODS FOR THE STUDY OF COLD COLLISIONS

##### A. Atom traps

###### 1. Light forces

It is well known that a light beam carries momentum and that the scattering of light by an object produces a force. This property of light was first demonstrated by Frish (1933) through the observation of a very small transverse deflection ( $3 \times 10^{-5}$  rad) in a sodium atomic beam exposed to light from a resonance lamp. With the invention of the laser, it became easier to observe effects of this kind because the strength of the force is greatly enhanced by the use of intense and highly directional light fields, as demonstrated by Ashkin (1970) with the manipulation of transparent dielectric spheres suspended in water. The results obtained by Frish and Ashkin raised the interest of using light forces to control the motion of neutral atoms. Although the understanding of light forces acting on atoms was already established by the end of the 1970s, unambiguous demonstration of atom cooling and trapping was not accomplished before the mid-80s. In this section we discuss some fundamental aspects of light forces and schemes employed to cool and trap neutral atoms.

The light force exerted on an atom can be of two types: a dissipative, spontaneous force and a conservative, dipole force. The spontaneous force arises from the impulse experienced by an atom when it absorbs or emits a quantum of photon momentum. When an atom scatters light, the resonant scattering cross section can be written as  $\sigma_0 = \lambda_0^2/2\pi$  where  $\lambda_0$  is the on-resonant wavelength. In the optical region of the electromagnetic spectrum the wavelengths of light are on the order of several hundreds of nanometers, so resonant scattering cross sections become quite large,  $\sim 10^{-9}$  cm<sup>2</sup>. Each photon absorbed transfers a quantum of momentum  $\hbar\vec{k}$  to the atom in the direction of propagation ( $\hbar$  is the Planck constant divided by  $2\pi$ , and  $k = 2\pi/\lambda$  is the magnitude of the wave vector associated with the optical field). The spontaneous emission following the absorption occurs in random directions; over many absorption-emission cycles, it averages to zero. As a result, the *net* spontaneous force acts on the atom in the direction of the light propagation, as shown schematically in Fig. 9. The saturated rate of photon scattering by spontaneous emission (one half the reciprocal of the excited-state lifetime) fixes the upper limit to the force magnitude. This force is sometimes called *radiation pressure*.

The dipole force can be readily understood by considering the light as a classical wave. It is simply the time-averaged force arising from the interaction of the transition dipole, induced by the oscillating electric field of the light, with the gradient of the electric field amplitude. Focusing the light beam controls the magnitude of this gradient, and detuning the optical frequency below or above the atomic transition controls the sign of the force acting on the atom. Tuning the light below resonance attracts the atom to the center of the light beam

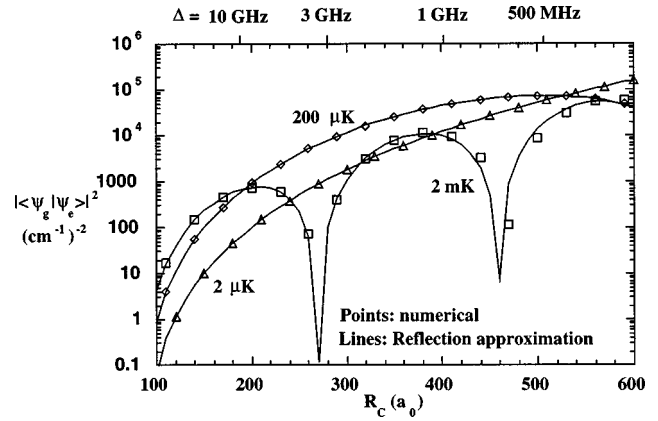


FIG. 8. The plots show the validity of the reflection approximation over a range of Condon points and collision energies for a typical case.

while tuning above resonance repels it. The dipole force is a stimulated process in which no net exchange of energy between the field and the atom takes place, but photons are absorbed from one mode and reappear by stimulated emission in another. Momentum conservation requires that the change of photon propagation direction from initial to final mode imparts a net recoil to the atom. Unlike the spontaneous force, there is in principle no upper limit to the magnitude of the dipole force since it is a function only of the field gradient and detuning.

We can bring these qualitative remarks into focus by considering the amplitude, phase, and frequency of a classical field interacting with an atomic transition dipole. A detailed development of the following results is out of the scope of the present work, but can be found elsewhere (Stenholm, 1986; Cohen-Tannoudji *et al.*, 1992). The usual approach is semiclassical and consists in treating the atom as a two-level quantum system and the radiation as a classical electromagnetic field (Cook, 1979). A full quantum approach can also be employed (Cook, 1980; Gordon and Ashkin, 1980), but it will not be discussed here.

The basic expression for the interaction *energy* is

$$U = -\vec{\mu} \cdot \vec{E}, \quad (35)$$

where  $\vec{\mu}$  is the transition dipole and  $\vec{E}$  is the electric field of the light. The *force* is then the negative of the spatial gradient of the potential,

$$\vec{F} = -\vec{\nabla}_R \cdot U = \mu \vec{\nabla}_R E, \quad (36)$$

where we have set  $\vec{\nabla}_R \cdot \mu$  equal to zero because there is no spatial variation of the dipole over the length scale of the optical field. The optical-cycle average of the force is expressed as

$$\langle \vec{F} \rangle = \langle \mu \vec{\nabla}_R E \rangle = \mu [(\vec{\nabla}_R E_0)u + (E_0 \vec{\nabla}_R(k_L R))v], \quad (37)$$

where  $u$  and  $v$  arise from the steady-state solutions of the optical Bloch equations,

$$u = \frac{\Omega}{2} \frac{\Delta\omega_L}{(\Delta\omega_L)^2 + (\Gamma/2)^2 + \Omega^2/2} \quad (38)$$

and

$$v = \frac{\Omega}{2} \frac{\Gamma/2}{(\Delta\omega_L)^2 + (\Gamma/2)^2 + \Omega^2/2}. \quad (39)$$

In Eqs. (38) and (39)  $\Delta\omega_L = \omega - \omega_0$  is the detuning of the optical field from the atomic transition frequency  $\omega_0$ ,  $\Gamma$  is the natural width of the atomic transition, and  $\Omega$  is termed the Rabi frequency and reflects the strength of the coupling between field and atom,

$$\Omega = -\frac{\vec{\mu} \cdot \vec{E}_0}{\hbar}. \quad (40)$$

In writing Eq. (37) we have made use of the fact that the time-average dipole has in-phase and in-quadrature components,

$$\langle \vec{\mu} \rangle = 2\vec{\mu}(u \cos \omega_L t - v \sin \omega_L t), \quad (41)$$

and the electric field of the light is given by the classical expression,

$$E = E_0[\cos(\omega t - k_L R)]. \quad (42)$$

The time-averaged force, Eq. (37), consists of two terms: the first term is proportional to the gradient of the electric field amplitude; the second term is proportional to the gradient of the phase. Incorporating Eqs. (38) and (39) into Eq. (37), we have for the two terms,

$$\begin{aligned} \langle \vec{F} \rangle = & \mu(\vec{\nabla}_R E_0) \frac{\Omega}{2} \left[ \frac{\Delta\omega_L}{(\Delta\omega_L)^2 + (\Gamma/2)^2 + \Omega^2/2} \right] \\ & + \mu(E_0 \vec{\nabla}_R(-k_L R)) \frac{\Omega}{2} \left[ \frac{\Gamma/2}{(\Delta\omega_L)^2 + (\Gamma/2)^2 + \Omega^2/2} \right]. \end{aligned} \quad (43)$$

The first term is the dipole force, sometimes called the trapping force,  $F_T$ , because it is a conservative force and can be integrated to define a trapping potential for the atom:

$$\vec{F}_T = \mu(\vec{\nabla}_R E_0) \frac{\Omega}{2} \left[ \frac{\Delta\omega_L}{(\Delta\omega_L)^2 + (\Gamma/2)^2 + \Omega^2/2} \right] \quad (44)$$

and

$$U_T = - \int F_T dR = \frac{\hbar \Delta\omega_L}{2} \ln \left[ 1 + \frac{\Omega^2/2}{(\Delta\omega_L)^2 + (\Gamma/2)^2} \right]. \quad (45)$$

The second term is the spontaneous force, sometimes called the cooling force,  $F_C$ , because it is a dissipative force and can be used to cool atoms,

$$\vec{F}_C = -\mu E_0 \vec{k}_L \frac{\Omega}{2} \left[ \frac{\Gamma/2}{(\Delta\omega_L)^2 + (\Gamma/2)^2 + \Omega^2/2} \right]. \quad (46)$$

Note that in Eq. (44) the line-shape function in square brackets is dispersive and changes sign as the detuning  $\Delta\omega_L$  changes sign from negative (red detuning) to positive (blue detuning). In Eq. (46) the line-shape function is absorptive, peaks at zero detuning and exhibits a

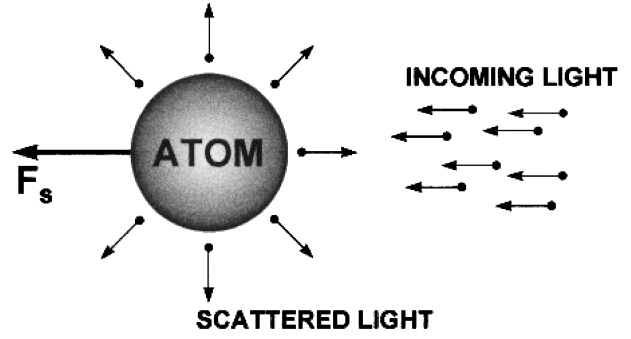


FIG. 9. Spontaneous emission following absorption occurs in random directions, but absorption from a light beam occurs along only one direction.

Lorentzian profile. These two equations can be recast to bring out more of their physical content. The dipole force can be expressed as

$$\vec{F}_T = -\frac{1}{2\Omega^2} \vec{\nabla} \Omega^2 \hbar \Delta\omega_L \left[ \frac{s}{1+s} \right], \quad (47)$$

where  $s$ , the *saturation parameter*, is defined to be

$$s = \frac{\Omega^2/2}{(\Delta\omega_L)^2 + (\Gamma/2)^2}. \quad (48)$$

In Eq. (48) the saturation parameter essentially defines a criterion to compare the time required for stimulated and spontaneous processes. If  $s \ll 1$  then spontaneous coupling of the atom to the vacuum modes of the field is fast compared to the stimulated Rabi oscillation, and the field is considered weak. If  $s \gg 1$  then the Rabi oscillation is fast compared to spontaneous emission and the field is said to be strong. With the help of the definition of the Rabi frequency, Eq. (40), and the light beam intensity,

$$I = \frac{1}{2} \epsilon_0 c E_0^2, \quad (49)$$

Eq. (47a) can be written in terms of the gradient of the light intensity, the saturation parameter, and the detuning,

$$\vec{F}_T = -\frac{1}{4I} (\vec{\nabla} I) \hbar \Delta\omega_L \left[ \frac{s}{1+s} \right]. \quad (50)$$

Note that negative  $\Delta\omega_L$  (red detuning) produces a force attracting the atom to the intensity maximum while positive  $\Delta\omega_L$  (blue-detuning) repels the atom away from the intensity maximum.

The spontaneous force or cooling force can also be written in terms of the saturation parameter and the spontaneous emission rate,

$$\vec{F}_C = \frac{\hbar \vec{k}_L \Gamma}{2} \left[ \frac{s}{1+s} \right], \quad (51)$$

which shows that this force is simply the rate of absorption and reemission of momentum quanta  $\hbar k_L$  carried by a photon in the light beam. Note that as  $s$  increases

beyond unity,  $\bar{F}_C$  approaches  $\hbar \tilde{k}_L \Gamma/2$ , the photon scattering rate for a saturated transition.

## 2. The magneto-optical trap (MOT)

### a. Basic notions

Pritchard *et al.* (1986) originally suggested that the spontaneous light force could be used to trap neutral atoms. The basic concept exploited the internal degrees of freedom of the atom as a way of circumventing the optical-Earnshaw theorem proved by Ashkin and Gordon (1983). This theorem states that if a force is proportional to the light intensity, its divergence must be null because the divergence of the Poynting vector, which expresses the directional flow of intensity, must be null through a volume without sources or sinks of radiation. This null divergence rules out the possibility of an inward restoring force everywhere on a closed surface. However, when the internal degrees of freedom of the atom are considered, they can change the proportionality between the force and the Poynting vector in a position-dependent way such that the optical-Earnshaw theorem does not apply. Spatial confinement is then possible with spontaneous light forces produced by counterpropagating optical beams. Using these ideas to circumvent the optical-Earnshaw theorem, Raab *et al.* (1987) demonstrated a trap configuration that is presently the most commonly employed. It uses a magnetic field gradient produced by a quadrupole field and three pairs of circularly polarized, counterpropagating optical beams, detuned to the red of the atomic transition and intercepting at right angles in the position where the magnetic field is zero. The magneto-optical trap exploits the position-dependent Zeeman shifts of the electronic levels when the atom moves in the radially increasing magnetic field. The use of circularly polarized light, red-detuned  $\sim \Gamma$  results in a spatially dependent transition probability whose net effect is to produce a restoring force that pushes the atom toward the origin.

To make clear how this trapping scheme works, consider a two-level atom with a  $J=0 \rightarrow J=1$  transition moving along the  $z$  direction (the same arguments will apply to the  $x$  and  $y$  directions). We apply a magnetic field  $B(z)$  increasing linearly with distance from the origin. The Zeeman shifts of the electronic levels are position-dependent, as shown in Fig. 10(a). We also apply counterpropagating optical fields along the  $\pm z$  directions carrying opposite circular polarizations and detuned to the red of the atomic transition. It is clear from Fig. 10 that an atom moving along  $+z$  will scatter  $\sigma^-$  photons at a faster rate than  $\sigma^+$  photons because the Zeeman effect will shift the  $\Delta M_J = -1$  transition closer to the light frequency.

$$F_{+z} = -\frac{\hbar k}{2} \Gamma$$

$$\times \frac{\Omega^2/2}{[\Delta + kv_z + (\mu_B/\hbar)(dB/dz)z]^2 + (\Gamma/2)^2 + \Omega^2/2}. \quad (52)$$

In a similar way, if the atom moves along  $-z$  it will scatter  $\sigma^+$  photons at a faster rate from the  $\Delta M_J = +1$  transition.

$$F_{-z} = +\frac{\hbar k}{2} \times \Gamma \frac{\Omega^2/2}{\left(\Delta - kv_z - \frac{\mu_B}{\hbar} \frac{dB}{dz} z\right)^2 + (\Gamma/2)^2 + \Omega^2/2}. \quad (53)$$

The atom will therefore experience a net restoring force pushing it back to the origin. If the light beams are red-detuned  $\sim \Gamma$ , then the Doppler shift of the atomic motion will introduce a velocity-dependent term to the restoring force such that, for small displacements and velocities, the total restoring force can be expressed as the sum of a term linear in velocity and a term linear in displacement,

$$F_{\text{MOT}} = F_{+z} + F_{-z} = -\alpha \dot{z} - Kz. \quad (54)$$

Equation (54) expresses the equation of motion of a damped harmonic oscillator with mass  $m$ ,

$$\ddot{z} + \frac{2\alpha}{m} \dot{z} + \frac{K}{m} z = 0. \quad (55)$$

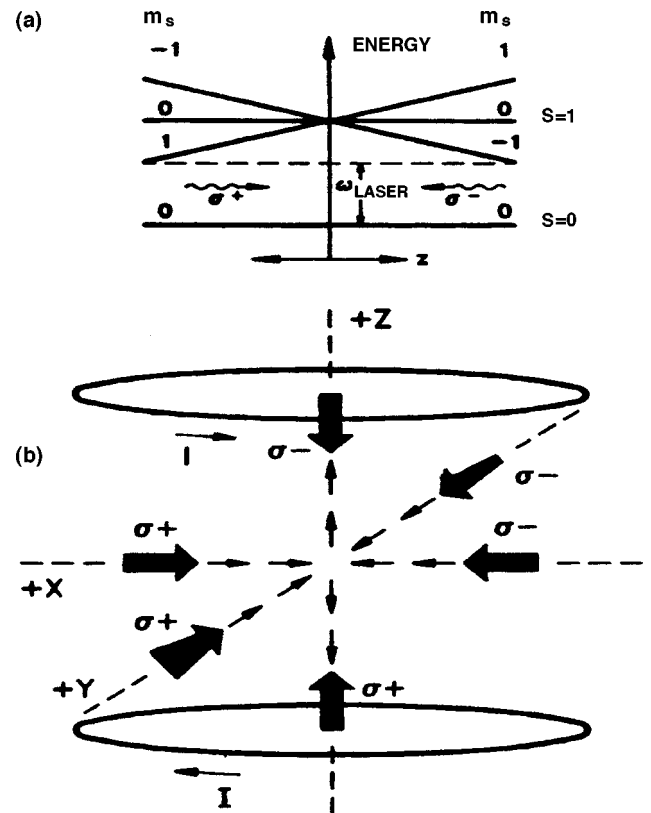


FIG. 10. MOT schema: (a) Energy level diagram showing shift of Zeeman levels as atom moves away from the  $z=0$  axis. Atom encounters a restoring force in either direction from counterpropagating light beams. (b) Typical optical arrangement for implementation of a magneto-optic trap.

The damping constant  $\alpha$  and the spring constant  $K$  can be written compactly in terms of the atomic and field parameters as

$$\alpha = \hbar k \Gamma \frac{16|\Delta'|(\Omega')^2(k/\Gamma)}{[1+2(\Omega')^2]^2\{1+4(\Delta')^2/[1+2(\Omega')^2]\}^2} \quad (56)$$

and

$$K = \hbar k \Gamma \frac{16|\Delta'|(\Omega')^2(d\omega_0/dz)}{[1+2(\Omega')^2]^2\{1+4(\Delta')^2/[1+2(\Omega')^2]\}^2}, \quad (57)$$

where  $\Omega'$ ,  $\Delta'$ , and  $d\omega_0/dz = [(\mu_B/\hbar)(dB/dz)]/\Gamma$  are  $\Gamma$  normalized analogues of the quantities defined earlier. Typical MOT operating conditions fix  $\Omega' = 1/2$ ,  $\Delta' = 1$ , so  $\alpha$  and  $K$  reduce (in mks units) to

$$\alpha(Nm^{-1}s) \approx (0.132)\hbar k^2 \quad (58)$$

and

$$K(Nm^{-1}) \approx (1.16 \times 10^{10})\hbar k \frac{dB}{dz}. \quad (59)$$

The extension of these results to three dimensions is straightforward if one takes into account that the quadrupole field gradient in the  $z$  direction is twice the gradient in the  $x, y$  directions, so that  $K_z = 2K_x = 2K_y$ . The velocity dependent damping term implies that kinetic energy  $E$  dissipates from the atom (or collection of atoms) as  $E/E_0 = e^{-(2\alpha/m)t}$  where  $m$  is the atomic mass and  $E_0$  the kinetic energy at the beginning of the cooling process. Therefore the dissipative force term cools the collection of atoms as well as combining with the displacement term to confine them. The damping time constant  $\tau = m/2\alpha$  is typically tens of microseconds. It is important to bear in mind that a MOT is anisotropic since the restoring force along the  $z$  axis of the quadrupole field is twice the restoring force in the  $xy$  plane. Furthermore a MOT provides a dissipative rather than a conservative trap, and it is therefore more accurate to characterize the maximum capture velocity rather than the trap “depth.”

Early experiments with magneto-optical trapped atoms were carried out by slowing an atomic beam to load the trap (Raab *et al.*, 1987; Walker *et al.*, 1990). Later, a continuous uncooled source was used for that purpose, suggesting that the trap could be loaded with the slow atoms of a room-temperature vapor (Cable *et al.*, 1990). The next advance in the development of magneto-optical trapping was the introduction of the vapor-cell magneto-optical trap (VCMOT). This variation captures cold atoms directly from the low-velocity edge of the Maxwell-Boltzmann distribution always present in a cell background vapor (Monroe *et al.*, 1990). Without the need to load the MOT from an atomic beam, experimental apparatuses became simpler; and now many groups around the world use the VCMOT for applications ranging from precision spectroscopy to optical control of reactive collisions.

#### b. Densities in a MOT

The VCMOT typically captures about a million atoms in a volume with less than one millimeter diameter, re-

sulting in densities  $\sim 10^{10} \text{ cm}^{-3}$ . Two processes limit the density attainable in a MOT are (1) collisional trap loss and (2) repulsive forces between atoms caused by reabsorption of scattered photons from the interior of the trap (Walker *et al.*, 1990; Sesko *et al.*, 1991). Collisional loss in turn arises from two sources: hot background atoms that knock cold atoms out of the MOT by elastic impact, and binary encounters between the cold atoms themselves. Trap loss due to cold collisions is the topic of Sec. V. The “photon-induced repulsion” or photon trapping arises when an atom near the MOT center spontaneously emits a photon which is reabsorbed by another atom before the photon can exit the MOT volume. This absorption results in an increase of  $2\hbar k$  in the relative momentum of the atomic pair and produces a repulsive force proportional to the product of the cross sections for absorption of the incident light beam and for the scattered fluorescence. When this outward repulsive force balances the confining force, a further increase in the number of trapped atoms leads to larger atomic clouds, but not to higher densities.

### 3. Dark SPOT MOT

In order to overcome the “photon-induced repulsion” effect, Ketterle *et al.* (1993) proposed a method that allows the atoms to be optically pumped to a “dark” hyperfine level of the atom ground state that does not interact with the trapping light. In a conventional MOT one usually employs an auxiliary “repumper” light beam, copropagating with the trapping beams but tuned to a neighboring transition between hyperfine levels of ground and excited states. The repumper recovers population that leaks out of the cycling transition between the two levels used to produce the MOT. As an example, Fig. 11 shows the trapping and repumping transitions usually employed in a conventional Na MOT. The scheme proposed by Ketterle *et al.* (1993), known as a dark spontaneous-force optical trap (dark SPOT), passes the repumper through a glass plate with a small black dot shadowing the beam such that the atoms at the trap center are not coupled back to the cycling transition but spend most of their time ( $\sim 99\%$ ) in the “dark” hyperfine level. Cooling and confinement continue to function on the periphery of the MOT but the center core experiences no outward light pressure. The dark SPOT increases density by almost two-orders of magnitude.

### 4. The far-off resonance trap (FORT)

Although a MOT functions as a versatile and robust “reaction cell” for studying cold collisions, light frequencies must tune close to atomic transitions, and an appreciable steady-state fraction of the atoms remain excited. Excited-state trap-loss collisions and photon-induced repulsion limit achievable densities.

A far-off resonance trap (FORT), in contrast, uses the dipole force rather than the spontaneous force to confine atoms and can therefore operate far from resonance with negligible population of excited states. The first atom confinement (Chu *et al.*, 1986) was reported using

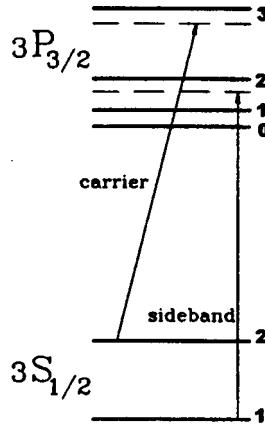


FIG. 11. Usual cooling (carrier) and repumping (sideband) transitions when optically cooling Na atoms. The repumper frequency is normally derived from the cooling transition frequency with electrooptic modulation. Dashed lines show that lasers are tuned about one natural linewidth to the red of the transition frequencies.

a dipole-force trap. A hybrid arrangement in which the dipole force confined atoms radially while the spontaneous force cooled them axially was used by a NIST-Maryland collaboration (Gould *et al.*, 1988) to study cold collisions, and a FORT was demonstrated by Miller *et al.* (1993a) for  $^{85}\text{Rb}$  atoms. The FORT consists of a single, linearly polarized, tightly focused Gaussian-mode beam tuned far to the red of resonance. The obvious advantage of large detunings is the suppression of photon absorption. Note from Eq. (46) that the spontaneous force, involving absorption and reemission, falls off as the square of the detuning while Eq. (45) shows that the potential derived from dipole force falls off only as the detuning itself. At large detunings and high field gradients (tight focus) Eq. (45) becomes

$$U \approx \frac{\hbar \Omega^2}{4\Delta \omega_L}, \quad (60)$$

which shows that the potential becomes directly proportional to light intensity and inversely proportional to detuning. Therefore at far detuning but high intensity the depth of the FORT can be maintained but most of the atoms will not absorb photons. The important advantages of FORTS compared to MOTS are (1) high density ( $\sim 10^{12} \text{ cm}^{-3}$ ) and (2) a well-defined polarization axis along which atoms can be aligned or oriented (spin polarized). The main disadvantage is the small number of trapped atoms due to small FORT volume. The best number achieved is about  $10^4$  atoms (Cline *et al.*, 1994a, 1994b).

## 5. Magnetic traps

Pure magnetic traps have also been used to study cold collisions, and they are critical for the study of dilute gas-phase Bose-Einstein condensates in which collisions figure importantly. We anticipate therefore that mag-

netic traps will play an increasingly important role in future collision studies in and near Bose-Einstein condensation conditions.

The most important distinguishing feature of all magnetic traps is that they do not require light to provide atom containment. Light-free traps reduce the rate of atom heating by photon absorption to zero, an apparently necessary condition for the attainment of Bose-Einstein condensation. Magnetic traps rely on the interaction of atomic spin with variously shaped magnetic fields and gradients to contain atoms. Assuming the spin adiabatically follows the magnetic field, the two governing equations for the potential  $U$  and force  $\vec{F}_B$  are

$$U = -\vec{\mu}_S \cdot \vec{B} = -\frac{g_s \mu_B}{\hbar} \vec{S} \cdot \vec{B} = -\frac{g_s \mu_B}{\hbar} M_S B \quad (61)$$

and

$$\vec{F}_B = -\frac{g_s \mu_B}{\hbar} M_S \vec{\nabla} B. \quad (62)$$

where  $\mu_S$  and  $\mu_B$  are the electron spin dipole moment and Bohr magneton respectively,  $M_S$  the  $z$ -component of  $\vec{S}$ , and  $g_s$  the Landé  $g$ -factor for the electron spin. If the atom has nonzero nuclear spin  $\vec{I}$  then  $\vec{F} = \vec{S} + \vec{I}$  substitutes for  $\vec{S}$  in Eq. (61), the  $g$  factor generalizes to

$$g_F \approx g_s \frac{F(F+1) + S(S+1) - I(I+1)}{2F(F+1)}, \quad (63)$$

and

$$\vec{F}_B = -\frac{g_F \mu_B}{\hbar} M_F \vec{\nabla} B. \quad (64)$$

Depending on the sign of  $\vec{F}_B$  with respect to  $\vec{B}$ , atoms in states whose energy increases or decreases with magnetic field are called “weak-field seekers” or “strong-field seekers,” respectively. For example, see Fig. 3. One could, in principle, trap atoms in any of these states, needing only to produce a minimum or a maximum in the magnetic field. Unfortunately only weak-field seekers can be trapped in a static magnetic field because such a field in free space can only have a minimum. Dynamic traps have been proposed to trap both weak- and strong-field seekers (Lovell *et al.*, 1985). Even when weak-field seeking states are not in the lowest hyperfine levels they can still be used for trapping because the transition rate for spontaneous magnetic dipole emission is  $\sim 10^{-10} \text{ sec}^{-1}$ . However, spin-changing collisions can limit the maximum attainable density.

The first static magnetic field trap for neutral atoms was demonstrated by Migdall *et al.* (1985). An anti-Helmholtz configuration (see Fig. 10), similar to a MOT, was used to produce an axially symmetric quadrupole magnetic field. Since this field design always has a central point of vanishing magnetic field, nonadiabatic Majorana transitions can take place as the atom passes through the zero point, transferring the population from a weak-field to a strong-field seeker and effectively ejecting the atom from the trap. This problem can be

overcome by using a magnetic bottle with no point of zero field (Gott *et al.*, 1962; Pritchard, 1983; Bagnato *et al.*, 1987; Hess *et al.*, 1987). The magnetic bottle, also called the Ioffe-Pritchard trap, was recently used to achieve a Bose-Einstein condensation in a sample of Na atoms pre-cooled in a MOT (Mewes *et al.*, 1996). Other approaches to eliminating the zero field point are the time-averaged orbiting potential trap (Anderson *et al.*, 1995) and an optical “plug” (Davis *et al.*, 1995) that consists of a blue-detuned intense optical beam aligned along the magnetic trap symmetry axis and producing a repulsive potential to prevent atoms from entering the null field region. Trap technology continues to develop and the recent achievement of Bose-Einstein condensation will stimulate more robust traps containing greater numbers of atoms. At present  $\sim 10^7$  atoms can be trapped in a Bose-Einstein condensate loaded from a MOT containing  $\sim 10^9$  atoms.

## B. Atom beams

Although MOTs and FORTs have proved productive and robust experimental tools for the investigation of ultracold collisions, they suffer from two shortcomings of any “reaction cell” technique: (1) collision kinetic energy or temperature cannot be varied over a wide range and (2) the isotropic distribution of molecular collision axes in the laboratory frame masks effects of light-field polarization on inelastic and reactive processes. Furthermore, probe beams in a MOT cannot explore close to the cooling transition without severely perturbing or destroying the MOT.

An alternative approach to atom traps is the study of collisions between and within atomic beams. In fact the application of thermal atomic and molecular beams to investigate inelastic and reactive collisions dates from the early sixties (Herschbach, 1966). It was not until the early eighties, however, that polarization and velocity-group selection led to detailed measurements of collision rate constants as a function of velocity, alignment, and orientation of the colliding partners (Wang and Weiner, 1990). Beginning the decade of the nineties, Thorsheim, *et al.* (1990) reported the first measurements of subthermal collisions in an atomic beam. In this experiment a single-mode laser beam excited a narrow velocity group from a thermal sodium atomic beam, and the rate of associative ionization *within the selected velocity group* was measured as a function of light polarization perpendicular and parallel to the beam axis. The effective collision temperature of 65 mK was just on the threshold of the subthermal regime, defined as  $T_S$ , the temperature at which the atomic radiative lifetime becomes comparable to the collision duration. For sodium excited to the  $3p^2P_{3/2}$ ,  $T_S$  is 64 mK (Julienne and Mies, 1989). Building on this experiment, Tsao *et al.* (1995) used a much narrower optical transition ( $5p^2P_{3/2}$ ) to select a velocity group from a collimated atomic beam and reported a rate constant for photoassociative ionization at 5.3 mK, well within the subthermal regime. Figure 12 shows a diagram of the experimental setup. Atoms

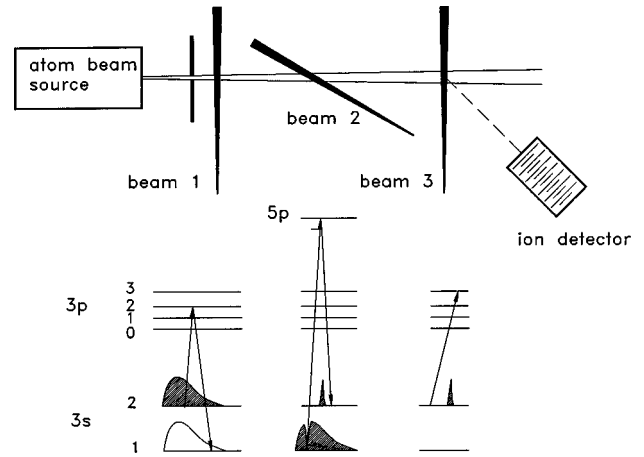


FIG. 12. Schematic of atomic beam experiment in which a narrow velocity group is selected (laser beam 2) and intravelocity group collisions are probed (laser beam 3). From Thorsheim *et al.* (1990).

emerging from a mechanically collimated thermal source interact with light in three stages: first, the atom beam crosses an optical “pump” beam tuned to transfer population from  $F=2$  to  $F=1$  of the ground state. Second, a velocity-group-selecting optical beam, tuned to the  $3s^2S_{1/2}$  ( $F=1$ )  $\rightarrow$   $5p^2P_{3/2}$  transition crosses the atomic beam at  $\sim 45^\circ$  and pumps a very narrow group to the previously emptied  $F=2$  level of the ground state. Finally, a third light beam, detuned  $\sim \Gamma$  to the red of the  $D_2$  transition, excites collision pairs from within the  $F=2$  velocity group to form the detected photoassociative ionization product ions. The production rate of the  $\text{Na}_2^+$  product ions is then measured as a function of intensity and polarization. Although the optical-velocity-selection technique achieves subthermal collision temperatures, it suffers from the disadvantage that only a small fraction of the atoms in the atomic beam participate, and signal levels are low.

Subjecting the axial or transverse velocity components of the beam to dissipative cooling dramatically compresses the phase space of the atom flux, resulting in dense, well-collimated atomic beams suitable for the study of atom optics, atom holography, or ultracold collision dynamics. Prodan *et al.* (1982) first demonstrated the importance of this phase-space compression. In fact atomic beams can now achieve “brightness” (atom beam flux density per unit solid angle) many times greater than the phase-space conservation limit imposed by the Liouville theorem (Pierce, 1954; Sheehy *et al.*, 1989; Kuyatt, 1967). Several groups have used MOT physics to make “atom funnels” or “2D MOTS” to cool and compress the transverse components of atom beams (Nellessen *et al.*, 1990; Riis *et al.*, 1990; Faultsich *et al.*, 1992; Hoogerland, 1993; Yu *et al.*, 1994; Swanson *et al.*, 1996; Tsao *et al.*, 1996) or have used ordinary magneto-optical traps as sources of slow, well-collimated beams (Myatt *et al.*, 1996; Lu *et al.*, 1996). Tsao (1996) has used axial phase-space compression to increase atom density in a velocity group prior to optical selection. Figure 13 shows how a cooling light beam counterpropagating to a

thermal atomic beam can compress the Maxwell-Boltzmann distribution into a relatively narrow range of velocities. Tsao *et al.* (1998) used this technique to investigate the polarization properties of optical suppression, an optically controlled collisional process described in Sec. VII. To date atom beams have not contributed as importantly to cold and ultracold collision dynamics as MOTs and FORTs, but their full potential has yet to be exploited.

## V. INELASTIC EXOERGIC COLLISIONS IN MOTS

An exoergic collision converts internal atomic energy to kinetic energy of the colliding species. When there is only one species in the trap (the usual case) this kinetic energy is equally divided between the two partners. If the net gain in kinetic energy exceeds the trapping potential or the ability of the trap to recapture, the atoms escape, and the exoergic collision leads to trap loss.

Of the several trapping possibilities described in the last section, by far the most popular choice for collision studies has been the magneto-optical trap (MOT). A MOT uses spatially dependent resonant scattering to cool and confine atoms. If these atoms also absorb the trapping light at the initial stage of a binary collision and approach each other on an excited molecular potential, then during the time of approach the colliding partners can undergo a fine-structure-changing collision or relax to the ground state by spontaneously emitting a photon. In either case electronic energy of the quasimolecule converts to nuclear kinetic energy. If both atoms are in their electronic ground states from the beginning to the end of the collision, only elastic and hyperfine-changing collisions can take place. Elastic collisions (identical scattering entrance and exit states) are not exoergic but figure importantly in the production of Bose-Einstein condensates. At the very lowest energies only  $s$ -waves contribute to the elastic scattering, and in this regime the collisional interaction is characterized by the scattering length. The sign and magnitude of the scattering length determine the properties of a weakly-interacting Bose gas and controls the rate of evaporative cooling, needed to achieve BEC. The hyperfine-changing collisions arise from ground state splitting of the alkali atoms into hyperfine levels due to various orientations of the nonzero nuclear spin. A transition from a higher to a lower molecular hyperfine level during the collisional encounter releases kinetic energy. In the absence of external light fields hyperfine-changing collisions often dominate trap heating and loss.

If the collision starts on the excited level, the long-range dipole-dipole interaction produces an interatomic potential varying as  $\pm C_3/R^3$ . The sign of the potential, attractive or repulsive, depends on the relative phase of the interacting dipoles. For the trap-loss processes that concern us in this chapter we concentrate on the attractive long-range potential,  $-C_3/R^3$ . Due to the extremely low energy of the collision, this long-range potential acts on the atomic motion even when the pair are as far apart as  $\lambda/2\pi$  (the inverse of the light field wave

vector  $k$ ). Since the collision time is comparable to or greater than the excited state life time, spontaneous emission can take place during the atomic encounter. If spontaneous emission occurs, the quasimolecule emits a photon red-shifted from atomic resonance and relaxes to the ground electronic state with some continuum distribution of the nuclear kinetic energy. This conversion of internal electronic energy to external nuclear kinetic energy can result in a considerable increase in the nuclear motion. If the velocity is not too high, the dissipative environment of the MOT is enough to cool this radiative heating, allowing the atom to remain trapped. However, if the transferred kinetic energy is greater than the recapture ability of the MOT, the atoms escape the trap. This process constitutes an important trap loss mechanism termed radiative escape, and was first pointed out by Vigué (1986). For alkalis there is also another exoergic process involving excited-ground collisions. Due to the existence of a fine structure in the excited state ( $P_{3/2}$  and  $P_{1/2}$ ), the atomic encounter can result in fine-structure-changing collision, releasing  $\Delta_{FS}$  of kinetic energy, shared equally between both atoms. For example in sodium  $\frac{1}{2}\Delta E_{FS}/k_B \approx 12$  K, which can easily cause the escape of both atoms from the MOT, typically 1 K deep.

These three effects, hyperfine-changing collisions, radiative escape, and fine-structure-changing collisions, are the main exoergic collisional processes that take place in a MOT. They are the dominant loss mechanisms which usually limit the maximum attainable density and number in MOTs. They are not, however, the only type of collision in the trap, as we shall see later.

### A. Excited-state trap-loss collisions

#### 1. Early quasistatic models

##### a. Gallagher-Pritchard model

Soon after the first observations of ultracold collisions in traps, Gallagher and Pritchard (1989) proposed a simple semiclassical model to describe the fine-structure-changing and radiative escape trap-loss processes. Figure 14 shows the two mechanisms involved. When atoms are relatively far apart they absorb a photon, promoting the system from the ground state to a long-range attractive molecular state. We denote the relevant molecular levels by their asymptotic energies. Thus,  $S+S$  represents two ground-state atoms, and  $S+P_{1/2}$  or  $S+P_{3/2}$  represents one ground and one excited state atom which can be in either one of the fine-structure levels.

For radiative escape, the process is described by

$$A + A + \hbar\omega \rightarrow A_2^* \rightarrow A + A + \hbar\omega' \quad (65)$$

with energy  $\hbar(\omega - \omega')/2$  transferred to each atom. The fine-structure-changing collision is represented by

$$A + A + \hbar\omega \rightarrow A^*(P_{3/2}) + A \rightarrow A^*(P_{1/2}) + A + \Delta E_{FS} \quad (66)$$

with  $\Delta E_{FS}/2$  transferred to each atom.

The Gallagher-Pritchard model begins by considering a pair of atoms at the internuclear separation  $R_0$ . If this

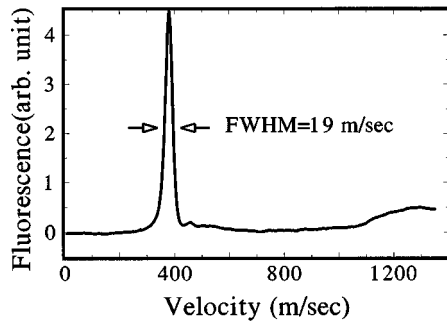


FIG. 13. The trace with the sharp peak is the velocity profile of axially cooled atomic beam. The broad low-amplitude trace shows the residual thermal velocity distribution from which the sharp peak was compressed. From Tsao *et al.* (1998).

pair is illuminated by a laser of frequency  $\omega_L$  and intensity  $I$ , the rate of molecular excitation is given by

$$\begin{aligned} \mathcal{R}(R_0, \omega_L, I) &= \left[ \frac{(\Gamma_M/2)^2}{[\Delta_M]^2 + (\Gamma_M/2)^2} \right] \frac{I \lambda^2}{\hbar \omega_L 2\pi} \\ &= \epsilon(\omega_L, R_0) \frac{I \lambda^2}{\hbar \omega_L 2\pi}, \end{aligned} \quad (67)$$

where  $\Delta_M = [\omega_L - \omega(R_0)]$ , and  $\omega(R_0) = \omega_A - C_3/\hbar R_0^3$  is the resonant frequency at  $R_0$ , and  $\omega_A$  is the atomic resonant frequency. The constant  $C_3$  characterizes the excited molecular potential,  $\lambda^2/2\pi$  is the photoabsorption cross section to all attractive molecular states (one half the atomic value), and  $I$  and  $\omega_L$  are the laser intensity and frequency. Finally  $\Gamma_M$  is the molecular spontaneous decay rate, here taken as twice the atomic rate,  $\Gamma_A$ .

After excitation at  $R_0$ , the atom pair begins to accelerate together on the  $-C_3/R^3$  potential, reaching the short-range zone where the fine-structure-changing collision and radiative escape processes leading to trap loss occur. The time to reach the short-range zone is essentially the same as to reach  $R=0$ . This time is easily calculated by integrating the equation of motion,

$$\begin{aligned} t(R_0) &= \left[ \frac{M}{4} \right]^{1/2} \int_0^{R_0} dR \left[ \frac{C_3}{R^3} - \frac{C_3}{R_0^3} \right]^{-1/2} \\ &= 0.747 \left[ \frac{MR_0^5}{4C_3} \right]^{1/2}, \end{aligned} \quad (68)$$

where  $M$  is the atomic mass. Defining  $\Delta = \omega_A - \omega_L$  as the detuning,  $R_\tau$  the interaction separation reached by the atoms (in one life time  $\tau = \Gamma_M^{-1}$ ), and  $\Delta_\tau$  the detuning at  $R_\tau$ . With these definitions, the time for the atoms to reach the short-range zone can be written as

$$t(R_0) = \left( \frac{\Delta_\tau}{\Delta} \right)^{5/6} \Gamma_M^{-1}, \quad (69)$$

and the probability of survival against spontaneous emission is given by  $\gamma = \exp[-\Gamma_M t(R_0)]$  or  $\gamma = \exp[(-\Delta_\tau/\Delta)^{5/6}]$ .

If the  $A^*-A$  pair reaches the short-range region (where fine-structure-changing collisions take place) before radiating, it rapidly traverses this zone twice, yield-

ing a probability for fine-structure-changing collisions (FCC) equal to  $\eta_J = 2P(1-P)$ , where  $P$  is the Landau-Zener single-transit curve-crossing probability. Repeated oscillations of the atoms through the crossing results in a probability  $P_{\text{FCC}}$  which is the sum of the probabilities at each traversal,

$$P_{\text{FCC}} = \eta_J \gamma + \eta_J (1 - \eta_J) \gamma^3 + \dots = \frac{\eta_J \gamma}{[1 - \gamma^2 + \eta_J \gamma^2]}. \quad (70)$$

If  $n$  is the total atomic density, the number of pairs with separation  $R_0 \rightarrow R_0 + dR_0$  is  $n^2 4\pi R_0^2 dR_0/2$ , and the total rate of fine-structure-changing collisions per unit of volume is the integration over all internuclear separations,

$$R_{\text{FCC}} = \frac{n^2}{2} \int_0^\infty dR_0 4\pi R_0^2 \mathcal{R}(R_0, \omega_L, I) P_{\text{FCC}}(R_0). \quad (71)$$

The rate constant between two colliding ground state atoms is then

$$k_{\text{FCC}} = \frac{1}{2} \int_0^\infty dR_0 4\pi R_0^2 \mathcal{R}(R_0, \omega_L, I) P_{\text{FCC}}(R_0). \quad (72)$$

Alternatively the rate constant can be expressed in terms of a binary collision between one excited and one unexcited atom,

$$R_{\text{FCC}} = n n^* k'_{\text{FCC}}, \quad (73)$$

where  $n^*$  is the excited atom density. At steady state, the rate of atom photo-excitation expressed as the product of photon flux, atom density, and absorption cross section (including line shape function) equals the rate of fluorescence,

$$(I/\hbar \omega_L) n (\lambda^2/\pi) \left[ \frac{\Gamma_A^2/4}{(\Delta_M)^2 + \Gamma_A^2/4} \right] = n^* \Gamma_A, \quad (74)$$

and combining Eqs. (67), (71), (73), and (74),

$$\begin{aligned} k'_{\text{FCC}} &= \frac{1}{4} \left[ \frac{(\Delta_M)^2 + \Gamma_A^2/4}{\Gamma_A/4} \right] \\ &\times \int_0^\infty dR_0 4\pi R_0^2 \epsilon(\omega_L, R_0) P_{\text{FCC}}(R_0). \end{aligned} \quad (75)$$

The fine-structure change is not the only loss mechanism in the trap. Radiative escape is also important. The rate of radiative escape (RE), per unit of volume, can be obtained from Eqs. (72) or (75), when  $P_{\text{FCC}}(R_0)$  is replaced by  $P_{\text{RE}}(R_0)$ , the probability of spontaneous emission during transit in an inner region,  $R < R_E$ . Here  $R_E$  is defined as the internuclear separation at which the kinetic energy acquired by the colliding pair is enough to escape from the magneto-optical trap. The probability  $P_{\text{RE}}(R_0)$  can be obtained as a series sum similar to Eq. (70). Defining the time spent at  $R < R_E$  as  $2t_E(R_0)$  obtained from an integration similar to Eq. (69), one writes  $P_{\text{RE}}(R_0)$  as

$$P_{\text{RE}}(R_0) = \frac{2t_E(R_0) \Gamma_M \gamma}{[1 - \gamma^2 + \eta_J \gamma^2]}. \quad (76)$$

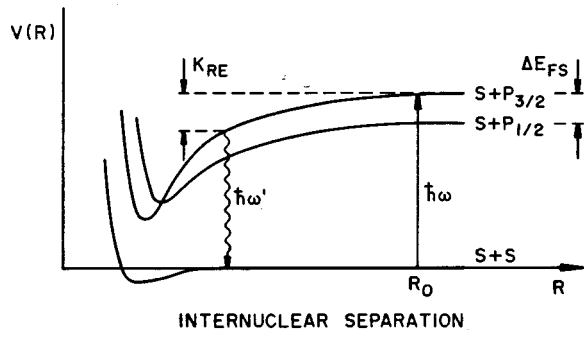


FIG. 14. Schematic diagram showing mechanisms of radiative escape and fine-structure-changing collisions. An  $\hbar\omega$  photon, red detuned  $\sim\Gamma_A$ , transfers the population to long-range attractive curve. Atoms accelerate radially along a molecular potential until either the molecule emits a photon  $\hbar\omega'$  (RE) or undergoes a crossing to a potential curve asymptotically dissociating to  ${}^2P_{1/2}+{}^2S_{1/2}$  (FCC).

The Gallagher-Pritchard model predicts that fine-structure-changing collisions dominate over radiative escape. Gallagher and Pritchard (1989) estimate  $\eta_J \sim 0.2$  for sodium collisions, resulting in a prediction of  $P_{\text{FCC}}/P_{\text{RE}} \sim 20$  for Na-magneto-optical trap loss.

#### b. Julienne-Vigué model

Julienne and Vigué (1991) proposed an elaboration, hereafter termed the JV model, which introduced the role of angular momentum and a thermal averaging procedure, employed realistic molecular states, and took into account the effects of retardation on molecular spontaneous emission decay rates. Like Gallagher and Pritchard, they neglected molecular hyperfine structure. The rate of fine-structure-changing collisions or radiative escape transition per unit of volume is written as

$$\frac{\text{rate}}{\text{volume}} = Kn^2 = \frac{1}{2d_g^2} \frac{\pi v}{k^2} \sum_{\epsilon, l} (2l+1) P_{\text{TL}}(\epsilon, l) \times P_{\text{ES}}(R, \epsilon, l, \Delta, I) n^2. \quad (77)$$

where  $n$  is the ground state density,  $v$  the asymptotic velocity for the atoms when they are far apart,  $k$  the wave vector associated with the momentum of the reduced particle,  $I$  the light intensity,  $d_g$  the ground state degeneracy, and the factor of 1/2 accounts for homonuclear symmetry. The summation is performed over all contributing attractive excited states indexed by  $\epsilon$ . The term  $P_{\text{TL}}(\epsilon, l)$  represents the probability that trap loss (either fine-structure-changing collisions or radiative escape) occurs at small internuclear separation  $R_{\text{TL}}$  after the atoms have drawn together. This  $P_{\text{TL}}(\epsilon, l)$  factor was evaluated using different methods and was shown to be nearly independent of the asymptotic energy of the atoms over a wide range of temperature. The JV expression Eq. (77) corresponds to the Gallagher-Pritchard expression Eq. (71). Note however that excitation, survival against spontaneous decay, and the collisional interaction are factored differently. In Gallagher and Pritchard,  $\mathcal{R}(R_0, \omega_L, I)$ , represents excitation and  $P_{\text{FCC}}$  or  $P_{\text{RE}}$

represents survival and collisional interaction together; in JV,  $P_{\text{ES}}$  represents excitation and survival and  $P_{\text{TL}}$  the probability of the collisional process itself. The excitation and survival probability,  $P_{\text{ES}}(R, \epsilon, \Delta, I)$ , represents the probability that an excited state  $\epsilon$  produced at a rate  $G(R')$  at some  $R' > R$  by light detuned  $\Delta$  and intensity  $I$  will survive without spontaneous radiative decay during the motion from  $R'$  to  $R$ . In Julienne-Vigué theory,  $P_{\text{ES}}$  can be written as

$$P_{\text{ES}}(R, \epsilon, l, \Delta, I) = \int_R^\infty G(R', \epsilon, \Delta, I) S_{Ei}^l(R, R', \epsilon) \frac{dR'}{v_{Ei}^l(R')} \quad (78)$$

where  $S_{Ei}^l(R, R', \epsilon)$  is the survival factor for the atom pair moving from  $R'$  to  $R$  on the excited state  $\epsilon$ , with angular momentum  $l$  and the initial kinetic energy  $Ei$ , starting from the ground state. The excitation rate is  $G(R', \epsilon, \Delta, I)$  and the excitation probability is given by  $G(R', \epsilon, \Delta, I) dR'/v_{Ei}^l(R')$ .

Trap-loss collision rates in alkali magneto-optical traps have been measured extensively, and the specific molecular mechanisms for fine-structure-changing collisions and radiative escape trap loss for this class of atoms have been discussed theoretically by Julienne and Vigué (1991). The molecular structure of the alkali metals are qualitatively similar, and the long range potentials are well known. The long-range potentials coming from the  $P_{3/2}+S_{1/2}$  separated Na atoms are shown in Fig. 15 and give rise to five attractive states ( $1_u, 0_g^-, 2_u, 1_g,$  and  $0_u^+$ ). Those states have different decay rates which makes the survival effect very sensitive to the initial excitation. As to the collisional interaction itself, Julienne and Vigué (1991) verified, using quantum scattering calculations, that the predictions of Dashkevskaya *et al.* (1969) about fine-structure-changing collisions were qualitatively correct. The calculations by Dashkevskaya *et al.* (1969) show that fine-structure-changing collisions arise from two principal mechanisms: spin-orbit (radial) coupling at short range and Coriolis (angular) coupling at long range and that gerade states contribute very little to the fine-structure-changing collisions process. Therefore Julienne and Vigué (1991) conclude that, of all the  ${}^2P_{3/2}+{}^2S_{1/2}$  entrance channel states, only  $0_u^+$  and  $2_u$  contribute significantly to the FCC cross section. Dashkevskaya (1979) points out three basic pathways for FCC: (1) spin-orbit mixing of the  $0_u^+$  components of the  $A^1\Sigma_u$  and  $b^3\Pi_u$  where they cross at short range, (2) Coriolis mixing of the  $\Omega=0,1,2$  components of  $b^3\Pi_u$ , and Coriolis coupling of  $0_u^+$  and  $1_u$  states at long range. The dominant mechanism for the light alkalis with relatively small spin-orbit terms (Li, Na, K) are the Coriolis couplings. For the heavy alkalis (Rb, Cs) the short-range spin-orbit mechanism prevails. Julienne and Vigué (1991) calculated fine-structure-changing collisions and radiative escape for all alkalis and obtained rate coefficients for trap loss combining fine-structure-changing collisions and radiative escape as shown in Fig. 16. Because the spin-orbit interaction in Li is small, fine-structure-changing collisions do not lead to appreciable

trap loss. It becomes important only if the trap depth is less than 250 mK. The radiative escape contribution for Li is also small due to the fast decay rate of the excited states, preventing close approach of the two partners along the accelerating  $-C_3/R^3$  excited-state potentials. As a result, Li is predicted to have the lowest trap loss rate of all the alkalis.

## 2. Theoretical approaches to excited-state trap loss

### a. Quasistatic theories

Both the Gallagher-Pritchard and Julienne-Vigué theories develop rate expressions that derive from the “quasistatic” picture of light-matter interaction. The idea is that the atoms approach each other sufficiently slowly such that at each internuclear separation  $R_c$  there is enough time to establish a steady state between rates of quasimolecule stimulated absorption and spontaneous emission. This steady state sets up the familiar Lorentzian line-shape function,  $(\Gamma_M/2)^2/(\Delta_M^2 + (\Gamma_M/2)^2)$ , for the probability of excited state population. This line-shape function permits off-resonant excitation around the Condon point  $R_c$  where  $\Delta_M=0$ . For a flat ground state  $V_g=0$  and excited state  $V_e=-C_3/R^3$  the detuning is  $\Delta=C_3/\hbar R_c^3$  and  $|d\Delta/dR_c|=3C_3/\hbar R_c^4$ . Thus at relatively large detuning the line-shape function is still rather narrow and the excitation is fairly well confined around  $R_c$ . At small detunings however, off-resonant excitation contributes significantly to the quasistatic rate constant, and further theoretical studies using quantum scattering with complex potentials (Boesten *et al.*, 1993; Boesten and Verhaar, 1994; Julienne *et al.*, 1995), optical Bloch equations (Band and Julienne, 1992; Band *et al.*, 1994) or quantum Monte Carlo methods (Lai *et al.*, 1993; Holland *et al.*, 1994) have shown that this off-resonant excitation picture is of dubious validity. These issues have been reviewed in detail by Suominen (1996). It is also worth noting that both the Gallagher-Pritchard and Julienne-Vigué theories factor the rate constant into two terms: the first term describing excitation and survival at long range, and the second term expressing the probability of the short-range trap-loss process itself. This decoupling of optical excitation and survival from the short-range collisional interaction provides a useful factorization even for theoretical approaches which do not invoke the quasistatic picture.

### b. Method of complex potentials

At weak field, where optical cycling of population between ground and excited states can be safely ignored, a tractable quantum mechanical treatment of collisional loss processes can be conveniently introduced by insertion of an imaginary term in the time-independent Hamiltonian. Boesten *et al.* (1993) and Julienne *et al.* (1995) have each developed complex potential models of ultracold collisions in order to test the semiclassical theories. Both found serious problems with existing semiclassical theories at small detuning. Again the approach is to factor the probability for trap loss into two

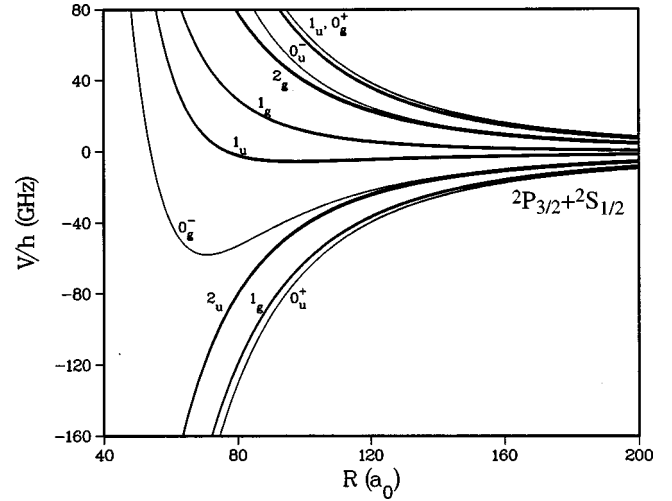


FIG. 15. Long-range potential curves of the first excited states of the Na dimer labeled by Hund’s case (c) notation. The number gives the projection of electron spin plus orbital angular momentum on the molecular axis. The  $g/u$  and  $+/-$  labels correspond to conventional point-group symmetry notation.

parts: (1) long-range excitation and survival,  $J(E,l,\Delta,I;\Gamma)$ , and (2) the short-range loss process itself,  $P_X(E,l)$ , where the subscript  $X$  denotes fine-structure or radiative escape and  $E,l$  are the total collision energy and angular momentum, respectively. The terms  $\Delta,I$  represent the detuning and intensity of the optical excitation with  $\Gamma$  the spontaneous decay rate. The overall probability for the process is therefore,

$$P(E,l,\Delta,I;\Gamma) = P_X(E,l)J(E,l,\Delta,I;\Gamma). \quad (79)$$

In principle the inclusion of a dissipative term like spontaneous decay means that the problem should be set up using the optical Bloch equations or quantum Monte Carlo methods which take dissipation into account naturally over a wide range of field strengths. However in the weak-field limit exact quantum scattering models with a complex potential suffice for testing the semiclassical Gallagher-Pritchard and Julienne-Vigué theories and developing alternative semiclassical models. Julienne *et al.* (1994), for example, studied a three-state model comprising the ground state entrance channel, an optically excited molecular state, and a fictitious probe state which simulates the collisional loss channel of the fine-structure or radiative escape processes. The trap-loss probability is then expressed in terms of the  $S$  matrix connecting the ground state ( $g$ ) to the probe state ( $p$ ),

$$P(E,l,\Delta,I;\Gamma) = |S_{gp}(E,l,\Delta,I;\Gamma)|^2 = P_{XQ}(E,l) \cdot J_Q(E,l,\Delta,I;\Gamma). \quad (80)$$

The subscript  $Q$  denotes quantum close coupling, and Julienne *et al.* (1994) compare  $J_Q$  to four semiclassical approximations for  $J$ : (1)  $J_{JV}$  from the semiclassical Julienne-Vigué model, (2)  $J_{BJ}$  from an optical-Bloch-equation calculation of Band and Julienne (1992), (3)  $J_{BV}$  from the Landau-Zener model of Boesten and Verhaar (1994), and (4)  $J_{LZ}$  from the Landau-Zener model

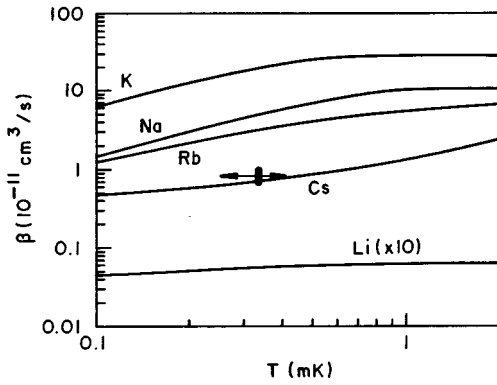


FIG. 16. Total trap-loss rate constants  $\beta$  as a function of temperature for the different alkali species. These rates are calculated by Julienne and Vigué (1991), and the solid points are measurements from Sesko *et al.* (1989). The arrow indicates the experimental uncertainty in temperature.

of Julienne *et al.* (1995). Both  $J_{BV}$  and  $J_{LZ}$  are variants of the celebrated Landau-Zener formula,

$$J_{LZ} \approx S_a e^{-A}, \quad (81)$$

where  $S_a$  is the survival factor and  $A$  is the familiar Landau-Zener argument,

$$A = \frac{2\pi |V_{ag}(I)|^2}{\hbar \left| \frac{dV_a}{dR} - \frac{dV_g}{dR} \right|_{R_c} v_a}. \quad (82)$$

In Eq. (82)  $V_{ag}$  is the optical coupling, proportional to the laser intensity, and the denominator is the product of the difference in slopes evaluated at the Condon point  $R_c$  and the local velocity  $v_a$ . The inner-region collisional interaction  $P_{XQ}(E, I)$  is insensitive to the intensity and detuning of the outer-region optical excitation  $\Delta, I$ , the decay rate  $\Gamma$ , or the collision energy  $E$ . Therefore the overall trap-loss probability, Eq. (80), is controlled by the behavior of  $J_Q(E, I, \Delta, I; \Gamma)$ . Figure 17 shows Cs trap-loss probabilities for the various  $J$ 's as a function of collision temperature and reveals two important points. First, the quantal close coupling  $J_Q$  confirms the conclusion of Boesten *et al.* (1993) which first pointed out a “quantum suppression” effect, i.e., that  $J$  for a Cs model falls by about four orders of magnitude below the semiclassical prediction,  $J_{BJ}$ , as the temperature decreases from 1 mK to 10  $\mu$ K. Second,  $J_{LZ}$  tracks the close-coupling results very closely even down into this “quantum suppression” region. At first glance the ability of the semiclassical Landau-Zener formula to follow the quantum scattering result even where the semiclassical optical-Bloch-equation and Julienne-Vigué theories fail may seem surprising. The very good agreement between  $J_Q$  and  $J_{LZ}$  simply means that the dramatic reduction in trap-loss probability below 1 mK can be interpreted essentially as poor survival against spontaneous emission when the approaching partners are locally excited at the Condon point at long range. The calculations in Fig. 17 were carried out with a detuning  $\Delta$  of one atomic line width  $\Gamma_A$ . To check this interpreta-

tion, further calculations were carried out at greater red detunings and with lighter alkalis. In both cases the “quantum suppression” effect was greatly diminished as an increased survival interpretation would lead one to expect. An experimental measurement of the reduction in trap-loss rate with temperature has been reported by Wallace *et al.* (1995) in  $^{85}\text{Rb}$  collisions.

### c. Two-photon distorted wave theory

Solts *et al.* (1995) have developed a distorted wave theory for evaluating weak-field, two-photon spectra, collision-induced energy redistribution, and radiative escape rates in cold atom traps. This theory complements the method of complex potentials discussed above and illustrates the connection between trap-loss spectra and photoassociation spectra. The two-photon distorted-wave collision theory is a rigorous quantum mechanical development, valid in the weak-field limit, and capable of treating multichannel collisional effects such as hyperfine structure. The theory concentrates on radiative escape trap-loss collisions,

$$A + A + \hbar\omega_L \rightarrow [A + A^*] \rightarrow A + A + \hbar\omega_S \quad (83)$$

treating the radiative coupling as weak perturbations, while fully taking into account the collision dynamics. The  $A$  term stands for an alkali atom or metastable rare-gas atom,  $[A + A^*]$  is a bound excited quasimolecule, and  $\omega_L, \omega_S$  are the exciting laser photon and reemitted fluorescent photon, respectively. When  $\omega_L$  is close to  $\omega_0$ , the  $A \leftrightarrow A^*$  atomic resonance frequency, so that the red-detuning  $\Delta_L = \omega_L - \omega_0$ , is within a few natural line widths of the atomic transition, the spectrum of  $\hbar\omega_S$  will appear continuous, and its asymmetrically peaked form is controlled by the pair distribution function dependence on  $\Delta_L$  and on radiative damping. For an example of this line shape see the corresponding trap-loss spectrum in Fig. 37. As  $|\Delta_L|$  increases, and the density of excited bound states decreases, the spectrum resolves into the discrete vibration-rotation progressions characteristic of photoassociation spectra. The state-to-state cross section for energy-specific ( $E_i \rightarrow E_f$ ) transitions is given by

$$\frac{d\sigma(E_i, E_f)}{dE_f} = \frac{2\pi^2}{k_i^2} \hbar \gamma |V_L|^2 Y(E_i, E_f), \quad (84)$$

where  $k_i^2 = 2\mu E_i / \hbar^2$  and  $V_L$  is the exciting laser coupling strength. The “characteristic strength” function  $Y(E_i, E_f)$  can be expressed as a partial wave expansion,

$$Y(E_i, E_f) = \sum_{l=0}^{l_{\max}} (2l+1) |\Theta_{fi}^{(l)}|^2, \quad (85)$$

where  $\Theta_{fi}^{(l)}$  is the two-photon  $T_{fi}$  matrix element ( $E_f, l | T_{fi} | E_i, l$ ) divided by the product of  $\Delta_L$  and  $\Delta_S = \omega_S - \omega_0$ . The summation over partial waves is effectively cut off by a centrifugal barrier. The trap-loss rate constant  $\beta_{RE}(T)$  is calculated by averaging over the thermal distribution of atoms at the temperature of the trap and integrating over the final energies exceeding the trap escape threshold  $\Delta_{RE}$ ,

$$\beta_{\text{RE}}(T) = \left( \frac{2\pi\hbar^2}{\mu k_B T} \right)^{3/2} \gamma |V_L|^2 \int_0^\infty dE_i I(\Delta_{\text{RE}}) e^{-E_i/k_B T}, \quad (86)$$

where  $k_B$  is the Boltzmann constant and

$$I(\Delta_{\text{RE}}) = \int_{\Delta_{\text{RE}}}^\infty dE_f Y(E_i, E_f). \quad (87)$$

At weak field the loss rate constant is directly proportional to the field intensity through the  $|V_L|^2$  term. Equation (84) shows that the state-to-state redistribution cross section is proportional to the ‘‘characteristic strength function.’’ Figure 18 shows the ‘‘spectrum’’ of  $Y(E_i, E_f)$  as a function of detuning  $\Delta_L$ , taking  $0_u^+$  state of  $\text{Na}_2$  as an example of an excited-state potential. The figure shows how the density of resonances decreases with increasing detuning. These lines, typical of the photoassociation spectra to be discussed in Sec. VI, are clearly resolved even to very small detuning because only one spinless excited state is involved. If other excited states and hyperfine structure were included, the overlapping resonances would blend together into an effective continuum at small detuning, but would resolve into typical photoassociation spectra at large detuning (see, for example, Fig. 57). In principle the two-photon distorted-wave theory could be applied to a real photoassociation spectrum (at weak field) including hyperfine structure and excited states. This theory presents a unified view of trap-loss and photoassociation spectroscopy that shows them to be two aspects of the same cold-collision interaction with the laser field, differing only in the detuning regime.

#### d. Optical Bloch equations

Both the Gallagher-Pritchard and Julienne-Vigué semiclassical models as well as the complex potential and two-photon distorted wave quantum scattering calculations assume an initial optical excitation and subsequent spontaneous decay, after which the decayed population no longer participates in the collisional process. This picture is valid as a weak-field limit, but at higher fields the decayed population can be reexcited, resulting in important modification of the overall probability of excitation at various points along the collision trajectory as well as changes in the ground-state kinetic energy. The need to treat dissipation at high field requires a density matrix approach; by introducing semiclassical trajectories, the time-dependent equations of motion governing the density matrix transform to the optical-Bloch equations. Although the optical Bloch equations treat population recycling properly in principle, problems arise when the time dependence of these equations maps to a spatial dependence. This mapping converts the time coordinate to a semiclassical reference trajectory; however, because the potentials of the ground and excited states are quite different, the state vectors evolving on these two potentials, in a diabatic representation, actually follow very different trajectories. Band and Julienne (1992) formulated two versions of an optical-

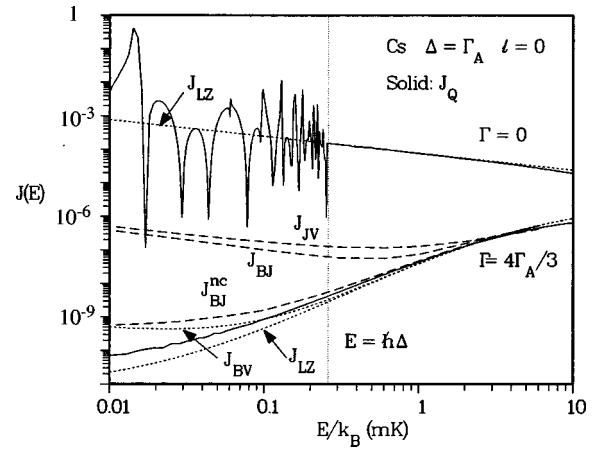


FIG. 17. Cs trap-loss probabilities for various  $J$ 's as a function of collision temperature. Notice the steep drop for  $J_{\text{BV}}$ ,  $J_{\text{LZ}}$ , and  $J_{\text{BJ}}^{\text{nc}}$ . Notice also that semiclassical theory  $J_{\text{JV}}$  completely misses this drop below about 1 mK. From Julienne *et al.* (1994).

Bloch-equation trap-loss theory in a diabatic representation and calculated the excitation-survival factor,  $J(E, l, \Delta, I; \gamma)$  of Eq. (79). One version applies correction factors to the initial reference trajectory so as to accurately reflect the actual semiclassical path followed by each state vector component. The other version makes no such corrections. Figure 17 shows that the ‘‘not corrected’’ version  $J_{\text{BJ}}^{\text{nc}}$  actually works much better than the ‘‘corrected’’ version  $J_{\text{BJ}}$ , although neither tracks the quantal results as well as  $J_{\text{LZ}}$ . The problem appears to be that the correction factors can successfully handle the diagonal terms of the density matrix, but fail when applied to the field-induced off-diagonal terms. These terms are important in a diabatic representation. Band *et al.* (1994) have recast the optical-Bloch-equation calculations in an adiabatic basis in which the field interaction is diagonalized and the interaction coherences are therefore eliminated. This approach yields much better results at low temperature, as can be seen in Fig. 19. A complete derivation of the adiabatic optical-Bloch-equation method is given by Suominen, Band, *et al.* (1998) including interpretative Landau-Zener models adapted to the strong field case.

Although numerical results using the optical-Bloch equations show reasonable agreement with experiments performed in Cs by Sesko *et al.* (1989) and Na by Marcassa *et al.* (1993), the quantum calculations of Boesten *et al.* (1993), Boesten and Verhaar (1994), Julienne *et al.* (1994), and Suominen *et al.* (1994) indicate that these results are fortuitous. A proper quantum treatment using two-state models would give rate coefficients more than one order of magnitude smaller than measured.

#### e. Quantum Monte Carlo methods

Suominen *et al.* (1994) have carried out a quantum Monte Carlo two-state model study of survival in the very low temperature regime in which  $J_Q$ ,  $J_{\text{BV}}$ ,  $J_{\text{LZ}}$  of Fig. 17 all show a dramatic reduction in the trap-loss

probability. The approach is to apply the Monte Carlo state vector method of Castin *et al.* (1993) to the time evolution of wave packets undergoing random quantum jumps (Lai *et al.*, 1993) during the course of the cold collision. By repeating the simulation many times, a statistical sample that approaches the density matrix is gradually built up. This approach treats spontaneous emission rigorously at all field strengths, taking into account not only population recycling but also ground-state kinetic energy redistribution. The motivation for the study was to provide definitive quantum mechanical benchmark calculations against which all approximate (but numerically more manageable) theories could be compared. Further motivation was to demonstrate, from an entirely different wave-packet, time-dependent approach, the surprising resilience and robustness of the Landau-Zener formula in the very low energy regime where a semiclassical expression would be normally suspect. Figure 20 shows the results of a diabatic optical-Bloch equation, a Monte Carlo wave packet, and a Landau-Zener calculation of the excited-state flux survival for Cs collisions at an energy of 100  $\mu$ K. The diabatic optical-Bloch equation clearly fails, and the Landau-Zener result appears as the semiclassical average of the wave packet result. The conclusions of this benchmark study are, therefore, (1) semiclassical, diabatic optical-Bloch-equation calculations cannot be trusted below 1 mK, (2) the quantal wave-packet calculations confirm previous findings that trap-loss collision probabilities drop off dramatically with temperature, and (3) the Landau-Zener results are in excellent accord with the oscillation-averaged fully quantal results.

Holland *et al.* (1994) have applied the wave-packet quantum Monte Carlo technique to consider radiative heating of an ensemble of two-level Cs atoms; i.e., the reduced mass of the two-body collision was chosen to be that of Cs and the excited state was chosen to have the  $C_3$  parameter of the attractive  $0_u^+$  state. Figure 21 shows how the Monte Carlo method reveals momentum distribution spreading due to reexcitation and population recycling. Note that the spreading is especially marked for lower values of the initial momentum and results in ensemble heating even if trap loss does not occur. Significant heating without trap loss may have an important bearing on the limiting temperatures and densities attainable in optical traps.

### 3. Assessment of theoretical approaches

#### a. Quasistatic vs dynamical

The quasistatic theories of GP and JV assume that, for any pair separation  $R_0$ , the colliding partners are moving slowly enough that the field-quasimolecule coupling sets up a steady state population distribution at  $R_0$  governed by the Lorentzian of Eqs. (67) or (74). The characteristic time to establish this distribution is on the order of the spontaneous emission lifetime. Under the influence of an attractive  $C_3/R^3$  potential the colliding nuclei rapidly pick up kinetic energy; therefore, at large detunings the time requirement to achieve the steady-

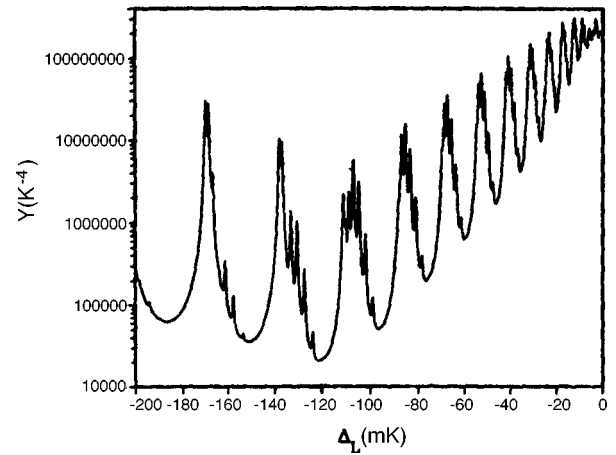


FIG. 18. Spectrum of the characteristic strength function,  $Y$ , as a function of detuning  $\Delta_L$ . The units of detuning in the figure are given in mK where 1 mK  $\approx$  20 MHz. Note that resonance peaks are resolvable even at small detuning due to the simplicity of the model calculation. See Solts *et al.* (1995).

state distribution is never fulfilled. At small detunings, where the nuclei accelerate more slowly, there *may* be sufficient time if the excitation is not too weak; but the governing Lorentzian distribution then implies very strong delocalization of excitation about the Condon point,  $R_C$ . This delocalization of excitation has been tested by quantum Monte Carlo wave packet studies (Suominen *et al.*, 1994). The results demonstrate that excitation is a “dynamical” process, sharply localized around  $R_C$  for all detunings, and established on a time scale of the order of the inverse of the excitation Rabi frequency. The quantum scattering complex potential studies and adiabatic OBE calculations confirm the dynamical picture, at least in the weak field limit. Furthermore the excitation-survival probability distribution itself can be factored into a survival term and an excitation term expressed by the Landau-Zener formula,  $J_{LZ} \approx S_a e^{-A}$  with  $A$  given by Eq. (82). Figure 17 shows that all dynamical theories correctly demonstrate the “quantum suppression” effect on trap-loss probabilities as temperature descends from the mK to the  $\mu$ K regime, while the quasistatic steady-state theories completely miss it. At higher excitation fields, where theory must correctly take into account spontaneous emission, population recycling between ground and excited states, and kinetic energy redistribution on the ground state, so far only the quantum Monte Carlo wave packet studies of Suominen *et al.* (1994) provide a reliable guide to the physics of collision processes. The calculational burden of these statistical samplings of the full density matrix has restricted these studies to two-level model systems. Studies of realistic potentials including hyperfine interaction are still beyond the scope of present calculational resources.

#### b. Small vs large detuning

The various theoretical approaches to trap loss at small detuning, i.e.,  $\Delta \leq 10 \Gamma_A$  from atomic resonance,

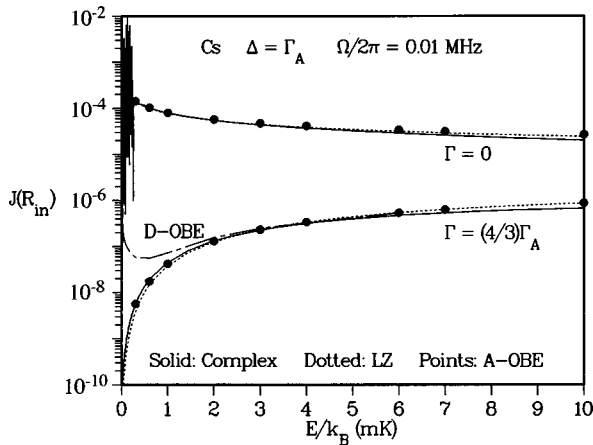


FIG. 19. Trap-loss probability as a function of temperature for complex potential, Landau-Zener, and adiabatic optical-Bloch equation approaches. Notice that the adiabatic optical-Bloch equation is much better than the diabatic version, from Band *et al.* (1994).

can at best provide a qualitative guide for understanding the process. No theory yet exists that is fully quantitative because small detuning implies an  $R_C$  typically on the order of  $\lambda/2\pi$ , where  $\lambda$  is the wavelength of the cooling transition. The large value of  $R_C$  leads to two major complications: (1) the long time scale for the atoms to be accelerated to small  $R$  where fine-structure-changing collisions or radiative escape energy exchange occurs gives a prominent role to spontaneous decay, and (2) the molecular hyperfine structure introduces great complexity into the long range potential curves. All theoretical treatments to date ignore (2), because of the computational intractability of the full problem, which is currently beyond the scope of any conceivable numerical computational solution. A full and proper treatment of the small detuning case requires the solution to the von Neumann equation of motion for the quantum density matrix  $\rho_{ij}(R, R')$  (Julienne, Smith, Burnett, 1993; Suominen *et al.*, 1994). This is now feasible with Monte Carlo simulations for two-state models, as demonstrated by Suominen *et al.* (1994), whose calculations provide the benchmarks against which any other two-state theories must be tested.

Unfortunately, all current theories of trap loss for small detuning suffer from the limitation of being restricted to two (or at least a very few) scattering channels. There are some general conclusions that can be extracted from these calculations, however. The first is that of the great usefulness of the semiclassical picture of localized excitation at the Condon point. As discussed in Sec. V.A.3.a above, the local equilibrium models of Gallagher and Pritchard and Julienne and Vigué give simple pictures for interpreting trap loss. As detuning changes from small (order of a few natural atomic widths) to large (many natural widths), these theories all show that the trap-loss rate first increases with the magnitude of the detuning (as survival improves due to excitation at smaller  $R$ ) then decreases (survival approaches unity, but the available phase space of pairs

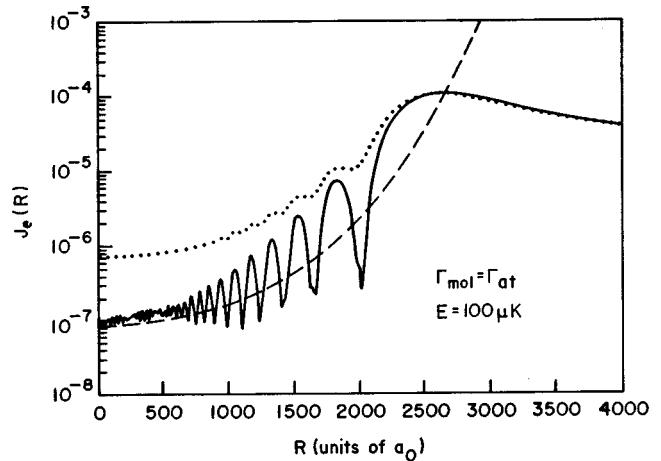


FIG. 20. Probability as a function of temperature for the diabatic optical-Bloch equation (dotted line), a wave packet (solid line), and Landau-Zener calculation (dashed line) of excited-state flux survival at collision energy of 100  $\mu\text{K}$ .

proportional to  $R^2$  decreases). Unfortunately, all of the quantum calculations show that in the small detuning regime the quasistatic picture with delocalized, Lorentzian excitation is fundamentally incorrect. The correct picture shows localized excitation at the Condon point followed by spontaneous decay as the atoms are accelerated together on the excited state. The Monte Carlo calculations even demonstrate that such a picture can even be extended to the strong field saturation regime of two state models: a semiclassical delayed decay model (Suominen *et al.*, 1997) works where decay is only calculated from the inner edge of a region of saturation about the Condon point.

In contrast, at large detuning the Gallagher-Pritchard and Julienne-Vigué theories do result in excitation localized near the Condon point because of the steep slope of the upper potential curve, and in fact Band and Julienne (1992) showed that the Gallagher-Pritchard theory becomes equivalent to the Landau-Zener+survival model which has now been demonstrated by the quantum calculations. In practice, this will be true for detunings on the order of 10 atomic line widths or more. The Gallagher-Pritchard theory is especially useful in this regime. The validity of the simple Gallagher-Pritchard formula has been verified in the trap-loss studies to the red of the  $S_{1/2}+P_{1/2}$  limit by Peters *et al.* (1994). Unfortunately, the semiclassical theories leave out the role of bound states of the excited potential, which are now well known from the detailed spectra measured by photoassociation spectroscopy at sufficiently large detuning, typically more than 100 linewidths from atomic resonance. There is a need for the development of a theory that bridges the gap between the large detuning photoassociation region and the intermediate detuning regime where the density of bound vibrational states is so high that the quasicontinuum approach of Gallagher and Pritchard applies. This bridging could be done by applying the complex potential method, which uses well-understood scattering algorithms, or the perturbative

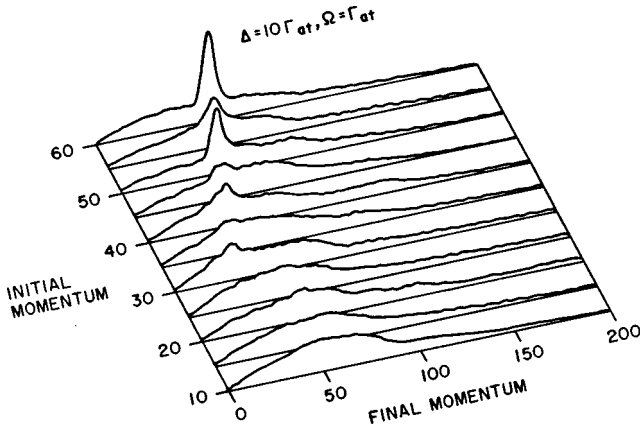


FIG. 21. Momentum distribution spreading due to reexcitation and population recycling. From Holland *et al.* (1994).

Franck-Condon approach of Solts, Ben-Reuven, and Julienne (1995).

Another main complication at small detuning is the extreme complexity of the molecular hyperfine structure (Walker and Pritchard, 1994; Julienne *et al.*, 1994; Lett, Julienne, and Phillips, 1996). A number of the experimental studies described below indicate a prominent role for hyperfine structure in determining the trap-loss rate. For example Fig. 22 shows the molecular hyperfine potentials originating from  ${}^2S + {}^2P_{3/2}$  Na atoms. The recent work of Fioretti *et al.* (1997) suggests that hyperfine optical pumping in a molecular environment during a collision may also be significant (see also Julienne and Mies, 1989). The fundamental difficulty with the two-state treatments in the older Gallagher-Pritchard, Julienne-Vigué, and optical-Bloch-equation studies is that the apparent agreement with experiment is only fortuitous. According to the quantum calculations, with their dynamical picture of the excitation, the predicted trap-loss rates will be much lower (an order of magnitude or more) for these same two-state models than rates given by the older semiclassical theories. Therefore there is a fundamental discrepancy that remains to be understood. There is considerable likelihood that the resolution of this problem will require understanding the role of the complex molecular hyperfine structure, with molecular optical pumping and spontaneous decay. Although the semiclassical optical Bloch equation methods showed clear problems in the diabatic formulation, there is some promise in an adiabatic formulation of the semiclassical optical-Bloch-equation method that appears much more accurate than the diabatic formulation (Suominen, Band, *et al.*, 1998). Since it is unlikely that a fully quantum density matrix treatment including hyperfine structure will be available in the foreseeable future, a possible approach to understanding small-detuning trap loss may lie with adiabatic optical-Bloch-equation or Landau-Zener semiclassical models (Boesten and Verhaar, 1994; Julienne *et al.*, 1994; Suominen, Band, *et al.*, 1998).

The situation is much better at somewhat larger detuning, i.e., large compared to the atomic spontaneous decay line width. When the detuning becomes suffi-

ciently large, the trap-loss process gives rise to a discrete spectrum of trap loss due to the bound states in the excited attractive molecular potentials. The Condon point is sufficiently small that many vibrational cycles are necessary before spontaneous decay can occur, and the spacing between vibrational levels becomes large compared to their natural linewidth. We will discuss this case in detail in Sec. VI on photoassociation spectroscopy. In this limit of large detuning, the theory is in excellent shape, because spontaneous emission can be treated as a perturbation on the normal conservative multichannel scattering theory, and fully quantitative calculations including all molecular hyperfine structure have been carried out in great detail, and with superb agreement with experiment.

It is within the realm of possible calculations to study a realistic system without hyperfine structure, such as Group II species like Mg, Ca, or Sr. All of these have  ${}^1S \rightarrow {}^1P$  transitions. We will show in Sec. VII on optical shielding how a full three-dimensional scattering treatment taking into account the degeneracy of the excited  $P$  level is possible. Monte Carlo simulations, as well as simpler models, of such a system appear to be feasible with advanced computation methods. Experimental studies of such a simple system would be very helpful in unraveling the complexities of small detuning trap loss. There is a realistic hope of testing proper theory against experimental measurements in such systems.

#### 4. Excited-state-trap loss measurements

In general, collisions in traps are investigated by either detecting the product resulting from the binary encounter or through loss of the colliding species from the trap. When an ultracold collision releases kinetic energy, the reaction rate can be measured by observing the time dependence of the number of atoms  $N$  either as the trap loads or as it decays. The equation governing the net loading rate of the trap is given by

$$\frac{dN}{dt} = L - \gamma N - \beta \int_v n^2(r,t) d^3r, \quad (88)$$

where  $L$  is the capture rate,  $\gamma$  the rate constant for collisions of trapped atoms with thermal background gas, and  $\beta$  the loss-rate constant due to collisions between trapped atoms. In general, spatial variation of the atomic density  $n(r,t)$  requires integration over the whole volume occupied by the atoms; however, the spatial density distribution of the trapped atoms can be in one of two possible limits: at low-density radiation trapping is negligible, and the trap spatial distribution is close to Gaussian; in the high-density limit Walker *et al.* (1990) showed that radiation trapping dominates and produces a constant spatial atom density. Thus in the low density limit the distribution  $n(r,t)$  can be expressed as  $n(r,t) = n_0(t) e^{-r^2/w^2}$ , and Eq. (88) becomes

$$\frac{dN}{dt} = L - \gamma N - \frac{\beta N^2}{(2\pi)^{3/2} w^3}. \quad (89)$$

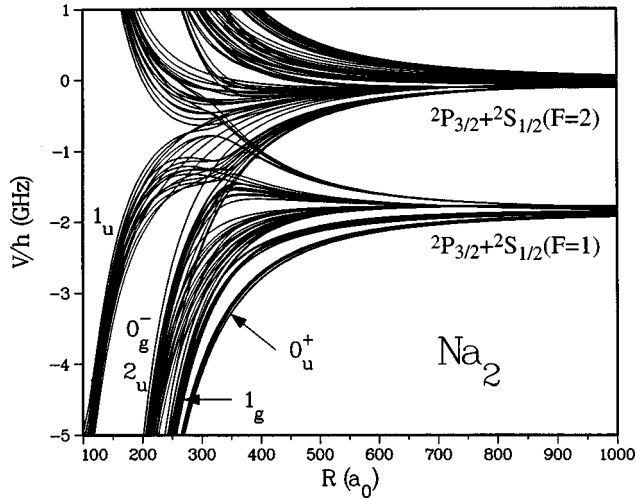


FIG. 22. Hyperfine molecular states near the  ${}^2S + {}^2P_{3/2}$  asymptote. The dense number of states gives rise to a large number of avoided crossings, state mixing, and congested spectra. From Lett, Julienne, and Phillips (1996).

This equation has a complicated solution as shown by Prentiss *et al.* (1988), but  $N(t)$  can be measured directly and  $\beta$  determined by curve fitting.

In the high-density limit, trap loading proceeds at constant density. As the number of atoms in the trap increases, the volume expands so that the density in the trap remains unchanged, and Eq. (88) takes the form

$$\frac{dN}{dt} = L - (\gamma + \beta n_c)N, \quad (90)$$

where  $n_c$  is the constant atomic density obtained in the trap. The value of  $n_c$  is characteristic of the trapping conditions. The factor  $\gamma + \beta n_c$  is determined by beginning with an empty trap, turning it on, and measuring the number of trapped atoms as a function of time. Equation (90) is then fit to the measurement. Examples of these  $N(t)$  transients obtained in a sodium MOT by Marcassa *et al.* (1993) are presented in Fig. 23, at several different MOT laser intensities. A semilog plot of the absolute value of  $1 - N/N_0$  versus  $t$  determines the slope equal to  $-(\gamma + \beta n_c)$  as shown in Fig. 24. The linearity of those plots confirms that trap loading takes place within the regime of constant density,  $n_c$ . These loading-curve fits ignore the very early times where the constant density regime has not yet been reached. The density  $n_c$  is obtained by first measuring the trap diameter with, for example, a charge-coupled-device (CCD) camera to determine the volume. Then fluorescence detection or absorption with an independent probe laser determines the number of trapped atoms. To extract  $\beta$ , the two-body trap-loss rate constant, it is necessary to devise an independent measurement of  $\gamma$ . This rate can be determined either by observing variations of  $(\gamma + \beta n_c)$  for different background pressures of the trapped gas or by operating the MOT with a very low number of trapped atoms such that the term  $\beta n_c$  is negligible compared with  $\gamma$ . Figure 24 shows the light-field-intensity dependence of  $-(\gamma$

$+\beta n_c)$  that is associated with the intensity-dependence of  $\beta$  since  $\gamma$  and  $n_c$  are insensitive to this parameter.

If the MOT is loaded from a slow atomic beam, the background-loss rate  $\gamma$  is normally very small and a convenient way to investigate  $\beta$  is to observe the decay of the trapped atoms as a function of time after the loading process has been completed and the source of atoms interrupted. In this case the capture rate  $L$  is no longer present in Eq. (88). Typical decay of a cesium MOT atomic fluorescence (Walker and Feng, 1994) as a function of time is shown in Fig. 25. In the initial stage, Fig. 25 shows a constant-density collision rate resulting in exponential decay. As the number of atoms decreases, the radiation trapping effect becomes weak enough that the density begins to drop while the trapped-atom distribution retains a Gaussian shape. In this regime the decay is non-exponential. Finally, when the number of atoms become very small, the intra-trap collisions are no longer important and the collisions with background gas cause the decay to once again become exponential in time, with a rate smaller than the first stage.

The trap-loss parameter  $\beta$  contains the probabilities for inelastic processes such as fine-structure-changing collisions, radiative escape, and photoassociation. To better understand the influence of applied optical fields on these processes, several research groups have performed studies of the dependence of  $\beta$  on various parameters, especially MOT laser frequency and intensity. Both the Gallagher-Pritchard and Julienne-Vigué models predict a  $\beta$  increasing linearly with MOT intensity; initial experiments sought to verify this behavior.

Investigation of the variation of  $\beta$  with MOT light intensity is straightforward to carry out. One can either load or unload the trap at different intensities and extract  $\beta$  from the transient behavior. If the experiment is performed by loading a MOT from a slow atomic beam, this technique works well over a wide range of intensities (Sesko *et al.*, 1989; Wallace *et al.*, 1992; Kawanaka, *et al.*, 1993; Ritchie, *et al.*, 1995). However, for vapor-cell loading where the  $\gamma$  term in Eq. (88) becomes significant, the steady-state number of atoms in the trap at low MOT intensity becomes too small for reliable measurements. In this case, the study of  $\beta$  as a function of intensity can be implemented by a sudden change of intensities as demonstrated by Santos *et al.* (1996). The basic idea is to switch between two different intensities in a short time interval. A large number of atoms is loaded into the trap at high intensity after which the intensity is suddenly attenuated by introducing a calibrated neutral density filter into the laser beam. At lower intensity the new loading and loss rates determine a new (lower) steady state number of atoms. The transient variation of the number of trapped atoms between the two limits determines  $\beta$  in the low intensity regime. Figure 26 shows a typical fluorescence-time spectrum using a sudden change of intensity, starting from a high steady-state number of atoms. The fast drop observed at the first instant of time corresponds to the decrease in the photon scattering rate due to the change in light intensity without variation in the number of trapped atoms. The

subsequent slow decay must be analyzed using Eq. (89) or Eq. (90) already described.

The investigation of  $\beta$  with MOT detuning is more difficult because the trap only operates over a narrow range of detunings  $\sim\Gamma$  to the red of the atomic resonance. Hoffmann *et al.* (1992) overcame this limitation by introducing an extra probe laser, which they called a “catalysis” laser. This idea was first introduced by Sesko *et al.* (1989). Although the added optical field does not act as a catalyst in the conventional chemical sense of increasing reaction rates without net consumption of the catalysis photon “reagent,” the term has been widely adopted anyway. As long as the frequency of this laser is not too close to the MOT or repumping transition, it does not affect the trapping and cooling processes; however, it can produce changes in the trap-loss rate. Hoffmann *et al.* (1992) assumed the effect of the catalysis laser on the trap-loss rate to be additive,  $\beta = \beta_t + \beta_c$ , where  $\beta_t$  represents the rate constant with only the trapping laser present and  $\beta_c$  the contribution of the catalysis laser. It is important to note, however, that Sanchez-Villicana *et al.* (1996) have demonstrated a “flux enhancement effect” (see discussion below in the section on rubidium trap loss and Fig. 38) that call the  $\beta$  additivity assumption into question. Detuning the catalysis laser ( $\Delta_c$ ) affects  $\beta$  and the number of atoms in the trap,  $N$ ,

$$N = \frac{L}{\gamma + \beta n_c f}, \quad (91)$$

where  $L, \gamma$  have their usual meaning—see Eq. (88)—and  $f = \int n^2(\mathbf{r}, t) d^3\mathbf{r} / n_c N$  is a measure of the deviation of the density distribution from the uniform density  $n_c$ . As the intensity  $I_c$  and detuning  $\Delta_c$  of the catalysis laser vary, the trap-loss constant  $\beta$  varies as,

$$\beta = \beta_t + \beta_c(\Delta_c) \frac{I_c(\Delta_c)}{I_{\text{ref}}}, \quad (92)$$

where  $I_{\text{ref}}$  is a reference laser intensity taken to be  $10 \text{ mW cm}^{-2}$ . Equation (91) shows that varying  $I_c$  and  $\Delta_c$  in turn will alter  $N$  and consequently the trap density,  $n$ . Unfortunately, the most difficult quantity to determine accurately in these experiments is the trap density, but Hoffmann *et al.* (1992) avoided this problem by adjusting  $I_c$  at each  $\Delta_c$  such that  $N$  and  $n$  remained constant over the entire range of detunings in the experiment. With the condition that the product  $\beta_c(\Delta_c) I_c(\Delta_c)$  be held invariant to maintain constant  $N$ , it was only necessary to measure the loading curve, Eq. (88), with and without the catalysis laser at one fixed detuning and intensity in order to obtain the absolute value of the  $\beta_c I_c$  product. Once known, measures of  $I_c(\Delta_c)$  determined absolute values of  $\beta_c(\Delta_c)$  over the entire detuning range of the experiment. The reliability of the catalysis laser method depends strongly on the assumption that the extra laser light affects only the atomic collisions and not the performance and characteristics of the MOT. This assumption is best justified if the catalysis laser is not tuned too close to the trapping and repump-

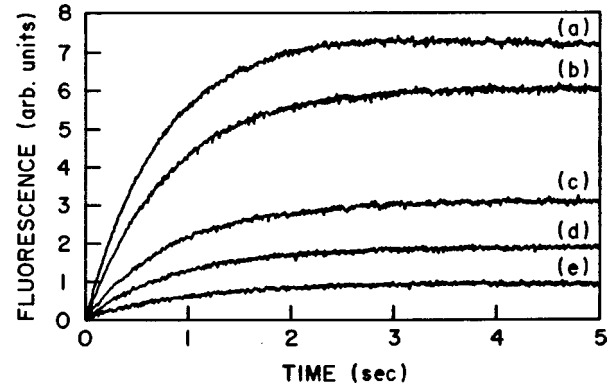


FIG. 23. Examples of trap loading rates in MOT (type-I trap with trapping laser tuned approximately one linewidth to the red of  $2S (F=2) \rightarrow 3P_{3/2}(F'=3)$ ) for several different MOT intensities: (a)  $96 \text{ mW cm}^{-2}$ , (b)  $70 \text{ mW cm}^{-2}$ , (c)  $36 \text{ mW cm}^{-2}$ , (d)  $23 \text{ mW cm}^{-2}$ , (e)  $16 \text{ mW cm}^{-2}$ . Curves are from Marcassa *et al.* (1993).

ing transitions and the power is not so high that light shifts begin to affect the MOT functioning.

Using these techniques to study trap loss, several specific cases have been investigated.

#### a. Sodium trap loss

Prentiss *et al.* (1988) carried out the first measurements of collisional losses in a MOT loaded from a cold sodium beam. In this work sudden interruption of the atomic beam stopped the loading at a well-defined instant of time and the subsequent fluorescence decay was recorded. At early times a nonexponential fluorescence decay was observed at a trap density  $\sim 7 \times 10^9 \text{ cm}^{-3}$ . Fit-

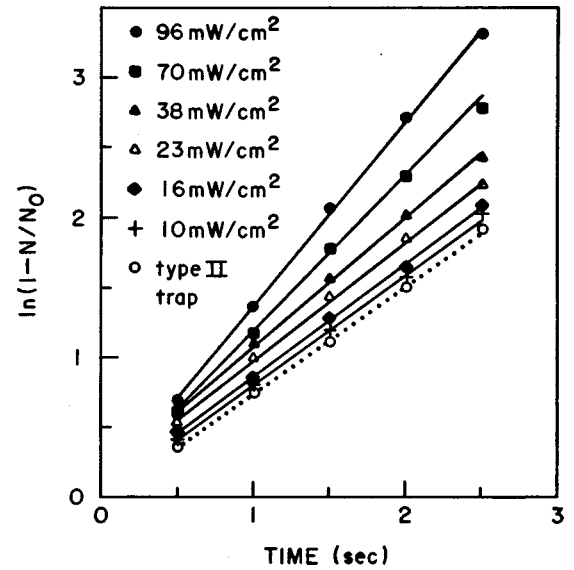


FIG. 24. Semilog plot of the integrated loading curves: absolute value of  $1 - N/N_0$  versus  $t$ . The slope,  $-(\gamma + \beta n_c)$ , determines the trap loss rate constant  $\beta$ . Results are for a type-I trap with trapping laser tuned approximately one linewidth to the red of  $2S (F=2) \rightarrow 3P_{3/2}(F'=3)$ . Curves are from Marcassa *et al.* (1993).

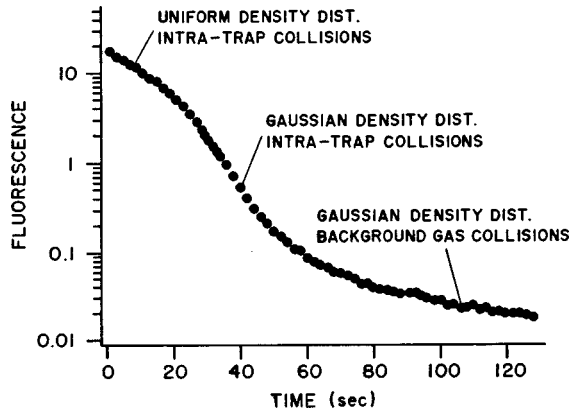


FIG. 25. Time evolution of MOT decay. From Walker and Feng (1994).

ting of the nonexponential decay with an equation like Eq. (89) permitted extraction of a value for  $\beta$ . Investigation of the variation of  $\beta$  with laser intensity is shown in Fig. 27. The data yielded a  $\beta$  invariant with intensity (within  $\pm 40\%$ ) over a range of 5 to 50 mW cm<sup>-2</sup>. Variations of the trap depth, realized through changes in the MOT magnetic field, indicated that  $\beta$  was insensitive to trap-depth changes as well. The absolute values of  $\beta$  were measured to be about  $4 \times 10^{-11}$  cm<sup>3</sup> s<sup>-1</sup> (within a factor of 5). Although Prentiss *et al.* (1988) could not readily explain the unexpected insensitivity of  $\beta$  to light intensity, they offered several possibilities for the observation including the effect of  $m_F$  hyperfine levels mixing and shifts of the atomic energy levels that occur during a collision. The surprising lack of intensity dependence in their results underscored the importance of investigating binary collisions in MOTs.

Marcassa *et al.* (1993) investigated  $\beta$  over a wider range of intensity, from 20 to 300 mW cm<sup>-2</sup>, using a Na vapor-cell-loaded MOT. In their report a definite light intensity dependence was indeed observed, and the apparent independence previously reported by Prentiss *et al.* (1988) was explained by the relatively narrow range over which the earlier experiments had been carried out. In the experiment of Marcassa *et al.* (1993) the MOT laser was tuned about 10 MHz to the red of the atomic cooling transition, and  $\beta$  extracted from the fluorescence growth curve recorded during MOT loading, starting from an empty trap. Densities in the MOT ranged from  $5 \times 10^9$  to  $2 \times 10^{10}$  cm<sup>-3</sup>, which is in the high-density limit where Eq. (90) governs the loading process. In order to distinguish  $\gamma$  from  $\beta n_c$  trap loss was measured using two tuning conditions, the type I and type II traps, described in Prentiss *et al.* (1988). The type II trap was operated in a density regime low enough so that trapped-atom collisions could be ignored and the slope of the fluorescence growth exponential determined  $\gamma$ . A calibrated telescope measured the MOT diameter from which the assumed spherical volume was calculated, and the atom number in the MOT was determined from fluorescence imaged onto a calibrated photomultiplier detection train. These two measurements determined  $n_c$ , and  $\beta$  was then calculated from Eq. (90).

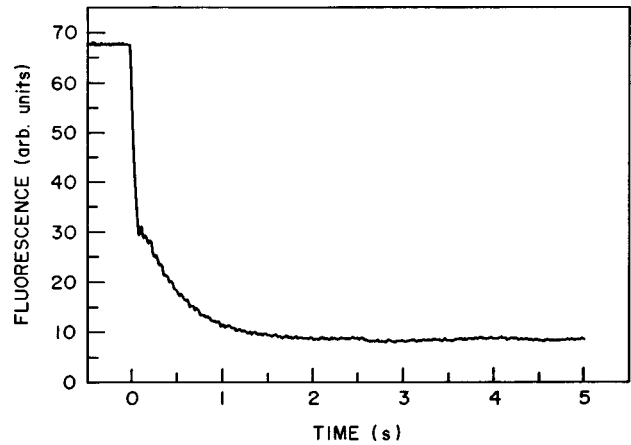


FIG. 26. Fluorescence-time spectrum. The abrupt drop at the initial moment is due to a change in light intensity without variation in the number of trapped atoms. From Santos *et al.* (1996).

The measured intensity dependence of  $\beta$  is shown in Fig. 28. Despite error bars of 50% or more, due essentially to uncertainties in the volume measurement, the expected increase of  $\beta$  with MOT intensity is unmistakable.

Band and Julienne (1992) proposed a new theory for trap loss, explicitly avoiding the local equilibrium assumption of the Gallagher-Pritchard and Julienne-Vigué models, and based on the optical-Bloch equations. The optical-Bloch-equation density-matrix approach to trap loss is appropriate to studies of optical field dependence because it naturally takes into account population recycling (optical excitation, decay, and reexcitation) at high field. In contrast Gallagher-Pritchard and Julienne-Vigué are weak-field theories in which spontaneous emission is treated as a simple loss term, and the decayed population never recycles. Marcassa *et al.* (1993) applied this optical-Bloch-equation theory to their intensity-dependence studies of Na trap loss by calculating  $\beta$  as a function of MOT intensity and comparing it to the measured values. A difficulty in making this comparison is knowledge of the minimum velocity that must be imparted to the atoms in order to escape from the MOT. Assuming single-atom escape velocities of 20 and 30 ms<sup>-1</sup>, Marcassa *et al.* (1993) calculated a radiative escape contribution to the total loss rate of 38% and 24% respectively with the remaining fraction due to fine-structure-changing collisions. Figure 28 plots the results from calculation and measurement. Although the model did not include hyperfine structure of the excited states, the agreement between theory and experiment is reasonably satisfactory, with theory somewhat higher than experiment. However, the assessment in Sec. V.A.3 indicates that this agreement is likely to be fortuitous. It is worthwhile to note that Marcassa *et al.* (1993), in the course of carrying out these  $\beta$  calculations, also reevaluated the  $P_{XQ}(E, l)$  factor of Eq. (79) for the fine-structure-changing collision probability, using quantum close-coupling calculations and accurate potential curves of Magnier *et al.* (1993). The results showed a fine-structure-changing collisions probability smaller by a

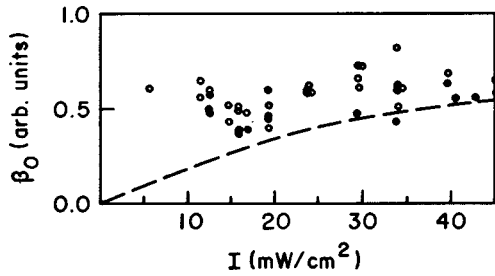


FIG. 27. Early experiment, Prentiss *et al.* (1988), measuring variation of trap loss rate constant in a Na MOT as a function of MOT intensity. The dashed line traces the calculated variation of the excited-state population.

factor of 2 than that estimated in Julienne and Vigué (1991) and underscores the necessity of using accurate molecular potential data in collisions calculations. Dulieu *et al.*, 1994 showed that fine-structure-changing collisions probabilities can be quite sensitive to the molecular potentials.

In a followup experiment Marcassa *et al.* (1997) used a catalysis laser to study Na trap loss as a function of red detuning. As discussed above, the number of atoms observed in the presence of the catalysis or probe laser is  $N = L/[\gamma + \beta(\Delta, I)n_c f]$  where  $\beta(\Delta, I) = \beta_t + \beta_c(\Delta)I/I_{\text{ref}}$ . As in Hoffmann *et al.* (1992) the intensity of the extra laser is adjusted at each detuning to keep  $N$  constant. From this condition Marcassa *et al.* (1997) determined  $\beta_c(\Delta)$ . Figure 29 shows the trap-loss spectrum for the catalysis laser detuned to the red of both the  $3s^2S_{1/2} + 3p^2P_{3/2}$  asymptote and the  $3s^2S_{1/2} + 3p^2P_{1/2}$  asymptote. The reason for measuring the trap-loss spectrum from both asymptotes is that both fine-structure-changing collisions and radiative escape contribute from the  $3s^2S_{1/2} + 3p^2P_{3/2}$  level, while only radiative escape contributes from the lower  $3s^2S_{1/2} + 3p^2P_{1/2}$  level. For comparison, the Gallagher-Pritchard theory is shown in the same figure as the solid line. The overall behavior is in good qualitative agreement with the model. Comparison between the absolute values shows that the amplitude of the trap-loss spectrum to the red of the  $3s^2S_{1/2} + 3p^2P_{1/2}$  asymptote is only 20% lower than the trap-loss spectrum near the  $3s^2S_{1/2} + 3p^2P_{1/2}$ . Therefore Marcassa *et al.* (1997) concluded that fine-structure-changing collisions is responsible for only 20% of trap loss, with radiative escape responsible for the remaining 80%. This result is in sharp disagreement with the calculations reported in Marcassa *et al.* (1993) in which radiative escape contributes about 30%. These disagreements indicate that the small-detuning trap-loss process and its detailed mechanisms are still poorly understood.

#### b. Cesium trap loss

Sesko *et al.* (1989) carried out the first collisional trap loss measurements on cesium using a MOT loaded from an atomic beam. In their experiment fluorescence decay was observed after loading. To ensure a constant half-width Gaussian profile for the whole investigated intensity range, the number of trapped atoms was kept low

( $\sim 3 \times 10^4$ ). Figure 30 shows the measured  $\beta$  as a function of trap laser intensity obtained by Sesko *et al.* (1989). Above  $4 \text{ mW cm}^{-2}$   $\beta$  increases with intensity due to the energy transfer collisions as radiative escape and fine-structure-changing collisions. Below  $4 \text{ mW cm}^{-2}$  the dramatic increase in  $\beta$  is due to hyperfine-changing collisions between ground-state atoms. For Cs, a change from  $6s^2S_{1/2}(F=4)$  to  $6s^2S_{1/2}(F=3)$  in one of the atoms participating in the collision transfers about  $5 \text{ ms}^{-1}$  of velocity to each atom. The Gallagher-Pritchard model is also included in Fig. 30 (solid line) showing a value a few times smaller than the measurement.

In the same experiment Sesko *et al.* (1989) also investigated the trap loss spectrum using a ‘‘catalysis’’ laser. They did not adjust the catalysis laser intensity at different detunings, as did Hoffmann *et al.* (1992) and Marcassa (1995), to maintain constant trap density, but instead measured the trap density at each point on the trap-loss curve, and measured the  $\beta$ -decay curve with and without the catalysis laser present. Their results are presented in Fig. 31, together with the Gallagher-Pritchard model (solid line). The scatter in the data reflects the difficulty of obtaining accurate measurement of the trap density.

In a recent work Fioretti *et al.* (1997) directly measured fine-structure-changing collisional losses from a cesium type I and type II MOT (Raab *et al.*, 1987), with the trapping light near the  $6s^2S_{1/2}(F=4) \rightarrow 6p^2P_{3/2}(F=5)$  and the repumping light near  $6s^2S_{1/2}(F=3) \rightarrow 6p^2P_{3/2}(F=4)$  for the type I trap and  $6s^2S_{1/2}(F=3) \rightarrow 6p^2P_{3/2}(F=2)$  for the type II trap, by detecting  $D1$  fluorescence emitted on the  $6p^2P_{1/2} \rightarrow 6s^2S_{1/2}$  transition. Measuring the counting rate of  $D1$  photons emitted, the efficiency of detection of both  $D2$  and  $D1$  light, and determining the trap density from the  $D2$  count rate and the spatial extent of the trap, Fioretti *et al.* (1997) derive an absolute value for fine-structure-changing collisions in the cesium MOT. They have examined the sensitivity of fine-structure-changing collisions to different excited-state hyperfine components by modifying the ground-state hyperfine population that starts the process. They fit their data with a model that requires molecular hyperfine optical pumping during the collision. Their measurement of  $\beta_{\text{FCC}}$  ( $2 \times 10^{-12} \text{ cm}^3 \text{ s}^{-1}$ ) and comparison with the previous measurement, Sesko *et al.* (1989), of the total  $\beta$  ( $8 \times 10^{-12} \text{ cm}^3 \text{ s}^{-1}$ ) leads to the conclusion that fine-structure-changing collisions contribute about 25% of the total (FCC+RE) loss rate constant. The Julienne-Vigué theory predicts about equal contributions from fine-structure-changing collisions and radiative escape, but it must be born in mind that the Fioretti *et al.* (1997) experiment was carried out under strong-field conditions (total trap intensity as high as  $150 \text{ mW cm}^{-2}$ ) and Julienne-Vigué is a weak-field theory that neglects hyperfine structure. Therefore it is not too surprising that theory and experiment are not in accord.

#### c. Rubidium trap loss

Wallace *et al.* (1992) carried out the first measurements of trap loss in rubidium, using a MOT similar to

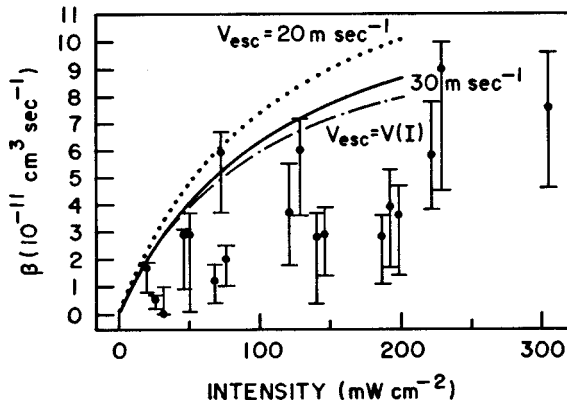


FIG. 28. Measurement of the trap loss rate constant as a function of MOT light intensity. The wider range of light intensity reveals an increase in  $\beta$  with MOT intensity. Dotted, full, and dot-dash curves are theory calculations using the optical-Bloch equation method of Band and Julienne (1992) with different assumptions about the maximum escape velocity of the MOT. The curve  $V_{\text{esc}}=V(I)$  results from a simple model in which the escape velocity is a function of the MOT intensity. Data are from Marcassa *et al.* (1993).

the one employed by Sesko *et al.* (1989) for the study of cesium. The MOT was loaded from a rubidium atomic beam slowed with a frequency-chirped diode laser source, and the trap loss determined by monitoring the atomic fluorescence decay. The trap-loss rate constant  $\beta$  was obtained by fitting the data to

$$\frac{dN}{dt} = -\gamma N - \beta \int_v n^2(r,t) d^3r, \quad (93)$$

which is just Eq. (88) with the loading rate  $L$  set to zero. The trap operates at sufficiently low densities ( $<2 \times 10^{10} \text{ cm}^3 \text{ s}^{-1}$ ) that radiation trapping effects can be ignored (Walker *et al.*, 1990). The rate constant for loss due to collisions with thermal background gas,  $\gamma$ , was constant and fixed by the background pressure of  $\sim 10^{-10}$  Torr. The number of atoms in the trap and the density of the trap are determined from (1) absorption measurements with a weak probe beam, (2) measurement of the excited-state population fraction obtained from selective photoionization of the Rb ( $5p^2P_{3/2}$ ) level, and (3) trap size determined by a digitized charge-coupled device (CCD) camera image. Figure 32 shows  $\beta$  plotted as a function of total trap intensity at a fixed detuning of 4.9 MHz to the red of the trapping transition for both rubidium isotopes,  $^{85}\text{Rb}$  and  $^{87}\text{Rb}$ . The behavior is similar to that of Cs (Sesko *et al.*, 1989), with  $\beta$  decreasing approximately linearly from high trap intensities to a minimum at a few  $\text{mW cm}^{-2}$ , and then increasing sharply as the trap intensity is further reduced. On the high-intensity side of the curve  $\beta$  behavior indicates trap loss due to a combination of radiative escape and fine-structure-changing collisions, although there is no way to separate the contributions of the two processes in this experiment. At low intensity the sharp increase of  $\beta$  is the signature of hyperfine-changing collision. In addition to this general behavior, the most

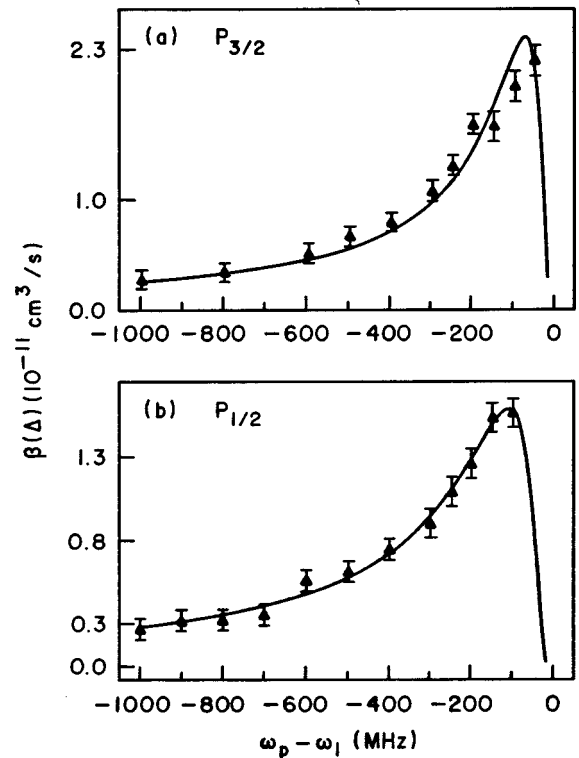


FIG. 29. Trap-loss spectrum in a Na MOT for catalysis laser detuned to the red from both atomic fine-structure asymptotes. From Marcassa *et al.* (1997).

striking feature of the high-intensity branch of the trap-loss curve is a strong isotope effect: the value of  $\beta$  for  $^{85}\text{Rb}$  is always a factor of  $3.3 (\pm 0.3)$  higher than for  $^{87}\text{Rb}$ . Wallace *et al.* (1992) point out that this isotope effect was not anticipated by either the Gallagher-Pritchard or Julienne-Vigué theories; furthermore, since the only significant difference between the two isotopes is their hyperfine structure, it probably results from the influence of long-range molecular hyperfine interactions on the fine-structure-changing collisions and radiative-escape loss mechanisms. The Connecticut group, led by P. L. Gould, also compared their determination of the absolute value of  $\beta$  for both isotopes at a trap intensity of  $10 \text{ mW cm}^{-2}$  to the Julienne-Vigué theory. The measured values are  $\beta = 3.4 \times 10^{-12} \text{ cm}^3 \text{ s}^{-1}$  and  $1.0 \times 10^{-12} \text{ cm}^3 \text{ s}^{-1}$  for  $^{85}\text{Rb}$  and  $^{87}\text{Rb}$ , respectively. The Julienne-Vigué theory calculates  $\beta = 1.7 \times 10^{-11} \text{ cm}^3 \text{ s}^{-1}$ , factors of 5 and 17, respectively, in disagreement with either experimental measurement. Since Wallace *et al.* (1992) quote an uncertainty of only  $\pm 40\%$  in their absolute  $\beta$  measurements, the disagreement between experiment and theory is large and real. In addition to ignoring hyperfine structure, it is important to remember the Julienne-Vigué is a weak-field theory and that the calculation of the fine-structure-changing collisions contribution is quite sensitive to  $P_{XQ}(E,l)$ , the accurate calculation of which, in turn, relies on accurate molecular potential energy curves. The strong sensitivity of the fine-structure-changing collisions probability to the molecular potentials has been examined by Dulieu *et al.*

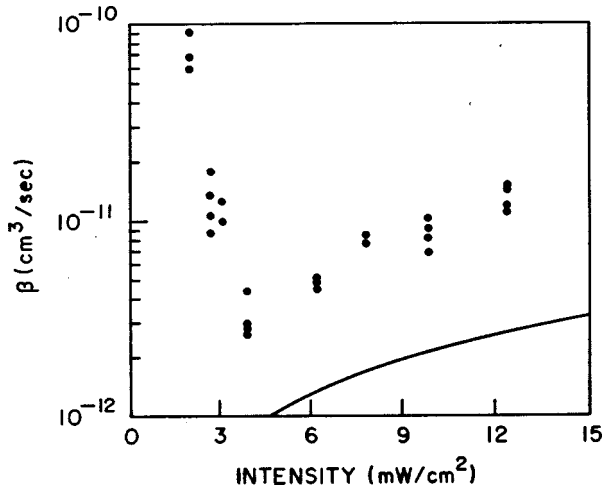


FIG. 30. Trap-loss rate constant  $\beta$  as a function of MOT intensity for Cs collisions: comparison of experiment with GP theory, from Sesko *et al.* (1989).

(1994). At this writing the accord between experiment and theory must be considered unsatisfactory.

On the low-intensity branch of Fig. 32, where  $\beta$  starts to increase due to hyperfine-changing collisions, the isotopic ordering of  $\beta$  reverses, and the trap intensity at which  $\beta$  reaches a minimum differs between the two isotopes by a factor of  $\sim 1.5$ . Since the ratio of the kinetic energy release due to hyperfine-changing collisions from  $^{87}\text{Rb}$  and  $^{85}\text{Rb}$  is  $6835\text{ MHz}/3036\text{ MHz} = 2.25$ , the factor of 1.5 at first appears surprising. However Wallace *et al.* (1992) point out that a MOT contains the atoms by position-dependent forces and velocity-dependent forces. If the velocity-dependent forces control, and if these forces vary linearly with trap intensity, then one would expect the trap-loss ratio to be equal to the ratio of velocities or  $\sqrt{6835\text{ MHz}/3036\text{ MHz}} = 1.5$  in accord with observation. At the very lowest trap intensities  $\beta$

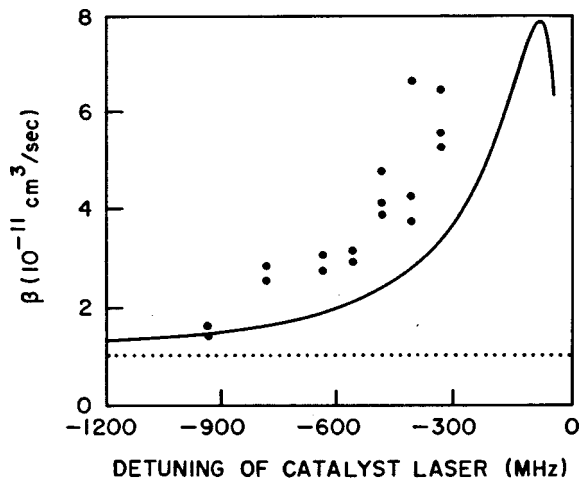


FIG. 31. Trap-loss spectrum in a Cs MOT using a "catalysis" laser (points), and comparison with GP theory (solid line). The dotted line shows the value of  $\beta$  without the "catalysis" laser. From Sesko *et al.* (1989).

levels off, and the Connecticut group concludes that under these conditions all the atoms undergoing the hyperfine-changing collisions process can escape. Therefore the  $\beta$  of this plateau is a measure of the hyperfine-changing collision rate. The measurements show a value of  $\sim 2 \times 10^{-11}\text{ cm}^3\text{ s}^{-1}$ .

At about the same time the Connecticut group was carrying out these rubidium trap-loss isotope studies, another group at the University of Wisconsin, led by T. Walker, started investigating  $^{85}\text{Rb}$ . In contrast to Wallace *et al.* (1992), the results reported by Hoffmann *et al.* (1992) were carried out in a vapor-loaded trap, not an atomic-beam loaded trap, and  $\beta$  was obtained by fitting Eq. (90) to the observed fluorescence loading curves. The Wisconsin group also used a catalysis laser to measure the trap-loss spectrum, i.e.,  $\beta$  as a function of red detuning of the catalysis laser from the trapping transition. Their results are displayed in Fig. 33. They compare their rubidium results to the earlier cesium study (Sesko *et al.*, 1989), and find the following differences: (1)  $\beta$  at the peak of the  $^{85}\text{Rb}$  trap-loss spectrum is about a factor of 3.5 smaller than  $\beta$  at the peak of the Cs trap-loss spectrum, (2) these peaks do not appear at the same detuning for the two species. Cesium  $\beta$  peaks at a detuning  $\approx 450\text{ MHz}$  while  $^{85}\text{Rb}$  peaks  $\approx 160\text{ MHz}$ . (3) Extrapolating their data to  $10\text{ mW cm}^{-2}$  and small detunings, Hoffmann *et al.* (1992) determine  $\beta = (3.6 \pm 1.5) \times 10^{-12}\text{ cm}^3\text{ s}^{-1}$ , a factor of 5 below the Julienne-Vigué calculation but in quite good agreement with the measurement of Wallace *et al.* (1992).

The striking and unexpected isotope effect reported by Wallace *et al.* (1992) stimulated further investigation by the Wisconsin group. Feng *et al.* (1993) carried out trap-loss studies on both rubidium isotopes similar to those already described by Hoffmann *et al.* (1992) for  $^{85}\text{Rb}$ . The trap-loss spectra show that for catalysis-laser detunings outside the excited-state hyperfine structure regime, about 400 MHz to the red of the trapping transition,  $\beta$  for both isotopes is the same. Within the hyperfine region, Feng *et al.* (1993) found approximately the same ratio of  $\beta_{85}/\beta_{87} \approx 3$  as Wallace *et al.* (1992). Furthermore, they observed a double-peaked structure in the  $^{87}\text{Rb}$   $\beta$  at 400 MHz red detuning, and difficulty in making reliable measurements left gaps or holes in the spectrum at detunings near the atomic hyperfine transitions. Figure 34 shows these features of  $^{87}\text{Rb}$  trap loss spectrum. These results clearly demonstrate that the isotope effect as well as the spectral "holes" are associated with trap-loss processes strongly modulated by molecular hyperfine structure. The Wisconsin group details their experimental method and summarizes the results in Hoffmann *et al.* (1994).

The important role of hyperfine structure in trap-loss dynamics demonstrated by the experiments of Wallace *et al.* (1992) and Feng *et al.* (1993) prompted the development of models proposed by Walker and Pritchard (1994) and Lett *et al.* (1995). In essence these studies extend the Gallagher-Pritchard picture of a single attractive excited state to multiple excited states with both attractive and repulsive branches. Figures 35(a) and

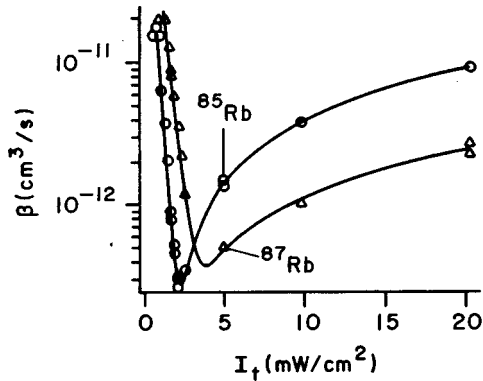


FIG. 32. Trap-loss spectrum for two isotopes of rubidium. Right-hand branch shows trap loss due FCC and RE. Left-hand branch shows trap loss due to HCC. From Wallace *et al.* (1992).

35(b) show the simplest, illustrative case. Potential curves 0 and  $E_1$  represent two closely spaced hyperfine levels of the excited state. The upper curve, 0, shows the familiar  $V(R) = -C_3/R^3$  long-range behavior while the lower level splits into  $\pm C_3/R^3$  corresponding to attractive and repulsive dipole-dipole interaction. Each of the attractive curves gives rise to a Gallagher-Pritchard-like trap-loss spectral profile resulting in an observed “doublet” as a catalysis (probe) laser detunes to the red, indicated in Fig. 35(b). The repulsive curve arising from  $E_1$  mixes with the attractive curve from 0 in a localized region around the crossing point. As the catalysis laser scans through the crossing, population in the attractive level leaks onto the repulsive curve, effectively rerouting scattering flux away from radiative escape and fine-structure-changing trap-loss processes occurring at smaller  $R$ . The result is hole burned in the trap-loss spectrum shown schematically by the dotted curve in Fig. 35(b). Lett *et al.* (1995) generalized this model to multiple levels with multiple crossings. In the case of  $^{87}\text{Rb}$ , for example, three hyperfine levels ( $F' = 3, 2, 1$ ) can be excited from the  $F = 2$  ground state. Very careful new trap-loss measurements were carried out in  $^{85}\text{Rb}$  right around the detuning region where structure in the trap-loss spectrum was expected. Figure 36 shows the results of these new measurements together with the former data of Hoffmann *et al.* (1992) and the hyperfine-structure model using  $2_u$  potential parameters and the Landau-Zener avoided-crossing probability  $P_{LZ} = 0.6$ . The agreement between the experimental points and the model appears quite satisfactory. Attempts to fit the data using long-range potentials other than the  $2_u$  in the model cannot reproduce consistently the data of Hoffmann *et al.* (1992) and these new results reported by Lett *et al.* (1995). Further application of the model to the  $^{87}\text{Rb}$  trap-loss data of Feng *et al.* (1993) also shows good agreement, and the model is successful with Cs data (although a printing error in Fig. 8 of Lett *et al.*, (1995), does not actually permit the comparison in that article; see, however, Corrigendum, 1995). The application of this hyperfine-level avoided crossing model leads to two major conclusions: (1) structure in the trap-loss spec-

trum is due to excitations of multiple hyperfine levels and avoided crossings between them, and (2) the major trap-loss mechanism is long-range radiative escape on the  $2_u$  potential curve. However, we must caution that using the molecular Hund’s case (c) symmetry label  $2_u$  for potential curves in a region of strong hyperfine-induced mixing is unwarranted. These results do suggest that a state characterized by weak optical coupling is implicated in the trap-loss mechanism.

Peters *et al.* (1994) greatly simplified the interpretation of trap-loss data by measuring  $\beta$  from collision partners excited near the  $\text{Rb}(5p^2P_{1/2}) + \text{Rb}(5s^2S_{1/2})$  asymptote. Since most hyperfine-level curve crossings are eliminated and the spacing between the levels is large, all of the attractive hyperfine levels converging on the  $\text{Rb}(5s^2S_{1/2}; F=2) + \text{Rb}(5p^2P_{1/2}; F'=1)$  will closely follow a  $C_3/R^3$  power law and their contributions to the total trap-loss rate constant should be simply additive. Furthermore, trap loss contributions to the red of the  $5p^2P_{1/2}$  asymptotes can only be due to the radiative escape process since energy conservation closes the fine-structure-changing collisions channel. The results shown in Fig. 37 confirm that under these simplified conditions there is no discernible isotope effect between  $^{85}\text{Rb}$  and  $^{87}\text{Rb}$ , that the Gallagher-Pritchard model works fairly well, but that multiple orbiting of the collision partners must be included to obtain good agreement between the measurements and the model. Another benchmark is the position of the peak in the trap-loss spectrum. For hyperfine levels converging on the  $\text{Rb}(5p^2P_{3/2}) + \text{Rb}(5s^2S_{1/2})$  asymptote the Gallagher-Pritchard model predicts this peak to be near a red detuning of about 115 MHz. Unfortunately this is also the region where curve-crossing and interactions among the hyperfine levels complicate the trap-loss spectrum. From the calculated shapes of the long-range potentials converging on the  $\text{Rb}(5s^2S_{1/2}; F=2) + \text{Rb}(5p^2P_{1/2}; F'=1)$  asymptote, however, Peters *et al.* (1994) calculate that the trap-loss peak should occur at about 25 MHz red detuning with no complicating hyperfine interactions to cloud the model prediction. Probing the trap with the “catalysis” laser so close to the trapping transition unfortunately leads to such strong trap perturbations that trap-loss measurements become unreliable. Therefore the Wisconsin group could not apply their measurement technique to test this particular prediction of the Gallagher-Pritchard model.

Very recently Sanchez-Villicana *et al.* (1996) have demonstrated a flux enhancement effect in ultracold collisions by comparing trap-loss rate constants in an atomic-beam-loaded rubidium MOT with trap and probe lasers present simultaneously or alternately and with the probe laser tuned as far as 1 GHz to the red of the MOT trapping transition. Figure 38 outlines the basic process. Scattering flux enters the collision on the  $5S + 5S$  ground state and is excited by the MOT laser at  $R_t$  (red detuning  $\sim \Gamma$ ) to one of the attractive  $-C_3/R^3$  potentials converging on the  $5S + 5P$  asymptote. The excited flux accelerates and spontaneously relaxes back to the ground state with increased kinetic energy, enabling

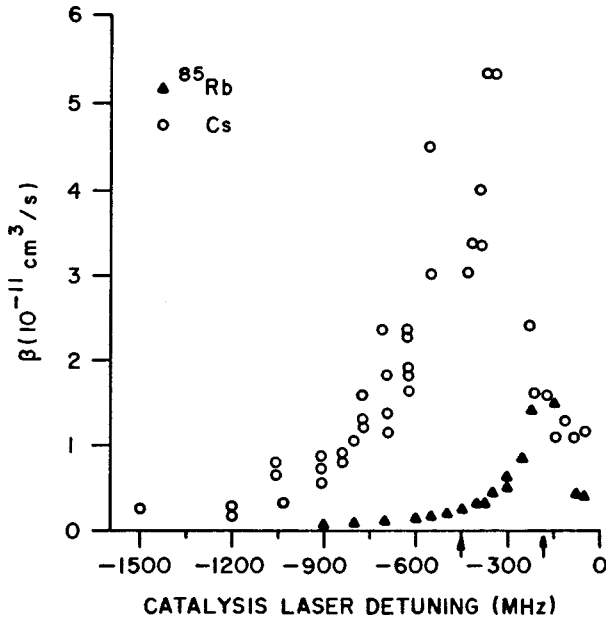


FIG. 33. Trap-loss spectrum of  $^{85}\text{Rb}$  measured by the Wisconsin group and compared to trap-loss spectrum of Cs. From Hoffmann *et al.* (1992).

higher partial-wave components to overcome their angular momentum barriers at closer internuclear separation. At some near-zone Condon point  $R_C$  (red detuning  $\sim 50\text{--}150\ \Gamma$ ) a probe laser reexcites the flux to the  $-C_3/R^3$  potential where it may undergo an inelastic trap-loss interaction (e.g., a short-range curve crossing leading to a fine-structure change). Sanchez-Villicana *et al.* (1997) measure an enhancement in the trap-loss constant  $\beta$  due to the combined effect of the trap and probe lasers by defining an enhancement factor  $\eta$ ,

$$\eta = \frac{\beta_{t+p} - \beta_t}{\beta_p}, \quad (94)$$

which is the difference between the trap-loss constant with both beams present simultaneously or alternately. Note that if there is no combined effect, then  $\eta$  would remain equal to one. This flux enhancement process is

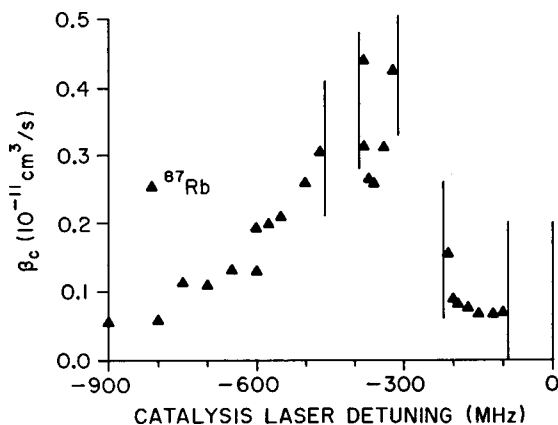


FIG. 34. Trap-loss spectrum of  $^{87}\text{Rb}$  showing “holes” due to hyperfine structure. From Feng *et al.* (1993).

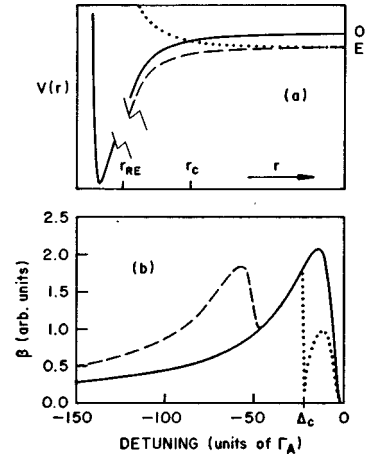


FIG. 35. Model of the influence of hyperfine structure on trap-loss spectra. From Lett *et al.* (1995).

significant because it might influence the results of any experiment where trap and probe beams are present simultaneously. The Connecticut group has also very recently reported a comprehensive study of trap-loss collisions in the  $^{85}\text{Rb}$  and  $^{87}\text{Rb}$  covering a wide range of trap parameters (Gensemer *et al.*, 1997).

#### d. Lithium trap loss

Although collisional trap loss occurs for all alkali species, lithium shows two unique features. First, the excited-state hyperfine structure is inverted with  $2p^2P_{3/2}(F'=3)$  lying lower than  $2p^2P_{3/2}(F'=2,1,0)$ . Therefore long-range attractive molecular states correlating to the  $2s^2S_{1/2}(F=2) + 2p^2P_{3/2}(F'=3)$  asymptote are less likely to be perturbed by hyperfine interactions and avoided crossings with higher-lying molecular states. Second, the fine-structure splitting,  $\Delta E_{\text{FS}}$ , between the  $2p^2P_{3/2}$  and  $2p^2P_{1/2}$  levels is sufficiently small that, by varying the trapping laser intensity, the MOT trap depth can be made comparable to the fine-structure-changing collisions energy release. In temperature units  $\Delta E_{\text{FS}}/k_B$  is only 0.48 K. A fine-structure-changing collision results in each atom leaving the binary encounter with one-half the exoergic energy. If the trap depth  $E_T$  is shallower than this  $\frac{1}{2}\Delta E_{\text{FS}}$ , then each atom can escape the trap and fine-structure-changing collisions becomes an important loss mechanism. However, if the trap deepens below  $\frac{1}{2}\Delta E_{\text{FS}}$ , the atoms cannot escape and the fine-structure-changing collisions mechanism no longer functions as a trap-loss process. In this situation, the remaining loss from radiative escape may be studied without the influence of fine-structure-changing collisions.

Kawanaka *et al.* (1993) reported the first measurement of  $\beta$  for  $^7\text{Li}$ . The experiment implemented an unusual four-beam MOT in which three of the beams point toward the vertex of an equilateral pyramid and the fourth beam counterpropagates along the axis of the pyramid, itself aligned with a trap-loading Li beam. The axial counterpropagating laser beam serves the double role of atomic beam slower and MOT confining laser. Total intensity in the MOT laser was  $30\ \text{mW cm}^{-2}$ , and

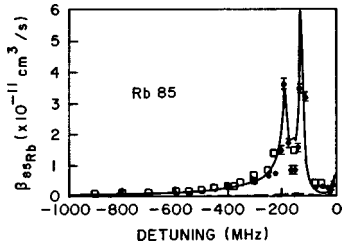


FIG. 36. Structure in the trap-loss spectrum of  $^{85}\text{Rb}$ , showing the influence of hyperfine structure. Solid curve is a model calculation. Full circles are the measurements of Lett *et al.* (1995), and the open squares are measurements from Hoffmann *et al.* (1992).

to change the trap depth, the MOT beams were on-off modulated at 500 kHz with the “on” time varying from  $\sim 30$  to 100% duty ratio. Values of  $\beta$  as a function of MOT duty ratio were extracted from curve fitting fluorescence decay. The trap was operated with a small number of atoms, such that the spatial density profile was always close to a Gaussian profile. As the duty ratio (or trap depth) was varied,  $\beta$  exhibited the behavior shown in Fig. 39. The value of  $\beta$  appears to show a plateau  $\sim 3 \times 10^{-12} \text{ m}^3 \text{ s}^{-1}$  at the minimum duty ratio of  $\sim 30\%$  (shallow trap). As the duty ratio increases (deeper trap) this value decreases rapidly about one order of magnitude, reaching a minimum value of  $\sim 3.2 \times 10^{-13} \text{ cm}^3 \text{ s}^{-1}$  at  $\sim 65\%$  duty ratio. As the MOT laser “on” duty ratio increases above this minimum point to 100%,  $\beta$  increases only slightly to  $\sim 5 \times 10^{-13} \text{ cm}^3 \text{ s}^{-1}$ . Kawanaka *et al.* (1993) interpret this  $\beta$  behavior as showing the contributions of both fine-structure-changing collisions and radiative escape below the minimum, but at higher duty ratios (deeper traps) the fine-structure-changing collisions process no longer contributes. Therefore above about 65% duty ratio the only source of collisional trap loss is radiative escape. If this interpretation is correct, then the duty ratio at which the minimum  $\beta$  occurs must be equivalent to  $E_T = \frac{1}{2} \Delta E_{\text{FS}}$ . Kawanaka *et al.* (1993) carried out a direct measurement of the trap depth at 100 percent duty ratio by applying the kick-and-recapture technique described by Raab *et al.* (1987). This measurement showed that the MOT is anisotropic with a depth of 0.64 K along the radial direction and 1.3 K along the axial direction. The trap-modulation technique effectively varies the average MOT intensity and therefore the average trap depth. A MOT operates with two kinds of restoring forces: proportional to position and proportional to velocity. If the position-dependent conservative force dominates, then the trap depth should be linear with the average MOT intensity. If the velocity-dependent dissipative force dominates then the trap capture ability should vary as the square root of the average MOT intensity. Given the direct measurement of the trap depth at 100% duty ratio and assuming a square-root dependence,  $\frac{1}{2} \Delta E_{\text{FS}}$  corresponds to about 60% duty ratio, near the minimum  $\beta$  and roughly consistent with the interpretation of a radiative-escape-only trap loss at duty ratios above 60–65%. It should be born in mind that the anisotropy of

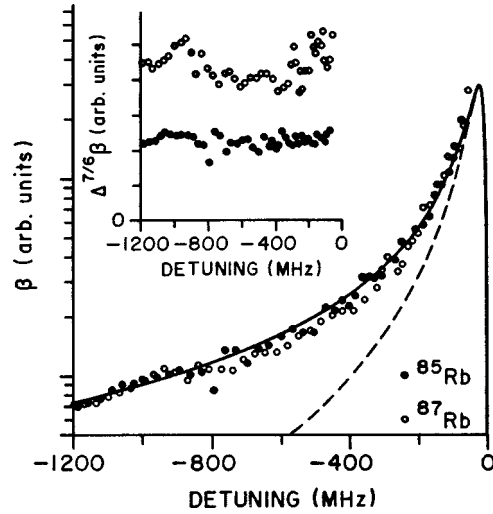


FIG. 37. Rubidium trap loss spectra from the Wisconsin group showing that no isotope effect is measurable for trap-loss collisions from the  $5p^2P_{1/2} + 5s^2S_{1/2}$  asymptote and that multiple orbiting must be included in any model of the trap loss process. Solid line is a model calculation including multiple orbits; dashed line shows the same model with a single orbit. From Peters *et al.* (1994).

the trap was not explicitly taken into account in these measurements. It should be further noted that value of  $\beta$  reported in the radiative-escape-only regime,  $\sim 5 \times 10^{-13} \text{ cm}^3 \text{ s}^{-1}$ , is about one order of magnitude greater than predicted either by the Gallagher-Pritchard or Julienne-Vigué models.

Ritchie *et al.* (1995) carried out another study of collisional trap loss in a  $^7\text{Li}$  MOT, measuring  $\beta$  over a wider range of intensities and several detunings. This study carefully took account of the anisotropy of the MOT trap depth by modeling and simulating atom escape velocities as a function of angle, intensity, and de-

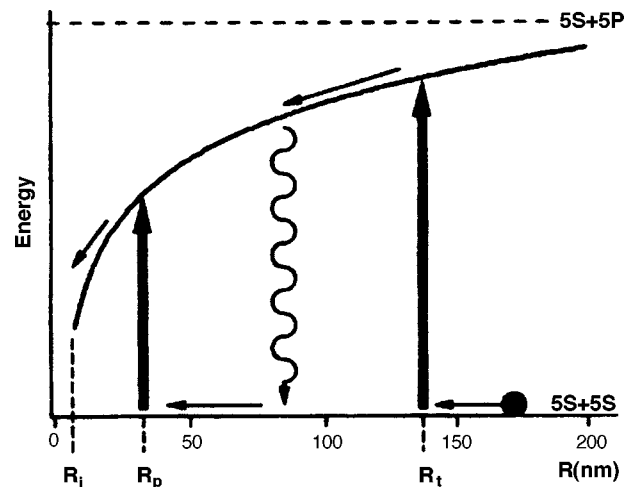


FIG. 38. Schematic of flux enhancement. The first excitation at  $R_t$  puts flux on the long-range  $C_3/R^3$  attractive potential. This excitation effectively pulls added flux into the small  $R$  region where it is probed by the second excitation at  $R_p$ . From Sanchez-Villicana *et al.* (1996).

tuning. In a separate study Ritchie *et al.* (1994) develop and examine this model in detail. The MOT setup used the conventional six-way orthogonal laser beam arrangement and was loaded from an optically-slowed atomic beam. The trap-loss rate constant  $\beta$  was extracted from fits to fluorescence decay after the loading was shut off. Figure 40 shows the measured  $\beta$  for four values of laser detuning and a range of intensities. For each of the four detunings the measured loss rate was largest at small intensities and decreased with MOT intensity until reaching a distinct minimum, which occurred at a different intensity for each detuning. Similar to the interpretation of Kawanaka *et al.* (1993), this  $\beta$  minimum is attributed to the suppression of fine-structure-changing collisions loss. At higher values of intensity the loss is due entirely to radiative escape. Also, shown in Fig. 40 are the results of an optical-Bloch-equations-theory calculation (Julienne *et al.*, 1994) for radiative escape trap-loss rates in Li. The optical-Bloch-equations approach is appropriate because the MOT intensities in this study reach as high as  $120 \text{ mW cm}^{-2}$  where weak-field theories such as Gallagher-Pritchard or Julienne-Vigué cannot be applied. In addition the optical-Bloch-equations theory was found not to fail for Li as it does for the heavier alkalis (Julienne *et al.*, 1994). The optical-Bloch-equations theory predicts a strong dependence on trap depth with  $\beta_{\text{RE}}$  scaling as  $E_T^{-3.0}$ , and therefore a thorough understanding of trap depth spatial and intensity dependence is crucial. To that end Ritchie *et al.* (1994) developed a model and carried out trajectory simulations of Li atoms subject to various conditions of intensity and detuning in the MOT. These simulations revealed that the trap depth  $E_T$  was highly dependent on  $\theta, \phi$  the polar and azimuthal angles with respect to the MOT symmetry axis. From the model spatial dependence Ritchie *et al.* (1995) were able to calculate  $\beta$  averaged over the different trap directions,

$$\beta = \frac{\beta_0}{4\pi} \int \left( \frac{E_0}{E_T} \right) d\Omega \quad (95)$$

where  $\beta_0$ ,  $E_0$  are the trap-loss rate constant and trap depth in the shallowest direction. The result showed a rather startling anisotropy with  $\beta/\beta_0 = 0.23 \pm 0.02$ , relatively independent of intensity and detuning. The graphs in Fig. 40 plot this averaged  $\beta$  as well as the calculated intensity  $I_c$  required to recapture an atom released in the shallowest direction with a kinetic energy equal to  $\frac{1}{2}\Delta E_{\text{FS}}$ . Except for the largest detuning, the agreement between the calculated  $I_c$  and the breakpoint in the  $\beta$  vs  $I$  plots (where  $\beta_{\text{FCC}} \rightarrow 0$ ) inspires confidence in the basic correctness of the model of Ritchie *et al.* (1994). In contrast, while the optical-Bloch-equation calculation gets about the correct value for  $\beta_{\text{RE}}$  near  $I_c$ , the predicted and observed trap depth dependences go in opposite directions. The culprit is probably molecular hyperfine structure, ignored in the application of the optical-Bloch-equation theory. At this writing the disagreement remains unresolved. It is, however, interesting to note that Ritchie *et al.* (1994) find that the increase in  $\beta_{\text{RE}}$

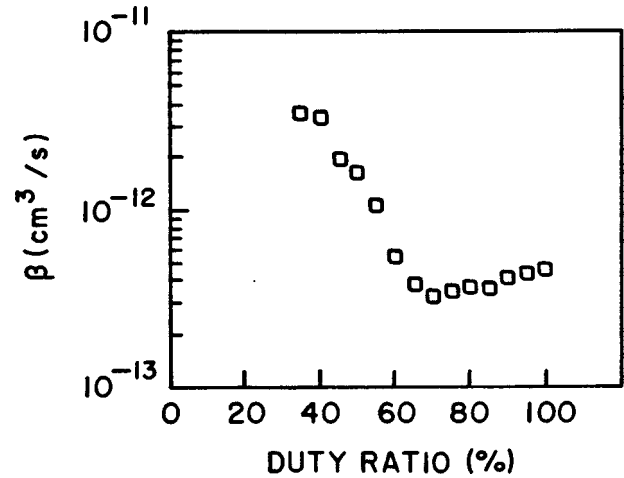


FIG. 39. Trap-loss rate constant  $\beta$  as function of “trap depth” (MOT duty ratio) for lithium atoms. Rapidly rising left-hand branch thought to be due to fine-structure-changing collisions and radiative escape, but as trap becomes deeper (increasing duty ratio) fine-structure-changing collisions no longer contributes. From Kawanaka *et al.* (1993).

with MOT intensity above the breakpoint can be well fit to a function proportional to the product of ground and excited state atomic fractions and that this fitting works over the range of detunings from  $\Delta = -2.3\Gamma$  to  $-4.1\Gamma$ . Such a fitting is more consistent with a Gallagher-Pritchard or Julienne-Vigué picture of radiative escape since the quasistatic theories should not be very sensitive to trap depth or detuning. At the high trap intensities of these experiments, however, the basic weak-field assumption of Gallagher-Pritchard and Julienne-Vigué cannot possibly be appropriate and the “agreement” is probably just fortuitous. Further work in application of theory is clearly needed.

#### e. Potassium trap loss

Potassium is the last stable atom in Group IA of the periodic table to be successfully confined in a MOT and on which cold-collisions have been investigated. The peculiarities of K atomic structure have precluded a conventional approach to trap-loss measurements. Williamson and Walker (1995) reported the first successful potassium MOT and the first studies of exoergic trap loss. The Wisconsin group trapped two isotopes,  $^{39}\text{K}$  and  $^{41}\text{K}$ , with natural isotopic abundances of 93 and 7% respectively; however, the very small excited-state hyperfine splittings of these isotopes required a modification of conventional MOT technique. The unusual fact is that, in the case of  $^{39}\text{K}$ , the splitting of the entire excited-state hyperfine manifold is only 33 MHz, and the separation between  $4p^2P_{3/2}(F'=3)$  and  $4p^2P_{3/2}(F'=2)$  is only 21 MHz. In the case of  $^{41}\text{K}$  the excited hyperfine manifold covers only 17 MHz. With a natural linewidth of 6.2 MHz, overlapping transitions from the  $4s^2S_{1/2}(F=2)$  ground state to adjacent hyperfine levels would lead to considerable optical pumping and heating as spontaneous emission populated the lower  $F=1$

ground state. To overcome this problem Williamson and Walker (1995) tuned the trapping and repumper lasers to the red of the entire hyperfine manifold, essentially treating the  $^2P_{3/2}$  fine-structure level of  $^{39}\text{K}$  as an unresolved line with  $\sim 30$  MHz width. Although optical pumping “population leakage” will certainly be higher when the maximum  $F|M_F|$  state cannot be populated uniquely, this tactic has at least the advantage that the capture range of K atom velocity extends to  $30\text{ ms}^{-1}$  an increase of about a factor of five over the capture range for Na. The increase in velocity capture range increases the MOT loading rate and partially compensates for optical pumping losses. The Wisconsin potassium MOT operates at high light intensity ( $470\text{ mW cm}^{-2}$  for  $^{39}\text{K}$ ) and with a large number of trapped atoms such that the loading proceeds mostly at constant density. For the  $^{41}\text{K}$  the MOT intensity goes as high as  $530\text{ mW cm}^{-2}$  with large beam diameter of 0.6 cm. Fitting trap-loading fluorescence curves to Eq. (90) yields the total loss rate constant  $\Gamma(n) = \gamma + \beta n$  where  $\gamma$  is the rate constant for collisions with hot background gas and  $\beta$  is the familiar trap loss rate constant for ultracold potassium collisions. The  $\beta$  rate constant is then determined by measuring the density dependence of the total trap loss rate,  $\Gamma$  at fixed detuning. The slope of this plot,  $d\Gamma/dn$ , yields  $\beta$ ; and this program is carried out over a range of detunings. Figure 41 shows the variation of  $\beta$  with the detuning  $\Delta$  for the  $^{39}\text{K}$  MOT. Although some variation of  $\beta$  with detuning is evident, the range is considerably narrower than the typical trap-loss spectra reported earlier by the Connecticut and Wisconsin groups for rubidium. Obtaining the detuning dependence of  $\beta$  from the density plots is clearly much more arduous than the using a catalysis laser so the difference in detuning range is not surprising. Williamson and Walker (1995) report that  $^{41}\text{K}$  shows even less detuning dependence than  $^{39}\text{K}$ . The trap-loss collision dynamics of K is much less well-studied than the other alkalis and investigations must continue to clarify the role played by the differences in hyperfine structure.

Another study of the dependence of trap-loss rate of a potassium MOT as a function of trap laser intensity was recently performed by Santos *et al.* (1996) using a MOT loaded from vapor. The loading measurements were carried out under conditions of constant trap density. To be able to measure a large range of intensities without compromising the trap performance, the sudden-change-of-intensity technique was used: the trap was loaded at high intensity, after which a neutral density filter was mechanically introduced, producing a low intensity condition. The transition between the two intensities regime causes a transient decay in the number of atoms that permits determination of  $\beta$ . The values of  $\beta$  measured for several intensities are plotted in Fig. 42, where each point is a result of fifteen independent measurements. From high intensities down to  $10\text{ mW cm}^{-2}$ ,  $\beta$  shows only small variation with a possible tendency of increasing with intensity. In this regime, indicated by a dashed line on Fig. 42, radiative escape and fine-structure-changing collisions are dominant losses. At about

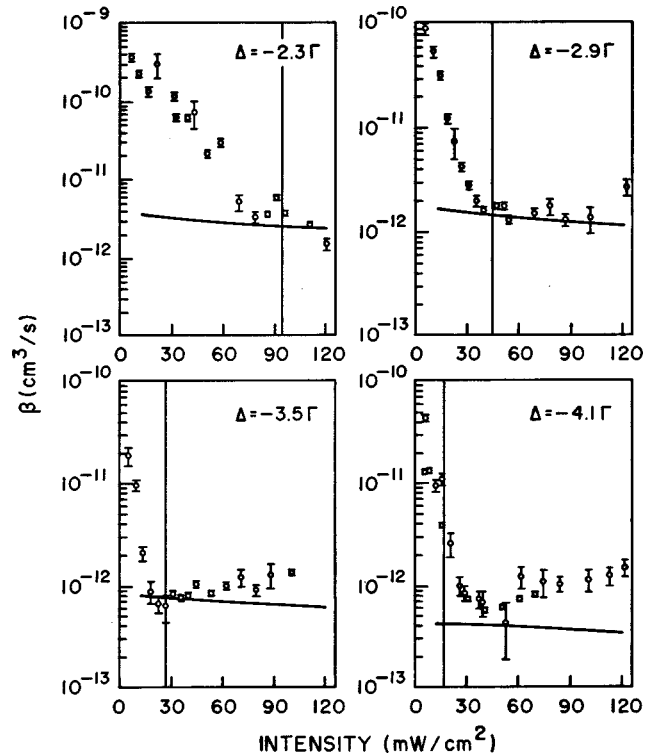


FIG. 40. Trap-loss rate constant  $\beta$  for four different detunings and a range of intensities in the Rice group’s Li MOT. The vertical lines in each plot denote  $I_c$  the calculated critical intensity required to recapture an atom released in the shallowest direction. From Ritchie *et al.* (1995).

$10\text{ mW cm}^{-2}$  an abrupt increase in  $\beta$  is observed, which is associated with hyperfine-changing collisions as observed in other systems. The HCC regime for trap loss is indicated in Fig. 42 as a dotted line.

#### f. Sodium-potassium mixed-species trap loss

All experiments and theories about exoergic collisions in atomic traps have considered only homonuclear systems. Santos *et al.* (1995) recently demonstrated that two different alkalis (Na/K) could be cooled and confined in the same MOT. This experiment opens the study of heteronuclear ultracold exoergic collisions.

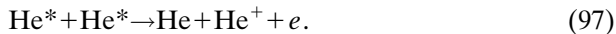
The mixed-alkali MOT of Santos *et al.* (1995) uses a glass vapor cell that contains a mixture of Na/K vapor at room temperature. The trapping laser beams for both alkalis (589 nm for Na and 766 nm for K) are combined using dichroic mirrors and enter the MOT cell copropagating. The optimum trapping conditions are similar to each alkali individually considered. Fluorescence detection measures the number of trapped atoms and a CCD camera measures the spatial distribution of each species. The sodium atomic cloud is located within the larger potassium cloud. To investigate the inter-species cold collision effects, Santos *et al.* (1995) measured the loading of the sodium trap in the presence and absence of the cold potassium cloud. As the sodium trap loaded, the net loading rate is expressed as

$$\frac{dN_{\text{Na}}}{dt} = L - \gamma N_{\text{Na}} - \beta n_{\text{Na}} N_{\text{Na}} - \beta' n_{\text{K}} N_{\text{Na}}. \quad (96)$$

where  $\gamma N_{\text{Na}}$  is the collision rate of trapped Na with hot background gas (both Na and K). Observing the transient behavior in a regime of constant density for both species, one can measure  $\beta'$  which is the cross-species trap-loss collision rate. The measured value for Na/K was  $\beta' = 3.0 \pm 1.5 \times 10^{-12} \text{ cm}^3 \text{ s}^{-1}$ . The loss-rate constant for Na/Na collisions was previously reported by Marcassa *et al.* (1993) to be  $\beta = 3 \pm 1 \times 10^{-11} \text{ cm}^3 \text{ s}^{-1}$ , about one order of magnitude larger than  $\beta'$  due to Na/K collisions. The Brazilian group, led by V. S. Bagnato, rationalized the marked difference by noting that the long-range, excited-state molecular potential in NaK arises from a *nonresonant* dipole-dipole interaction and varies only as  $-C_6/R^6$  instead of the familiar  $-C_3/R^3$  as in the homonuclear case. They argued that the Na/K atom pairs excited at long range will experience much less acceleration along their line of centers with consequent reduction in the survival probability factor [see, for example, Eq. (78) or (81)] of the rate constant. An alternative interpretation could be that the  $-C_6/R^6$  interaction implies a much reduced phase space available for the initial excitation due to the much smaller Condon point.

#### g. Rare-gas metastable loss in MOTs and optical lattices

Rare gas metastable atoms can also be trapped in MOTs and give rise to trap loss by Penning or associative ionization collisions. Bardou *et al.* (1992) have carried out an unusual variation on the trap-loss experiment by decelerating a beam of helium metastable atoms,  $\text{He}(2^3S_1)$ , and capturing the slowed atoms in a MOT. The cooling transition is between the  $2^3S_1$  “ground state” and the  $2^3P_2$  excited state ( $\lambda = 1.083 \mu\text{m}$ ). They carried out trap-decay measurements by shutting off the loading beam and observing the non-exponential decay of the *ions* rather than the usual fluorescence. By fitting the usual trap-loss equations to the ion decay curves, they determined a trap loss rate from Penning ionization,



The MOT contains a significant fraction of  $2^3P_2$  as well as  $2^3S_1$  so the  $\text{He}^*$  collisions could be between any combination of these two species. Bardou *et al.* determine  $\beta = 7_{-5}^{+21} \times 10^{-8} \text{ cm}^3 \text{ sec}^{-1}$  which is a remarkably big number. In fact the formula—Eq. (48), given in Julienne and Mies (1989)—calculated from the S-matrix unitarity condition, shows that an upper bound to the Penning ionization rate constant for collisions between  $\text{He}(^3S_1)$  atoms approaching on the  $^1\Sigma_g^+$  molecular state will be  $2 \times 10^{-9} \text{ cm}^3 \text{ sec}^{-1}$  at  $T_{\text{MOT}} = 1 \text{ mK}$ . The fact that the measured  $\beta$  is more than an order of magnitude higher than the *s*-wave unitarity limit may mean that collisions between  $\text{He}(^3S_1)$  and  $\text{He}(^3P_2)$  play an important role. Julienne *et al.* (1993) confirmed this conjecture by showing that the unitarity limit increases by a factor of  $(l_{\text{max}} + 1)^2$  where  $l_{\text{max}}$  partial waves are captured by the ex-

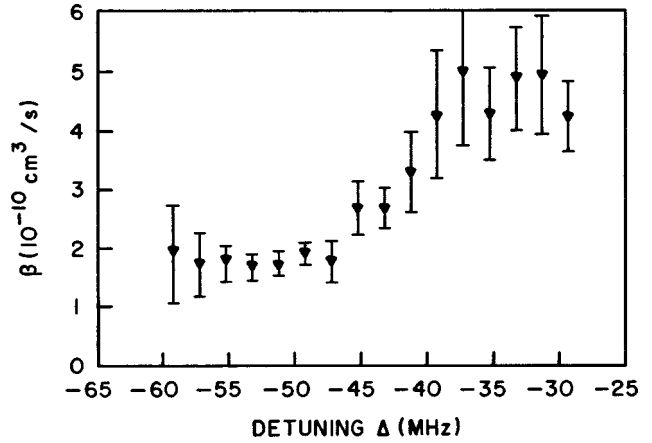


FIG. 41. Trap-loss spectrum of  $^{39}\text{K}$  in the potassium MOT of the Wisconsin group. From Williamson and Walker (1995).

cited state. At 1 mK  $l_{\text{max}}$  is about 5. Bardou *et al.* probed the role of the excited state by modulating the trapping light and observing the effect on the ion production rate. The decline was dramatic, and by varying the density in the MOT they were able to determine  $\beta_P = 14 \times 10^{-8} \text{ cm}^3 \text{ sec}^{-1}$ . Therefore their measured  $\beta = 7_{-5}^{+21} \times 10^{-8} \text{ cm}^3 \text{ sec}^{-1}$  is an average of  $\beta_S$  and  $\beta_P$ , weighted by the product of relative ground-state population for *S-S* collisions and the product of ground- and excited-state population for *S-P* collisions. Both kinds of collisions contribute a loss-rate constant several orders of magnitude greater than fine-structure-changing collisions or radiative escape in the alkalis. As a consequence Bardou *et al.* report a steady state density in the MOT of about  $10^8 \text{ cm}^{-3}$ , about two orders of magnitude lower than the density of a typical alkali MOT. Very recently Mastwijk *et al.* (1998) have reported a new measurement of the rate constant for Penning and associative ionization in metastable He trapped in a MOT. Their reported result,  $(1.9 \pm 0.8) \times 10^{-9} \text{ cm}^3 \text{ s}^{-1}$ , is about two orders of magnitude smaller than that of Bardou. At this writing the discrepancy has not been resolved. Katori and Shimizu (1994) and Wahlhout *et al.* (1995) have also measured trap-loss rates of ionizing collisions in metastable Kr and Xe traps.

An interesting variation on “trap loss” in ionizing collisions is the modification of collision rates in optical lattices which constrain atomic motion in a periodic potential. Kunugita *et al.* (1997) measured a reduced collision rate in a Kr lattice and Lawall *et al.* (1998) measured both suppression and enhancement in a Xe lattice. Boisseau and Vigué (1996) discuss how *very* long-range molecular interactions in a light field might be modified in optical lattices. Finally we note that Katori *et al.* (1995) have measured a quantum statistical effect on ionizing collision rates of metastable Kr. The collision rate for the spin-polarized fermionic isotope  $^{83}\text{Kr}$  decreased relative to the collision rate in the unpolarized gas. The decrease was attributed to the threshold laws for *p*-waves (which contribute to the spin-polarized case) that differed from those for *s* waves (which only-

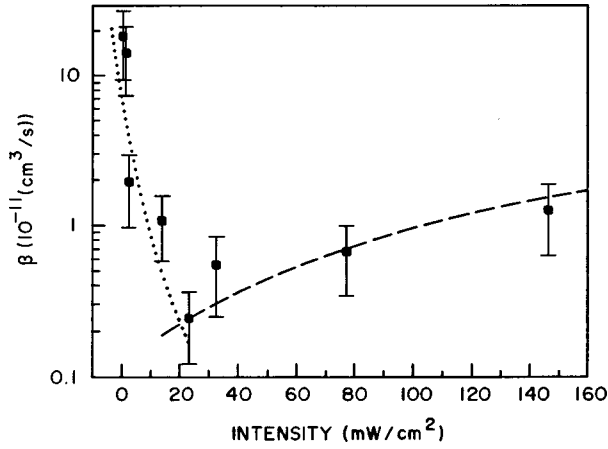


FIG. 42. Intensity dependence of the trap-loss rate constant  $\beta$  in the São Carlos potassium MOT. From Santos *et al.* (1996).

contribute in the spin-unpolarized case). For a discussion of these threshold laws see Sec. III.B.

### B. Ground-state trap-loss collisions

Trap-loss processes such as radiative escape and fine-structure-changing collisions always start with collision partners approaching on an excited long-range attractive molecular potential. Collisions on the molecular ground state divide into two categories: elastic collisions and hyperfine-changing collisions. Exoergic hyperfine-changing collisions can also lead to loss if the trap is made sufficiently shallow such that the velocity gained by each atom from the hyperfine-changing collisions kinetic energy release exceeds the maximum capture velocity of the trap.

#### 1. Hyperfine-changing collisions

If atoms have nuclear spin  $\vec{I}$  then the coupling of this nuclear spin to the total electronic angular momentum  $\vec{J}$  results in hyperfine states  $\vec{F} = \vec{J} + \vec{I}$  with projection  $M_F$  along some axis of quantization. In binary collisions this axis is always taken to be the line joining the two nuclei with the hyperfine states of the two partners labeled  $F_1 M_{F_1}$  and  $F_2 M_{F_2}$ . The manifold of molecular hyperfine states  $\vec{F}_m$  is constructed from vector pairing of the atomic states in the usual way,  $\vec{F}_m = \vec{F}_1 + \vec{F}_2$ . In the asymptotic limit of internuclear separation the molecular hyperfine states are products of the atomic hyperfine states,  $|F_1 M_{F_1}\rangle |F_2 M_{F_2}\rangle$ , and their energy levels are the sum of their constituent atomic hyperfine energies. Figure 4 illustrates these molecular potentials near their asymptotic limit for the case of  $^{87}\text{Rb}$ . It is customary to label the asymptotic energy levels by  $F_1 F_2$ . For example the ground state of Na splits into two hyperfine levels,  $F=1, 2$  by the vector coupling of  $J=1/2$  to the nuclear spin  $I=3/2$ . The energy difference between the two hyperfine levels is 1772 MHz. The molecular hyperfine asymptotes are labeled  $F_1 F_2 = 1+1, 1+2, 2+2$  with each asymptote separated by 1772 MHz. If during a collisional encounter the exit channel lies on a lower hyper-

fine level than the entrance channel, the energy difference appears as the kinetic energy of the receding partners. In homonuclear collisions each partner receives half the kinetic-energy release and an increment in velocity  $v_{\text{HCC}} = \sqrt{\Delta E_{\text{HCC}}/m}$ . If this velocity increment exceeds the capture velocity of the MOT, the hyperfine-changing collision leads to trap loss.

Two physical processes govern the change of hyperfine level: spin exchange and spin dipole-dipole interaction. Spin exchange occurs when the charge clouds of the two colliding partners begin to overlap. The electron spins  $\vec{S}_1, \vec{S}_2$  decouple from the nuclear spins and recouple to form molecular electron spin states  $\vec{S} = \vec{S}_1 + \vec{S}_2$ . The atomic nuclear spins also recouple to form molecular nuclear spin states  $\vec{I} = \vec{I}_1 + \vec{I}_2$  such that  $\vec{F}_m = \vec{S} + \vec{I}$  is conserved and  $M_F = M_{F_1} + M_{F_2}$ . In the exchange region the asymptotic hyperfine states  $|F_1 M_{F_1}\rangle |F_2 M_{F_2}\rangle$  transform to linear combinations that lead to a finite probability that the postcollisional population of asymptotic states differs from the entrance channel. In contrast to the exchange interaction the long-range spin-dipole interaction is usually weaker by several orders of magnitude, because it derives from relativistic spin-dependent forces proportional to the square of the fine-structure constant. Later we will enlarge the discussion of ground-state collisions and these physical processes in the context of Bose-Einstein condensates (Stoof *et al.*, 1988). For the present discussion of trap-loss processes it suffices to note that in a MOT endoergic inelastic channels are generally closed by energy conservation, but the exoergic hyperfine-changing collisions channels can lead to trap loss.

#### a. Cesium and rubidium

Earlier we noted that Sesko *et al.* (1989) observed a rapid increase in  $\beta$  as the intensity of their Cs MOT dropped below  $4 \text{ mW cm}^{-2}$ . They interpreted this loss as due to hyperfine-changing collisions, but could not infer directly  $\beta_{\text{HCC}}$ , the rate constant for the hyperfine-changing collisions process itself, because even at the lowest MOT laser intensity the trap loss  $\beta$  does not become independent of the trap depth. Sesko *et al.* (1989) state a  $\beta_{\text{HCC}}$  estimation between  $10^{-10}$  and  $10^{-11} \text{ cm}^3 \text{ sec}^{-1}$ . Wallace *et al.* (1992) also observed a rapidly rising branch of  $\beta$  as a function of decreasing MOT laser intensity below about  $2.5 \text{ mW cm}^{-2}$  in a  $^{85}\text{Rb}$  MOT and below about  $4 \text{ mW cm}^{-2}$  in a  $^{87}\text{Rb}$  MOT. They also reported a strong isotope effect in  $\beta$  and showed that the ratio of  $\beta_{85}/\beta_{87}$  at constant trap intensity supported the view that MOT velocity-dependent forces rather than position-dependent forces dominate atom capture and trapping in the MOT environment. Furthermore, at the lowest MOT intensities  $\beta$  shows some sign of becoming independent of MOT capture velocity which would imply a direct measure of  $\beta_{\text{HCC}}$ . Wallace *et al.* (1992) estimated this  $\beta_{\text{HCC}}$  to be about the same for both isotopes,  $\sim 2 \times 10^{-11} \text{ cm}^3 \text{ sec}^{-1}$ . If MOTs functioned as spatially isotropic, conservative potentials,

then one would expect a very sharp threshold for loss as the trapping laser intensity decreases below the minimum required to contain the hyperfine-changing collisions kinetic energy release. In fact, to first approximation, the MOT restoring forces are the sum of a velocity-dependent dissipative term and a spatially-dependent term, so it is more accurate to characterize a MOT by its capture velocity rather than the trap “depth.” This capture velocity is a complicated function of trapping laser detuning, intensity, spot size, magnetic field gradient, and, as Ritchie *et al.* (1994) have shown in detail for a Li MOT, exhibits spatial anisotropy. Therefore, as the MOT laser intensity decreases, the trap will start to leak in the shallowest directions (along the MOT symmetry axis for a six-beam MOT) first. As MOT laser intensity continues to decrease, the leak rate will increase until  $\beta$  reaches a constant value where atoms are no longer contained in any direction. Ritchie *et al.* (1994, 1995) have shown how a detailed trap simulation can be used to extract  $\beta_{\text{FCC}}$  from the intensity dependence of MOT performance for fine-structure-changing collisions in Li, but a similar analysis to extract  $\beta_{\text{HCC}}$  has not yet been attempted.

#### b. Sodium

Marcassa *et al.* (1993) could not maintain their Na MOT at intensities sufficiently low to measure  $\beta$  on the rapidly rising branch where HCC is thought to become the dominant trap-loss process. Although similar hyperfine-changing collisions losses have been observed in Cs (Sesko *et al.*, 1989), Rb (Wallace *et al.*, 1992), and K (Santos *et al.*, 1996), the low-intensity branch is more difficult to observe in Na because the threshold for its occurrence starts at MOT intensities already weak compared to the saturation intensity of the atomic cooling transition. At such low intensities the vapor-loaded MOT barely functions. However, starting from a slow atomic beam Shang *et al.* (1994) succeeded in efficiently loading a Na MOT to investigate trap losses over a wide range of MOT intensity, including the low-intensity  $\beta$  branch. Another novel aspect of their work is the investigation of trap loss with all ground-state trapped atoms prepared in *either* the  $3s^2S_{1/2}(F=1)$  hyperfine level, *or* the  $3s^2S_{1/2}(F=2)$  level. The motivation was to show directly that, since only collisions between atoms prepared in the  $F=2$  level can lead to hyperfine-changing collisions, only they exhibit the low-intensity  $\beta$  branch. Their trap-loss measurements presented in Fig. 43 confirm that  $F=1$  collisions do not exhibit the rapidly-rising  $\beta$  signature of hyperfine-changing collisions. In contrast, for atoms trapped in the  $F=2$  ground state, Shang *et al.* (1994) did observe the conventional decrease of  $\beta$  as MOT intensity decreases, until a minimum is reached at about  $4 \text{ mW cm}^{-2}$ . Below  $4 \text{ mW cm}^{-2}$  hyperfine-changing collisions dominate, and the loss rate increases rapidly. For atoms in the  $F=1$  hyperfine level the hyperfine-changing collisions exoergic channel is closed, and  $\beta$  exhibits no rapidly rising branch below the  $4 \text{ mW cm}^{-2}$  minimum. To obtain a trap with atoms predominantly in the  $F=1$  ground hyperfine level, Shang

*et al.* (1994) used the type II trap described by Prentiss *et al.* (1988) and later used by Marcassa *et al.* (1993). The values measured by Shang *et al.* (1994) are in reasonable agreement with theory presented in Marcassa *et al.* (1993) in which  $\beta$  from fine-structure-changing and radiative escape were calculated using the optical-Bloch-equation approach of Band and Julienne (1992) and accurate  $\text{Na}_2$  potential curves from Magnier *et al.* (1993). We have previously discussed the limitations of the optical-Bloch-equation approach in Sec. V.A.3. The solid line in Fig. 43 shows the theory calculation. Comparison between  $\beta_{F1}$  and  $\beta_{F2}$  on the high intensity branch shows that trap-loss rate from  $F=1$  collisions is greater than  $F=2$  collisions by about a factor of three over the intensity range from 20 to  $90 \text{ mW cm}^{-2}$ . From about 4 to  $20 \text{ mW cm}^{-2}$   $\beta_{F2}$  drops by about two orders of magnitude from  $\sim 2 \times 10^{-10} \text{ cm}^3 \text{ sec}^{-1}$  to  $\sim 2 \times 10^{-12} \text{ cm}^3 \text{ sec}^{-1}$ . Shang *et al.* (1994) speculate that sub-Doppler cooling in this intensity range may slow the collision rate. Differences in molecular hyperfine structure between  $F=2$  collisions and  $F=1$  collisions may also play a role. At present the dramatic drop in  $\beta_{F2}$  is not clearly explained.

The most recent contribution to ground-state trap loss in sodium corresponds to a study of collisional loss rate of Na in a MOT operating on the D1 line (Marcassa *et al.*, 1996). Although the idea of trapping alkalis using the D1 resonance is straightforward, only recently has it been demonstrated by Flemming *et al.* (1996). The performance of a D1 trap alone in a vapor cell is very poor and requires loading from an external source of cold atoms. Therefore, Marcassa *et al.* (1996) used a conventional MOT operating on the D2 line for loading the D1 MOT. Atoms are loaded by capturing and cooling them in a conventional D2 MOT with the D1 optical beams superposed in the MOT configuration. After loading, the D2-line laser is turned off, but the cold atoms remain trapped in the D1 MOT. The number of trapped atoms is determined during the D2 MOT. As previously,  $\beta_{D1}$  is extracted from the fluorescence decay during the D1-line cycle. The measured  $\beta_{D1}$  from several intensities of laser at a detuning of about  $-10 \text{ MHz}$  from  $3S_{1/2}(F=2) \rightarrow 3P_{1/2}(F=2)$ , and the repumper close to  $3S_{1/2}(F=1) \rightarrow 3P_{1/2}(F=2)$ , is presented in Fig. 44. In the range from  $200 \text{ mW cm}^{-2}$  to about  $65 \text{ mW cm}^{-2}$  no significant variation in  $\beta$  is observed. At about  $65 \text{ mW cm}^{-2}$  the collisional loss rate increases considerably. At this point of rapid increase, the trap has become shallow enough to make hyperfine-changing collisions an important loss mechanism. For a trap operating at the D2 line the intensity at which this rapid increase occurs is about  $5 \text{ mW cm}^{-2}$  (Shang *et al.*, 1994), about 10 times smaller than for the D1-line trap. As a consequence the trap depth of the D1-line trap is about 1/10 of the D2-line trap at comparable intensities. This considerable decrease in trap depth is attributed to the several possible “dark states” that can occur in the D1-line trap.

#### 2. Summary comparison of trap-loss rate constants

Many research groups have carried out hyperfine-changing collisions trap loss experiments in MOTs with

varied instrumental design parameters, different MOT laser intensities, spot sizes, and detunings, and a host of atoms all with their own resonance lines and lifetimes. It would be desirable to organize these measurements on a common basis so as to identify the critical factors resulting in a particular determination of  $\beta$ . We present here a simple model of MOT atom confinement from which we derive a parameter  $\Theta$  that correlates well with the measurements discussed in the preceding subsections.

We assume that an atom pair subject to a hyperfine-changing collisions collision receives an extra quantity of energy  $\Delta E_{\text{HCC}}$  corresponding to the exoergicity of the transition and that each atom of mass  $m$  carries away half the velocity increase,

$$v = \left[ \frac{\Delta E_{\text{HCC}}}{m} \right]^{1/2}. \quad (98)$$

We further assume that the atom travels outward from the center of the trap to the radius of the MOT  $w$  subject only to the dissipative velocity-dependent decelerating force. Wallace *et al.* (1992) cite evidence from their isotopic studies in a Rb MOT that the velocity-dependent force dominates over the position-dependent restoring force. Thus

$$F = -\alpha v \quad (99)$$

and

$$v(z) = \left[ \frac{\Delta E_{\text{HCC}}}{m} \right]^{1/2} - \frac{\alpha}{m} z. \quad (100)$$

The maximum capture velocity is defined by

$$v(w) = 0, \quad (101)$$

so

$$\frac{\alpha}{m} w = \left[ \frac{\Delta E_{\text{HCC}}}{m} \right]^{1/2} = v_{\text{max}}. \quad (102)$$

Now, from Eq. (56),

$$\alpha = \frac{16\hbar k^2 \Omega^2 \Delta \Gamma}{(4\Delta^2 + \Gamma^2 + 2\Omega^2)^2}, \quad (103)$$

so at relatively large detunings and low intensities the second two terms in the denominator of Eq. (103) can be ignored and writing the MOT intensity  $I$  in terms of the Rabi frequency  $\Omega$ ,

$$\Omega^2 = \frac{I}{I_{\text{sat}}} \Gamma^2, \quad (104)$$

we have

$$v_{\text{max}} = \frac{\hbar k^2 I w \Gamma^3}{\Delta^3 I_{\text{sat}} m}. \quad (105)$$

Removing all the constant terms we define a trap capture parameter  $\Theta$  as

$$\Theta = \frac{1}{\lambda^2} \frac{\Gamma^3}{\Delta^3} \frac{I}{I_{\text{sat}}} \frac{w}{m}. \quad (106)$$

Figure 45 shows  $\beta$  plotted against  $\Theta$  for all the alkalis discussed above. Note that for heteronuclear collisions

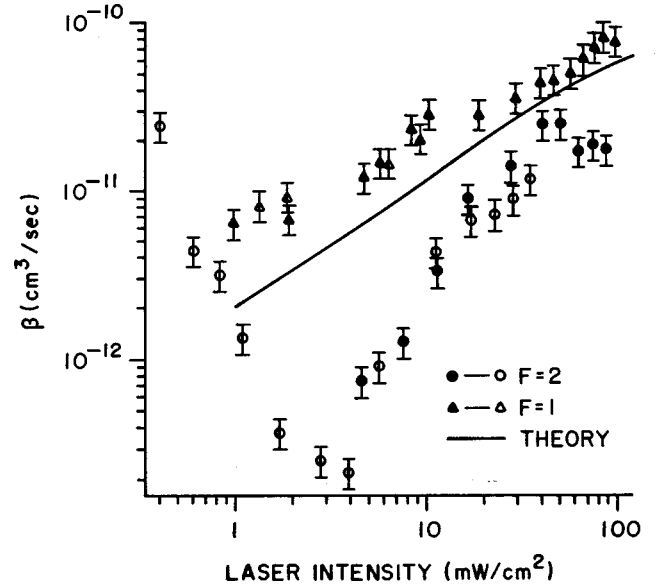


FIG. 43. Trap-loss due to hyperfine changing collisions is possible for  $F=2$  collisions but not possible for  $F=1$  collisions. The absence of a rapidly rising branch at low intensity for  $F=1$  collisions confirms the trap-loss process at low trap depth. From Shang *et al.* (1994).

Eq. (106) must be modified by substituting  $(m_1/2)(1 + m_1/m_2)$  for  $m$  where  $m_1$  is the mass of the species of the observed trap loss.

## VI. PHOTOASSOCIATION SPECTROSCOPY

### A. Introduction

If, while approaching on an unbound ground state potential, two atoms absorb a photon and couple to an excited bound molecular state, they are said to undergo photoassociation. Figure 46 diagrams the process. At long range electrostatic dispersion forces give rise to the ground-state molecular potential varying as  $C_6/R^6$ . If the two atoms are homonuclear, then a resonant dipole-dipole interaction sets up  $\pm C_3/R^3$  excited-state repulsive and attractive potentials. Figure 47 shows the actual long-range excited potential curves for the sodium dimer, originating from the  $^2S_{1/2} + ^2P_{3/2}$  and  $^2S_{1/2} + ^2P_{1/2}$  separated atom states. For cold and ultracold photoassociation processes the long-range attractive potentials play the key role; the repulsive potentials figure importantly in optical shielding and suppression, the subject of Sec. VII. In the presence of a photon with frequency  $\omega_p$  the colliding pair with kinetic energy  $k_B T$  couples from the ground state to the attractive molecular state in a free-bound transition near the Condon point  $R_C$ , the point at which the difference potential just matches  $\hbar\omega_p$ .

Scanning the probe laser  $\omega_p$  excites population of vibration-rotation states in the excited bound potential and generates a free-bound spectrum. This general class of measurements is called photoassociative spectroscopy and can be observed in several different ways. The ob-

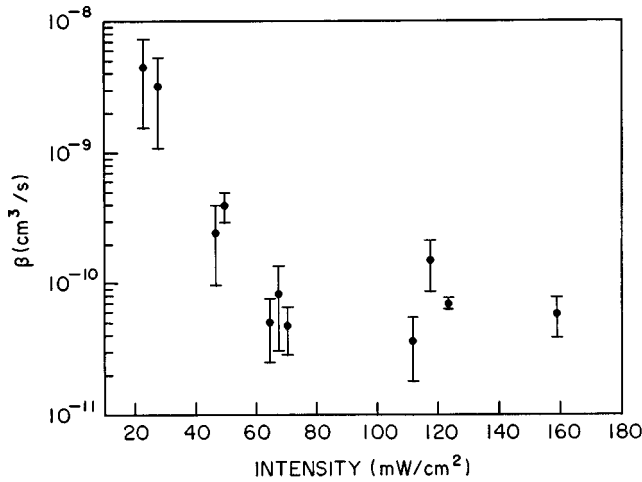


FIG. 44. Trap-loss from a Na MOT formed on the D1 resonance line as a function of MOT laser intensity (trap depth). From Marcassa *et al.* (1996).

servation may consist of bound state decay by spontaneous emission, most probably as the nuclei move slowly around the outer turning point, to some distribution of continuum states on the ground potential controlled by bound-free nuclear Franck-Condon overlap factors. The free atoms then recede on the ground state with some distribution of kinetic energy. In a MOT or a FORT, this radiative escape process can be an important source of loss if each atom receives enough kinetic energy to overcome trap restoring forces. As  $\omega_p$  passes through the free-bound resonances, the loss channel opens, and the number of atoms in the trap sharply diminishes. Thus scanning  $\omega_p$  generates a high-resolution fluorescence-loss spectrum. The excited bound quasimolecule may also decay around the inner turning point to bound levels of the ground molecular state. Since the stable dimers are usually not confined by MOT fields, this cold-molecule production is another trap-loss channel, although the branching ratio to ground-state bound molecules is usually small, only a few percent of the total loss rate.

Instead of observing the spectrum by spontaneous decay and trap loss, a second probe photon may excite the long-range bound quasimolecule to a higher excited state (or manifold of states) from which the molecule may undergo direct photoionization or autoionization within some range of internuclear separation. If this second photon comes from the same light source as the first, the process is called “one-color” photoassociative spectroscopy; if from an independently tunable source then it is called “two-color” photoassociative spectroscopy. When the ultimate product of the photoassociation is a molecular ion, the process is called photoassociative ionization. Heinzen (1995) has provided a good introductory review of photoassociation and optical shielding (the subject of the next section).

## B. Photoassociation at ambient and cold temperatures

The first measurement of a free-bound photoassociative absorption appeared long before the development

of optical cooling and trapping, about two decades ago, when Scheingraber and Vidal (1977) reported the observation of photoassociation in collisions between magnesium atoms. In this experiment fixed uv lines from an argon ion laser excited free-bound transitions from the thermal continuum population of the ground  $X^1\Sigma_g^+$  state to bound levels of the  $A^1\Sigma_u^+$  state of  $Mg_2$ . Scheingraber and Vidal analyzed the subsequent fluorescence to bound and continuum states from which they inferred the photoassociative process. The first unambiguous photoassociation *excitation spectrum*, however, was measured by Inou *et al.* (1982) in collisions between Xe and Cl at 300 K. In both these early experiments the excitation was not very selective due to the broad thermal distribution of populated continuum ground states. Jones *et al.* (1993) with a technically much improved experiment reported beautiful free-bound vibration progressions in KrF and XeI  $X \rightarrow B$  transitions; furthermore, from the intensity envelope modulation they were able to extract the functional dependence of the transition moment on the internuclear separation. Although individual vibrational levels of the  $B$  state were clearly resolved, the underlying rotational manifolds were not. Jones *et al.* (1993) simulated the photoassociation structure and line shapes by assuming a thermal distribution of rotational levels at 300 K. Photoassociation and dissociation processes prior to the cold and ultracold epoch have been reviewed by Tellinghuisen (1985).

A decade after Scheingraber and Vidal reported the first observation of photoassociation, Thorsheim *et al.* (1987) proposed that high-resolution free-bound molecular spectroscopy should be possible using optically cooled and confined atoms. Figure 48 shows a portion of their calculated  $X \rightarrow A$  absorption spectrum at 10 mK for sodium atoms. This figure illustrates how cold temperatures compress the Maxwell-Boltzmann distribution to the point where individual rotational transitions in the free-bound absorption are clearly resolvable. The marked differences in peak intensities indicate scattering resonances, and the asymmetry in the line shapes, tailing off to the red, reflect the thermal distribution of ground-state collision energies at 10 mK. Figure 49 plots the photon-flux-normalized absorption rate coefficient for singlet  $X^1\Sigma_g^+ \rightarrow A^1\Sigma_u^+$  and triplet  $a^3\Sigma_u^+ \rightarrow 1^3\Sigma_g^+$  molecular transitions over a broad range of photon excitation, red-detuned from the Na ( $^2S \rightarrow ^2P$ ) atomic resonance line. The strongly modulated intensity envelopes are called Condon modulations, and they reflect the overlap between the ground state continuum wave functions and the bound excited vibrational wave functions. These can be understood from the reflection approximation described in Eq. (32). We shall see later that these Condon modulations reveal detailed information about the ground state scattering wave function and potential from which accurate  $s$ -wave scattering lengths can be determined. Thorsheim *et al.* (1987), therefore, predicted all the notable features of ultracold photoassociation spectroscopy later to be developed in many experiments: (1) precision measurement of vibration-rotation progressions from which accurate excited-state potential

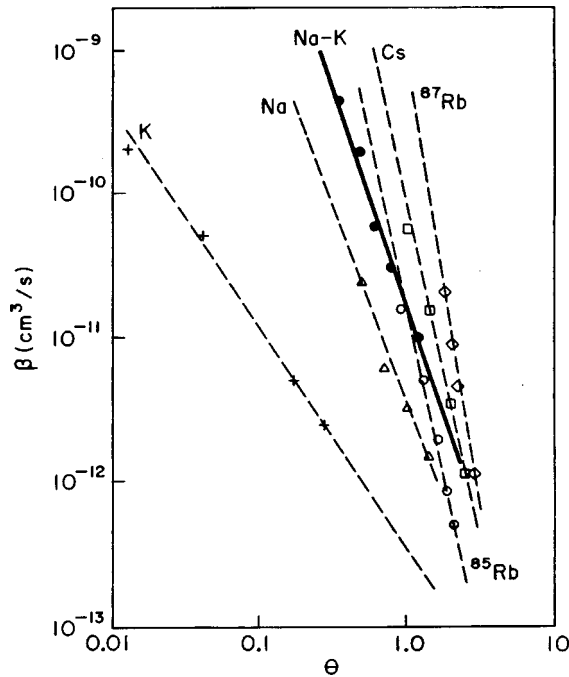


FIG. 45. Summary plot of the trap-loss constant  $\beta$  as a function of the trap-loss parameter  $\Theta$  for all the alkali systems studied to date.

parameters can be determined, (2) line profile measurements and analysis to determine collision temperature and threshold behavior, and (3) spectral intensity modulation from which the ground state potential, the scattering wave function, and the  $s$ -wave scattering length can be characterized with great accuracy.

An important difference distinguishes ambient temperature photoassociation in rare-gas halide systems and sub-millidegree-Kelvin temperature photoassociation in cooled and confined alkali systems. At temperatures found in MOTs and FORTs (and within selected veloc-

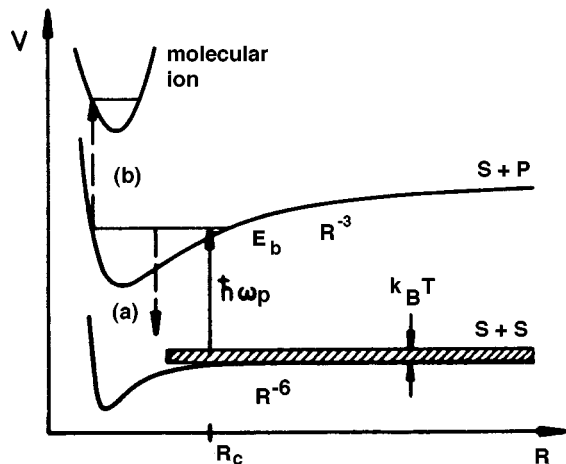


FIG. 46. Diagram of the photoassociation process. First excitation ( $\hbar\omega_p$ ) is followed by (a) spontaneous or stimulated emission back to bound or continuum levels of the ground state or (b) second excitation to the molecular ion (photoassociative ionization).

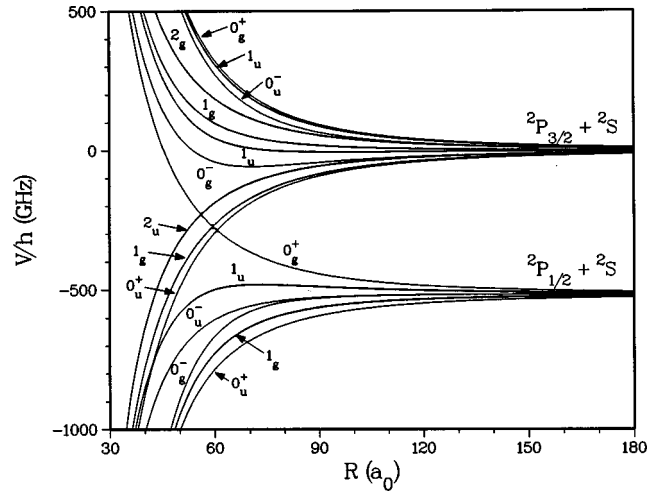


FIG. 47. Long-range potential curves of the first excited states of the Na dimer labeled by Hund's case (c) notation. The number gives the projection of electron spin plus orbital angular momentum on the molecular axis. The  $g/u$  and  $+/-$  labels correspond to conventional point-group symmetry notation.

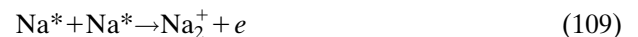
ity groups in atomic beams) the collision dynamics are controlled by long-range electrostatic interactions, and Condon points  $R_C$  are typically at tens to hundreds of  $a_0$ . In the case of the rare-gas halides the Condon points are in the short-range region of chemical binding, and therefore free-bound transitions take place at much smaller internuclear distances, typically less than ten  $a_0$ . For the colliding  $A, B$  quasimolecule the pair density  $n$  as a function of  $R$  is given by

$$n = n_A n_B 4\pi R^2 e^{-V(R)/kT} \quad (107)$$

so the density of pairs varies as the square of the internuclear separation. Although the pair-density  $R$  dependence favors long-range photoassociation, the atomic reactant densities are quite different with the  $n_A n_B$  product on the order of  $10^{35} \text{ cm}^{-6}$  for rare-gas halide photoassociation and only about  $10^{22} \text{ cm}^{-6}$  for optically trapped atoms. Therefore the effective pair density available for rare-gas halide photoassociation greatly exceeds that for cold alkali photoassociation, permitting fluorescence detection and dispersion by high resolution (but inefficient) monochromators.

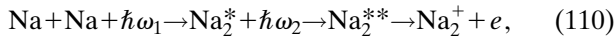
### C. Associative and photoassociative ionization

Conventional associative ionization occurring at ambient temperature proceeds in two steps: excitation of isolated atoms followed by molecular autoionization as the two atoms approach on excited molecular potentials. In sodium for example (Weiner *et al.*, 1989),

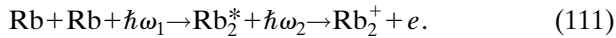


The collision event lasts a few picoseconds, fast compared to radiative relaxation of the excited atomic states ( $\sim$  tens of nanoseconds). Therefore the incoming atomic

excited states can be treated as stationary states of the system Hamiltonian, and spontaneous radiative loss does not play a significant role. In contrast, cold and ultracold photoassociative ionization must always start on ground states because the atoms move so slowly that radiative lifetimes become short compared to the collision duration. The partners must be close enough at the Condon point, where the initial photon absorption takes place, so that a significant fraction of the excited scattering flux survives radiative relaxation and goes on to populate the final inelastic channel. Thus photoassociative ionization is also a two-step process: (1) photoexcitation of the incoming scattering flux from the molecular ground-state continuum to specific vibration-rotation levels of a bound molecular state; and (2) subsequent photon excitation either to a doubly-excited molecular autoionizing state or directly to the molecular photoionization continuum. For example, in the case of sodium collisions, the principal route is through doubly-excited autoionization (Julienne and Heather, 1991),



whereas for rubidium atoms the only available route is direct photoionization in the second step (Leonhardt and Weiner, 1995),



Collisional ionization can play an important role in plasmas, flames, and atmospheric and interstellar physics and chemistry. Models of these phenomena depend critically on the accurate determination of absolute cross sections and rate coefficients. The rate coefficient is the quantity closest to what an experiment actually measures and can be regarded as the cross section averaged over the collision velocity distribution,

$$K = \int_0^\infty v \sigma(v) f(v) dv. \quad (112)$$

The velocity distribution  $f(v)$  depends on the conditions of the experiment. In cell and trap experiments it is usually a Maxwell-Boltzmann distribution at some well-defined temperature, but  $f(v)$  in atomic beam experiments, arising from optical excitation velocity selection, deviates radically from the normal thermal distribution (Tsao *et al.*, 1995). The actual signal count rate  $d(X_2^+)/dt$  relates to the rate coefficient through

$$\frac{1}{V\alpha} \frac{d(X_2^+)}{dt} = K[X]^2, \quad (113)$$

where  $V$  is the interaction volume,  $\alpha$  the ion detection efficiency, and  $[X]$  the atom density. If rate constant or cross section measurements are carried out in crossed or single atomic beams (Weiner *et al.*, 1989; Thorsheim *et al.*, 1990; Tsao *et al.*, 1995) special care is necessary to determine the interaction volume and atomic density.

Photoassociative ionization was the first measured collisional process observed between cooled and trapped atoms (Gould *et al.*, 1988). The experiment was performed with atomic sodium confined in a hybrid laser

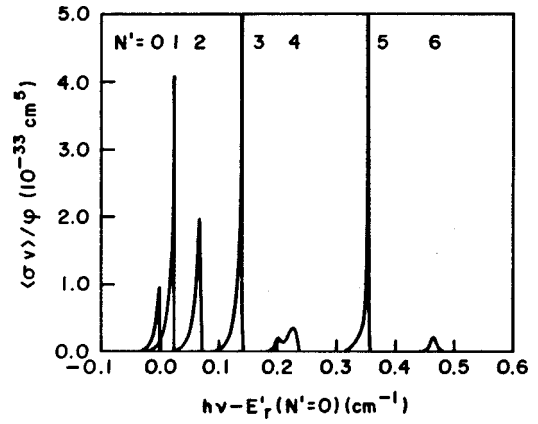


FIG. 48. Calculated free-bound photoassociation spectrum at 10 mK. From Thorsheim *et al.* (1987).

trap, utilizing both the spontaneous radiation pressure and the dipole force. The trap had two counterpropagating, circularly polarized Gaussian laser beams brought to separate foci such that longitudinal confinement along the beam axis was achieved by the spontaneous force and transversal confinement by the dipole force. The trap was embedded in a large ( $\sim 1$  cm diameter) conventional optical molasses loaded from a slowed atomic beam. The two focused laser beams comprising the dipole trap were alternately chopped with a  $3 \mu\text{sec}$  “trap cycle,” to avoid standing-wave heating. This trap cycle for each beam was interspersed with a  $3 \mu\text{sec}$  “molasses cycle” to keep the atoms cold. The trap beams were detuned about 700 MHz to the red of the  $3s^2S_{1/2}(F=2) \rightarrow 3p^2P_{3/2}(F=3)$  transition while the molasses was detuned only about one natural linewidth ( $\sim 10$  MHz). The atoms captured from the molasses ( $\sim 10^7 \text{ cm}^{-3}$ ) were compressed to a much higher excited atom density ( $\sim 5 \times 10^9 \text{ cm}^{-3}$ ) in the trap. The temperature was measured to be about  $750 \mu\text{K}$ . Ions formed in the trap were accelerated and focused toward a charged-particle detector. To assure the identity of the counted ions, Gould *et al.* carried out a time-of-flight measurement; the re-

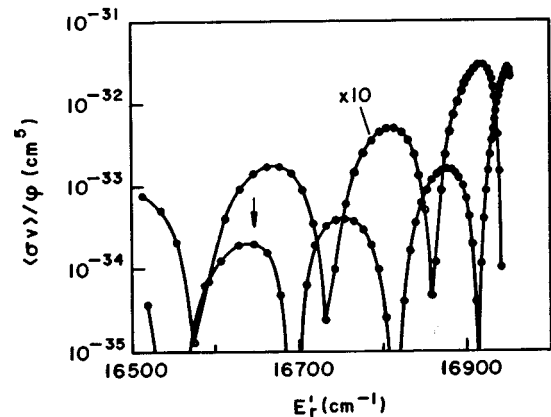


FIG. 49. Calculated absorption spectrum of photoassociation in Na at 10 mK, showing Condon fluctuations. The curve labeled “ $\times 10$ ” refers to  $^3\Sigma_g \rightarrow ^3\Sigma_u$  while the other curve refers to  $^1\Sigma_g \rightarrow ^1\Sigma_u$  transitions. From Thorsheim *et al.* (1987).

sults of which, shown in Fig. 50, clearly establish the  $\text{Na}_2^+$  ion product. The linearity of the ion rate with the square of the atomic density in the trap, supported the view that the detected  $\text{Na}_2^+$  ions were produced in a binary collision. After careful measurement of ion rate, trap volume and excited atom density, the value for the rate coefficient was determined to be  $K = (1.1^{+1.3}_{-0.5}) \times 10^{-11} \text{ cm}^3 \text{ sec}^{-1}$ . Gould *et al.* (1988), following conventional wisdom, interpreted the ion production as coming from collisions between two *excited* atoms,

$$\frac{dN_I}{dt} = K \int n_e^2(\vec{r}) d^3\vec{r} = K \bar{n}_e N_e, \quad (114)$$

where  $dN_I/dt$  is the ion production rate,  $n_e(\vec{r})$  the excited-state density,  $N_e$  the number of excited atoms in the trap  $[= \int n_e(\vec{r}) d^3\vec{r}]$ , and  $\bar{n}_e$  the “effective” excited-state trap density. The value for  $K$  was then determined from these measured parameters. Assuming an average collision velocity of  $130 \text{ cm s}^{-1}$ , equivalent to a trap temperature of  $750 \mu\text{K}$ , the corresponding cross section was determined to be  $\sigma = (8.6^{+10.0}_{-3.8}) \times 10^{-14} \text{ cm}^2$ . In contrast, the cross section at  $\sim 575 \text{ K}$  had been previously determined to be  $\sim 1.5 \times 10^{-16} \text{ cm}^2$  (Bonnano *et al.*, 1983, 1985; Wang *et al.*, 1986; Wang *et al.*, 1987). Gould *et al.* (1988) rationalized the difference in cross section size by invoking the difference in de Broglie wavelengths, the number of participating partial waves, and the temperature dependence of the ionization channel probability. The quantal expression for the cross section in terms of partial wave contributions  $l$  and inelastic scattering probability  $S_{12}$  is

$$\begin{aligned} \sigma_{12}(\epsilon) &= \left( \frac{\pi}{k^2} \right) \sum_{l=0}^{\infty} (2l+1) |S_{12}(\epsilon, l)|^2 \\ &\cong \pi \left( \frac{\lambda_{dB}}{2\pi} \right)^2 (l_{\max} + 1)^2 P_{12}, \end{aligned} \quad (115)$$

where  $\lambda_{dB}$  is the entrance channel de Broglie wavelength and  $P_{12}$  is the probability of the ionizing collision channel averaged over all contributing partial waves of which  $l_{\max}$  is the greatest. The ratio of the  $(l_{\max} + 1)^2$  between  $575 \text{ K}$  and  $750 \mu\text{K}$  is about 400 and the de Broglie wavelength ratio factor varies inversely with temperature. Therefore in order that the cross section ratio be consistent with low- and high-temperature experiments,  $\sigma_{12}(575 \text{ K})/\sigma_{12}(750 \mu\text{K}) \sim 1.7 \times 10^{-3}$ , Gould *et al.* (1988) concluded that  $P_{12}$  must be about three times greater at  $575 \text{ K}$  than at  $750 \mu\text{K}$ .

However, it soon became clear that the conventional picture of associative ionization, starting from the excited atomic states, could not be appropriate in the cold regime. Julienne (1988) pointed out the essential problem with this picture. In the molasses cycle the optical field is only red-detuned by one linewidth, and the atoms must therefore be excited at very long range, near  $1800 a_0$ . The collision travel time to the close internuclear separation where associative ionization takes place is long compared to the radiative lifetime, and most of the population decays to the ground state before reach-

ing the autoionization zone. During the trap cycle, however, the excitation takes place at much closer internuclear distances due to a 70-linewidth red detuning and high-intensity field dressing. Therefore one might expect excitation survival to be better during the trap cycle than during the molasses cycle, and the NIST group, led by W. D. Phillips, set up an experiment to test the predicted cycle dependence of the ion rate.

Lett *et al.* (1991) performed a new experiment using the same hybrid trap. This time however, the experiment measured ion rates and fluorescence separately as the hybrid trap oscillated between “trap” and “molasses” cycles. The results from this experiment are shown in Fig. 51. While keeping the total number and density of atoms (excited atoms plus ground state atoms) essentially the same over the two cycles and while the excited state *fraction* changed only by about a factor of two, the ion rate increased in the trapping cycle by factors ranging from 20 to 200 with most observations falling between 40 and 100. This verified the predicted effect qualitatively even if the magnitude was smaller than the estimated  $10^4$  factor of Julienne (1988). This modulation ratio is orders of magnitude more than would be expected if excited atoms were the origin of the associative ionization signal. Furthermore, by detuning the trapping lasers over 4 GHz to the red, Lett *et al.* (1991) continued to measure ion production at rates comparable to those measured near the atomic resonance. At such large detunings reduction in atomic excited state population would have led to reductions in ion rate by over four orders of magnitude had the excited atoms been the origin of the collisional ionization. Not only did far off-resonance trap cycle detuning maintain the ion production rate, Lett *et al.* (1991) observed evidence of peak structure in the ion signal as the dipole trap cycle detuned to the red.

To interpret the experiment of Lett *et al.* (1991), Julienne and Heather (1991) proposed a mechanism which has become the standard picture for cold and ultracold photoassociative ionization. Figure 52 details the model. Two colliding atoms approach on the molecular ground-state potential. During the molasses cycle with the optical fields detuned only about one linewidth to the red of atomic resonance, the initial excitation occurs at very long range, around a Condon point at  $1800 a_0$ . A second Condon point at  $1000 a_0$  takes the population to a  $1_u$  doubly excited potential that, at shorter internuclear distance, joins adiabatically to a  $^3\Sigma_u^+$  potential, thought to be the principal short-range entrance channel to associative ionization (Dulieu *et al.*, 1991; Henriet *et al.*, 1991). More recent calculations suggest other entrance channels are important as well (Dulieu *et al.* 1994). The long-range optical coupling to excited potentials in regions with little curvature implies that spontaneous radiative relaxation will depopulate these channels before the approaching partners reach the region of small internuclear separation where associative ionization takes place. The overall probability for collisional ionization during the molasses cycle remains therefore quite low. In contrast, during the trap cycle the optical fields are

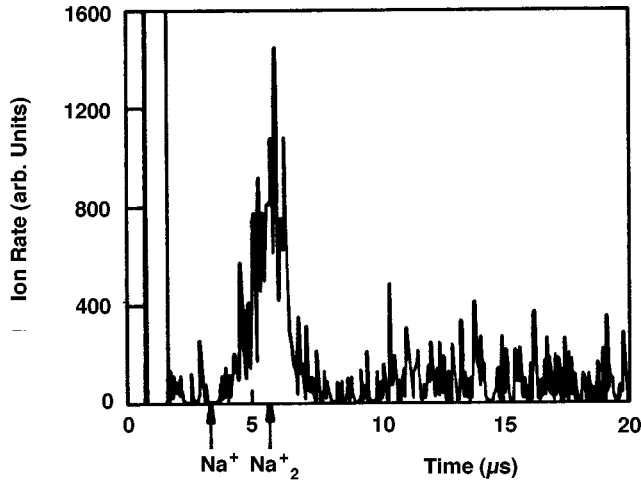


FIG. 50. Time-of-flight spectrum clearly showing that the ions detected are  $\text{Na}_2^+$  and not the atomic ion. From Gould *et al.* (1988).

detuned 60 linewidths to the red of resonance, the first Condon point occurs at  $450 a_0$ ; and, if the trap cycle field couples to the  $0_g^-$  long-range molecular state (Stwalley *et al.*, 1978), the second Condon point occurs at  $60 a_0$ . Survival against radiative relaxation improves greatly because the optical coupling occurs at much shorter range where excited-state potential curvature accelerates the two atoms together. Julienne and Heather (1991) calculate about a three-order-of-magnitude enhancement in the rate constant for collisional ionization during the trap cycle. The dashed and solid arrows in Fig. 52 indicate the molasses cycle and trap cycle pathways, respectively. The strong collisional ionization rate constant enhancement in the trap cycle calculated by Julienne and Heather (1991) is roughly consistent with the measurements of Lett *et al.* (1991), although the calculated modulation ratio is somewhat greater than what was actually observed. Furthermore, Julienne and Heather calculate structure in the trap detuning spectrum. As the optical fields in the dipole trap tune to the red, a rather congested series of ion peaks appear which Julienne and Heather ascribed to free-bound association resonances corresponding to vibration-rotation bound levels in the  $1_g$  or the  $0_g^-$  molecular excited states. The density of peaks corresponded roughly to what Lett *et al.* (1991) had observed; these two tentative findings together were the first evidences of a new photoassociation spectroscopy. In a subsequent full paper expanding on their earlier report, Heather and Julienne (1993) introduced the term, “photoassociative ionization” to distinguish the two-step optical excitation of the quasimolecule from the conventional associative ionization collision between excited atomic states. In a very recent paper, Pillet *et al.* (1997) have developed a perturbative quantum approach to the theory of photoassociation which can be applied to the whole family of alkali homonuclear molecules. This study presents a useful table of photoassociation rates which reveals an important trend toward lower rates of molecule formation as the alkali

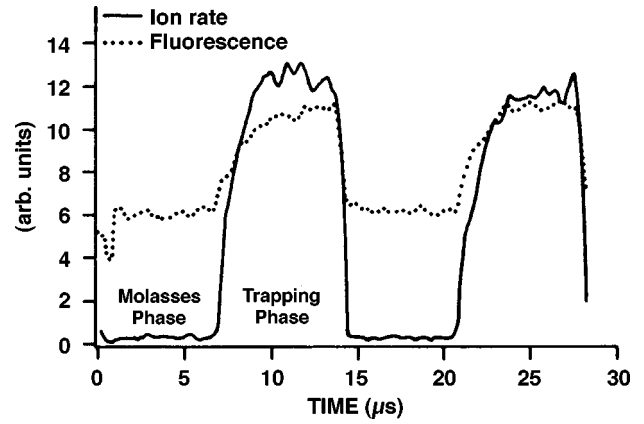


FIG. 51. Trap modulation experiment showing much greater depth of ion intensity modulation (by more than one order of magnitude) than fluorescence or atom number modulation, demonstrating that excited atoms are not the origin of the associative ionizing collisions. From Lett *et al.* (1991).

mass increases and provides a helpful guide to experiments designed to detect ultracold molecule production.

#### 1. Photoassociative ionization at small detuning

When near-resonant light couples ground and excited molecular states of colliding atoms, spontaneous emission occurs during the collision with high probability. Collision problems involving strong coupling to one or more optical field modes and with radiative dissipation can only be properly treated by solving the Liouville equation of motion for the quantum density matrix of particles plus field,

$$\frac{d}{dt}\rho(t) = \frac{1}{i\hbar}[H, \rho(t)], \quad (116)$$

where  $\rho(t)$  is the density matrix describing the states of the quasimolecule and the radiation field and  $H = H_{\text{molec}} + H_{\text{field}} + H_{\text{int}}$  is the Hamiltonian for the system of quasimolecule, radiation field, and the coupling between the two. Photoassociative ionization during the molasses cycle of the NIST hybrid trap or within the confines of a magneto-optical trap correspond to this situation. Bagnato, Marcassa, Wang, *et al.* (1993), therefore, undertook to investigate the photoassociative ionization (PAI) rate constant in a sodium MOT as a function of MOT optical field intensity. The essential idea was to measure the dependence of the PAI rate constant on MOT intensity and compare it to rate constants calculated from an optical-Bloch-equation theory, based on Eq. (116), proposed earlier by Band and Julienne (1992). Bagnato, Marcassa, Wang *et al.* (1993) also compared the experimental results to the Gallagher-Pritchard model or “local equilibrium,” model discussed at length in Sec. V. The results are shown in Fig. 53. The semiclassical optical-Bloch-equation theory agrees well with the experiment at the low end of the intensity scale, but the measured rate constants appear to increase less rapidly with increasing intensity than the calculations and to flatten around  $100 \text{ mW cm}^{-2}$ . The local equilib-

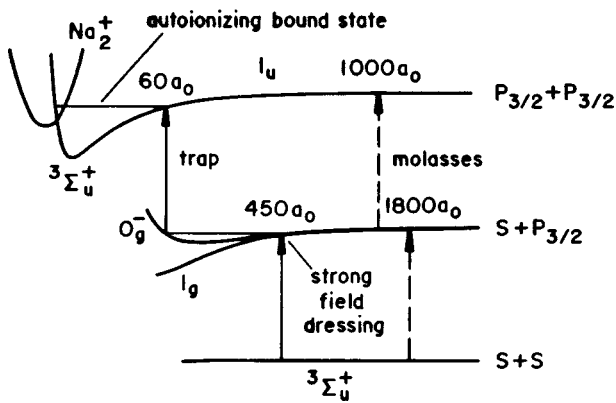


FIG. 52. Photoassociative ionization in Na collisions. From Heather and Julienne (1993).

rium model builds on the quasistatic theory of collision broadening, treats the molecule-field interaction perturbatively, and does not attempt to solve a density matrix equation of motion. The term “local equilibrium” comes from the characteristic of this theory that, at any Condon point, the detuning dependence of the optical excitation takes the form of a Lorentzian line shape. The key assumption, therefore, of the local equilibrium model is that at any internuclear separation the quasimolecule has time to reach “equilibrium” with the modes of the radiation field. In both the optical-Bloch-equation and local equilibrium models, calculation of the rate constant requires determining two probabilities: first the probability that a two-step optical excitation-survival process (first to the  $1_g$  or  $0_g^-$ , then to the  $1_u$ ) brings the two atoms together near  $R \sim 6a_0$  on the doubly excited autoionizing  $3\Sigma_u^+$  potential; second, the probability that the autoionization takes place. Both models require the molecular autoionization probability and rely on measurements reported in the literature (Huennekens and Gallagher, 1983; Bonanno *et al.*, 1983). The two models differ significantly in the calculation of the first step, the optical excitation probability. Figure 53 shows that the local equilibrium theory overestimates the PAI rates by about one order of magnitude. Neither theory takes into account the extensive molecular hyperfine structure of the excited states, and the evidence from trap loss experiments (see Sec. V) indicates that models of collision dynamics at small detuning that ignore molecular excited-state hyperfine structure usually fail.

Recently Blangé *et al.* (1997) have performed photo-dissociation fragmentation spectroscopy on the  $\text{Na}_2^+$  ions produced by PAI in a conventional Na MOT. They succeeded in determining the internal vibrational level distribution of  $\text{Na}_2^+$  produced by the cold collision; authors interpreted the distribution to infer the mechanism for this PAI process.

## 2. PAI and molecular hyperfine structure

Exploring the off-resonance detuning dependence of PAI, Wagshul *et al.* (1993) discovered important effects

of molecular ground-state hyperfine structure. With a MOT loaded from a Zeeman-slowed atomic beam, together with an extra probe laser, Wagshul *et al.* alternated trapping and probing with a 50% duty cycle. Trap on/off periods varied from 2 to 100  $\mu\text{sec}$ , and ions were counted only during the probe period. In this scheme a large range of probe laser detuning could be explored without the complicating effects of the MOT fields (trap and repumper) and without compromising the trap performance. Total probe laser intensity ( $\sim 3 \text{ W cm}^{-2}$ ) was much greater than the trapping laser ( $\sim 35 \text{ mW cm}^{-2}$ ) but had a similar geometrical configuration and polarization to minimize perturbations on the MOT. Figure 54 shows the spectrum obtained by Wagshul *et al.* (1993) in the region between the two hyperfine ground state transitions,  $F=2 \rightarrow F'=3$  and  $F=1 \rightarrow F'=2$ . A broad resonance structure rises sharply about halfway between the two ground-state hyperfine transitions and extends to the blue. The quadratic dependence of the amplitude of this feature with the probe laser intensity is consistent with a two-photon process. Observing variations in the peak intensity as the relative population between the two ground-state hyperfine levels were varied, Wagshul *et al.* concluded that the observed spectrum arises from the collision of two ground-state atoms, each of which is in a different ground-state hyperfine level. The interpretation of Fig. 54 can be understood in the following way. Atoms in different hyperfine ground states collide on the potential labeled  $F=1 + F=2$ . The photon required for a two-step excitation to the doubly excited level falls halfway between the potentials labeled  $1+P$  and  $2+P$ . Where the attractive  $2+P$  potential crosses this line, the transition becomes doubly resonant. The observed threshold for this process is within 10 MHz of the prediction. Light to the red of this frequency cannot provide enough energy to reach the  $P+P$  potential starting from the  $F=1 + F=2$  asymptote of the ground state. Light to the blue of the threshold frequency follows the following route. First the optical field couples to the  $2+P$  curve at larger internuclear separation. The atoms then begin to accelerate together on the  $2+P$  potential until they reach a Condon point where the exciting light becomes resonant with a transition to the  $P+P$  curve. This broad PAI feature shows substructure consistent with free-bound transitions to an intermediate attractive state. Wagshul *et al.* (1993) carried out a model calculation of the PAI feature by applying their earlier two-step model (Julienne and Heather, 1991; Heather and Julienne, 1993) and incorporating the ground-state hyperfine levels. The calculated structure resembles the experimental feature, but appears to be less congested; This is probably because the model neglects the multitudinous number of excited-state hyperfine levels.

## 3. Two-color PAI

The work of Wagshul *et al.* (1993) brought to light the importance of ground-state hyperfine structure in early studies of PAI spectroscopy. They used a one-color probe to excite the two-step PAI process. Bagnato, Mar-

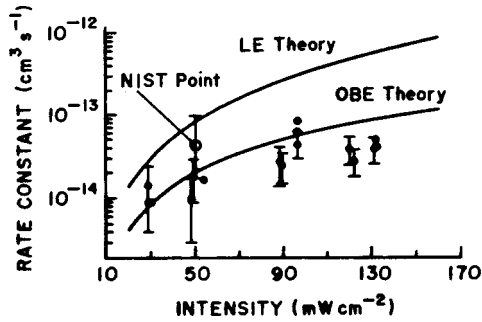


FIG. 53. Photoassociative ionization rate constant as a function of MOT light intensity. MOT laser detuned to the red of resonance about one natural linewidth. From Bagnato, Marcassa, Wang, *et al.* (1993).

marcassa, Tsao, *et al.* (1993) investigated the same PAI processes, using two different laser frequencies, one of which could be independently varied, and starting with different initial states for the colliding atoms. Atomic sodium was cooled and trapped in a MOT loaded from the low-velocity tail of background vapor. The trapping frequency  $\omega_1$  was red detuned as usual about one linewidth from cycling transition  $3s^2S_{1/2}(F=2) \rightarrow 3p^2P_{3/2}(F'=3)$ , and the repumper  $\omega_2$  was tuned close to  $3s^2S_{1/2}(F=1) \rightarrow 3p^2P_{3/2}(F'=2)$ . Depending on their relative intensity, these two frequencies could pump different relative populations into the two ground-state hyperfine levels  $F=1$  and  $F=2$ . A channeltron detector measured the PAI ion signal as a function of the frequency of a third, tunable probe laser  $\omega_p$ . Figures 55(a) and 55(b) show the PAI profiles as  $\omega_p$  scans to the blue of  $\omega_1$  and  $\omega_2$ . In Fig. 55(a) the intensity of  $\omega_1$  is stronger than  $\omega_2$  by a factor of three, and the inset above the line profiles shows the interpretation of the excitation routes. Both atomic hyperfine levels have significant population so  $\omega_1$  and  $\omega_2$  can couple all three molecular entrance channels (1+1, 1+2, 2+2) to the 1+P and 2+P attractive excited-state levels. Then  $\omega_p$  scanning to the blue couples these two singly excited levels to the doubly excited autoionizing P+P curve. To test this interpretation Bagnato, Marcassa, Tsao, *et al.* (1993) reversed the relative intensities in  $\omega_1$  and  $\omega_2$  so as to pump most of the atomic population to the  $F=2$  level. The effect is to depopulate the 1+1 molecular entrance channel, and panel (b) of Fig. 55 shows that the amplitude of the PAI profile degrading to the blue of  $\omega_2$  is greatly attenuated, consistent with this entrance channel depopulation. A common feature of all the measurements is the asymmetry in the PAI profile. As the probe laser scans to the blue, starting from the atomic transitions near  $\omega_1$  and  $\omega_2$ , the PAI signal rises rapidly to a peak  $\sim 400$  MHz detuning from the atomic limit, then exhibits a slow decay over a range of about 2 GHz. The asymmetric shape of this two-color PAI spectrum was modeled by Gallagher (1991) and arises from the action of four factors: (1) first excitation from the ground state at the initial Condon point  $R_i$ , (2) spontaneous emission as the atoms approach on the first attractive excited state until they reach the second Condon Point  $R_2$ , (3)

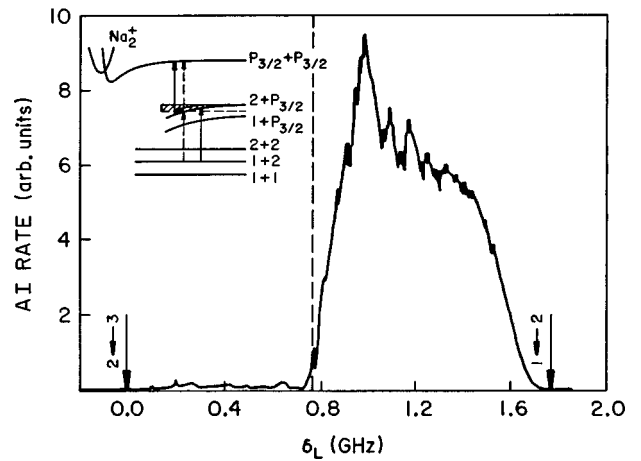


FIG. 54. Two-photon PAI spectrum arising from collisions on different ground-state hyperfine levels. From Wagshul *et al.* (1993).

second excitation from the first attractive state to the doubly excited state at  $R_2$ , and (4) spontaneous emission at the atoms approach the autoionization zone on the doubly excited state. Once the atoms are within  $R_{PAI}$ , the zone where the quasimolecule can autoionize, the four excitation-decay factors must be multiplied by the autoionizing probability in order to calculate an overall ion production rate. Detuning of  $\omega_p$  to the blue effectively increases the time between the first and second optical excitations. For short times (small blue detunings) the initially excited population does not have time to undergo appreciable radiative decay before excitation to the doubly excited level, yet the strong accelerating influence of the attractive  $C_3/R^3$  potential shortens the travel time between  $R_2$  and  $R_{PAI}$  where the atoms enter the autoionizing region. These two factors account for the rapid rise in PAI rate at small blue detunings. As  $\omega_p$  continues to scan to the blue, radiative depopulation of the first excited state starts to become significant and the overall PAI probability diminishes slowly. For atoms surviving to  $R_2$  on the first excited state, the increased radial acceleration tends to minimize radiative decay on the doubly excited state once the population undergoes the second excitation at  $R_2$ . However, the probability of that excitation begins to diminish with increased acceleration because the atoms pass through the optical resonance around the Condon point  $R_2$  with greater velocity. The overall effect is a slow diminution of the PAI production rate as  $\omega_p$  scans further to the blue. Although the asymmetric shape calculated by Gallagher is in satisfactory accord with the measurements of Bagnato, Marcassa, Tsao, *et al.* (1993) the absolute values of the rate constants differ by about an order of magnitude. Furthermore the position of the peak in the measured PAI profile is blue-shifted from Gallagher's model by about 200 MHz. These discrepancies could be accounted for by effects discussed previously in the section on trap loss, specifically (1) neglect of hyperfine structure and (2) semiclassical treatment at small detuning.

Bagnato, Marcassa, Tsao, *et al.* (1993) also investigated two-color PAI by prepumping all the atoms into either the  $F=1$  or the  $F=2$  and probing with only two frequencies:  $\omega_p, \omega_1$  or  $\omega_p, \omega_2$ . Figures 56(a) and 56(b) show the results with insets of the excitation routes. Panel (a) shows the spectrum with two principal features when only  $F=1$  is populated so that incoming scattering flux appears only on the  $1+1$  asymptote. The onset of the right-most features occurs at about twice the ground-state hyperfine splitting to the blue of  $\omega_1$ . The asymmetric shape degraded to the blue is characteristic of initial excitation to an attractive state at long range by fixed frequency  $\omega_1$  followed by a second excitation to the doubly excited level by scanning frequency  $\omega_p$ . The right inset above the feature shows the excitation pathway. It appears that the profile has a structure that must come from bound states of the doubly excited manifold. This structure remains to be investigated thoroughly. The central peak, immediately to the blue of  $\omega_2$ , is quadratic in the probe laser intensity, suggesting a two-photon single frequency process similar to that observed by Wagshul *et al.* (1993). The inset shows that  $\omega_p$  carries population to some mixed state of  $1+P$  and  $2+P$ , and a second photon takes the population to the doubly excited level. Panel b shows the spectrum obtained when only  $F=2$  is populated. Incoming scattering flux appears only on the  $2+2$  asymptote, and the onset of the feature begins about 250 MHz to the red of  $\omega_1$  and degrades to the red over a range of about 2 GHz. Structure is clearly visible and the inset above the feature shows that the scanning frequency  $\omega_p$  excites vibration-rotation levels associated with a bound singly excited states while  $\omega_2$  transfers population to the doubly excited level. Note that the left and right insets show how the fixed and scanning frequencies exchange roles. A PAI profile degrading to the blue means  $\omega_p$  couples the strongly attractive, singly excited state (or states) to the relatively flat, doubly excited level above it. A profile degrading to the red implies  $\omega_p$  coupling from the strongly attractive manifold to the flat  $2+2$  entrance channel below it. The fixed frequency  $\omega_1$  or  $\omega_2$  determines where on the absolute frequency scale these two-step excitation profiles appear. The red-degraded, structured profile reveal bound states of the singly excited manifold very close to the dissociation limit where molecular hyperfine coupling produces a complicated and congested spectrum. This structure was analyzed by Bagnato *et al.* (1994) to be associated with a  $0_g^-$  bound vibrational level progression, but extensive hyperfine mixing near dissociation render these symmetry labels ambiguous. Further probing to the red of the hyperfine region (Ratliff *et al.*, 1994) reveals a much simpler, highly resolved spectrum, opening the very fruitful field of precision PAI spectroscopy, reviewed in the next section.

In very recent work, Jones *et al.* (1997) have measured two-color spectra in which the first step populates a specific state in the  $0_g^-$  or the  $1_g$   $\text{Na}_2$  molecular electronic potentials. Then a second high-resolution light beam

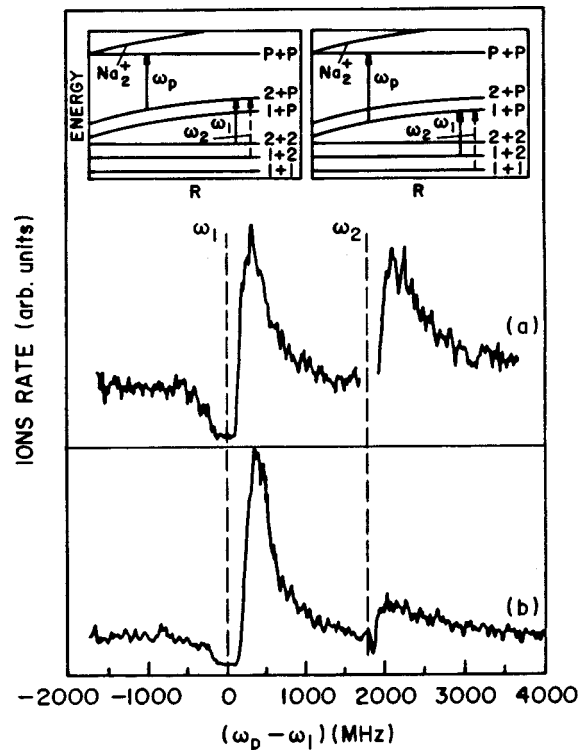


FIG. 55. Two-color photoassociative ionization. Inset shows MOT ( $\omega_1$ ) and repumper ( $\omega_2$ ) fixed frequencies and sweeping probe ( $\omega_p$ ) frequency. From Bagnato, Marcassa, Tsao *et al.* (1993).

scans transitions either upward leading to autoionizing potentials near the  $3P+3P$  doubly excited asymptote or downward back to the manifold of potentials associated with the  $\text{Na}_2$  ground electronic state. This study obtains spectroscopic constants for several levels of a doubly excited  $1_u$  state, demonstrates the appearance of a new form of Condon internal diffraction from bound $\rightarrow$ free transitions just above the  $3P_{3/2}+3P_{3/2}$  dissociation limit, and discusses the use of photoassociation as a source of cold molecules. This work pioneers the high-resolution photoassociation spectroscopy of the doubly excited states of  $\text{Na}_2$  and begins to unravel the similarities and differences between the mechanisms of associative ionization at high temperature and photoassociative ionization in the ultracold regime.

In a parallel theoretical study, Dulieu *et al.* (1997) have shown that five molecular symmetries,  $^1\Sigma_g^+$ ,  $^3\Sigma_u^+$ ,  $^1\Pi_u$ ,  $^3\Pi_u$ ,  $^1\Delta_g$  of the doubly excited states are likely to contribute to the molecular autoionization. They identify the peaks observed by Jones *et al.* (1997) and attributed to a doubly excited  $1_u$  state (Hund's case (c) coupling), as belonging to the  $^1\Pi_u$  member (Hund's case (a) coupling) of the five molecular symmetries. Exactly how the short range  $^1\Pi_u$  joins to the long range  $1_u$  is still the subject of continuing investigation (Huynh *et al.*, 1997). It appears, however, that the autoionization rate of this  $^1\Pi_u$  state precludes it from significantly contributing to the associative ionization process at thermal energies.

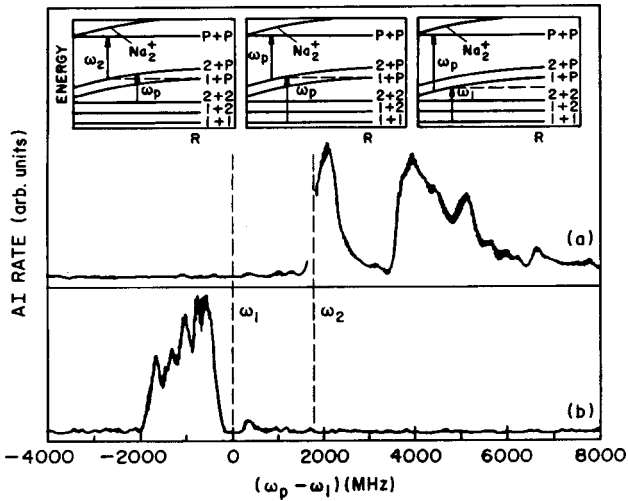


FIG. 56. Two-color photoassociative ionization. Insets above features describe excitation routes. Frequencies are labeled as in the previous figure. From Bagnato, Marcassa, Tsao, *et al.* (1993).

#### D. Photoassociation spectroscopy in MOTs and FORTs

Although early cold alkali photoassociative ionization experiments explored different excitation and ionization pathways and confirmed the essential mechanisms of the process, the full potential of photoassociation as a versatile and powerful spectroscopic technique of unprecedented precision could not be realized until scanning probe fields could explore beyond the hyperfine coupling zone of irregular and congested spectra. Two back-to-back articles appearing in *Physical Review Letters* signaled a breakthrough in measuring photoassociation spectra well beyond this region. The NIST group continued to investigate photoassociative ionization sodium, first with a strong probe laser and a conventional MOT (Lett *et al.*, 1993), then with a “dark spot” MOT which increased their ionization signal about a hundred fold (Ratliff *et al.*, 1994). In contrast the University of Texas group, led by D. J. Heinzen, used a far-off-resonance optical trap (FORT) to capture rubidium atoms (Miller *et al.*, 1993a) and to measure photoassociation spectra by measuring fluorescence loss from the trap as a function of trap frequency (Miller *et al.*, 1993b). These two experiments opened a new domain of precision spectroscopy from which molecular potentials, scattering dynamics, atomic lifetimes, and scattering lengths have all been determined with an accuracy unattainable by conventional methods. An excellent review of PAI has recently appeared (Lett *et al.*, 1996), lucidly explaining developments up to about mid-1995.

##### 1. Sodium

The NIST group first reported a PAI spectrum (Lett *et al.*, 1993) showing regular vibrational progressions by scanning a probe laser to the red of the MOT cycling transition. The setup used the same conventional MOT and dedicated, retroreflected probe laser source that Wagshul *et al.* (1993) employed to study hyperfine ef-

fects. The PAI spectrum showed two regular progressions, one strong series ranging from about 5 to 100 GHz to the red of the MOT cycling transition and a second weaker series discernible from 15 to 40 GHz red detuning. These regular features are the vibrational series corresponding to long-range molecular potentials of the singly excited  $\text{Na}_2$  molecule. The  $C_3/R^3$  form of these long-range potentials arises from the resonant dipole-dipole interaction between an excited  $\text{Na}^*(3p)$  atom and a ground state  $\text{Na}(3s)$  atom. Four optically active excited molecular potentials supporting vibrational levels and correlating to the  ${}^2S_{1/2} + {}^2P_{3/2}$  asymptote are candidates for the observed regular progressions. In Hund’s case (c) coupling these states are labeled  $1_u$ ,  $0_g^-$ ,  $1_g$ , and  $0_u^+$ . They will have different effective  $C_3$  coefficients and their vibrational progressions will have different hyperfine substructure. Both of these characteristics serve to identify states to which the spectra belong.

LeRoy and Bernstein (1970) and Stwalley (1970) have shown that in this long-range regime the spacing between vibrational levels can be described analytically by

$$\frac{dE(v)}{dv} = \hbar \left( \frac{2\pi}{\mu} \right) \frac{\Gamma(4/3)}{\Gamma(5/6)} \frac{3}{C_3^{1/3}} [D - E(v)]^{5/6}, \quad (117)$$

which integrates to

$$E_v - D = \left( \frac{a}{C_3^2} \right) (v - v_d)^6, \quad (118)$$

where  $v$  is the vibrational quantum number counted from the top of the well, and  $v_d$  is the effective quantum number at the apparent dissociation. The number  $v_d$  is a fraction between 0 and 1. The first bound vibrational level below dissociation is always labeled  $v = 1$ . The term  $D$  denotes the dissociation energy, and  $a$  is a collection of constants including the reduced mass,  $\mu$ . The NIST group fit a plot of  $(E_v - D)^{1/6}$  vs  $(v - v_d)$  to the centroids of the peaks for the strong and weak series. From the slope they determined  $C_3 = 10.37 \pm 0.07$  a.u. for the strong series and  $C_3 = 10.8 \pm 0.7$  a.u. for the weak series. The calculated Hund’s case (c)  $C_3$  constants for the optically active excited states clearly narrowed the possible identification of the strong and weak series to  $1_g$  and  $0_u^+$ . The measured peak widths, due to hyperfine substructure, were  $\sim 1$  GHz, consistent with calculations for  $1_g$  but not for  $0_u^+$ . According to Williams and Julienne (1994), the  $0_u^+$  state should show about one third the hyperfine substructure as the  $1_g$  state. Therefore, *both* the strong and weak series must belong to the  $1_g$ . Since the apparent dissociation energy determined from Eq. (118) for the two series differs by about the ground-state hyperfine splitting, Lett *et al.* (1993) concluded that the origin of the strong and weak progressions arose from 2+2 collisions and 2+1 collisions, respectively. However, one may ask, Why is it that the average measured  $C_3$  lies near 10.6 a.u. with uncertainty of about 0.7% while the best  $C_3$  value for the  $1_g$  state is 9.55 a.u., a difference of about 8%? The reason is that the  $1_g$  potential originates from diagonalizing a  $3 \times 3$  potential matrix, and  $C_3$  is only independent of  $R$  in the region of

internuclear separation where the binding energies of the states is much less than the atomic fine structure splitting, i.e.,  $C_3/R^3 \ll \Delta E_{FS}$ . In this range of  $R$  the  $C_3$  term is *independent* of  $R$ . At shorter internuclear separation the diagonalized adiabatic states will fit to  $C_3$  constants that depend on the range of  $R$  over which the potential is sampled. Williams and Julienne (1994) report that fitting vibrational eigenvalues obtained from adiabatic electronic-rotational-hyperfine molecular potentials to Eq. (118) yields a  $C_3$  in agreement with the measured value of the strong series within experimental error *as long as the measured and calculated values span the same range in the progression*. The  $C_3$  extracted from such fits can be used to obtain a precision measurement of the excited atom lifetime. Section VI.E reviews precision measurement of excited state lifetimes.

Ratliff *et al.* (1994) improved the NIST experiment by substituting a “dark spot” MOT (Ketterle *et al.*, 1993) for the conventional MOT, increasing the ion signal by two orders of magnitude and permitting a probe scan over  $172 \text{ cm}^{-1}$  to the red of the trapping transition. Figure 57 shows the full range of this photoassociative ionization spectrum. These new results revealed the  $1_g$ ,  $0_u^+$ , and  $0_g^-$  states, identified by the energy range over which they were observed, vibrational and rotational spacing, and the extent of the hyperfine structure. Furthermore, alternately chopping the trap and probe lasers at 50 KHz while slowly scanning the probe permitted two kinds of measurements: (1) trap-loss spectra during the trap phase, as measured by ions produced by the trapping lasers, and (2) ionization production during the probe phase. Figure 58 shows how these two complementary spectra helped distinguish the various progressions. The long progression of the  $1_g$  state shows clearly the change of coupling regime from Hund’s case (c) to Hund’s case (a) at closer range. Hund’s case (a) labels the state  $^1\Pi_g$  and the vibrational lines split into rotational progressions. The molecular transition giving rise to this progression is  $^3\Sigma_u^- \rightarrow 1_g$  (or  $^1\Pi_g$  at close range); however, the triplet character diminishes as the coupling scheme transforms from Hund’s case (c) to (a), and the natural line width diminishes to less than 0.1 MHz. Therefore at closer range (detunings  $\geq 50 \text{ cm}^{-1}$ ) the spectral resolution is limited only by the probe laser width ( $\sim 2 \text{ MHz}$ ) permitting analysis of the line profiles of the resolved rotational progressions.

The individual rotational line profiles show structure and asymmetries due to the finite temperature of the MOT, residual hyperfine splitting and quantum threshold effects. Figure 59 shows the measured rotational line shapes obtained by Ratliff *et al.* (1994) for the  $v=48$  vibrational level of the  $1_g$  state. Evidence of hyperfine contributions can be seen in the incompletely resolved substructure of  $J=1$  and  $J=2$  profiles. An analysis of these rotational line shapes have been carried out by Napolitano *et al.* (1994), the results of which are shown in Fig. 60. The intensity of the photoassociation spectrum is proportional to the thermally averaged rate coefficient. The quantum scattering expression for the rate

coefficient in terms of the scattering matrix  $S$  and the scattering partial waves  $l$  is written as

$$K_p(T, \omega) = \frac{k_B}{h Q_T} \sum_{l=0}^{\infty} (2l+1) \times \int_0^{\infty} |S_p(E, l, \omega)|^2 e^{-E/k_B T} \frac{dE}{k_B T}, \quad (119)$$

where  $S_p(E, l, \omega)$  is the  $S$ -matrix element for product channel  $p$ ,  $Q_T = (2\pi \mu k_B T / h^2)^{3/2}$  is the translational partition function,  $k_B$  is Boltzmann’s constant,  $E = \hbar k^2 / 2\mu$  is the asymptotic kinetic energy of the colliding ground state  $^2S$  atoms, and the other terms in the expression have their usual meanings. At relatively large detunings where the vibration-rotation lines are isolated from each other, Napolitano *et al.* (1994) used quantum scattering calculations with a complex potential to show that the form of  $S_p(E, l, \omega)$  around a scattering resonance can be modeled as

$$|S_p(E, l, \omega)|^2 = \frac{\Gamma_p \Gamma_s(E, l)}{(E - \Delta_b)^2 + (\Gamma/2)^2}, \quad (120)$$

where  $\Delta_b$  is the probe laser detuning from the bound rovibronic state of the excited level of the free-bound transition,  $\Gamma_p$  is the decay width to the collision product (whatever that decay process might be) and  $\Gamma_s(E, l)$  is the stimulated rate connecting the ground and excited levels. The  $\Gamma$  term in the denominator is the sum of  $\Gamma_p$  and  $\Gamma_s$ , plus any other decay processes that affect the level in question. Since  $\Gamma_s = 2\pi P_{ge}(E)$ , where  $P_{ge}(E)$  is defined by Eq. (28),  $\Gamma_s$  exhibits the Wigner-law threshold behavior due to the quantum properties of the ground-state wave function as described in Sec. III.B. This threshold behavior has the form of  $\Gamma_s \approx A_l E^{(2l+1)/2}$  as  $E \rightarrow 0$ . Three partial waves,  $s, p, d$  contribute to the scattering amplitude of the  $J$ -levels of Fig. 60; their influence can most easily be seen on the blue (right-hand) slope of each profile. Note especially in the  $J=2$  panel of Fig. 60 the very sharp onset to the profile, illustrating the influence of the Wigner threshold law for the  $s$ -wave contribution (close to infinite slope as  $E \rightarrow 0$ ). On the red side of the profile, the intensity falls off as  $e^{-\Delta_b/k_B T}$  and at first thought one might expect to extract a collision temperature from the slope of a semilog plot. However, the  $s, p, d$  contributions to the line shapes all yield somewhat different effective temperatures, again due to the influence of the Wigner threshold law operating on  $\Gamma_s$ . In order to extract a meaningful temperature from the experimental line shape therefore the fractional partial wave contributions to the profile must be known. It is also worth noting that the particular admixture of partial waves at a particular temperature will shift the peak positions of the lines, and the line “position” must be found by modeling the onset on the blue side of the profile (Jones, Julienne, *et al.*, 1996).

Recently, a combination of high resolution photoassociative spectroscopy of cold Na together with conventional molecular spectroscopy using atomic beams and heat pipe, permitted Jones, Maleki, *et al.* (1996) to per-

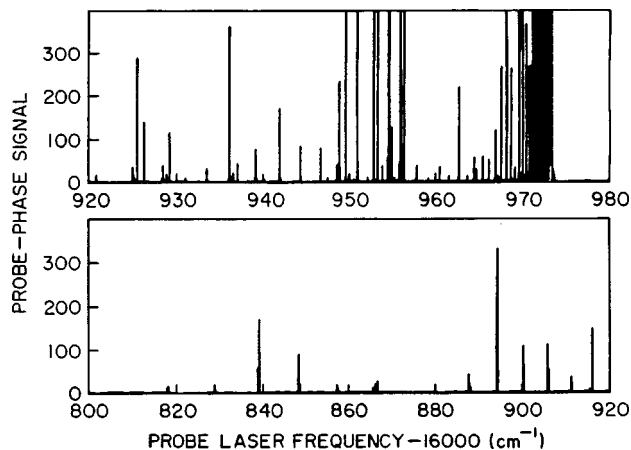


FIG. 57. Photoassociative ionization spectrum of Na collisions from the NIST dark-spot MOT. From Ratliff *et al.* (1994).

form a direct measurement of the ground-state dissociation energy ( $D_0$ ) of  $\text{Na}_2$  with unprecedented precision. Combining three spectroscopic measurements, Jones, Maleki, *et al.* (1996) obtained  $D_0$  for the  $X^1\Sigma_g^+$  ground state as  $D_0 = 5942.6880(49) \text{ cm}^{-1}$ , making this the most accurately known dissociation energy of any chemically bound neutral molecule. This result demonstrates how cold photoassociation spectroscopy can complement conventional spectroscopy with a considerable increase in resolution.

Additional two-color experiments have revealed other interesting details about the PAI process. Molenaar *et al.* (1996) have reported a two-color PAI spectrum in a Na MOT in which they determine high-lying vibrational levels of the  $0_g^-$  and observe a predissociation of this state at a curve-crossing interaction between the  $0_g^-$  and the ground-state  $^2S_{1/2}$  ( $F=1$ ) hyperfine level. Similar spectra near the  $0_g^-$  dissociation have been reported by Bagnato *et al.* (1994).

## 2. Rubidium

Although the atom trap most commonly used for collision studies has been the MOT, Miller *et al.* (1993a) pioneered the use of the far-off-resonance trap (FORT) to study photoassociation experiments in Rb. The advantages of the FORT over the MOT are (1) relative simplicity (no magnetic fields), (2) very low excited state population and therefore little diffusional heating, (3) high density ( $10^{12} \text{ cm}^{-3}$ ) and (4) a well-defined polarization axis along which atoms can be aligned or oriented. The disadvantage is the relatively low number of atoms ( $\sim 10^4$ ) trapped in the small volume ( $\sim 5 \times 10^{-9} \text{ cm}^3$ ). In the experiment of Miller *et al.* (1993b), the FORT was loaded from a MOT by spatially superposing the focused FORT laser on the MOT and alternately chopping the two kinds of traps. At the end of the load sequence fluorescence detection probes the number of atoms in the FORT. In the first version of the experiment, the FORT laser itself was swept in frequency from  $50 \text{ cm}^{-1}$  to  $980 \text{ cm}^{-1}$  to the red of the atomic resonance. As the laser scanned through the bound state reso-

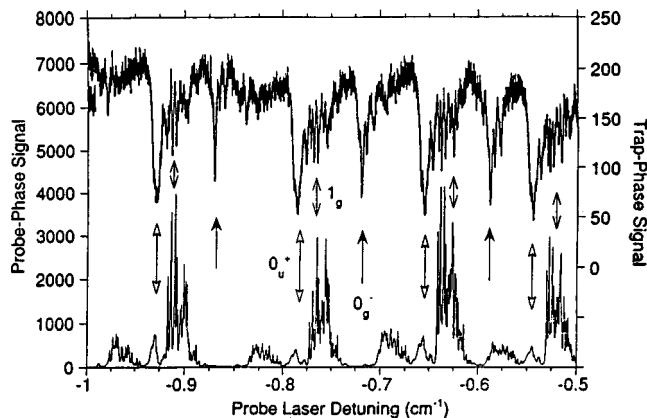


FIG. 58. Top spectrum shows trap-loss dips as probe laser scans through molecular rotational progressions. Bottom ion spectrum shows complementary photoassociative ionization signals. From Ratliff *et al.* (1994).

nances, the free-bound association peaks were detected by measuring the resulting loss of atoms from the FORT. Figure 61 shows the results of the trap-loss spectra. The increase of the background intensity as the dissociation limit is approached represents an increase in the Franck-Condon overlap and is also a consequence of the increase in the atomic density in the trap. The solid and dashed vertical lines on the top of the spectra of Fig. 61 identify two vibrational series. Comparison of these series with energy eigenvalues of model potentials by Movre and Pichler (1977), Krauss and Stevens (1990), and Bussery and Aubert-Frecon (1985a, 1985b) identify them as the  $1_g$  and  $0_g^-$  states. A noticeable feature in the spectrum obtained by Miller *et al.* (1993b) is the slow oscillation in the intensity of the lines. Thorsheim *et al.* (1987) predicted these Condon modulations. They arise from the Franck-Condon overlap of the ground- and excited-state wave functions, and the oscillations reflect the nodes and antinodes of the scattering wave function on the entrance ground-state channel. This is a consequence of the reflection principle in Eq. (32). Changing

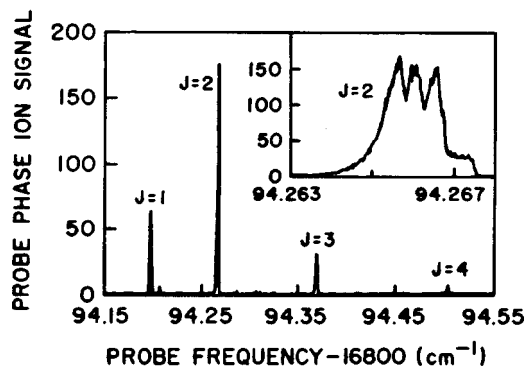


FIG. 59. High resolution photoassociative ionization spectrum of rotational levels associated with  $v=48$  of the long-range  $1_g$  state of  $\text{Na}_2$ . Note residual hyperfine splitting in the  $J=2$  inset. From Ratliff *et al.* (1994).

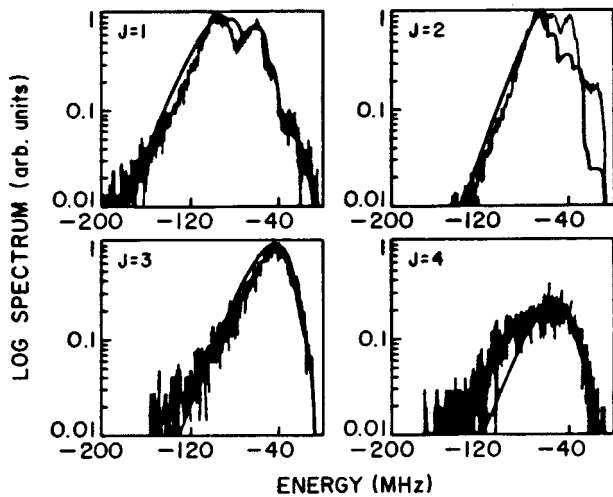


FIG. 60. High resolution line profile measurements and theory on rotational progression associated with  $v=48$  of the long-range excited  $1_g$  state of  $\text{Na}_2$ . From Napolitano *et al.* (1994).

the excitation frequency changes the Condon point  $R_C$  so that the spectrum tracks the shape of the ground-state wave function.

In a second version of this experiment Cline *et al.* (1994a, 1994b) separated the trapping and scanning functions with two different lasers: one laser at fixed frequency produced the FORT while a probe laser scanned through the resonances. The two lasers, probe and FORT, were alternately chopped to avoid spectral distortion from light shifts and power broadening. Miller *et al.* (1993b) restricted themselves to a spectral region from  $50 \text{ cm}^{-1}$  to  $980 \text{ cm}^{-1}$  below the  $2^2S_{1/2} + 2^2P_{1/2}$  dissociation limit of  $\text{Rb}_2$ . The two-color experiment (Cline *et al.*, 1994a, 1994b) enabled a greatly increased spectral range and the identification of the  $0_g^-$  “pure-long-range” state, the  $1_g$ , and the  $0_u^+$ . The high-resolution photoassociation spectrum is shown in Fig. 62. From this high-resolution spectra Cline *et al.* (1994a, 1994b) determined the  $C_3$  coefficient for two molecular excited states of  $\text{Rb}_2$ . The values are:  $C_3(0_u^+) = (14.64 \pm 0.7)$  a.u. and  $C_3(1_g) = (14.29 \pm 0.7)$  a.u. The spectra also show that the  $0_u^+$  lines are broadened by predissociation to the  $5^2S_{1/2} + 5^2P_{1/2}$  asymptote from spin-orbit mixing of the  $0_u^+$  components of  $A^1\Sigma_u^+$  and  $b^3\Pi_u$  at short range. This broadening is evidence of the fine-structure-charging collisions trap-loss process discussed in Sec. V. Recently the Texas group, in collaboration with the Eindhoven theory group, extended their experiments to a two-color photoassociation spectroscopy in which the second color couples population from the initially excited  $0_g^-$  to the last 12 vibrational levels of the  $^{85}\text{Rb}_2$  ground state (Tsai *et al.*, 1997). This high-precision spectroscopic data permits accurate determination of interaction parameters and collision properties of Rb ultracold collisions including the scattering length and the position of Feshbach resonances (see Sec. VIII.B), both of which are very important for Bose-Einstein condensation in ultracold Rb.

As an alternative to trap-loss spectroscopy Leonhardt and Weiner (1995, 1996) investigated  $\text{Rb}_2$  photoassociation spectra by direct photoassociative ionization. Figure 63(b) illustrates the main steps in this experiment. Atoms held in a vapor-cell-loaded MOT are illuminated with two light beams: a probe beam  $\omega_p$  scans through the resonances of the singly excited  $\text{Rb}_2$  long-range potential while a second, transfer laser at fixed frequency  $\omega_t$  directly photoionizes the bound excited molecule to high-lying vibrational states of  $\text{Rb}_2^+$ . This direct two-color photoassociative ionization process does not compete with an open autoionizing channel, as in sodium [Fig. 63(a)], because the manifold of doubly excited states  $P+P$  lies below the minimum in the dimer ion potential. Sweeping the probe laser to the red of the atomic resonance and counting the ions, Leonhardt and Weiner (1995, 1996) produced the photoassociative spectrum shown in Fig. 64 where the FORT trap-loss spectrum obtained by Cline *et al.* (1994a, 1994b) has been added for comparison. The direct  $\text{Rb}_2$  PAI spectrum appears to show only one molecular state progression. In fact, comparison with the FORT experiment shows that the  $0_g^-$  progression is absent in the photoassociative ionization spectrum. The measured series is assigned to the  $1_g$  state and the determination of the potential constant resulted in  $C_3(1_g) = (14.43 \pm 0.23)$  a.u. in good agreement with the value determined by Cline *et al.* (1994a, 1994b). Direct PAI should be widely applicable to many trappable species, but requires the densities of a dark spot MOT or a FORT to compete effectively with fluorescence trap-loss spectroscopy.

### 3. Lithium

The Rice University group, lead by R. G. Hulet, has performed a series of experiments in an atomic-beam-loaded MOT of  $^6\text{Li}$  and  $^7\text{Li}$ . Photoassociation trap-loss fluorescence spectroscopy has been carried out on both isotopes and the resulting data has been used to determine  $C_3$  coefficients, atomic lifetimes, and scattering lengths. The Rice group reported the basic spectroscopy, experimental technique, and analysis late in 1995 (Abraham, Ritchie, *et al.*, 1995). Earlier in the year the same group determined a precise atomic radiative lifetime for the Li ( $2p$ ) level using the same photoassociation spectral data (McAlexander *et al.*, 1995). A sample of the  $^6\text{Li}_2$  spectrum reported by McAlexander *et al.* (1995) is shown in Fig. 65. Indicated in the figure are the vibronic series for the  $1^1\Sigma_u^+$  and  $1^3\Sigma_g^+$  states which converge on the  $2s^2S_{1/2} + 2p^2P_{1/2}$  asymptotic limit. Three rotational lines ( $N=0, 1$ , and  $2$ ) are resolvable in the  $1^3\Sigma_g^+$  series as shown in the inset of Fig. 65. The  $N=0$  line is used for the series analysis to construct part of the  $1^3\Sigma_g^+$  interaction potential. The basic approach is to fit together a molecular potential at short, medium, and long range from various sources of calculated potentials and spectral data. At long range beyond  $20a_0$  the potential is approximated analytically by the form

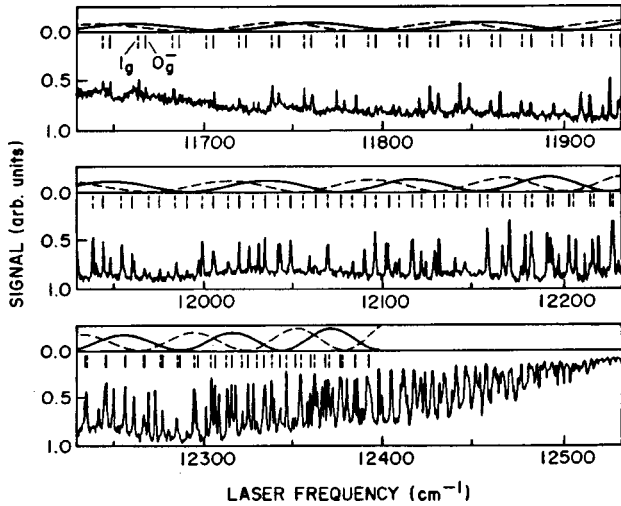


FIG. 61. Photoassociation FORT trap-loss fluorescence spectrum of  $\text{Rb}_2$ . From Miller *et al.* (1993b).

$$V \approx -\frac{C_3}{R^3} - \frac{C_6}{R^6} - \frac{C_8}{R^8}, \quad (121)$$

where  $C_3$  is due to the dominant resonant dipole interaction, and the other two dispersion terms are quite small compared to the dipole term. At very short range, less than  $4.7a_0$ , and then from  $7.8a_0$  to  $20a_0$  the potential uses *ab initio* calculations. In the region between  $4.7a_0$  and  $7.8a_0$  conventional spectroscopy yields an accurate Rydberg-Klein-Rees (RKR) potential. The different potential segments are then pieced together with a cubic spline and the spectral positions are calculated while  $C_3$  is varied as a free parameter until the best fit is obtained. McAlexander *et al.* (1995) finally report a  $C_3(1^3\Sigma_g^+) = 11.048 \pm 0.066$  a.u. This  $C_3$  is then used to calculate a lifetime for the Li ( $2p$ ) level. Deriving lifetimes from photoassociation spectra will be discussed in Sec. VI.E. In more recent work, Abraham, McAlexander, Stoof, and Hulet (1996) reported spectra of hyperfine resolved vibrational levels of the  $1^1\Sigma_u^+$  and  $3^3\Sigma_g^+$  states of both lithium isotopes, obtained via photoassociation. A simple first-order perturbation theory analysis accounts for the frequency splittings and relative transition strengths of the observed hyperfine features.

#### 4. Potassium

The research groups of Stwalley and Gould at the University of Connecticut have joined forces to mount a comprehensive study of the photoassociation spectroscopy in ultracold  $^{39}\text{K}$  collisions. Implementation of a MOT in potassium presents an unusual situation among the alkalis. All the excited-state hyperfine levels are spaced within 34 MHz, making it impossible to identify well-defined cycling and repumping transitions to cool and maintain the MOT. Nevertheless, following Williamson and Walker (1995), the Connecticut group was able to realize a working potassium MOT by essentially treating the whole group of excited hyperfine levels as a single “line” and tuning the cooling laser 40 MHz to the

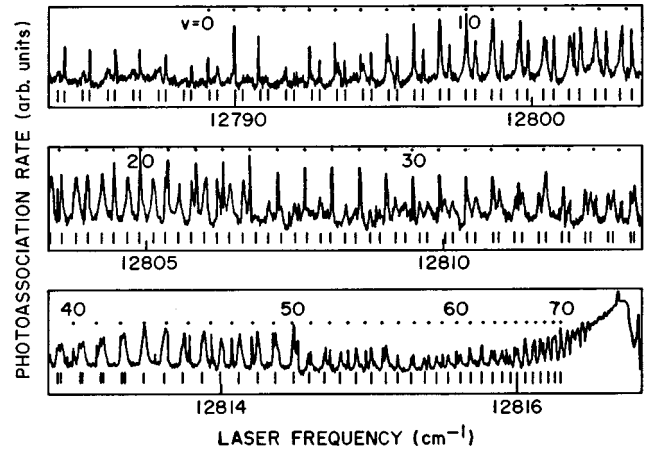


FIG. 62. Cline *et al.* (1994a, 1994b) separated the trapping and scanning functions with two different lasers: one laser at fixed frequency produced the FORT while a probe laser scanned through the resonances.

red of the  $^{39}\text{K } 4s^2S_{1/2}(F=2) \rightarrow 4p^2P_{3/2}(F'=3)$  transition. The “repumping” beam was set 462 MHz to the red of the same transition, equal to the splitting between the ground-state hyperfine levels. A potassium MOT requires relatively high intensity:  $90 \text{ mW cm}^{-2}$  for the “cooling” laser and  $40 \text{ mW cm}^{-2}$  for the “repumper,” although both beams undoubtedly fulfill both cooling and repumping functions. Wang *et al.* (1996a) report a MOT performance of  $\sim 2 \times 10^7$  captured atoms, a density  $\sim 3 \times 10^{10} \text{ cm}^{-3}$ , at a temperature  $\sim 500 \mu\text{K}$ . Insertion of a dark-spot disk (Ketterle *et al.*, 1993) in the horizontal components of the “repumper” beam enhanced the photoassociation rate by about one order of magnitude. With this potassium MOT, the Connecticut group carried out cold photoassociation spectroscopy by measuring trap-loss fluorescence as an intense ( $1\text{--}2 \text{ W cm}^{-2}$ ) probe laser scanned about  $7 \text{ cm}^{-1}$  to the red of the  $S_{1/2}(F=2) \rightarrow P_{3/2}(F'=3)$  reference. Figure 66 shows an example of the regular progressions observed. In their initial report Wang *et al.* (1996a) identified the  $0_g^-$ ,  $0_u^+$ , and  $1_g^-$  states associated with the  $S_{1/2} + P_{3/2}$  asymptote. In a followup study on the “pure long-range” states, Wang *et al.* (1996b) determined the molecular constants of the  $0_g^-$  and the  $C_3$  constants for the  $0_u^+$  and  $1_g^-$  states. They also pointed out the utility of the  $0_g^-$  as an intermediate “window” state to access even higher-lying states  $K_2$  by optical-optical double resonance. Very recently Wang, Wang, Gould, and Stwalley (1997) have observed optical-optical double resonance PAI spectroscopy near the  $^{39}\text{K}(4s) + ^{39}\text{K}(4d,5d,6d,7s)$  asymptotes, using the  $v'=0$  level of the  $0_g^-$  as the intermediate “window.” The Connecticut team has also reported a comprehensive study of the long-range interactions in potassium binary atom collisions (Wang, Gould, Stwalley, 1998b). They have observed the six long-range states of  $0_u^+$ ,  $1_g^-$ , and  $0_g^-$  symmetry, three dissociating to the  $4s^2S_{1/2} + 4p^2P_{3/2}$  asymptote and three to the  $4s^2S_{1/2} + 4p^2P_{1/2}$  asymptote. Furthermore their analysis has determined the  $C_3^{\Pi}$  and  $C_3^{\Sigma}$  constants from

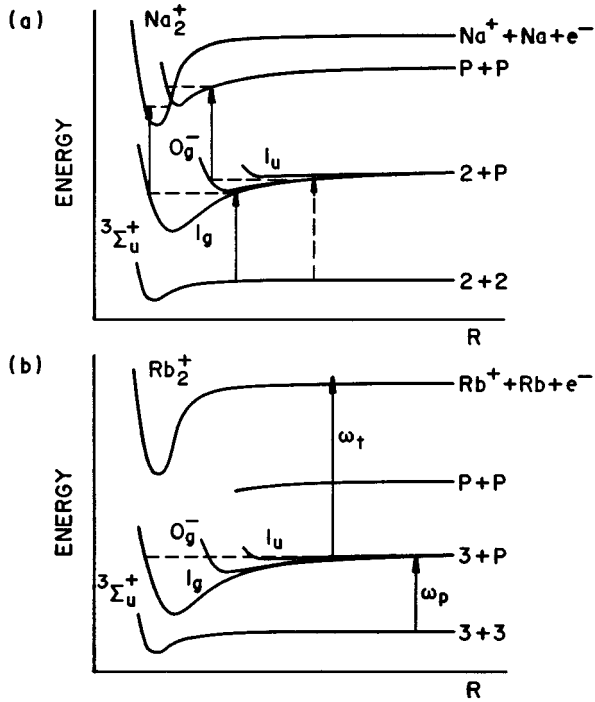


FIG. 63. PAI in sodium and rubidium collisions: (a) Potential diagram of  $\text{Na}_2$  and  $\text{Na}_2^+$  showing doubly excited asymptote above  $\text{Na}_2^+$  ionization threshold. (b) Potential diagram of  $\text{Rb}_2$  and  $\text{Rb}_2^+$  showing doubly excited asymptote below  $\text{Rb}_2^+$  threshold.

the  $0_g^-$  “pure long-range” state, from which they extract a precise measure of the  $K(4p)$  radiative lifetime, as well as the  $C_6^{\text{II}}$  and  $C_6^{\Sigma}$  constants. More recently, they have identified for the first time in an alkali dimer spectrum the pure long range  $1_u$  state (X. Wang, H. Wang *et al.*, 1998). Finally Wang, Gould, and Stwalley (1998a) have very recently reported direct observation of predissociation due to fine-structure interaction in the photoassociation spectra of  $K_2$ .

#### E. Atomic lifetimes from photoassociation spectroscopy

Because cold atoms collide at temperatures corresponding to kinetic energy distributions of order equal

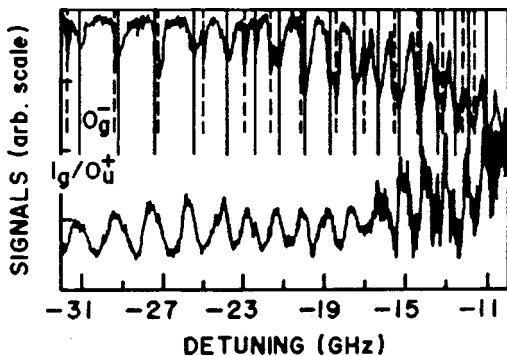


FIG. 64. Direct photoassociative ionization of  $^{85}\text{Rb}$  collisions in a MOT. The upper trace is the trap-loss spectrum from Texas FORT, and the lower trace is the  $\text{Rb}_2^+$  ion signal from the direct PAI. From Leonhardt and Weiner (1995).

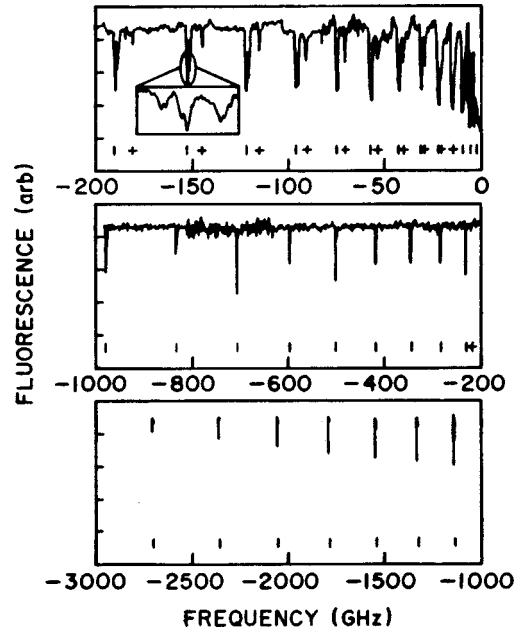


FIG. 65. Photoassociation spectrum from a  $^6\text{Li}$  MOT. Inset shows rotational substructure on vibrational lines. From McAlexander *et al.* (1995).

to or less than the spontaneous emission linewidth of their cooling transition, they are particularly sensitive to binary interactions when the partners are far apart. The dominant long-range interaction between identical atoms, one resonantly excited and the other in the ground state, is the dipole-dipole potential discussed many years ago by King and van Vleck (1939). They showed that this interaction potential between atom  $A$  in excited state  $P$  and atom  $B$  in ground state  $S$  is given by

$$V(R) = \pm \frac{1}{R^3} [\langle d_x \rangle^2 + \langle d_y \rangle^2 - 2\langle d_z \rangle^2], \quad (122)$$

where  $\langle d_q \rangle$ ,  $q=x,y,z$  are the transition dipole matrix elements between the two states. Normally the  $z$  axis is taken as the line joining the two atom centers, and  $C_3$  constants are then defined in terms of the transition dipoles as a “transverse” component,

$$C_3^{\text{II}} = \langle d_x \rangle^2 = \langle d_y \rangle^2 \quad (123)$$

and an “axial” component,

$$C_3^{\Sigma} = 2\langle d_z \rangle^2 = 2C_3^{\text{II}}. \quad (124)$$

The transition moments themselves are related to the atomic excited state lifetime  $\tau$  through the average rate of spontaneous photon emission  $\Gamma$ , written in mks units,

$$\Gamma = \tau^{-1} = \frac{16\pi^3 \nu^3}{3\epsilon_0 h c^3} \langle d_q \rangle^2.$$

With  $C_3^{\text{II}}$  also written in mks units,

$$C_3^{\text{II}} = \frac{1}{4\pi\epsilon_0} \langle d_q \rangle^2, \quad (125)$$

the atomic lifetime can be written in terms of  $C_3$  as

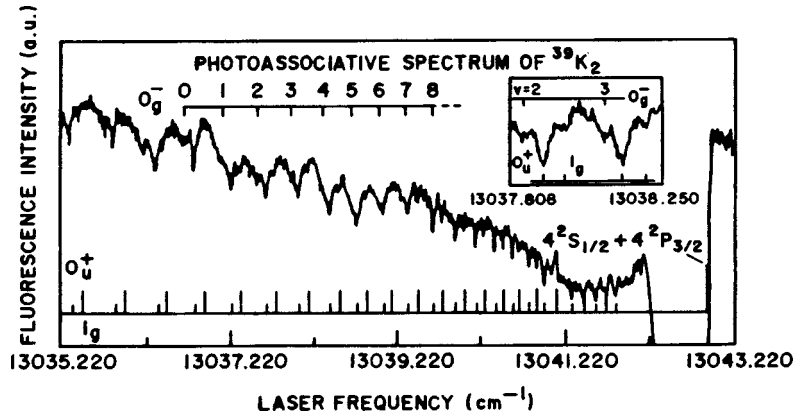


FIG. 66. Trap-loss fluorescence spectrum from photoassociation of  $^{39}\text{K}$ . From Wang *et al.* (1996a).

$$\tau = \frac{3\hbar}{4C_3^{\text{II}}} \left( \frac{\lambda}{2\pi} \right)^3 \quad (126)$$

Therefore, a precise determination of  $C_3^{\text{II}}$  from cold photoassociation spectroscopy will determine a precise measure of the atomic excited-state lifetime.

For most molecular states that exhibit strong chemical binding, however, the long-range, dipole-dipole interaction is only one of several  $R$ -dependent interaction terms in the Hamiltonian. At close range the electron clouds from each atom interpenetrate and give rise to electron-nuclear attraction, electron-electron repulsion terms, as well as attractive quantum mechanical electron exchange terms which decrease exponentially with increasing  $R$ . In this near zone the electron orbital angular momentum, with a molecular axis projection denoted by  $\Lambda$ , strongly couples to the internuclear axis, and the electron spin  $S$ , orbital angular momentum, and axis rotation angular momenta are coupled in a scheme called Hund's case (a), with states designated by the notation  $^S\Lambda$ . At greater internuclear separation, beyond the exchange interaction, the interatomic interaction is described by resonant dipole-dipole and dispersion terms varying with inverse powers of  $R$ ,  $V(R) \sim \pm C_3/R^3 - C_6/R^6 - C_8/R^8$ . At sufficiently large distances, where the energy separations between the different Hund's case (a) states become small compared to the atomic fine-structure splitting, electron orbital and spin angular momentum couple strongly together to form a total electronic angular momentum, whose projection on the molecular axis is designated  $\Omega$ . The total electronic angular momentum couples with nuclear rotation to form a total angular momentum called Hund's case (c), with states labeled by  $\Omega$ . This scheme is used to label the potentials in Fig. 47.

In order to extract  $C_3$  from observed spectral line positions, it is necessary to understand all the terms in the molecular Hamiltonian, which have contributions from the interatomic interactions, molecular rotation, and fine and hyperfine structure. Fortunately, these can all be taken into account with great precision and detail in the case of photoassociation, where the spectra are due to single molecular states. Although a complete quantitative theory of the rotating molecule with hyperfine struc-

ture can be developed (Tiesinga *et al.*, 1997) it is much easier to use simpler models, which are also highly quantitative (Jones, Julienne, *et al.*, 1996). The Hamiltonian of Movre and Pichler provides such a model. It includes the interatomic and fine-structure interactions (although rotation and hyperfine terms could be readily added). Only states with the same projection  $\Omega$  of total electronic angular momentum on the interatomic axis can couple to one another ( $\Omega = \Lambda + \Sigma$ , where  $\Lambda$  and  $\Sigma$  are the respective projections of orbital and spin angular momenta on the axis). At long range the off-diagonal interatomic interaction due to the resonant dipole coupling, proportional to  $C_3/R^3$ , mixes different states of the same  $\Omega$ . Diagonalizing the Movre-Pichler Hamiltonian gives the adiabatic molecular potential curves shown in Fig. 47. Therefore each individual adiabatic curve, such as  $1_g$  or  $0_g^-$ , has its own characteristic  $C_3$  coefficient at long range.

A good example of the Movre-Pichler analysis is provided by the two pure long-range  $0_g^-$  states dissociating to  $S+P$ . These result from a spin-orbit avoided crossing between two Hund's case (a) basis states: a repulsive  $^3\Pi_{0g}$  potential which goes as  $+C_3/R^3$  and an attractive  $^3\Sigma_{0g}$  potential which goes as  $-2C_3/R^3$ . The two adiabatic  $0_g^-$  potentials are found by diagonalizing the potential matrix (Jones, Julienne *et al.*, 1996):

$$V_{\text{MP}} = \begin{pmatrix} \Pi & \Sigma \\ \frac{C_3}{R^3} - \frac{2\Delta_{\text{FS}}}{3} & \frac{\sqrt{2}\Delta_{\text{FS}}}{3} \\ \frac{\sqrt{2}\Delta_{\text{FS}}}{3} & -\frac{2C_3}{R^3} - \frac{\Delta_{\text{FS}}}{3} \end{pmatrix} \begin{matrix} \Pi \\ \Sigma \end{matrix}, \quad (127)$$

where  $\Delta_{\text{FS}}$  is the atomic spin-orbit splitting ( $\Delta_{\text{FS}} = 515.520$  GHz for Na) and the zero of energy is the  $^2S_{1/2} + ^2P_{3/2}$  asymptote. Diagonalizing this matrix gives the two  $0_g^-$  states in Fig. 47, the upper going to  $^2P_{3/2} + ^2S_{1/2}$ , and the lower to  $^2P_{1/2} + ^2S_{1/2}$ . The upper  $0_g^-$  potential has a shallow well and is shown in Fig. 15. Although both curves are characterized by only a single atomic transition dipole matrix element, the diagonalization is  $R$  dependent, and the effective  $C_3$  value associated with a particular adiabatic curve is  $R$  dependent,

changing from a long-range value characteristic of Hund's case (c) coupling to a short range value characteristic of Hund's case (a) coupling. For example, the attractive Hund's case (c)  $1_g$  state from  ${}^2P_{3/2} + {}^2S_{1/2}$  changes to a Hund's case (a)  ${}^1\Pi_g$  state at short range. We have already seen Sec. VI how the  $C_3$  value found from fitting spectra for this state changes with the range of levels fitted. At short range the potentials are also affected by other terms in the electronic Hamiltonian. As  $R$  decreases, these terms can be ordered qualitatively: the van der Waals dispersion terms  $C_6/R^6$  first begin to play a role, then the exchange-overlap interaction due to overlapping atomic orbitals on the two atoms, and finally the strong chemical bonding at very small  $R$ . The effects of all of these terms must be taken into account, the specific details depending on the particular state being analyzed. The  $0_g^-$  state is especially useful in this regard, since it depends mainly on  $C_3$  and to a lesser extent on the dispersion energy.

The Rice group used the lower  ${}^3\Sigma_g^+$  state of  $\text{Li}_2$  (McAlexander *et al.*, 1995). Since this state is chemically bound with a large binding energy, the potential must be very accurately known over a wide range of  $R$  in order to use  $C_3$  as a free-variable fitting parameter to minimize differences between a constructed model potential and measured data. The accuracy of the lifetime determination was limited to 0.6% by the use of *ab initio* calculated potentials over a range of  $R$  (from  $7.8a_0$  to  $20a_0$ ) where spectroscopic data was unavailable. In an update to this experiment (McAlexander *et al.*, 1996) the Rice group was able to shrink the error bars even more by applying essentially the same approach but using an experimentally derived potential over the range of  $R$  where they had previously relied on calculations; moreover, by analyzing the hyperfine spectrum (Abraham, McAlexander, Stoof, and Hulet, 1996), they reduced the uncertainty in the vibrational energies. The reported uncertainty in the Li ( $2P$ ) lifetime from these measurements is 0.03%.

The "pure" long-range states, first proposed by Stwalley *et al.* (1978), support bound vibrational levels with turning points entirely outside the region where exchange potential makes significant contributions. The molecular potential therefore includes only the power series terms with atomic coefficients  $C_3, C_6, C_8 \dots$  and the constant atomic spin-orbit term. Transition moments and the atomic lifetimes can then be calculated from Eqs. (125) and (126). The NIST (Jones, Julienne, *et al.*, 1996) and Connecticut (Wang *et al.*, 1996a, 1996b) groups have followed this approach to study sodium and potassium respectively. Both groups used the "pure" long-range  $0_g^-$  state described by the Movre-Pichler Hamiltonian, Eq. (127), to obtain  $P$ -state lifetimes with uncertainties around the 0.1% level. As in the case of lithium, at this level of precision, retardation effects (Casimir and Polder, 1948; McLone and Power, 1964; Meath, 1968) have to be taken into account. This means that, in Eq. (127), the  $C_3$  term has to be replaced by  $f^{\Pi/\Sigma} \cdot C_3$  for the respective  $\Pi$  and  $\Sigma$  states where  $f^{\Pi/\Sigma}$  are the retardation correction factors,

$$f^{\Pi} = \cos\left(\frac{2\pi R}{\lambda}\right) + \left(\frac{2\pi R}{\lambda}\right) \sin\left(\frac{2\pi R}{\lambda}\right) - \left(\frac{2\pi R}{\lambda}\right)^2 \cos\left(\frac{2\pi R}{\lambda}\right) \approx 1 - \frac{(2\pi R/\lambda)^2}{2} \quad (128)$$

and

$$f^{\Sigma} = \cos\left(\frac{2\pi R}{\lambda}\right) + \left(\frac{2\pi R}{\lambda}\right) \sin\left(\frac{2\pi R}{\lambda}\right) \approx 1 + \frac{\left(\frac{2\pi R}{\lambda}\right)^2}{2}. \quad (129)$$

The significance of this factor can be gauged by comparing the magnitude of the retardation correction (121 MHz) to the experimental precision ( $\pm 5$  MHz) for the case of  $\text{Na}_2 0_g^-$  (Jones, Julienne, *et al.*, 1996).

Table II summarizes the results on precision lifetime measurements. The current best lifetimes for Li, Na, K, and Rb are from photoassociation spectroscopy. Only the Cs lifetime is based on conventional methods (Rafac *et al.*, 1994). The  $C_3$  coefficients for the five attractive states from  ${}^2P_{3/2} + {}^2S_{1/2}$  can be found by using the  $d^2$  from Table II with the formulas in Table I of Julienne and Vigué (1991).

#### F. Precision measurement of scattering length by photoassociative spectroscopy

As the kinetic energy of a binary collision approaches zero, the number of partial waves contributing to the elastic collision reduces to the  $s$  wave, and the information inherent in the scattering event can be characterized by the scattering length, as defined by Eq. (20),

$$A_0 = -\lim_{k \rightarrow 0} \left( \frac{1}{k \cot \eta_0} \right) \quad (130)$$

where  $k = 2\pi/\lambda_{dB}$  is the wave vector,  $\lambda_{dB}$  is the de Broglie wavelength of the reduced mass particle, and  $\eta_0$  is the  $s$ -wave phase shift due to the scattering potential. The role of the scattering length in ultracold ground state collisions is examined in detail in Sec. III.B. The sign and magnitude of  $A_0$  is crucially important to the attainment of Bose-Einstein condensation in a dilute gas (Cornell, 1996). Binary collisions with positive scattering length lead to large, stable condensates while negative scattering lengths do not, and the rate of evaporative cooling of the gas—necessary to achieve critical densities and temperatures of the BEC transition—depends on the square of the scattering length (Ketterle and Van Druten, 1996).

Photoassociation spectroscopy has played a pivotal role in determining accurate and precise values for the scattering length in collisions of Li, Na, and Rb, the three gases in which the quantum degenerate phase has been observed. The essential idea is to use photoassociative spectroscopy to probe the phase of the ground-state wave function with great precision. Two approaches have been most fruitful: (1) determination of the nodal positions of the ground-state wave function from the

relative intensities of spectral features, and (2) determination of the spectral position of the last ground bound state below the dissociation limit. The first approach takes advantage of the fact that photoassociative spectroscopy line intensities are sensitive to the amplitude of the ground-state wave function for each contributing partial wave near the Condon point of the transition, as indicated by Eq. (32). In particular, the slowly varying “Condon modulations” (Thorsheim *et al.*, 1987; Julienne, 1996) have minima that reveal the position of the ground-state wave-function nodes. A quantum scattering calculation tunes the model ground-state potentials until the relative spectral intensities in the calculation match those determined by the photoassociative spectroscopy experiment. The calculated phase shift then determines the scattering length  $A_0$  for the model. Although all three alkalis yielded excellent results to this line of attack, each one presented unique features of photoassociative spectroscopy analysis. The second approach uses a two-photon photoassociative spectroscopy to locate the exact position of the last bound states. After the initial free-bound photoassociation transition a second probe laser stimulates the excited population downward to the last bound vibrational level of the ground state. The detunings of the two probe lasers determine the spectral position of the last bound state, which in turn fixes the threshold phase of the ground-state potential within highly constrained limits. A quantum scattering calculation of the  $s$ -wave elastic phase shift then yields the scattering length. Both of these strategies have been used to good advantage.

### 1. Lithium

The Rice group led by R. G. Hulet determined the scattering length of collisions between two  ${}^7\text{Li}$  atoms in the  $F=2$ ,  $M_F=2$  state by using the two-photon technique to determine the last bound vibrational level of the  ${}^7\text{Li}_2(a^3\Sigma_u^+)$  triplet ground state (Abraham, McAlexander, *et al.*, 1995; Côté, Dalgarno, Sun, and Hulet, 1995). They set up a conventional lithium MOT and tuned a photoassociating laser to the  $v=64$  level of the  $1^3\Sigma_g^+$  bound excited state, using trap-loss fluorescence to find the free-bound transitions. Then a *second* probe connected this bound excited state back to high-lying bound states of the  $a^3\Sigma_u^+$  ground state. Resonances with the second probe were detected by an *increase* in the fluorescence base line, representing an anti-trap-loss fluorescence peak. Figure 67(a) shows the schematic of the stimulated excitation and deexcitation scheme, and Fig. 67(b) shows the peak in the MOT fluorescence as the second probe sweeps over the last bound vibrational level of the ground state. The difference frequency between the two probes, measured with a spectrum analyzer, permitted precise determination of the  $a^3\Sigma_u^+$  last bound-state energy with respect to the dissociation asymptote. Comparison of this energy with an accurate model potential identified the vibrational level with the  $v=10$  quantum number. Although the model potentials used to identify the last bound state (Moerdijk and Ver-

TABLE II. Atomic lifetimes and transition moments.

Atom	Lifetime, $\tau$ (ns)	$d^2$ (a.u.)
${}^7\text{Li}^a$ ( $2P_{1/2}$ )	27.102 (2) <sup>b</sup> (7) <sup>c</sup>	11.0028 (8) <sup>b</sup> (28) <sup>c</sup>
$\text{Na}^d$ ( $3P_{3/2}$ )	16.230 (16) <sup>b</sup>	6.219 (6) <sup>b</sup>
${}^{39}\text{K}^e$ ( $4P_{3/2}$ )	26.34 (5) <sup>b</sup>	8.445 (14) <sup>b</sup>
$\text{Rb}^f$ ( $5P_{3/2}$ )	26.23 (6) <sup>b</sup>	8.938 (20) <sup>b</sup>
$\text{Cs}^g$ ( $6P_{1/2}$ )	34.934 (94) <sup>b</sup>	10.115 (27) <sup>b</sup>

<sup>a</sup> McAlexander *et al.* (1996).

<sup>b</sup> One standard deviation.

<sup>c</sup> Systematic uncertainty.

<sup>d</sup> Jones, Julienne *et al.* (1996).

<sup>e</sup> Wang, Li, *et al.* (1997).

<sup>f</sup> Freeland *et al.* (1997).

<sup>g</sup> Rafac *et al.* (1994).

haar, 1994; Moerdijk, Stwalley, *et al.*, 1994; Côté *et al.*, 1994) were sufficient for that purpose, they both predicted a  $v=10$  binding energy of 11.4 GHz whereas the Rice group directly measured  $12.47 \pm 0.04$  GHz. The next step therefore was to modify the dissociation energy  $D_e$  of the potential of Côté *et al.* so that  $v=10$  level matched the measurement. The newly modified, fine-tuned model potential was then input to a quantum scattering calculation to determine the  $s$ -wave phase shift in the limit of zero temperature. Equation (130) then determined the scattering length. The final result, taking into account uncertainties in the long-range coefficients of the model potential, was found to be  $A_T(2,2) = -27.3 \pm 0.8$  a.u. where  $A_T(2,2)$  signifies the scattering length of the triplet potential starting from the  $F=2$ ,  $M_F=2$  doubly polarized atomic state.

In more recent work the Rice group used the Condon modulations in  $X^1\Sigma_g^+ \rightarrow A^1\Sigma_u^+$  photoassociation line intensities to determine the scattering lengths in  ${}^6\text{Li}$  and  ${}^7\text{Li}$  collisions (Abraham, McAlexander, Gerton, and Hulet, 1996). Figure 68 shows a plot of the photoassociation line intensities for the three possible combinations of atomic hyperfine levels (1+1, 1+2, 2+2) in the case of  ${}^7\text{Li}$  collisions. The minima, corresponding to nodes in the ground-state wave function, occur at slightly different positions for each of the hyperfine asymptotes. Varying the model potential of Côté *et al.* (1994), until the scattering lengths give the best fit to the node positions, resulted in  $A_S(1,1) = 39 \pm 3$  a.u.,  $A_S(2,1) = 33 \pm 5$  a.u., and  $A_S(2,2) = 31 \pm 3$  a.u. for  ${}^7\text{Li}$  collisions. In the case of  ${}^6\text{Li}$  the ground-state splittings were too close to resolve minima from the different hyperfine levels so the final result was reported as  $A_S = 47 \pm 3$  a.u. for  ${}^6\text{Li}$  collisions.

Finally in the most recent work (Abraham *et al.*, 1997) the Rice group completed the cycle in the lithium spectroscopy by determining the  $s$ -wave triplet scattering length in  ${}^6\text{Li}$ . Once again, as in the case of the boson isotope  ${}^7\text{Li}$ , they used the two-photon photoassociation technique to determine the precise energy of a bound state ( $v=9$ ) of the  $a^3\Sigma_u^+$  triplet ground state of  ${}^6\text{Li}_2$ . The result is also once again a negative scattering length, but of very large amplitude ( $A_T = -2160 \pm 250$  a.u.)

which indicates a near-threshold resonance lying just above the dissociation limit of the  $a^3\Sigma_u^+$  state.

## 2. Sodium

The NIST group also used the relative intensities of their photoassociative ionization spectra to determine the scattering length in Na collisions (Tiesinga *et al.*, 1996), but they were able to take advantage of a particularly fortuitous circumstance. One of the nodes of the ground state  $p$  wave (the “last” node before the wave assumes an oscillation characteristic of the 500  $\mu\text{K}$  temperature) appears directly below  $v=0$  vibrational level of the pure long-range  $0_g^-$  state. This  $p$ -wave node suppresses the intensity of photoassociation transitions to odd rotational levels of this  $v=0$  state and produces large variations in the rotational progression intensities for higher vibrational levels of the  $0_g^-$  state as well. Figure 69 shows the relative positions of the ground-state  $p$  wave, the  $0_g^-$  state, and the ionization pathway. Figure 70 shows how the  $J=1$  and  $J=3$  intensities are strongly suppressed in the  $v=0$  rotational progression because they arise from the  $p$ -wave contribution to the collision but then reappear in the  $v=1$  and  $v=5$  spectra. By varying parameters in the singlet  $X^1\Sigma_g^+$  and triplet  $a^3\Sigma_u^+$  ground states, the NIST group was able to reproduce the relative intensities and line shapes of the PAI spectra. The fine-tuning of the potentials shifted the  $p$ -wave and  $s$ -wave nodes to positions of best-fit to the spectra, and from these nodal positions the scattering lengths for collisions between atoms in  $F=1$ ,  $M_F=-1$  could be determined within narrow constraints. The result is  $A_{1,-1} = 52 \pm 5$  a.u.

## 3. Rubidium

The Texas group led by D. J. Heinzen, in collaboration with the Eindhoven theory group led by B. J. Verhaar, has carried out measurements of the scattering length in  $^{85}\text{Rb}$  collisions using a FORT in which the atoms were doubly spin polarized (Gardner *et al.*, 1995). The atoms approach only on the ground state  $a^3\Sigma_u^+$ , and the photoassociation trap-loss fluorescence spectroscopy measures vibration-rotation progressions in the  $a^3\Sigma_u^+ \rightarrow 0_g^-$  transition. Here the  $0_g^-$  state is *not* the pure long-range state but at short range becomes a component of the  $^3\Sigma_g^+$  molecular state dissociating to  $^2S_{1/2} + ^2P_{1/2}$ . Figure 71 shows how the electron and nuclear spin polarization restrict the populated  $0_g^-$  rotational states to even-numbered levels. Unlike the sodium case, with the  $0_g^-$  state from  $^2S_{1/2} + ^2P_{3/2}$ , in which more than one partial wave contributed to various members of the rotational progression, the  $0_g^-$  state from  $^2S_{1/2} + ^2P_{1/2}$  has a one-to-one correspondence between the  $J$  level and scattering partial wave. The intensity of each  $J$  peak effectively measures the amplitude of each partial wave. The energies of the  $J=0$  levels of five vibrational states were used to determine the product of the transition dipoles,  $d(P_{1/2})d(P_{3/2})$ , from a fit to the  $C_3/R^3$  potential in the range of  $R$  ( $\sim 41$ – $47$  a.u.), where the photo-

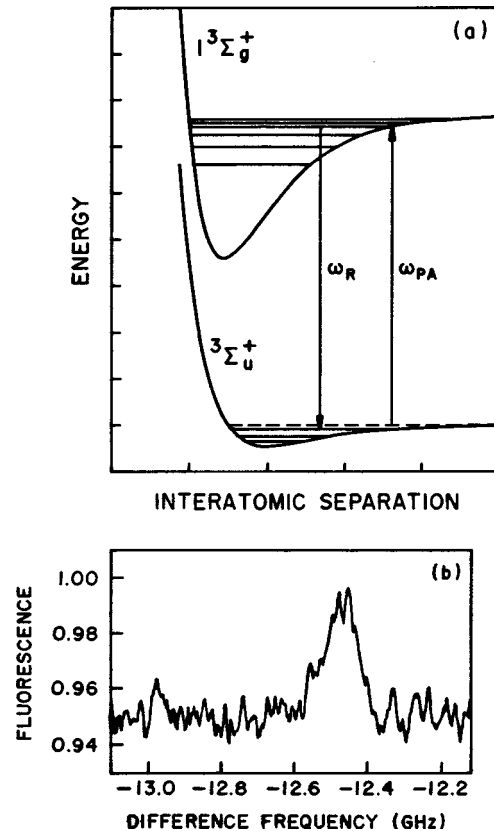


FIG. 67. Determination of the last bound state in  $^7\text{Li}_2(a^3\Sigma_u^+)$ : (a) Schematic of the stimulated excitation and deexcitation scheme. (b) Peak in the MOT fluorescence as the second probe sweeps over the last vibrational level of the ground state. From Abraham, McAlexander, *et al.* (1995).

association spectra are measured. A line-shape analysis similar to Napolitano *et al.* (1994) was then carried out on the  $J=0$  and  $J=2$  features from which a triplet scattering length  $-1000a_0 < a_T(^{85}\text{Rb}) < -60a_0$  was extracted. Using a  $\sqrt{m}$  scaling procedure and a model triplet potential, the Texas group concluded that the triplet scattering length for  $^{87}\text{Rb}$  fell in the range,  $+85a_0 < a_T(^{87}\text{Rb}) < +140a_0$ . These measurements showed that Bose-Einstein condensation was not favorable for the triplet state of  $^{85}\text{Rb}$  but was possible for  $^{87}\text{Rb}$ . In a followup experiment on shape resonances in  $^{85}\text{Rb}$  collisions (Boesten *et al.*, 1996) the same group was able to narrow the range of triplet scattering length to  $-500a_0 < a_T(^{85}\text{Rb}) < -300a_0$ , confirming that  $^{85}\text{Rb}$  would not produce large, stable condensates.

Table III summarizes the  $s$ -wave scattering length determinations for various isotopes and states of the three alkalis measured to date,

## VII. OPTICAL SHIELDING AND SUPPRESSION

### A. Introduction

Photoassociation uses optical fields to produce bound molecules from free atoms. Optical fields can also prevent atoms from closely approaching, thereby *shielding* them from short-range inelastic or reactive interactions

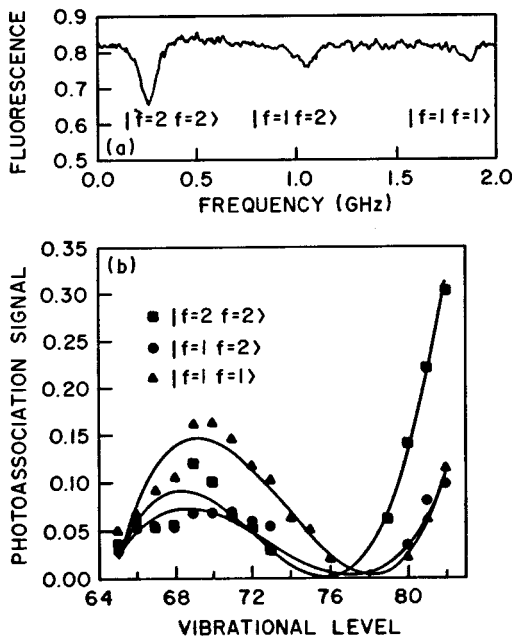


FIG. 68.  ${}^7\text{Li}$  collisions: (a) Plot of the photoassociation line intensities for the three possible combinations of atomic hyperfine levels. (b) Condon fluctuations showing nodes occurring at slightly different positions for each of the hyperfine asymptotes. From Abraham, McAlexander, Stoof, and Hulet, 1996.

and *suppressing* the rates of these processes. Recently several groups have demonstrated shielding and suppression by shining an optical field on a cold atom sample. Figure 72(a) shows how a simple semiclassical picture can be used to interpret the shielding effect as the rerouting of a ground-state entrance channel scattering flux to an excited repulsive curve at an internuclear distance localized around a Condon point. An optical field, blue detuned with respect to the asymptotic atomic transition, resonantly couples the ground and excited states. In the cold and ultracold regime particles approach on the ground state with very little kinetic energy. Excitation to the repulsive state effectively halts their approach in the immediate vicinity of the Condon point, and the scattering flux then exits either on the repulsive excited state or on the ground state. Figure 72(b) shows how this picture can be represented as a Landau-Zener avoided crossing of field-dressed potentials. As the blue-detuned suppressor laser intensity increases, the avoided crossing gap around the Condon point widens, and the semiclassical particle moves through the optical coupling region adiabatically. The flux effectively enters and exits on the ground state, and the collision becomes elastic. The Landau-Zener probability that the particle remain on the ground state as it passes once through the interaction region is

$$P_g = P_s = \exp\left(-\frac{2\pi\hbar\Omega^2}{\alpha v}\right), \quad (131)$$

where  $\alpha$  is the slope of the difference potential evaluated at the Condon point,

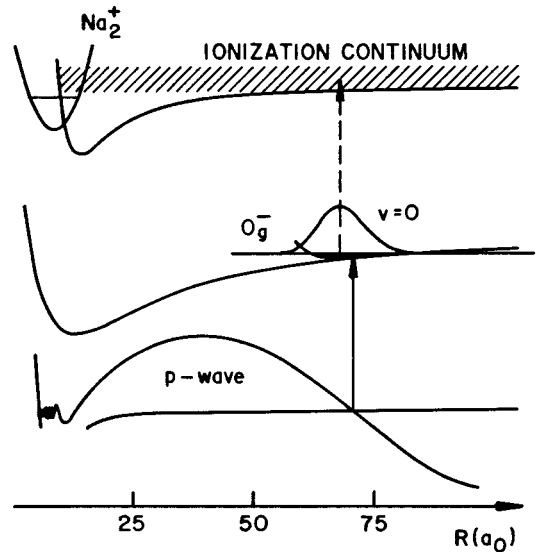


FIG. 69. Relative position of the ground state  $p$ -wave, the  $0_g^-$  state, and the ionization pathway. From Tiesinga *et al.* (1996).

$$\alpha = \left. \frac{d\Delta}{dR} \right|_{R_C} = \left. \frac{d[U_e(R) - U_g(R)]}{dR} \right|_{R_C}, \quad (132)$$

$v$  being the local velocity of the semiclassical particle, and  $\Omega$  the Rabi frequency of the optical coupling,

$$\frac{\Omega_{ge}}{2\pi} = 17.35 \text{ MHz} \times \sqrt{I(\text{W cm}^{-2})} \times d_{ge}(\text{a.u.}). \quad (133)$$

In Eq. (133)  $I$  is the shielding optical field intensity and  $d_{ge}$  is the transition dipole moment in atomic units. Equation (131) expresses the probability of penetration through the crossing region with the scattering flux remaining on the ground state. This probability is often

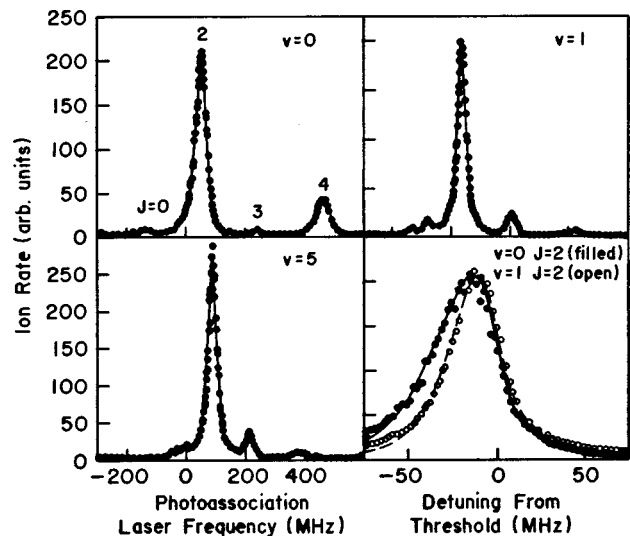


FIG. 70. Note how in Na photoassociative ionization ( ${}^3\Sigma_u^- \rightarrow 0_g^-$ ) the  $J=1$  and  $J=3$  intensities are strongly suppressed in the  $v=0$  rotational progression because they arise from the  $p$ -wave contribution to the collision but then reappear in the  $v=1$  and  $v=5$  spectra. From Tiesinga *et al.* (1996).

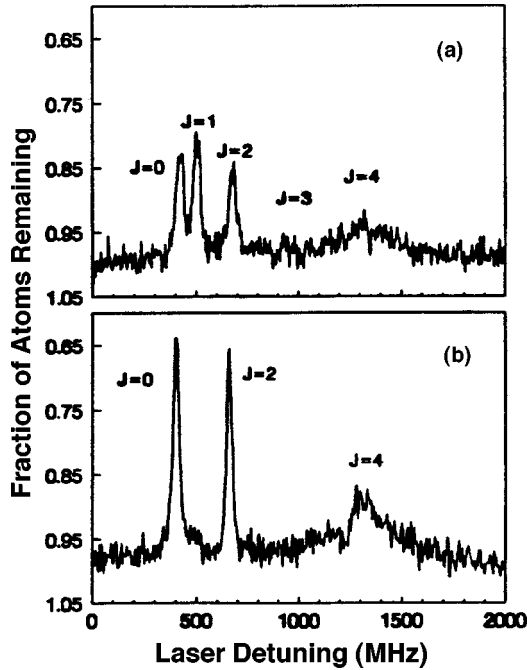


FIG. 71. Rubidium photoassociative ionization spectra showing the effects of spin polarization: (a) Rb photoassociative ionization spectrum unpolarized. (b) Rb photoassociative ionization spectrum from doubly spin-polarized atoms. Note restriction to even-numbered rotational levels. From Gardner *et al.* (1995).

termed the “shielding measure,”  $P_S$ . The probability of transferring to the excited state at the crossing is given by

$$P_e = 1 - \exp\left(-\frac{2\pi\hbar\Omega^2}{\alpha v}\right), \quad (134)$$

and the probability of exiting the collision on the excited state asymptote after traversing the crossing region twice is

$$P_e^\infty = P_e P_g = P_e(1 - P_e) = 1 - P_g^\infty. \quad (135)$$

According to Eqs. (131) and (135) the probability of the scattering flux exiting the collision on the ground state approaches unity as  $I$  increases to a strong field. However, as we shall see in Sec. VII.F, other effects enter at high field to modify this simple behavior. In addition, such Landau-Zener models are necessarily phenomenological in nature, since there are a multiplicity of potential curves (see Fig. 22) and an effective value of the molecular transition dipole strength  $d_{ge}$  must be chosen to fit the data.

## B. Optical suppression of trap loss

Evidence for optical manipulation of trap-loss processes was first reported by Bali *et al.* (1994) in  $^{85}\text{Rb}$  collisions in a MOT. In this experiment scattering flux entering on the ground state transfers to excited repulsive molecular states by means of a control or “catalysis” laser tuned 5–20 GHz to the blue of the cooling

frequency. When the blue detuning of the control laser becomes greater than about 10 GHz, the scattering partners, receding from each other along the repulsive potential, gather sufficient kinetic energy to escape the trap. The control laser thus produces a “trap-loss” channel, the rate of which is characterized by a trap-loss decay constant  $\beta(I)$ , a function of the control laser intensity  $I$ . Figure 73 shows the increase of  $\beta$  up to about  $6 \text{ W cm}^{-2}$ . Above this point the trap-loss rate constant begins to *decrease*, indicating a suppression of the loss channel with increasing control laser intensity. Bali *et al.* interpret this suppression in terms of the dressed-state Landau-Zener crossing model depicted in Fig. 72. The suppression of  $\beta$  is a consequence of the increasingly avoided crossing between the ground atom-field state  $|g;N\rangle$  and the excited atom-field state  $|e;N-1\rangle$ . As the control laser intensity increases, incoming flux on  $|g;N\rangle$  begins to propagate adiabatically near the crossing and recedes along the same channel from which it entered. A followup study by this Wisconsin group (Hoffmann *et al.*, 1996) used a blue-detuned laser to excite incoming collision flux population from the ground level to repulsive excited levels in a Rb MOT. The kinetic energy gained by the atoms dissociating along the excited repulsive potential probed the limits of capture velocity as a function of MOT parameters.

The Connecticut group of Gould and coworkers has also studied shielding and suppression in ground-state hyperfine-changing collisions (Sanchez-Villicana *et al.*, 1995). As discussed in Sec. V.B, exoergic hyperfine-changing collisions can also lead to loss of atoms from a trap if it is made sufficiently shallow (by decreasing the trapping light intensity) such that the velocity gained by each atom from the hyperfine-changing-collisions kinetic-energy release exceeds the maximum capture velocity of the trap. In earlier studies, Wallace *et al.* (1992) observed a rapidly rising branch of  $\beta$ , the trap-loss rate constant, as a function of decreasing MOT laser intensity below about  $2.5 \text{ mW cm}^{-2}$  in a  $^{85}\text{Rb}$  MOT and below about  $4 \text{ mW cm}^{-2}$  in a  $^{87}\text{Rb}$  MOT. They interpreted this rapid rise as due to hyperfine-changing-collisions kinetic-energy release. In order to suppress this source of trap loss Sanchez-Villicana *et al.* (1995) imposed a light field on their  $^{87}\text{Rb}$  MOT blue-detuned 500 MHz with respect to the  $S_{1/2} + P_{3/2}$  asymptote. This suppressor light field couples the incoming ground-state collision flux to a repulsive excited-state potential at a Condon point  $R_C \sim 32 \text{ nm}$ , effectively preventing the atoms from approaching significantly closer. The atoms recede, either along the excited-state potential or along the ground-state potential, before reaching the internuclear distance where hyperfine-changing collisions takes place ( $\leq 10 \text{ nm}$ ). The blue-detuned light field effectively shields the atomic collision from the hyperfine-changing-collisions loss process by preventing the atoms from approaching close enough for it to take place. Figure 74 shows the effectiveness of this shielding action as a function of suppression intensity by plotting the ratio of trap loss rate constant  $\beta/\beta_0$  with and without the suppressor laser present. Sanchez-Villicana *et al.* (1995)

TABLE III. Scattering lengths ( $a_0$ ).

	$A_s$	$A_t = A_{f_{\max} m_{\max}}$	$A_{1-1}$	$A_{3,-3}$	$A_{1,-1/2}$
${}^6\text{Li}_2^a$	$+45.5 \pm 2.5$	$-2160 \pm 250$			
${}^7\text{Li}_2^b$	$+33 \pm 2$	$-27.6 \pm 0.5$			
${}^6\text{Li}{}^7\text{Li}^a$	$-20 \pm 10$	$+40.9 \pm 0.2$			
${}^{23}\text{Na}_2^b$		$+85 \pm 3$	$+52 \pm 5$		
${}^{39}\text{K}_2^c$	$+132 \leftrightarrow +144$	$-1200 \leftrightarrow -60$			
${}^{41}\text{K}_2^c$	$+80 \leftrightarrow +88$	$+25 \leftrightarrow +60$			
${}^{39}\text{K}_2^d$	$+278 \pm 14$	$+81.1 \pm 2.4$			
${}^{40}\text{K}_2^d$	$+158 \pm 3$	$+1.7 \pm 4.4$			
${}^{41}\text{K}_2^d$	$+121 \pm 2$	$+286 \pm 36$			
${}^{85}\text{Rb}_2^e$		$-500 \leftrightarrow -300$			
${}^{85}\text{Rb}_2^f$	$+4500 \leftrightarrow +\infty$ $-\infty \leftrightarrow -1200$	$-440 \pm 140$			
${}^{87}\text{Rb}_2^e$		$+85 \leftrightarrow 140$			
${}^{87}\text{Rb}_2^g$		$+103 \pm 5$	$+103 \pm 5$		$+103 \pm 5$
${}^{133}\text{Cs}_2^h$		$>260$			
${}^{133}\text{Cs}_2^i$				$ 46 \pm 12 $	

<sup>a</sup> Abraham *et al.* (1997).

<sup>b</sup> Tiesinga *et al.* (1996).

<sup>c</sup> Boesten, Vogels, *et al.* (1996).

<sup>d</sup> Côté and Dalgnaro (1997); Côté and Stwalley (1997).

<sup>e</sup> Boesten, Tsai, *et al.* (1996).

<sup>f</sup> Tsai *et al.* (1997).

<sup>g</sup> Julienne *et al.* (1997).

<sup>h</sup> Arndt *et al.* (1997).

<sup>i</sup> Monroe *et al.* (1993).

compare their measurements to the simple Landau-Zener model of the shielding effect (see Fig. 72) and find reasonably good agreement.

The use of blue-detuned optical fields to suppress hyperfine-changing collisions has also been studied in cold sodium collisions. Muniz *et al.* (1997) employed a novel sequential trapping technique to capture Na atoms in a MOT sufficiently shallow to observe the hyperfine-

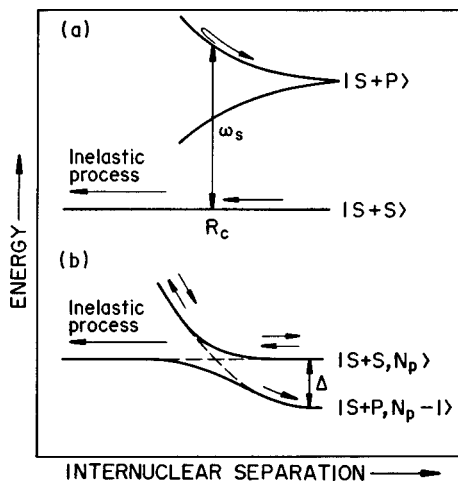


FIG. 72. Simple one-dimensional models of optical suppression: (a) Conventional semiclassical picture of optical suppression. Atoms approach on the ground state and are excited in a localized region around  $R_c$  by light of frequency  $\omega_s$  to a repulsive excited state. (b) Dressed-state picture where asymptotic states are atom-field states and the optical coupling appears as a Landau-Zener avoided crossing.

changing-collisions loss effect. The Brazil group captured  $10^7 - 10^8$  atoms in a relatively deep MOT operating near the  $D_2$  line of Na. They then transferred these cooled atoms to a much shallower MOT operating near the  $D_1$  line, the collisional loss from which is due principally to hyperfine-changing collisions. Then with a suppressor laser, blue-detuned 600 MHz with respect to the  $S_{1/2} + P_{3/2}$  asymptote, Muniz *et al.* (1997) measured the suppression of hyperfine-changing collisions. Figure 75 shows a plot of the fractional decrease in hyperfine-changing-collisions rate constant,  $\theta = (\beta_0 - \beta) / \beta_0$  vs suppression laser intensity,  $I$ . Both Sanchez-Villicana *et al.* (1995) and Muniz *et al.* (1997) compared their results to the simple Landau-Zener model, the diagram of which is shown in Fig. 72. From Fig. 74 it appears that the Landau-Zener model underestimates the suppression effect somewhat in  ${}^{87}\text{Rb}$  collisions, while Muniz *et al.* (1997) find the model overestimates the effect in Na collisions. This model and its appropriateness to optical suppression and shielding is discussed in more detail in the next section. Muniz *et al.* (1997) also compare their results to a more sophisticated three-dimensional, multichannel close-coupling calculation described in Sec. VII.F.

### C. Optical shielding and suppression in photoassociative ionization

Although trap-loss studies have played a major role in revealing the nature of cold and ultracold collisions, to date photoassociative ionization (PAI) has been the only collisional process where the product is directly de-

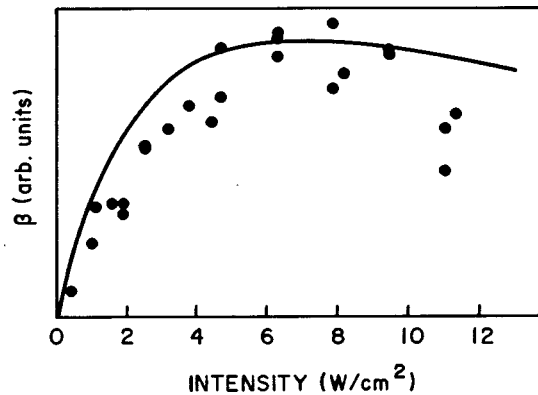


FIG. 73. Trap loss  $\beta$  as a function of control laser intensity. From Bali *et al.* (1994).

tected, although very recent results from Wang, Wang, *et al.* (1998) and Fioretti *et al.* (1997) indicate direct observation of fine-structure changing processes in K and Cs ultracold collisions, respectively. As discussed in Sec. VI on photoassociation, the PAI process takes place in two steps. Reactant partners first approach on the ground-state potential. Near the outer Condon point  $R_C$ , where an optical field  $\hbar\omega_1$  couples the ground and excited states, population transfers to the long-range attractive state, which accelerates the two atoms together. At shorter internuclear distance, near an inner Condon point, a second optical field  $\hbar\omega_2$  couples the population in the long-range attractive state either to a doubly excited state that subsequently autoionizes or to the ionization continuum directly. Optical shielding intervenes at the first step. Rather than transferring population to the long-range attractive potential at the first Condon point, an optical field  $\hbar\omega_3$ , tuned to the blue of the excited-state asymptote, transfers population to a repulsive curve from which it exits the collision on the excited asymptote with kinetic energy approximately equal to the blue detuning of  $\hbar\omega_3$ . This process is analogous to the weak-field, trap-loss mechanism described by Bali *et al.* (1994). As the intensity of the suppressor field increases, scattering flux begins to exit on the ground state with negligible increase in kinetic energy, and the collision partners become *elastically* shielded from short-range interactions. Optical suppression of photoassociative ionization was first reported by Marcassa *et al.* (1994) in a conventional MOT setup. Four different optical frequencies were used for the following: (a) to produce the MOT ( $\omega_1, \omega_2$ ), (b) to generate the suppressor frequency ( $\omega_3$ ), and (c) to probe the PAI inelastic channel ( $\omega_p$ ). Electro-optic modulation of the repumper  $\omega_2$  produced sideband frequencies  $\omega_3, \omega_4$ . Although  $\omega_4$  was not necessary to observe the suppression effect, its presence added new features consistent with the interpretation of suppression and shielding described here. Figure 76 shows the coupling and schematic routing of the incoming flux. Figure 76(a) shows the familiar two-step PAI process with no suppression. After excitation to the attractive  $2+P$  level, the frequency  $\omega_2$  transfers scattering flux in a second step to the  $P+P$  level from which associative ionization takes place. As  $\omega_p$  tunes to the red

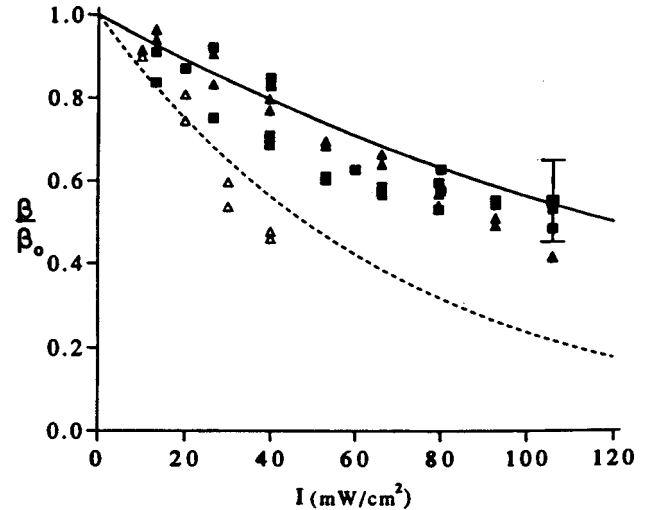


FIG. 74. Suppression ratio  $\beta/\beta_0$  vs suppression laser intensity  $I$  for detunings of 500 MHz (solid points) and 250 MHz (open points). Differently shaped symbols represent data from different runs. The solid and dashed lines show the Landau-Zener model calculations for the two detunings. From Sanchez-Villicana *et al.* (1995).

of the Condon point  $R_2$ , it can no longer, in combination with  $\omega_2$ , couple to the doubly excited level, and an abrupt cutoff of the PAI signal is predicted at that frequency. Figure 76(b) shows what happens when a suppressor frequency  $\omega_3$  is imposed on the trap. With  $\omega_p$  tuned to the *red* of  $\omega_3$ , scattering flux on the  $F=2, F'=2$  entrance channel diverts to the *repulsive*  $2+P$  curve around the suppressor Condon point  $R_3$ , and exits via the excited or ground state, depending on the intensity of the suppressor field. Figure 76(c) depicts what happens when  $\omega_p$  tunes to the *blue* of  $\omega_3$ . In this case the incoming flux transfers to the *attractive*  $2+P$  curve around the Condon point  $R_p$ . However, now  $\omega_3$  and  $\omega_4$  add to  $\omega_2$  to enhance the probability of second-step excitation to the  $P+P$  level. Therefore PAI should be enhanced with respect to the PAI rate represented in Fig. 76(a). Furthermore the cutoff to PAI should be extended to the left of  $R_2$  because  $\omega_4$  is the blue sideband of  $\omega_2$ , appearing 1.1 GHz higher frequency. Figure 77 shows a plot PAI count rate vs  $\omega_p$  detuning with and without  $\omega_3$  and  $\omega_4$ . All three predicted features—suppression, enhancement, and cutoff—extension, are evident and appear where expected.

The dependence of any shielding or suppression effect on the intensity of the optical field is obviously of great interest and importance. Marcassa *et al.* (1994) described model two-state calculations at three levels of elaboration: (1) time-dependent Monte Carlo wavefunction simulations of wave-packet dynamics, (2) quantum close-coupling calculations without excited-state spontaneous emission, and (3) a very simple estimate based on a dressed-state Landau-Zener avoided crossing model. The result of the calculations were in close agreement among themselves and within about 15% of the experiment, given that an effective value of  $d_{ge}$  in Eq. (133) had to be selected in order to give the model

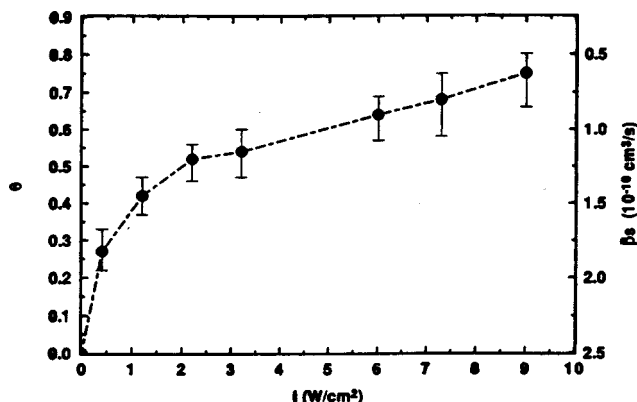


FIG. 75. Fractional suppression  $\theta$  vs suppressor laser intensity for a  $D1$  trapping laser intensity of  $40 \text{ mW cm}^{-2}$ . From Muniz *et al.* (1997).

an intensity scale that could be compared with the experimental one. However, laser source limitations precluded intensity measurements above  $\sim 1 \text{ W cm}^{-2}$ . In a followup article Marcassa *et al.* (1995) were able to measure the suppression power dependence up to  $8 \text{ W cm}^{-2}$ . Figure 78 plots the fractional intensity of the PAI signal as a function of suppressor power density. The experimental results are shown together with calculations from quantum close coupling and the Landau-Zener semiclassical model. Agreement is good at low field, but above about  $5 \text{ W cm}^{-2}$  the data tend to lie above the theory curve, suggesting that the intensity dependence of suppression “saturates” at an efficiency less than 100%. Calculated values do not lie outside the statistical error bars on the data points, however, so these data do not establish a “saturation” effect at high field beyond question.

Zilio *et al.* (1996) continued to investigate the high-field behavior of optical suppression of PAI, by measuring the rate dependence on the polarization (circular or linear) of the probe beam  $\omega_p$ . They found that as the suppressor field increased above about  $1 \text{ W cm}^{-2}$ , circular polarization became markedly more effective at suppressing PAI, but that neither linear nor circular polarization suppressed the PAI rate to the extent predicted by the simple weak-field Landau-Zener model. Figure 79(a) shows the shielding measure  $P_S$  as function of suppressor field intensity, and Fig. 79(b) shows the results of a close-coupling, strong-field model calculation of the process (Napolitano *et al.*, 1997). The model calculation shows the correct ordering of the polarization dependence and the magnitude of the shielding measure (which is considerably less than the Landau-Zener prediction) although the curvature of the experiment and theory plots have the opposite sign. This close-coupling calculation will be discussed in more detail in Sec. VII.F on strong-field theories of optical shielding. In very recent work, Tsao *et al.* (1998) investigated the alignment effect of linear polarization by measuring  $P_S$  with the suppressor beam E-field aligned parallel and perpendicular to a highly collimated and velocity-selected atomic beam. They compared their results to the predic-

tions of the close-coupling high-field model of Napolitano *et al.* (1997) and found reasonably good agreement. Figure 80 summarizes the experimental result and comparison with the model calculation.

#### D. Optical shielding in xenon and krypton collisional ionization

Another example of optical shielding in ionizing collisions of metastable xenon has been reported by the NIST group (Walhout *et al.*, 1995). The experiment takes place in a MOT with the cooling transition between the metastable “ground state”  $6s[\frac{3}{2}]_2$ , and the excited state  $6p[\frac{5}{2}]_3$ . This intermediate coupling notation refers to the core total electronic angular momentum in square brackets, and the subscript refers to the total electronic angular momentum of the atom (core + outer electron). The MOT is time chopped with a  $150 \mu\text{sec}$  period and an “on” duty cycle of  $\frac{2}{3}$ . Measurements were carried out in the probe cycle (MOT off) and the trap cycle (MOT on). Experiments in the probe cycle start with a control (or “catalysis”) laser sweeping over a range of detuning from about 1.5 GHz to the red of the cooling transition to 500 MHz to the blue. The control laser induces a strong enhancement of the ionization rate over a red detuning range of about 500 MHz, peaking at 20 MHz, and produces suppression at blue detunings over several hundred megahertz. The maximum suppression factor ( $\sim 5$ ), occurring at 200 MHz blue, appears to “saturate” at the highest control laser power of  $0.5 \text{ W cm}^{-2}$ . With the MOT beams illuminating the sample the experiments show an even more dramatic suppression effect. Figure 81 shows the suppression factor, which is the ratio of ionization rate constant with and without the control laser, plotted against control laser detuning. At about 250 MHz blue detuning the suppression factor reaches a maximum of greater than 30. The interpretation is similar to that of the sodium case (Marcassa *et al.*, 1994). Without the control field present, reactant scattering flux, approaching on the metastable ground state, is transferred to an attractive excited state at far internuclear separation by the trapping laser. The colliding partners start to accelerate toward each other and, during their inward journey, radiatively relax back to the metastable ground state. The consequent increase in kinetic energy allows the colliding partners to surmount centrifugal barriers that would otherwise have prevented higher partial waves from penetrating to internuclear distances where Penning and associative ionization take place. The net result is an increase in the ionization rate constant during the MOT “on” cycle. With the control laser present and tuned to the blue of the trapping transition, the previously accelerated incoming scattering flux is diverted to a repulsive excited state before reaching the ionization region. The colliding atoms are prevented from approaching further, and the result is the observed marked reduction in ionization rate constant.

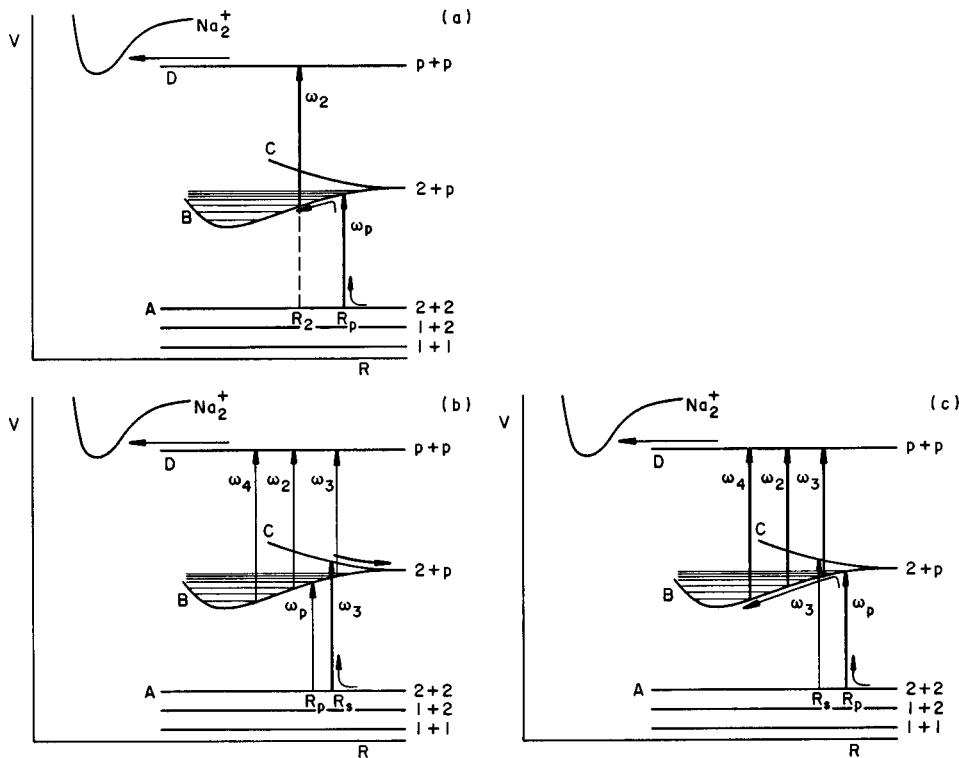


FIG. 76. Schematic of transitions showing photoassociative ionization and optical suppression of photoassociative ionization: (a) Two-step PAI process; (b) suppressor frequency  $\omega_3$  imposed on the collision, rerouting incoming flux to the repulsive excited curve; (c) with  $\omega_p$  tuned to the right of  $\omega_3$ , photoassociative ionization takes place with enhanced probability due to addition of  $\omega_3$  and  $\omega_4$ . From Marcassa *et al.* (1994).

An experiment similar to the xenon work has also been carried out in a krypton MOT by Katori and Shimizu (1994). Analogous to the xenon case, the cooling transition cycles between  $5s[\frac{3}{2}]_2 \leftrightarrow 5p[\frac{5}{2}]_3$ , and a control laser sweeps from red to blue over the cooling transition from about  $-600$  MHz to  $+100$  MHz. Suppression of the ionization rate was again observed with the control laser tuned to the blue. The power in the control laser was only about  $4 \text{ mW cm}^{-2}$ , and the suppression factor peaked at a blue detuning of about  $20$  MHz. Although this detuning is very close to the trapping transition, apparently the low power in the suppression laser and time chopping of the MOT cycle and probe cycle permitted ionization rate constant measurements without disruption of the MOT itself. Katori and Shimizu (1994) also determined the ratio of rate constants between associative and Penning ionization and found it to be  $\approx 1/10$ . The power dependence of the suppression effect was not investigated over a very wide range of control laser power. The maximum power density was only  $25 \text{ mW cm}^{-2}$ , so no firm conclusions concerning strong field effects can be drawn from this report.

### E. Optical shielding in Rb collisions

In very recent work Sukenik *et al.* (1997) have observed evidence of optical suppression in two-photon “energy pooling” collisions in  $^{85}\text{Rb}$  and  $^{87}\text{Rb}$  MOTs. This study is a two-color experiment in which one frequency  $\omega_1$  tunes  $90$  MHz to the red of the  $5S_{1/2}(F=1) \rightarrow 5P_{1/2}(F'=1)$   $^{87}\text{Rb}$  resonance transition (or the  $5S_{1/2}(F=2) \rightarrow 5P_{1/2}(F'=2)$   $^{85}\text{Rb}$  resonance transition) and populates singly excited attractive states originating

from the  $5S_{1/2}+5P_{1/2}$  asymptote. A second color  $\omega_2$ , tunes  $0-2$  GHz to the blue of  $5S_{1/2}(F=1) \rightarrow 5P_{1/2}(F'=2)$   $^{87}\text{Rb}$  transition (or  $5S_{1/2}(F=2) \rightarrow 5P_{1/2}(F'=3)$   $^{85}\text{Rb}$  transition). Violet photons are observed from the “energy pooling” energy transfer collision,

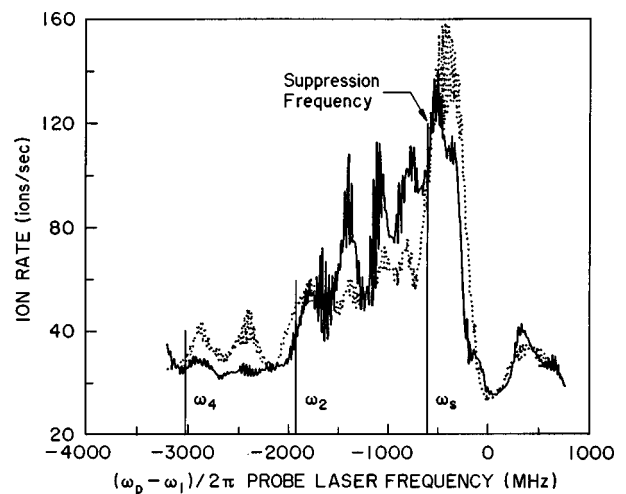


FIG. 77. Effect of optical suppression on the photoassociative ionization spectrum observed in a Na MOT. Solid curve is the photoassociative ionization spectrum without the suppression field  $\omega_s$  present. Dotted curve shows the photoassociative ionization spectrum  $\omega_s$  present. Note enhancement of signal to the right of  $\omega_s$ , suppression to the left. Note also the cutoff of the photoassociative ionization signal to the left of  $\omega_2$  without the suppression field and the extension of this cutoff to  $\omega_4$  when  $\omega_s$  is present. From Marcassa *et al.* (1994).

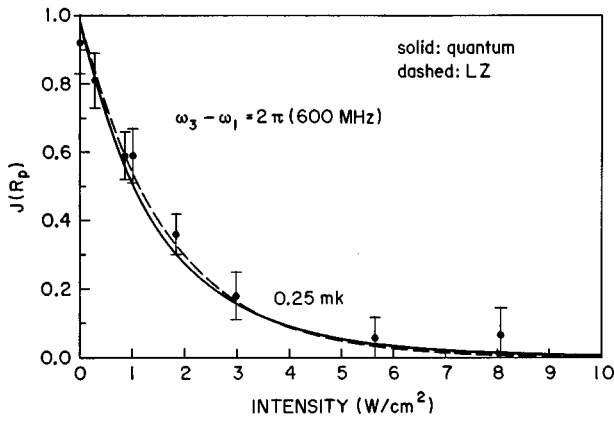
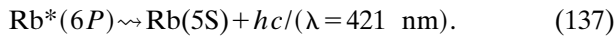


FIG. 78. Shielding parameter  $P_s$  as a function of suppressor field intensity. From Marcassa *et al.* (1995).

followed by subsequent emission from the excited Rb atom,



The spectrum of the violet photon emission was recorded as a function of  $\omega_2$  detuning. Sukenik *et al.*

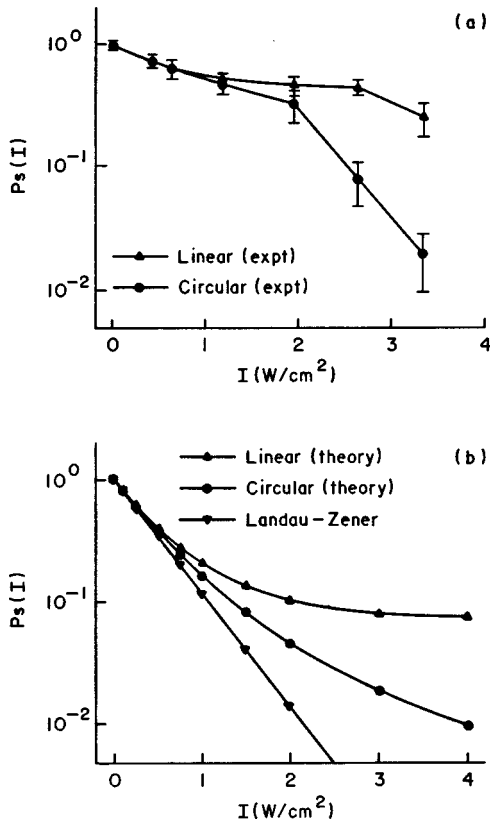


FIG. 79. Comparison of experiment and theory in optical suppression in Na: (a) Experimental results showing increased effectiveness of optical suppression by circularly polarized light at higher field intensities. From Zilio *et al.* (1996). (b) Theory calculations in good qualitative agreement with experimental results. Also shown is the Landau-Zener results which considerably overestimates suppression at high fields. From Napolitano *et al.* (1997).

(1997) report deep modulations in the fluorescence intensity. They attribute this detuning modulation to transitions in which  $\omega_2$  couples singly excited hyperfine levels, populated by  $\omega_1$  excitation, to doubly excited molecular hyperfine levels. Studies of  $\omega_1$  and  $\omega_2$  intensity dependencies show saturation in both colors. The  $\omega_1$  saturation is due to depletion of the ground-state reactant flux. The  $\omega_2$  saturation is ascribed to optical shielding due to the blue color coupling of the ground state and repulsive singly excited states. Thus  $\omega_2$  is thought to play a double role: (1) opening the energy-pooling channel by populating doubly excited molecular states at long range, and (2) suppressing two-step photon transitions by coupling incoming ground-state flux to repulsive curves originating from the  $5S+5P$  asymptotes.

## F. Theories of optical shielding

Weak-field theories applied to either Na or Xe experiments do not produce the experimentally measured dependence of ionization rate on blue-detuned optical-field power density. In particular a serious attempt to capture all the physics of strong-field optical shielding must take into account the effects of light shifts, saturation, rapid Rabi cycling at high fields, light polarization, and spontaneous decay. Suominen *et al.* (1995) investigated these factors (except light polarization) within the simplifying context of two-state models in which the angular dependence of the suppressor field Rabi coupling was replaced by a spherical average. The essential motivation was to investigate the conditions under which the naive Landau-Zener formulas—(Eqs. (131) and (134))—break down and what modifications can be made, if any, to retain a semiclassical picture of the shielding dynamic. Suominen *et al.* (1995) identify three different characteristic times whose relative duration determines the validity of various approximations. These

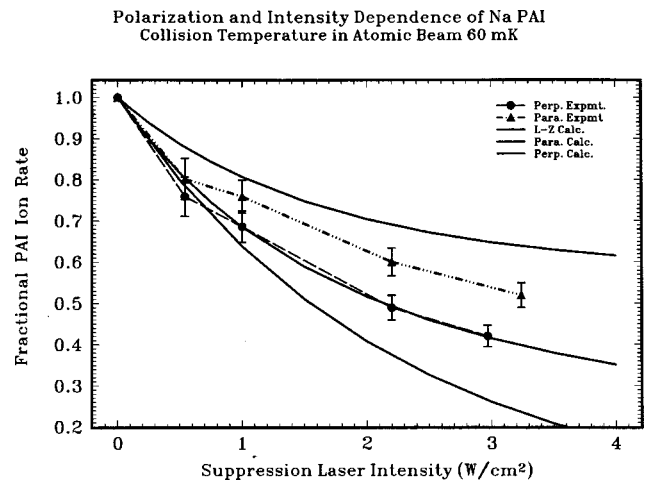


FIG. 80. Alignment dependence of optical suppression of Na photoassociative ionization collisions in a beam. Results show perpendicular polarization more effective than parallel and the *L-Z* formula overestimates effect at higher fields. From Tsao *et al.* (1998).

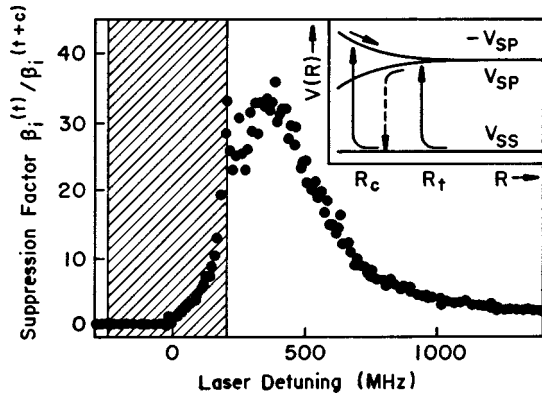


FIG. 81. Suppression factor as a function of control laser detuning in Xe collisions. These data show the suppression factor in the “trap” cycle with the MOT on. From Walhout *et al.* (1995).

times follow: (1) the lifetime against spontaneous decay  $\tau_\gamma$ , (2) the time  $\tau_{tp} \approx \mu v / \alpha$  for a wave packet to travel from the excitation Condon point  $R_C$  to the turning point  $R_{tp}$  on the repulsive potential, with  $\mu v$  the local momentum; and (3) the time it takes a wave packet to traverse half the Landau-Zener interaction region  $\tau_\Omega \approx \frac{1}{2} \hbar \Omega / \alpha v$ , where  $v$ ,  $\Omega$ , and  $\alpha$  have been defined in Eqs. (131), (133), and (132). Note that  $\tau_\Omega$  is the only one of these characteristic times that depends on the shielding field intensity and reflects the increasing “repulsion” of the dressed potentials with increasing  $\Omega$  at the avoided crossing. If  $\tau_\gamma$  is long compared to both  $\tau_{tp}$  and  $\tau_\Omega$ , spontaneous decay can be ignored and the weak-field Landau-Zener formulas are appropriate. If  $\tau_\gamma$  becomes less than  $\tau_{tp}$  but still remains long compared to  $\tau_\Omega$ , then spontaneous emission can be included by calculating the excitation probability with the Landau-Zener formula, Eq. (131), followed by radiative decay. In this case the shielding probability becomes

$$P_S = P_g + P_e [1 - \exp(-\gamma \tau_{tp})] = 1 - P_e \exp(-\gamma \tau_{tp}). \quad (138)$$

If  $\tau_\gamma$  becomes shorter than  $\tau_{tp}$  and  $\tau_\Omega$ , then excitation and spontaneous emission cannot be separated because Rabi cycling is taking place around  $R_C$ . As the shielding field intensity increases, eventually  $\tau_\Omega$  become greater than both  $\tau_{tp}$  and  $\tau_\gamma$ , and the semiclassical particle or wave packet never passes entirely through the interaction region before undergoing Rabi cycling and spontaneous decay. In this high-field regime one would not expect the Landau-Zener approach to be very useful. Suominen *et al.* (1995) investigated all these relative time scales by comparing the Landau-Zener models to quantum Monte Carlo wave-packet calculations, the ultimate arbiter for the usefulness of any semiclassical two-level model. They found that, as expected, the Landau-Zener, Eq. (131), and modified Landau-Zener, Eq. (138), expressions fail with increasing  $\Omega$  but that another modification of the Landau-Zener expression,

$$P_S = 1 - P_e \exp[-\gamma(\tau_{tp} - \tau_\Omega)], \quad (139)$$

actually tracks the Monte Carlo calculations quite well.

The overall conclusion is that Landau-Zener and its modifications remain surprisingly robust even under conditions where one would expect them to fail, at least within the confines of a two-state system. Real collisions of course involve many more than two states, and the next question is to what extent off-resonant states can influence the conclusions of the two-state studies.

Suominen, Burnett, and Julienne (1996) investigated this issue by carrying out Monte Carlo wave-function (MCWF) calculations on a model three-state system consisting of a flat ground state and two excited states varying as  $\pm C_3/R^3$ . First they investigated the effect of the off-resonant state (the repulsive  $+C_3/R^3$  state) on the probability of inelastic trap-loss processes excited by a red-detuned laser resonant with the attractive ( $-C_3/R^3$ ) state at some Condon point  $R_C$ . The results showed that as the red-detuned laser Rabi frequency increased, the two-state and three-state MCWF calculations yielded essentially the same increasing probability of excited-state population while the simple weak-field Landau-Zener model predicted a low-level saturation of this excited-state population. Aside from the inclusion of the off-resonant state, the essential difference between the MCWF calculations and the Landau-Zener approach is that at high fields the MCWF method takes into account population recycling due to successive excitations after spontaneous emission. The Landau-Zener approach makes the weak-field assumption that excitation and spontaneous emission are decoupled so that after excitation to the attractive state, followed by spontaneous emission back to the ground state, reexcitation never occurs. Off-resonant population of the repulsive  $+C_3/R^3$  state appears to have little effect on the results. Next, Suominen, Burnett, and Julienne (1996) switched the roles of the attractive and repulsive excited states by investigating the influence of the off-resonant state (the attractive  $-C_3/R^3$  state) on optical shielding when a blue-detuned laser is resonant with the repulsive ( $+C_3/R^3$ ) state at some Condon point  $R_C$ . They found that at weak field the results agreed with Landau-Zener, calculations, but that at strong field the shielding measure  $P_S$  did not approach zero but began to *increase* due to the off-resonant population of the attractive excited state. This behavior is not observed in the experiments of Zilio *et al.* (1996) and Walhout *et al.* (1995), where  $P_S$  saturates with increasing shielding field intensity at levels above those predicted by Landau-Zener but shows no evidence of a subsequent rise. The experimental results cannot be explained therefore by the presence of off-resonant states, but must be due to some other high-field effects.

At the same time that Suominen, Burnett, and Julienne (1996) were carrying out the MCWF calculation to investigate the role of off-resonant states in a three-state model of shielding, they and their experimental co-authors (Suominen, Burnett, Julienne, *et al.*, 1996) investigated to what extent a two-state Landau-Zener type of theory could explain the experimental results of Walhout *et al.* (1995). Both the alkali experiments (Maraccasa *et al.*, 1994; Zilio *et al.*, 1996) and the xenon experi-

ments show that suppression and shielding are less than predicted by very simple two-state avoided-crossing models, but Fig. 82 shows that the extent of the shielding “saturation” as a function of shielding laser intensity is much more dramatic in the results of Walhout *et al.* (1995). The results of Fig. 82 were recorded with the MOT light turned off and only the blue-detuned control laser present. By inserting an averaged *distribution* of molecular Rabi frequencies in the Landau-Zener exponential argument, Suominen, Burnett, Julienne, *et al.* (1996) were able to get good agreement with these xenon experimental results. At first glance it might seem reasonable to use such a distribution since the MOT experiment does not restrict the angle  $\theta$  between the collision axis and the control laser polarization axis, and the Rabi frequency could be written as  $\Omega = \Omega_0 \sin \theta$ . The problem is that there is no real justification for averaging  $\Omega$  over  $\theta$  since the  $P, Q, R$  branches are all available for optical coupling. Furthermore the experimental results show that *relative* shielding is much more pronounced when both the blue-detuned control laser and the red-detuned MOT lasers are turned on. With both red and blue colors present the extent of the shielding effect resembles much more closely the alkali results, and application of the Landau-Zener formula with a distribution of Rabi frequencies does *not* give good agreement. Although various *ad hoc* adaptations of the Landau-Zener formula can yield a satisfactory comparison with the xenon measurements, a clear, justifiable, and consistent physical picture does not emerge from these calculations.

Very recently Yurovsky and Ben-Reuven (1997) have proposed a Landau-Zener approach in which the three-dimensional nature of the collision has been incorporated into the theory. By calculating the Landau-Zener probability at multiple crossings, where incoming  $^1\Sigma_g$  ground-state  $s$  and  $d$  waves couple through  $P, Q, R$  branches to a  $^1\Pi_u$  repulsive excited state, several pathways are traced out through which the incoming flux can penetrate to the inner region, thereby rendering the shielding less efficient than predicted by the naive one-dimensional Landau-Zener model. Yurovsky and Ben-Reuven calculated the shielding measure  $P_S$  as a function of shielding laser intensity for three detunings and compared to the measured results in xenon collisions (Suominen, Burnett, Julienne, *et al.*, 1996). Although the three-dimensional Landau-Zener theory better reflects the “saturation” behavior of  $P_S$  than does the one-dimensional Landau-Zener theory, the xenon measurements still show a stronger saturation than either the one- or three-dimensional versions of the two-state Landau-Zener model.

Motivated by the experimental results of Marcassa *et al.* (1995), Zilio *et al.* (1996), and Walhout *et al.* (1995), Napolitano *et al.* (1997) developed a full three-dimensional, close-coupled, quantum scattering approach to optical suppression of ultracold collision rates. This work differs from the MCWF approach of Suominen *et al.* (1995) and Suominen, Burnett, and Julienne (1996) in that the calculations are not restricted to two

or three states or to only  $s$ -wave scattering. Although it does not take spontaneous radiation explicitly into account, Suominen *et al.* (1995) has shown that at large enough blue detuning the decay of the upper state can be neglected, and Napolitano *et al.* (1997) carried out their model calculations in a detuning regime where spontaneous emission can be safely ignored. The model collision examined is

$$A(^1S) + A(^1S) + P(\vec{\epsilon}_q, \hbar\omega_L) \rightarrow A(^1S) + A(^1P), \quad (140)$$

where  $A(^1S)$  and  $A(^1P)$  are atoms in the  $^1S$  and  $^1P$  ground and excited states, respectively, and  $P(\vec{\epsilon}_q, \hbar\omega_L)$  represents a photon of energy  $\hbar\omega_L$  and unit polarization vector  $\vec{\epsilon}_q$  with  $q=0$  for linear polarization and  $q=\pm 1$  for circular polarizations. In order to keep the number of channels to a manageable size, nuclear and electron spins were excluded; however, the model does represent real scattering of the spinless alkaline earths (group IIA) and serves as a qualitative guide for understanding the behavior of the Na and Xe experiments. The problem is set up with the atoms far apart in an asymptotic field-dressed atomic basis within a space-fixed frame defined by  $\vec{\epsilon}_q$ . As the atoms approach, this space-fixed basis correlates to a molecular body-fixed basis through the unitary transformation of the symmetric top eigenfunctions; these molecular basis states are then coupled by the radiation field. This coupling is normally localized around a Condon point  $R_C$  defined by the blue detuning of the shielding laser field. The molecular state formed from a pair of  $^1S$  ground-state atoms ( $^1\Sigma_g^+$ ) and the states formed by a  $^1S, ^1P$  ground-excited pair ( $^1\Sigma_u^+, ^1\Pi_u$ ) constitute the four-state molecular basis ( $^1\Pi_u$  is doubly degenerate). The goal is to calculate the probability that scattering flux incoming on the molecular ground state will (1) penetrate to the inner region where reactive and inelastic processes can take place, (2) transfer and exit on the  $^1\Pi_u$  excited state, or (3) elastically scatter on the ground state.

The results of the quantum close-coupling calculations show that the shielding parameter  $P_S$  is markedly sensitive to both optical field intensity and to polarization, with circular polarization shielding more effectively than linear polarization. Napolitano *et al.* (1997) interpret the polarization effect as the difference in the number of angular momentum branches ( $P, Q, R$ ) through which the ground and excited states can couple. For example Fig. 83 shows that when two partial waves  $l=0, 2$  cross in the region of the Condon point, the angular momentum selection rules result in different coupling for linear and circularly polarized light. For linear polarization the entrance  $d$  wave couples only through the  $P$  and  $R$  branches, while for circularly polarized light the  $P, Q, R$  branches couple. The result is that circular polarization results in more “avoidedness” at the crossing than does linear polarization. Figure 79 demonstrates a qualitative agreement between close-coupling calculations and the results of Zilio *et al.* (1996) both in the amplitude of the shielding measure  $P_S$  and in the ordering of the light polarization. A further result of the close-coupling theory is the prediction of anisotropy in shielding as a

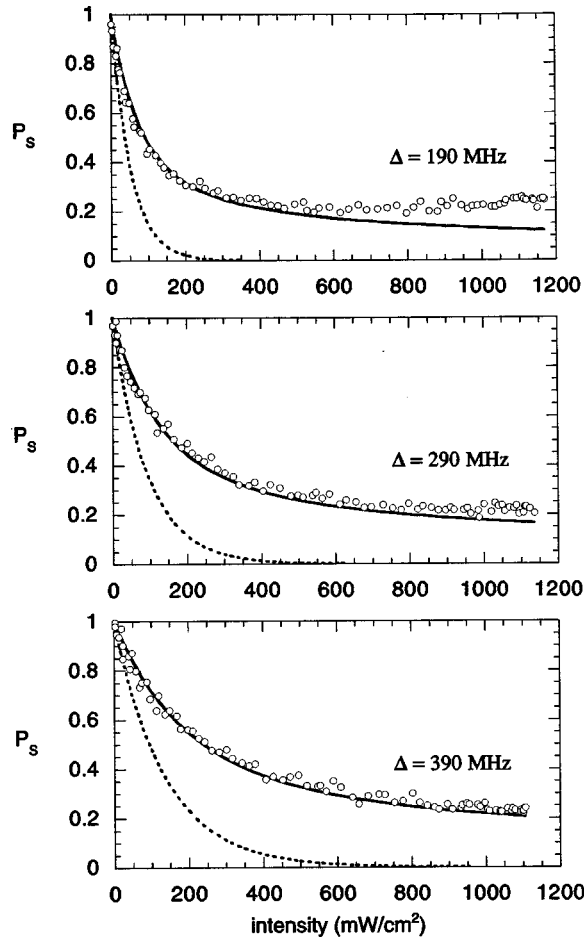


FIG. 82. Penetration measure ( $1 - P_s$ ) as function of laser intensity for three values of blue detuning of the control or shielding laser in Walhout *et al.* (1995). Circles are experimental points; solid line, the theory of Suominen, Burnett, Julienne, *et al.* (1996); dotted line, the standard Landau-Zener calculation.

function of the linear polarization alignment with respect to the molecular collision axis. This behavior was confirmed in a beam experiment by Tsao *et al.* (1998).

Most shielding and suppression studies, both experimental and theoretical, have focused on the dependence of  $P_s$  as a function of optical field intensity at some fixed blue detuning. Band and Tuvi (1995) have predicted, however, that by varying the relative detuning of the red and blue light fields in a sodium PAI experiment, as well as their intensities, one can produce interesting effects such as field-dressed “reaction barriers,” the height and width of which can be controlled by the suppression field detuning and intensity. These barriers would be observable as resonances in the PAI signal as a function of blue detuning. The resonance positions should also shift and broaden with increasing suppression intensity. To date we are aware of no experimental efforts undertaken to investigate these interesting predictions of a model calculation, but shielding and suppression should provide new opportunities for optical control of inelastic processes.

## VIII. GROUND-STATE COLLISIONS

Most of this review has focused on collisions of cold, trapped atoms in a light field. Understanding such collisions is clearly a significant issue for atoms trapped by optical methods, and historically this subject has received much attention by the laser cooling community. However, there also is great interest in ground-state collisions of cold neutral atoms in the absence of light. Most of the early interest in this area was in the context of the cryogenic hydrogen maser or the attempt to achieve Bose-Einstein condensation (BEC) of trapped doubly spin-polarized hydrogen. More recently the interest has turned to new areas such as pressure shifts in atomic clocks or the achievement of BEC in alkali systems. The actual realization of BEC in  $^{87}\text{Rb}$  (Anderson *et al.*, 1995),  $^{23}\text{Na}$  (Davis *et al.*, 1995), and  $^7\text{Li}$  (Bradley *et al.*, 1995; Bradley *et al.*, 1997) has given a tremendous impetus to the study of collisions in the ultracold regime. Collisions are important to all aspects of condensates and condensate dynamics. The process of evaporative cooling that leads to condensate formation relies on elastic collisions to thermalize the atoms. The highly successful mean field theory of condensates depends on the sign and magnitude of the  $s$ -wave scattering length to parametrize the atom interaction energy that determines the mean field wave function. The success of evaporative cooling, and having a reasonably long lifetime of the condensate, depend on having sufficiently small inelastic collision rates that remove trapped atoms through destructive processes. Therefore, ground-state elastic and inelastic collision rates, and their dependence on magnetic or electromagnetic fields, is a subject of considerable current interest.

This section will review work on ground-state collisions of trapped atoms in the regime below 1 mK, with particular emphasis on the ultracold regime below 1  $\mu\text{K}$ . The work on ground-state collisions could easily be the subject of a major review in its own right, so our review will be limited in scope. We do not in any way claim to be exhaustive in our treatment. We will use a historical approach, as we have done for collisions in a light field, and try to cover some of the key concepts and measurements. The first section will review the early work in the field, including a brief survey of the work on hydrogen. A second section will discuss the role of collisions in BEC.

### A. Early work

We noted in Sec. III B that the quantum properties are quite well known for collisions where the de Broglie wavelength is long compared to the range of the potential. We confine our interest here to the special case of the collision of two neutral atoms at temperatures of less than 1 K. Interest in this subject was stimulated in the 1980’s by two developments: the possibility of achieving Bose-Einstein condensation with magnetically trapped spin-polarized hydrogen (Stwalley and Nosanow, 1976; Laloë, 1980; Silvera and Walraven, 1980; Silvera and

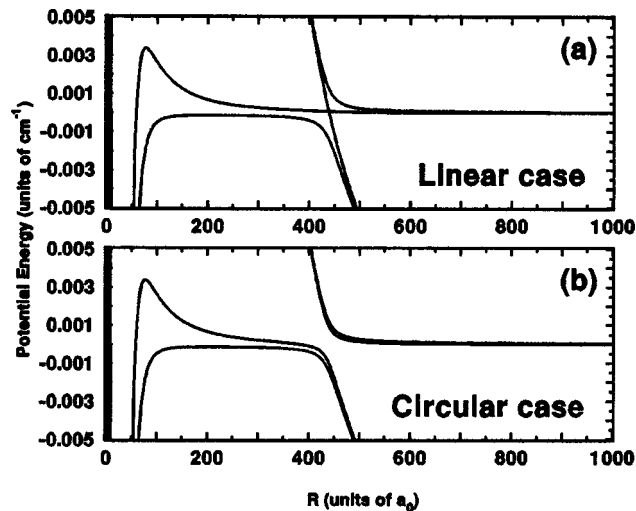


FIG. 83. Schematic of close-coupling, strong-field model of optical suppression: (a) Two partial waves,  $s$  and  $p$ , optically coupled from the  $^1\Sigma_g$  to  $^1\Pi_u$ , with linear polarization. Note that the  $d$  wave couples only through  $P, R$  branches. (b) Same coupling but with circular polarization. Coupling is through  $P, Q, R$  branches. From Napolitano *et al.* (1997).

Walraven, 1986), and the prospects of unparalleled frequency stability of the cryogenic hydrogen maser (Crampton *et al.*, 1978; Hess, Kochanski, *et al.*, 1986; Hurlimann, *et al.*, 1986; Walsworth, *et al.*, 1986). The ground-state hydrogen atom has a  $^2S$  electronic state and a nuclear spin quantum number of  $1/2$ . Coupling of the electron and nuclear spins gives rise to the well-known  $F=0$  and  $F=1$  hyperfine levels of the ground state. The transition between these two levels is the hydrogen maser transition, and the doubly spin polarized level,  $F=1, M=1$ , with both electron and nuclear spins having maximum projection along the same axis, is the one for which BEC is possible in a magnetic atom trap. Both the hydrogen maser and the phenomenon of BEC are strongly affected by atomic collisions of ground-state hydrogen atoms. Collisions cause pressure-dependent frequency shifts in the maser transition frequency that must be understood and controlled (Kleppner *et al.*, 1965; Crampton and Wang, 1975; Verhaar *et al.*, 1987; Koelman, Crampton, *et al.*, 1988), and they cause destructive relaxation of the spin-polarized H atoms that can prevent the achievement of BEC (Cline *et al.*, 1981; Sprik *et al.*, 1982; Ahn *et al.*, 1983; van Roijen *et al.*, 1988).

These developments stimulated in the 1980's theoretical calculations for low-temperature collision properties of atomic H and its isotopes. Earlier work (Dalgarno, 1961; Allison, 1972) had laid the groundwork for understanding inelastic spin exchange collisions by which two H atoms in the  $F=1$  state undergo a transition so that one or both of the atoms exit the collision in the  $F=0$  state. Berlinsky and Shizgal (1980) extended these calculations of the spin exchange cross section and collisional frequency shift of the hyperfine transition to the low-temperature limit. These early calculations were based on extending the high temperature theory, based

on knowing the phase shifts of the ground state molecular hydrogen  $^1\Sigma_g$  and  $^3\Sigma_u$  potentials alone without explicit inclusion of the hyperfine structure of the separated atoms. A proper quantum mechanical theory based on numerical solution of the coupled-channel Schrödinger equation for the atoms with hyperfine structure, also known as the close coupling method, was introduced by the Eindhoven group, and applied to frequency shifts in hydrogen masers (Verhaar *et al.*, 1987; Koelman, Crampton *et al.*, 1988; Maan *et al.*, 1990) and relaxation of doubly spin-polarized hydrogen in a magnetic trap (Ahn *et al.*, 1983; Lagendijk, 1986; Stoof *et al.*, 1988). The close coupling method is a powerful numerical tool and is the method of choice for quantitative calculations on ground-state collisions. It is the best method currently available and has been applied to a variety of species, including mixed species. A recent discussion of the multichannel scattering theory for cold collisions has been given by Gao (1997).

Collisions of species other than hydrogen have been investigated. Ung and Stwalley (1980) looked at collisions of hydrogen and deuterium in cold magnetic traps to assess the role of deuterium impurities in a cold spin-polarized hydrogen gas. Koelman *et al.* (1987) and Koelman, Stoof, *et al.* (1988) calculated the lifetime of a spin-polarized deuterium gas; Tiesinga *et al.* (1990) and Tiesinga, Crampton, *et al.* (1993) examined frequency shifts in the cryogenic deuterium maser. More recently Jamieson *et al.* (1996) have calculated collisional frequency shifts for the  $1S-2S$  two-photon transition in hydrogen. Tiesinga *et al.* (1991) calculated that the relaxation rate coefficient for doubly spin-polarized Na would be about ten times larger than for spin-polarized hydrogen. Tiesinga, Verhaar, *et al.* (1992) also calculated that the frequency shift in a cesium atomic fountain clock (Kasevich *et al.*, 1989; Clairon *et al.*, 1991) might be large enough to limit the anticipated accuracy of such a clock. The use of neutral atoms in ultra-precise atomic clocks is discussed by Gibble and Chu (1992). Gibble and Chu (1993) measured large collisional frequency shifts in a Cs fountain. These have been verified by an experiment of Ghezali *et al.*, 1996. Verhaar *et al.* (1993) argue that other cold collision properties can be deduced from these clock-shift measurements, namely, that doubly spin-polarized  $^{133}\text{Cs}$  probably has a large negative scattering length; they criticize the opposite conclusion drawn from the same data by Gribakin and Flambaum (1993), due to restrictive approximations used by the latter. Gibble and Verhaar (1995) suggest that clock frequency shifts might be eliminated by using  $^{137}\text{Cs}$ . Kokkelmans *et al.* (1997) use accurate collisional calculations for both isotopes of Rb to suggest that a Rb atomic clock will offer better performance than a Cs one. Gibble, Chang, and Legere (1995) have directly measured the  $s$ -wave scattering cross section and angular distribution in Cs atom collisions in an atomic fountain experiment at a temperature of  $T=0.89 \mu\text{K}$ .

## B. Bose-Einstein condensation

One of the major motivating factors in the study of collisions of cold ground-state neutral atoms has been

the quest to achieve Bose-Einstein condensation (BEC). This is a phase transition occurring in a gas of identical bosons when the phase space density becomes large enough, namely, when there is about one particle per cubic thermal de Broglie wavelength. The specific criterion for condensation is (Lee and Yang, 1958)

$$n \left( \frac{2\pi\hbar^2}{m\kappa T} \right)^{3/2} > 2.612, \quad (141)$$

where  $n$  represents atom density. In the condensate, there is a macroscopic occupation by a large number of atoms of the single ground state of the many-body system, whereas in a normal thermal gas many momentum states are occupied with very small probability of occupying any given one. Achieving BEC means making the density large enough, or the temperature low enough, that Eq. (141) is satisfied. The early work with spin-polarized hydrogen aimed at reaching high enough density using conventional refrigeration techniques. Unfortunately, this proved to be impossible due to the losses caused by collisions or surface recombination when the density was increased. An alternative approach was developed by using a magnetic trap without walls (Hess *et al.*, 1987) and evaporative cooling (Masuhara, 1988) to reach much lower temperatures. The idea is to keep the density sufficiently low to prevent harmful collisions. The long quest to achieve BEC for atomic hydrogen was finally successful in 1998 (Fried *et al.*, 1998), three years after the first demonstration with cold, trapped alkali atoms.

The success of laser cooling for alkali atoms gave an impetus to achieving BEC using an alkali species. These are similar to hydrogen in that they have  $^2S$  ground electronic states with two hyperfine levels due to the nuclear spin (see Fig. 3). All alkali species have an isotope with odd nuclear spin, making the atom a composite boson. Unlike hydrogen, the alkali dimer  $^3\Sigma_u$  state supports bound states; however, a metastable condensate is possible because of the long time scale required to make dimer bound states via three-body recombination at low condensate density. Ordinary laser cooling methods produce density and temperature conditions many orders of magnitude away from satisfying the phase-space density criterion in Eq. (141). The process of evaporative cooling was seen as a viable route to reaching BEC, and several groups set out to make it work. This approach was spectacularly successful, and within a few months of each other in 1995, three groups reached the regime of quantum degeneracy required for BEC. The first unambiguous demonstration of BEC in an evaporatively cooled atomic gas was reported by the NIST/JILA group (Anderson *et al.*, 1995) for doubly spin polarized  $^{87}\text{Rb}$ , followed by evidence of BEC for doubly spin-polarized  $^7\text{Li}$  by a group at Rice University (Bradley *et al.*, 1995), then BEC was demonstrated at MIT (Davis *et al.*, 1995) in the  $F=1, M=-1$  lower hyperfine component of  $^{23}\text{Na}$ . A much clearer demonstration of BEC for the  $^7\text{Li}$  system was given later (Bradley *et al.*, 1997). As of mid-1997, at least three additional groups have used similar evaporative cooling and trap

designs to achieve BEC in  $^{87}\text{Rb}$  and  $^{23}\text{Na}$ , and other attempts remain in progress elsewhere. A large literature on the subject of BEC has already been generated. Some introductory articles on the subject are given by Burnett (1996), Cornell (1996), and Townsend, Ketterle, and Stringari (1997).

Ground-state collisions play a crucial role both in the formation of a condensate and in determining its properties. A crucial step in the formation of a condensate is the achievement of critical density and temperature by “evaporative cooling,” the process by which hot atoms are removed from the confined ensemble while the remaining gas thermalizes to a lower temperature (Hess, 1986). Elastic collisions are necessary for evaporative cooling to work, and the stability and properties of the condensate itself depend on the sign and magnitude of the elastic scattering length. Two- and three-body inelastic collisions cause destructive processes that determine the condensate lifetime. Therefore, these collisions have been of as much interest for alkali species as for hydrogen and have been the object of numerous experimental and theoretical studies.

First, the process of evaporation depends on elastic momentum transfer collisions to thermalize the gas of trapped atoms as the trapping potential is lowered. These elastic collisions represent “good” collisions, and they have cross sections orders of magnitude larger for alkali species than for hydrogen. During evaporation, the rate of inelastic collisions that destroy the trapped hyperfine level, the so-called “bad” collisions, must remain much less than the rate of elastic collisions. An excellent description of the role of these two types of collisions is given in the review on evaporative cooling by Ketterle and Van Druten (1996). Long before alkali evaporative cooling was achieved, Tiesinga, Moerdijk, and Verhaar, and Stoof (1992) calculated that the ratio of the “good” to “bad” collisions appears to be very favorable for both the  $F=4, M=4$  and  $F=3, M=-3$  trappable states of  $^{133}\text{Cs}$ , having a value on the order of 1000. Precise predictions were not possible due to uncertainties in the interatomic potentials. Monroe *et al.* (1993) used time-dependent relaxation of trapped atoms to measure the elastic cross section for  $F=3, M=-3$  near 30  $\mu\text{K}$  to be large and independent of temperature between 30 and 250  $\mu\text{K}$ ,  $1.5(4) \times 10^{-12} \text{ cm}^2$ , implying a scattering length magnitude near  $46(12)a_0$ , if the cross section is assumed to be due to  $s$ -wave collisions. Newbury, Myatt, and Wieman (1995) similarly measured the elastic cross section for the  $F=1, M=-1$  state of  $^{87}\text{Rb}$  to be  $5.4(1.3) \times 10^{-12} \text{ cm}^2$ , implying a scattering length magnitude of  $88(21)a_0$ , as indicated in Table III. Measurements on thermalization in a  $F=1, M=-1$   $^{23}\text{Na}$  trap by Davis, Mewes, Joffe *et al.* (1995) deduced a scattering length of  $92(25)a_0$  for this level. A very recent study by Arndt *et al.* (1997) of thermalization of doubly spin-polarized  $^{133}\text{Cs}$   $F=4, M=4$  showed that the scattering length magnitude was very large,  $>260a_0$ , and the elastic scattering cross section was near the upper bound given by the  $s$ -wave unitarity limit  $8\pi/k^2$ , between 5 and 50  $\mu\text{K}$ . All of these experimental studies

measured total cross section only, and therefore were not able to determine the sign of the scattering length. Verhaar *et al.* (1993), however, calculated the sign to be negative for  $^{133}\text{Cs}$   $F=4$ ,  $M=4$ .

The second way in which atomic interactions profoundly affect the properties of a condensate is through their effect on the energy of the condensate. The effect of atom-atom interactions in the many-body Hamiltonian can be parametrized in the  $T \rightarrow 0$  limit in terms of the two-body scattering length (Huang and Yang, 1956). This use of the exact two-body  $T$  matrix in an energy expression is actually a rigorous procedure, and can be fully justified as a valid approximation (Stoof, Bijlsma, and Houbiers, 1996). One simple theory that has been very successful in characterizing the basic properties of actual condensates is based on a mean-field, or Hartree-Fock, description of the condensate wave function, which is found from the equation (Edwards and Burnett, 1995)

$$\left( -\frac{\hbar^2}{2m} \nabla^2 + V_{\text{trap}} + NU_0 |\Psi|^2 \right) \Psi = \mu \Psi. \quad (142)$$

Here  $V_{\text{trap}}$  is the trapping potential that confines the condensate,

$$U_0 = \frac{4\pi\hbar^2}{m} A_0 \quad (143)$$

represents the atom-atom interaction energy, which is proportional to the  $s$ -wave scattering length for the trapped atomic state, and  $\mu$  is the chemical potential—that is, the energy needed to add one more particle to a condensate having  $N$  atoms. The condensate wave function in this equation, called the Gross-Pitaevski equation or the nonlinear Schrödinger equation, can be interpreted as the single ground-state orbital occupied by each boson in the product many-body wave function  $\Phi(1 \dots N) = \prod_{i=1}^N \Psi(i)$ . The wave function  $\Psi$  could also be interpreted as the order parameter for the phase transition that produces the condensate.

The effect of atom interactions manifests itself in the nonlinear Schrödinger equation in the mean-field term proportional to the local condensate density,  $N|\Psi|^2$ , and the coupling parameter  $U_0$  proportional to the  $s$ -wave scattering length  $A_0$ . In an ideal gas, with no atom interactions,  $A_0=0$ , and this term vanishes. Equation (142) shows that the condensate wave function in such an ideal gas case just becomes that for the zero-point motion in the trap, that is, the ground state of the trapping potential. For typical alkali traps, which are harmonic to a good approximation, the zero-point motion typically has a frequency on the order of 50 to 1000 Hz, and a range on the order of 100  $\mu\text{m}$  to a few  $\mu\text{m}$ . For comparison,  $k_B T/h = 20$  kHz at  $T = 1$   $\mu\text{K}$ . In actuality, as atoms are added to the condensate the atom interaction term becomes the dominant term affecting the condensate wave function, and the shape of the condensate depends strongly on the size of the  $U_0$  term, which is proportional to the product  $NA_0$ . The sign of the scattering length is crucial here. If  $A_0$  is positive, the inter-

action energy increases as more atoms are added ( $N$  increases) to the condensate. The condensate is stable and becomes larger in size as more atoms are added. In fact, a very simple approximation, called the Thomas-Fermi approximation, gives the condensate density  $n$  by neglecting the kinetic energy term in Eq. (142) in relation to the other terms:

$$n = N|\Psi|^2 = \frac{\mu - V_{\text{trap}}}{U_0}. \quad (144)$$

This equation is remarkably accurate except near the edge of the trap where  $\mu - V_{\text{trap}}$  approaches 0 or becomes negative, and it describes condensates of  $^{87}\text{Rb}$   $F=2$ ,  $M=2$  and  $F=1$ ,  $M=-1$  and  $^{23}\text{Na}$   $F=1$ ,  $M=-1$ , all of which have positive scattering length. Condensates of such species can be made with more than  $10^6$  atoms. On the other hand, if the scattering length is negative, as for  $^7\text{Li}$ , increasing the number of particles in the trap makes the interaction energy term in Eq. (142) become more negative. The wave function contracts as more particles are added, and, in fact, only about 1000 atoms can be added to a  $^7\text{Li}$  condensate before it becomes unstable and can hold no more atoms (Dodd *et al.*, 1996; Bradley *et al.*, 1997; Bergeman, 1997). A condensate with negative scattering length is not possible in a uniform homogeneous gas, but in an atom trap the presence of zero-point motion does permit the existence of a very small condensate, as is the case for  $^7\text{Li}$ .

It is perhaps not obvious why a collisional property like a scattering length determines the energetics of the interacting particles. A simple motivational argument to indicate why this is the case can be given in relation to Fig. 5 in Sec. III.B. The long wavelength scattering wave has its phase shifted near  $R=0$  by the interaction potential. From the perspective of the asymptotic wave the effective origin of the oscillation near  $R=0$  is shifted by the presence of the potential, to  $R=A_0 > 0$  for the case of positive  $A_0$  and to  $R=A_0 < 0$  for the case of negative  $A_0$ , as Fig. 5(b) shows. The kinetic energy associated with the long wavelength asymptotic wave is affected by this shift in effective origin of oscillation. If one thinks of the two-particle system in terms of a single effective mass particle in a box, the left-hand wall of the box at  $R=0$  is moved to larger or smaller  $R$ , depending on the sign of the scattering length. What is important for the energetics is whether the change in energy is positive or negative, relative to noninteracting atoms (the box with a wall at  $R=0$ ). Given that the energy of the ground state of a reduced mass particle of mass  $m/2$  in a box is  $(\hbar^2/m)(\pi/L)^2$ , it is easy to work out that changing the length of the box from  $L$  to  $L+A_0$  changes the energy by an amount proportional to  $A_0/m$ , thus lowering the energy for the case of negative  $A_0$  and raising it for the case of positive  $A_0$ . A rigorous analysis gives the coupling term in Eq. (143).

The gas thermalization studies that measure the elastic scattering cross section cannot determine the sign of the scattering length. The sign can be determined from photoassociation spectroscopy, which is sensitive to the shape and phase of the ground-state collisional wave

function. Much tighter constraints have also been placed on the magnitudes of scattering lengths by photoassociation studies. This work was summarized in Sec. VI. Of course, observation of the condensate properties determines the sign as well. Even the magnitude of the scattering length can be found by measuring the expansion of the condensate when the trapping potential is removed, since the expansion rate depends on the strength of the interaction term in the initial condensate. This has been done for both the  $^{87}\text{Rb}$  (Holland *et al.*, 1997) and  $^{23}\text{Na}$  (Mewes *et al.*, 1996; Castin and Dum, 1996; Ketterle and Miesner, 1997) condensates, confirming the magnitude of the scattering lengths determined more precisely by other means. Before the determinations by photoassociation spectroscopy, the sign and magnitude of the scattering lengths have also been estimated from the best available interatomic potentials based on spectroscopically derived potential wells and the long-range van der Waals potentials. This was done for  $^7\text{Li}$  (Moerdijk and Verhaar, 1994; Moerdijk, Stwalley, *et al.*, 1994) and  $^{23}\text{Na}$  (Côte and Dalgarno, 1994; Moerdijk and Verhaar, 1994; Moerdijk and Verhaar, 1995), but the accuracy is not as good as for later determinations by photoassociation spectroscopy. Boesten *et al.* (1996) have used spectroscopic data on K to calculate threshold scattering properties of  $^{39}\text{K}$  and  $^{41}\text{K}$ . Côte *et al.* (Côte and Dalgarno, 1997; Côte and Stwalley, 1997) show that revised ground-state potentials for the  $\text{K}_2$  molecule need to be used, and these give different scattering lengths than the calculation of Boesten *et al.* (1996). The existence of photoassociation spectra for  $\text{K}_2$  should permit determination of more accurate threshold scattering properties of both isotopes in the future.

The third way in which collisions are significant for BEC is the role of inelastic collisions, which change the state of the trapped species. This process can produce untrapped states, as well as cause heating by releasing kinetic energy in the inelastic process. For example, if two doubly spin-polarized atoms collide and produce one or two atoms in the lower hyperfine state, then one or two units of the ground-state hyperfine splitting is given to the atoms, to be shared equally among them. Since this splitting is typically many hundreds of mK, the atoms easily escape the shallow traps designed to hold atoms at a few  $\mu\text{K}$  or less. We have already discussed how these “bad” collisions can affect the process of evaporative cooling. Fortunately, the ratio of “good” to “bad” collisions is favorable in many cases, so that evaporation actually works well and results in BEC. One case where evaporation appears to be unlikely due to “bad” collisions is the case of doubly spin-polarized  $^{133}\text{Cs}$ . Very recent experiments by (Soding *et al.*, 1998) found that the inelastic rate coefficient for destruction of doubly spin-polarized  $^{133}\text{Cs}$  atoms is so large, about three orders of magnitude larger than predicted by Tiesinga, Moerdijk, Verhaar, and Stoof (1992) that evaporative cooling of this level will be impossible. Leo *et al.* (1998) explain this unusually large inelastic collision rate as being due to a second-order spin-enhancement of the effective spin-dipolar coupling. Evaporative cooling of

the lower hyperfine level,  $^{133}\text{Cs}$   $F=3$ ,  $M=-3$  may still be feasible, given the relatively low collisional destruction rate for this level (Monroe *et al.*, 1993). The sign of the scattering length for this level is still not certain.

Measuring an inelastic collision rate in a condensate, compared to the corresponding collision rate in a thermal gas, provides a way to probe the quantum mechanical coherence properties of the condensate. Burt *et al.* (1997) have shown how this can be done. Although the first-order coherence of a condensate can be measured by observing the interference pattern of two overlapping condensates (Andrews *et al.*, 1997), collisions probe higher-order coherence properties related to the different nature of the density fluctuations in a thermal gas and in a condensate. For example, for ordinary thermal fluctuations, the average of the square of the density is two times larger than the square of the average density, whereas, for a condensate, these two quantities are equal. The second- and third-order coherence functions,  $g^{(2)}(0)$  and  $g^{(3)}(0)$ , respectively, measure this effect, where the argument 0 implies that two or three particles are found at the same position;  $g^{(2)}(0)=2!$  and  $g^{(3)}(0)=3!$  for thermal gases, and both are 1 for a condensate. Thus atoms are bunched in a thermal source, but not in a condensate, analogous to photons in a thermal source and a laser. Kagan *et al.* (1985) suggested that the three-body recombination rate might provide a way to measure this property, since the rate coefficient for three-body recombination would be  $3!=6$  times smaller in a condensate than in a thermal gas. Burt *et al.* (1997) in fact have done just this, measuring  $g^{(3)}(0)=7.4(2)$  by comparing the measured three-body recombination rates for thermal and condensed  $^{87}\text{Rb}$  in the  $F=1$ ,  $M=-1$  level.

Condensate coherence can also be probed with two-body inelastic collisions as well as three-body ones, as described by Ketterle and Miesner (1997). Stoof *et al.* (1989) use a collision theory viewpoint to show the difference of collision rates in a thermal gas and a condensate, showing that the corresponding rate for a two-body collision in a condensate is 2 times smaller than for the thermal gas. Burnett *et al.* (1996) point out that a condensate will have a two-body photoassociation spectrum, which will also show the factor of 2 decrease in rate coefficient relative to a thermal gas. In addition, a condensate photoassociation spectrum would probe the two-body part of the many-body wave function in much more detail than an overall collision rate, since it probes the wave function over a range of interparticle separations instead of just yielding  $g^{(2)}(0)$ , as an overall collision rate does. Photoassociation should be readily observable in a condensate, since at the frequencies of photoassociation lines, the light absorption rate due to two-body photoassociation at typical condensate densities will greatly exceed the light scattering rate by free atoms. An interesting question about photoassociation in a condensate is whether a three-body spectrum could be observed in which excited triatomic molecules are formed from three nearby ground-state atoms. If so, this

could provide a means for a finer grained probing of three-body effects in a condensate.

Inelastic collisions, including three-body recombination, are important for condensates and condensate formation because these can lead to heating or removal of atoms from the system. We discussed above how “bad” collisions can affect evaporative cooling. The lifetime of a condensate itself will be determined by collision processes. If the vacuum is not sufficiently low, hot background gas species can collide with trapped or condensed atoms, thereby transferring momentum to the atoms. Since the background gas atoms typically have energies on the order of 300 K, the cold atoms receive enough momentum to be ejected from the trap. There is also the possibility that some glancing collisions may transfer a very slight amount of momentum, producing hot but still trapped atoms. This could be a source of heating processes of unknown origin that have been observed in magnetic atom traps (Monroe, 1993; Mewes *et al.*, 1996). Even if the vacuum is good enough, inelastic collisions among the trapped species themselves can limit the lifetime of the trapped gas or condensate. If the collision rate coefficient for the destructive process is  $K_{in}^{(k)}$  for a  $k$ -body collision, the trap lifetime is  $(K_{in}^{(k)}n^k)^{-1}$ . For a nominal  $10^{14}$  cm<sup>-3</sup> atom density in a condensate, a one-second lifetime results from a two-body rate coefficient of  $10^{-14}$  cm<sup>3</sup> s<sup>-1</sup> or a three-body rate coefficient of  $10^{-28}$  cm<sup>3</sup> s<sup>-1</sup>. These rate coefficients will be very dependent on the species and the particular hyperfine level which is trapped. The only hyperfine levels for which trapping and condensation are possible are those for which the inelastic rate coefficients are sufficiently low.

We noted above how two-body inelastic collision rate coefficients must be small in relation to elastic collision rate coefficients in order for evaporative cooling to work. This is true for the  $F=2, M=2$  <sup>87</sup>Rb and <sup>7</sup>Li species and  $F=1, M=-1$  <sup>23</sup>Na species that have been condensed. The inelastic rate is small for the doubly spin-polarized species for the reasons discussed in Sec. VIII above. It is small for  $F=1, M=-1$  collisions for basically the same reason. An inelastic collision requires a weak spin-dipolar mechanism, since the sum of atomic  $M$  is not conserved, and, additionally, the exit channel is a  $d$ -wave for an  $s$ -wave entrance channel. The small amplitude of the threshold  $d$ -wave leads to very small collisional destruction of  $F=1, M=-1$  for weak magnetic fields. The success of sympathetic cooling, and observation of a dual condensate of <sup>87</sup>Rb  $F=1, M=-1$  and  $F=2, M=2$  (Myatt *et al.*, 1997), raises the obvious theoretical question of why the inelastic collision rate coefficient for the destructive collision of these two species was found to be so small,  $2.8 \times 10^{-14}$  cm<sup>3</sup> s<sup>-1</sup>. This inelastic process, which produces two  $F=1$  hot atoms, goes by the spin-exchange mechanism, and normally would be expected to be several orders of magnitude larger. Three theory groups immediately answered the puzzle by showing that this observation meant that <sup>87</sup>Rb had a very special property, namely the scattering lengths of both the  $^1\Sigma_g$  and  $^3\Sigma_u$  states are nearly the

same, and in fact, all scattering lengths between any two hyperfine levels of <sup>87</sup>Rb are nearly the same (Julienne *et al.*, 1997; Kokkelmans, Boesten, and Verhaar, 1997; Burke, Bohn, *et al.*, 1997a, 1997b). The existence of nearly identical scattering lengths is a sufficient condition for the inelastic rate coefficient to be as small as it is. It is not a necessary condition, since a threshold scattering resonance could also lead to a low inelastic rate coefficient. Such a resonance does not exist for <sup>87</sup>Rb, however. Julienne *et al.* (1997) pointed out that reconciling the existing data on <sup>87</sup>Rb required that the scattering lengths for collisions between any two pairs of  $F=2, M=2$  or  $F=1, M=-1$  differ by no more than  $4a_0$  and have a value of  $103 \pm 5a_0$ . Both Julienne *et al.* (1997) and Kokkelmans, Boesten, and Verhaar (1997) calculated that the inelastic collisional destruction rate coefficient for collisions of <sup>23</sup>Na  $F=2, M=2$  and  $F=1, M=-1$  would be 3 to 4 orders of magnitude larger than the one measured for <sup>87</sup>Rb. Consequently a dual species condensate would be impossible for <sup>23</sup>Na. The issue of inelastic collision rate coefficients is crucial for the prospects of sympathetic cooling, which offers an attractive path for cooling species that cannot be cooled evaporatively, and needs to be investigated for mixed alkali species. For example, cooling is desirable for spin-polarized fermionic species such as <sup>6</sup>Li, which may exhibit interesting Cooper pairing effects in the quantum degenerate regime (Stoof *et al.*, 1996). Spin-polarized fermionic species cannot be cooled evaporatively, since only  $p$ -wave collisions are allowed, and these are strongly suppressed at low  $T$  (see Sec. III.B).

Two-body rate coefficients for inelastic processes tend to be small for species that can be condensed, since otherwise the bad collisions will limit the trap density. But as density increases, three-body collisions will eventually provide a limit on trap density and lifetime. Three-body collisions produce a diatomic molecule and a free atom. These two products share the kinetic energy released due to the binding energy of the molecule. This is usually enough energy that the particles do not remain trapped; in any case, the molecule is unlikely to be trapped. Three-body collisions for spin-polarized hydrogen were studied by De Goey *et al.* (1986, 1988). The collision rate coefficient is unusually small for this system, since the ground-state triplet potential does not support any bound states in which to recombine, and making ground-state singlet molecules requires a very weak spin-dipolar transition. The rate coefficient for alkali systems is orders of magnitude larger than for hydrogen, since the triplet potentials support several bound states with small binding energy. Moerdijk, Boesten, and Verhaar (1996) calculate the three-body rate coefficients for doubly spin-polarized <sup>7</sup>Li, <sup>23</sup>Na, and <sup>87</sup>Rb to be 2.6, 2.0, and  $0.04 \times 10^{-28}$  cm<sup>3</sup> s<sup>-1</sup>, respectively. Moerdijk and Verhaar (1996) differ from the suggestion of Esry *et al.* (1996) that the three-body rate coefficient may be strongly suppressed at low  $T$ . Fedichev, Reynolds, and Shlyapnikov (1996) give a simple formula based on the scattering length for the case when the last bound state in the potential is bound weakly enough.

Burt *et al.* (1997) note that this theory gives the magnitude of their measured three-body rate coefficient for  $F=1$ ,  $M=-1$   $^{87}\text{Rb}$ .

One of the more interesting prospects for tailoring the collisional properties of ground-state species is to make use of an external field to modify the threshold collision dynamics and consequently change either the sign or magnitude of the scattering length or modify inelastic collision rates. This prospect was raised by Tiesinga, Verhaar, and Stoof (1993), who proposed that threshold scattering properties for  $^{133}\text{Cs}$  could be changed by a magnetic field. This is possible because of the rapid variation in collision properties associated with a threshold scattering resonance. For example, a magnetic field can move a molecular bound state to be located at just the threshold energy for the collision energy of two levels of the lower hyperfine manifold. Moerdijk, Verhaar, and Axelsson (1995) discussed the role of resonances for  $^6\text{Li}$ ,  $^7\text{Li}$ , and  $^{23}\text{Na}$ . Although an experimental attempt to locate predicted resonances in  $^{87}\text{Rb}$  was unsuccessful (Newbury *et al.*, 1995), there is no doubt that such scattering resonances will exist. The question is whether they exist in experimentally accessible regimes of magnetic fields. Using much more refined calculations of threshold scattering derived from photoassociation spectroscopy, Vogels *et al.* (1997) make specific predictions that resonances in scattering of the  $F=2$ ,  $M=-2$  lower hyperfine level of  $^{85}\text{Rb}$  will occur in experimentally accessible ranges of magnetic field. Boesten *et al.* (1996) calculate that  $^{41}\text{K}$  may offer good prospects for magnetic field tuning of the scattering length. The MIT BEC group, led by W. Ketterle (Inouye *et al.*, 1998) has recently reported an observation of magnetically induced Feshbach resonance effects on condensate mean-field energy and lifetime for Na  $F=1$ ,  $M=+1$  confined in an optical trap.

External fields other than magnetic ones can also change the scattering lengths. Fedichev, Kagan, *et al.* (1996) proposed that an optical field tuned near resonance with a photoassociation transition can be used to vary the ground-state scattering length but not cause excessive inelastic scattering. Napolitano, Weiner, and Julienne (1997), while investigating optical shielding (Sec. VII), calculated that large changes in elastic scattering rates can be produced by light detuned by about 100 natural linewidths to the blue of atomic resonance. This was partly because the optically induced mixing with the ground state of an excited repulsive excited state with the  $1/R^3$  long-range form greatly changed the ground-state collision by inducing contribution from angular momenta other than  $s$  waves. The problem with using light to change ground-state collision rates is that the light can also induce harmful inelastic processes as well, and the free atoms also scatter off-resonant light and experience heating due to the photon recoil. Such effects must be minimized in order for optical methods to be practical. Bohn and Julienne (1997) considered the proposal of Fedichev, Kagan, *et al.* (1996) in more detail for the cases of  $^7\text{Li}$  and  $^{87}\text{Rb}$ , giving simple formulas for estimating the light-induced changes, and showed that

there may be ranges of intensity and detuning where useful changes can be effected. Finally, the radiofrequency (rf) fields used in evaporative cooling can change collision rates. Agosta *et al.* (1989) showed how the strong rf field in a microwave trap will modify collisions. Moerdijk, Verhaar, and Nagtegaal (1996) showed that the rf fields used in evaporative cooling would make negligible changes in the collision rates of  $F=1$ ,  $M=-1$   $^{23}\text{Na}$  or  $F=2$ ,  $M=2$   $^{87}\text{Rb}$  in a magnetic trap. Suominen, Tiesinga, and Julienne (1998) concur with this analysis for these species, but show that typical rf fields for evaporative cooling can cause enhanced inelastic collisional relaxation of  $F=2$ ,  $M=2$   $^{23}\text{Na}$ . This is because rf-induced nonadiabatic transitions due to motion in the trap lead to production of other  $M$  levels, which decay with very large spin-exchange rate coefficients (Kokkelmans, Boesten, *et al.*, 1997; Julienne *et al.*, 1997).

One species that has been suggested as a viable candidate for BEC is the metastable  $^3S_1$  state of the He atom (Shlyapnikov *et al.*, 1994). This long-lived species can be cooled and trapped (Bardou *et al.*, 1992), and Fedichev, Reynolds, Rahmanov, and Shlyapnikov (1996) calculated that the collisional ionization rate coefficient is so small for the  $J=1$ ,  $M=1$  level that a polarized gas of such a species might be stable long enough to make trapping and condensation possible. The polarized gas is stable because a collision of two  $j=1$ ,  $m=1$  atoms only occurs on the  $^5\Sigma_g$  potential of the  $\text{He}_2$  dimer, for which Penning ionization is forbidden. A gas of metastable atoms is only stable if complete polarization is maintained. An unpolarized sample would rapidly destroy itself due to very fast Penning ionization collisions (Julienne and Mies, 1989; Bardou *et al.*, 1992). The Penning ionization rate coefficient for other spin-polarized  $J=2$  metastable noble gases is not known. Recent experiments on cold, trapped  $J=2$ ,  $M=2$  Xe metastable atoms indicate that collisional ionization of the polarized gas is comparable to that for the unpolarized gas (Rolston, 1997).

## IX. FUTURE DIRECTIONS

At this writing (March 1998) cold and ultracold collisions continue to stimulate the imagination of researchers with new avenues of investigation opening at an accelerating pace. In this section we briefly sketch some topics that appear particularly promising and significant.

Collisions in a light field present several intriguing areas of investigation. For example proposals for cooling and trapping molecules have recently appeared (Band and Julienne, 1995; Doyle *et al.*, 1995; Bahns *et al.*, 1996; Côté and Dalgarno, 1997) that would extend a Doppler-free precision spectroscopy to species not susceptible to direct optical cooling and may provide the starting point for building trapped clusters. Fioretti *et al.* (1998) recently reported the observation of translationally cold  $\text{Cs}_2$  molecules that fell out of a MOT following photoassociation of cold Cs atoms. Julienne *et al.* (1998) propose that cold molecules can be efficiently made by a stimulated Raman process in a Bose-Einstein condensate.

The prospects for producing cold molecules raises numerous issues about collisions between two cold molecules, or a cold molecule and a cold atom (Balakrishnan, Forrey *et al.*, 1997; Balakrishnan, Kharchenko, *et al.*, 1997). Multiple-color experiments, in which double-resonance optical excitation accesses “pure long-range” intermediate states, have begun the spectroscopic characterization of heretofore inaccessible highly excited and cold molecular Rydberg states (Wang, Gould, and Stwalley, 1998b). Two recent reports describe the production of a “frozen Rydberg gas” after excitation of atomic Rydberg states in cold Cs (Mourachko, *et al.* 1998) and Rb (Anderson, *et al.*, 1998). These experiments reveal novel many-body phenomena in a dilute gas. Collisions within and between highly collimated, dense, bright atomic beams reveal alignment and orientation features of ultracold collisions that are usually obscured by spatial averaging in trap collisions. A few steps have already been taken in this direction (Weiner, 1989; Thorsheim *et al.*, 1990; Wang and Weiner, 1990; Tsao *et al.*, 1998), but these only indicate the potential for future studies. For example atomic beam collisions will lead to a simplification of the analysis of photoassociation spectra through alignment and spin polarization (Gardner, *et al.*, 1995). Spin orientation effects suppressing Penning ionization in He metastable and other rare-gas metastable collisions can be also directly probed in beams. Doery *et al.* (1998) have calculated the long range-potentials of noble gas dimers, showing the existence of pure long-range states that could be probed by photoassociation spectroscopy. Tiesinga *et al.* (1998) have developed computational methods that treat explicitly nuclear and electron spin and permit accurate calculations of molecular hyperfine structure in photassociation spectra. Atom association between mixed species confined in “dual MOTs” will extend precision molecular spectroscopy from homonuclear to heteronuclear diatomic species. Initial studies with dual MOTs are already under active investigation (Santos *et al.*, 1995; Shaffer *et al.*, 1997). Development of convenient laser sources in the blue and near-UV regions of the spectrum will more readily permit cooling and trapping of Group IIA atoms such as Mg, Ca, Sr, and Ba. The common isotopes of the alkaline earths have no nuclear spin and therefore exhibit no hyperfine interaction. Photoassociation spectra and trap-loss spectra should therefore be interpretable with a rigorous, unifying, quantitative theory, including effects of strong light fields and spontaneous emission. The study of optical shielding and suppression in nuclear-spin-free systems will also permit rigorous comparison of experiment and theory. Up to the present most cold and ultracold collision measurements have been carried out in the frequency domain. Precision molecular spectroscopy has been the dominant influence. Some collision processes, however, lend themselves to the time domain; the observation of ultracold collisions in real time (Boesten *et al.*, 1996; Gensemer and Gould, 1997; Orzel *et al.*, 1998) and with wave packets (Varde *et al.*, 1997) may open a fruit-

ful new avenue for studies of dynamics and molecule formation complementary to high-precision frequency spectroscopy.

Ground-state collisions will continue to play an invaluable role as a probe of dilute, gas-phase quantum statistical condensates. Output coupling of confined BECs for the purpose of realizing beams of atoms in a single quantum state, “atom lasers” (Mewes, *et al.*, 1997) will need to address the issue of collision-limited coherence times. Details of scattering lengths between mixed species will determine the feasibility of sympathetic cooling (Myatt *et al.*, 1997) as a useful technique for extending BEC to a greater range of atomic or molecular systems. For example, Burke *et al.* (1997a, 1997b) discuss how  $^{87}\text{Rb}$  can be used for sympathetic cooling of the  $^{85}\text{Rb}$  isotope, which is difficult to cool directly because of a small elastic collision cross section in the relevant temperature range. Control of the sign and magnitude of the scattering length by magnetic (Vogels *et al.*, 1997; Burke *et al.*, 1997a, 1997b; Inouye *et al.*, 1998), rf, or optical field (Fedichev, Kagan, *et al.*, 1996) manipulation will be the focus of intensive efforts because a large positive scattering length provides the only demonstrated route to BEC via evaporative cooling.

Although we have discussed the principal future directions of which we are aware, the field of cold and ultracold collisions is presently germinating new ideas at such a rate that any assessment purporting to characterize the overall direction or emphasis even in the near term would be foolhardy. The only certitude one can express without fear of contradiction will be the need to update and supercede this review with another in the near future.

## ACKNOWLEDGMENTS

Financial support from the National Science Foundation, the Army Research Office, the Office of Naval Research, the FAPESP, CNPq, and CAPES is gratefully acknowledged.

## REFERENCES

- Abraham, E. R. I., W. I. McAlexander, J. M. Gerton, and R. G. Hulet, 1996, “Singlet  $s$ -wave scattering lengths of  $^6\text{Li}$  and  $^7\text{Li}$ ,” *Phys. Rev. A* **53**, R3713–R3715.
- Abraham, E. R. I., W. I. McAlexander, J. M. Gerton, and R. G. Hulet, 1997, “Triplet  $s$ -wave resonance in  $^6\text{Li}$  collisions and scattering lengths of  $^6\text{Li}$  and  $^7\text{Li}$ ,” *Phys. Rev. A* **55**, R3299–3302.
- Abraham, E. R. I., W. I. McAlexander, C. A. Sackett, and R. G. Hulet, 1995, “Spectroscopic determination of the  $s$ -wave scattering length of lithium,” *Phys. Rev. Lett.* **74**, 1315–1318.
- Abraham, E. R. I., W. I. McAlexander, H. T. C. Stoof, and R. G. Hulet, 1996, “Hyperfine structure in photoassociative spectra of  $^6\text{Li}_2$  and  $^7\text{Li}_2$ ,” *Phys. Rev. A* **53**, 3092–3097.
- Abraham, E. R. I., N. W. M. Ritchie, W. I. McAlexander, and R. G. Hulet, 1995, “Photoassociative spectroscopy of long-range states of ultracold  $^6\text{Li}_2$  and  $^7\text{Li}_2$ ,” *J. Chem. Phys.* **103**, 7773–7778.

- Adams, C. S., O. Carnal, and J. Mlynek, 1994, "Atom interferometry," *Adv. At. Mol. Opt. Phys.* **34**, 1–33.
- Adams, C. S., and E. Riis, 1997, "Laser cooling and trapping of neutral atoms," *Prog. Quantum Electron.* **21**, 1–79.
- Adams, C. S., M. Sigel, and J. Mlynek, 1994, "Atom optics," *Phys. Rep.* **240**, 143–210.
- Agosta, Ch., I. F. Silvera, H. T. C. Stoof, and B. J. Verhaar, 1989, "Trapping of neutral atoms with resonant microwave radiation," *Phys. Rev. Lett.* **62**, 2361–2364.
- Ahn, R. M. C., J. P. H. W. van den Eijnde, and B. J. Verhaar, 1983, "Calculation of nuclear spin relaxation rate for spin-polarized atomic hydrogen," *Phys. Rev. B* **27**, 5424–5432.
- Allison, A. C., 1972, "Spin-change frequency shifts in H-H collisions," *Phys. Rev. A* **5**, 2695–2696.
- Allison, A., and A. Dalgarno, 1969, "Spin change in collisions of hydrogen atoms," *Astrophys. J.* **158**, 423–425.
- Anderson, M. H., J. R. Ensher, M. R. Matthews, C. E. Wieman, and E. A. Cornell, 1995, "Observation of Bose-Einstein condensation in a dilute atomic vapor," *Science* **269**, 198–201.
- Anderson, W. R., J. R. Veal, and T. F. Gallagher, 1998, "Resonant dipole-dipole energy transfer in a nearly frozen Rydberg gas," *Phys. Rev. Lett.* **80**, 249–252.
- Andrews, M. R., C. G. Townsend, H.-J. Miesner, D. S. Durfee, D. M. Kurn, and W. Ketterle, 1997, "Observation of interference between two Bose-Einstein condensates," *Science* **275**, 637–641.
- Arndt, M., M. Ben Dahan, D. Guery-Odelin, M. W. Reynolds, and J. Dalibard, 1997, "Observation of a zero-energy resonance in Cs-Cs collisions," *Phys. Rev. Lett.* **79**, 625–628.
- Ashkin, A., 1970, "Acceleration and trapping of particles by radiation pressure," *Phys. Rev. Lett.* **24**, 156–159.
- Ashkin, A., 1978, "Trapping of atoms by resonance radiation pressure," *Phys. Rev. Lett.* **40**, 729–732.
- Ashkin, A., and J. P. Gordon, 1983, "Stability of radiation-pressure particle traps: An optical Earnshaw theorem," *Opt. Lett.* **8**, 511–513.
- Bagnato, V. S., G. P. Lafyatis, A. C. Martin, E. L. Raab, R. Ahmad-Bitar, and D. E. Pritchard, 1987, "Continuous stopping and trapping of neutral atoms," *Phys. Rev. Lett.* **58**, 2194–2197.
- Bagnato, V. S., L. Marcassa, C.-C. Tsao, Y. Wang, and J. Weiner, 1993, "Two-color spectroscopy of colliding ultracold atoms," *Phys. Rev. Lett.* **70**, 3225–3228.
- Bagnato, V. S., L. Marcassa, Y. Wang, J. Weiner, P. S. Julienne, and Y. B. Band, 1993, "Ultracold photoassociative ionization collisions in a magneto-optical trap: The optical-field-intensity dependence in a radiatively dissipative environment," *Phys. Rev. A* **48**, R2523–R2526.
- Bagnato, V. S., J. Weiner, P. S. Julienne, and C. J. Williams, 1994, "Long-Range Molecular States and Ultracold Photoassociative Ionization Collisions," *Laser Phys.* **4**, 1062–1065.
- Bahns, J. T., W. C. Stwalley, and P. L. Gould, 1996, "Laser cooling of molecules: A sequential scheme for rotation, translation, and vibration," *J. Chem. Phys.* **104**, 9689–9697.
- Balakrishnan, N., R. C. Forrey, and A. Dalgarno, 1997, "Threshold phenomena in ultracold atom-molecule collisions," *Chem. Phys. Lett.* **280**, 1–4.
- Balakrishnan, N., V. Kharchenko, R. C. Forrey, A. Dalgarno, 1997, "Complex scattering lengths in multi channel atom-molecule collision," *Chem. Phys. Lett.* **280**, 5–8.
- Bali, S., D. Hoffmann, and T. Walker, 1994, "Novel intensity dependence of ultracold collisions involving repulsive states," *Europhys. Lett.* **27**, 273–277.
- Band, Y. B., and P. S. Julienne, 1992, "Optical-Bloch-equation method for cold-atom collisions: Cs loss from optical traps," *Phys. Rev. A* **46**, 330–343.
- Band, Y. B., and P. S. Julienne, 1995, "Ultracold-molecule production by laser-cooled atom photoassociation," *Phys. Rev. A* **51**, R4317–R4320.
- Band, Y. B., and I. Tuvi, 1995, "Reduced optical shielding of collisional loss for laser-cooled atoms," *Phys. Rev. A* **51**, R4329–R4332.
- Band, Y. B., I. Tuvi, K.-A. Suominen, K. Burnett, and P. S. Julienne, 1994, "Loss from magneto-optical traps in strong laser fields," *Phys. Rev. A* **50**, R2826–R2829.
- Bardou, F., O. Emile, J.-M. Courty, C. I. Westbrook, and A. Aspect, 1992, "Magneto-optical trapping of metastable helium: Collisions in the presence of resonant light," *Europhys. Lett.* **20**, 681–686.
- Baylis, W. E., J. Pascale, and F. Rossi, 1987, "Polarization and electronic excitation in nonreactive collisions: Basic formulation for quantum calculations of collisions between  $^2P$ -state alkali-metal atoms and  $H_2$  or  $D_2$ ," *Phys. Rev. A* **36**, 4212–4218.
- Bergeman, T., 1997, "Hartree-Fock calculations of Bose-Einstein condensation of  $^7Li$  atoms in a harmonic trap for  $T > 0$ ," *Phys. Rev. A* **55**, 3658–3669.
- Berlinsky, A. J., and B. Shizgal, 1980, "Spin-exchange scattering cross sections for hydrogen atoms at low temperatures," *Can. J. Phys.* **58**, 881–885.
- Bethe, H., 1935, "Theory of disintegration of nuclei by neutrons," *Phys. Rev.* **47**, 747–759.
- Blangé, J. J., J. M. Zijlstra, A. Amelink, X. Urbain, H. Rudolph, P. van der Straten, H. C. W. Beijerinck, and H. G. M. Heideman, 1997, "Vibrational State Distribution of  $Na_2^+$  Ions Created in Ultracold Collisions," *Phys. Rev. Lett.* **78**, 3089–3092.
- Boesten, H. M. J. M., C. C. Tsai, B. J. Verhaar, and D. J. Heinzen, 1996, "Observation of a Shape Resonance in Cold-Atom Scattering by Pulsed Photoassociation," *Phys. Rev. Lett.* **77**, 5194–5197.
- Boesten, H. M. J. M., and B. J. Verhaar, 1994, "Simple quantum-mechanical picture of cold optical collisions," *Phys. Rev. A* **49**, 4240.
- Boesten, H. M. J. M., B. J. Verhaar, and E. Tiesinga, 1993, "Quantum suppression of collisional loss rates in optical traps," *Phys. Rev. A* **48**, 1428–1433.
- Boesten, H. M. J. M., J. M. Vogels, J. G. C. Tempelaars, and B. J. Verhaar, 1996, "Properties of cold collisions of  $^{39}K$  atoms and of  $^{41}K$  atoms in relation to Bose-Einstein condensation," *Phys. Rev. A* **54**, R3726–R3729.
- Bohn, J. L., and P. S. Julienne, 1996, "Semianalytic treatment of two-color photoassociation spectroscopy and control of cold atoms," *Phys. Rev. A* **54**, R4637–R4640.
- Bohn, J., and P. S. Julienne, 1997, "Prospects for influencing scattering lengths with far-off-resonant light," *Phys. Rev. A* **56**, 1486–1491.
- Boisseau, C., E. Audouard, and J. Vigué, 1998, "Quantization of the highest levels in a molecular potential," *Europhys. Lett.* **41**, 349–354.
- Boisseau, C., and J. Vigué, 1996, "Laser-dressed molecular interactions at long range," *Opt. Commun.* **127**, 251–256.
- Bonanno, R., J. Boulmer, and J. Weiner, 1983, "Determination of the absolute rate constant for associative ionization in crossed-beam collision between  $Na\ 3^2P_{3/2}$  atoms," *Phys. Rev. A* **28**, 604–608.

- Bradley, C. C., C. A. Sackett, and R. G. Hulet, 1997, "Bose-Einstein condensation of lithium: Observation of limited condensate number," *Phys. Rev. Lett.* **78**, 985–988.
- Bradley, C. C., C. A. Sackett, J. J. Tollett, and R. G. Hulet, 1995, "Evidence of Bose-Einstein Condensation in an Atomic Gas with Attractive Interactions," *Phys. Rev. Lett.* **75**, 1687–1690.
- Burke, J. P., J. L. Bohn, B. D. Esry, and Chris H. Greene, 1997a, "Impact of the  $^{87}\text{Rb}$  singlet scattering length on suppressing inelastic collisions," *Phys. Rev. A* **55**, R2511–R2514.
- Burke, J. P., J. L. Bohn, B. D. Esry, and C. H. Greene, 1998, "Prospects for mixed-isotope Bose-Einstein condensation in rubidium," *Phys. Rev. Lett.* **80**, 2097–2108.
- Burnett, K., 1996, "Bose-Einstein Condensation with evaporatively cooled atoms," *Contemp. Phys.* **37**, 1–14.
- Burnett, K., P. S. Julienne, and K.-A. Suominen, 1996, "Laser driven collisions between atoms in a Bose-Einstein condensed gas," *Phys. Rev. Lett.* **77**, 1416–1419.
- Burt, E. A., R. W. Ghrist, C. J. Myatt, M. J. Holland, E. A. Cornell, and C. E. Wieman, 1997, "Coherence, correlations, and collisions: what one learns about Bose-Einstein condensates from their decay," *Phys. Rev. Lett.* **79**, 337–340.
- Bussery, B., and M. Aubert-Frecon, 1985a, "Potential energy curves and vibration-rotation energies for the two purely long-range bound states  $1_u$  and  $0_g^-$  of the alkali dimers  $M_2$  dissociating to  $M(ns^2S_{1/2}) + M(np^2P_{3/2})$  with  $M=\text{Na, K, Rb, and Cs}$ ," *J. Mol. Spectrosc.* **113**, 21–27.
- Bussery, B., and M. Aubert-Frecon, 1985b, "Multipolar long-range electrostatic, dispersion, and induction energy terms for the interactions between two identical alkali atoms Li, Na, K, Rb, and Cs in various electronic states," *J. Chem. Phys.* **82**, 3224–3234.
- Cable, A., M. Prentiss, and N. P. Bigelow, 1990, "Observation of sodium atoms in a magnetic molasses trap loaded by a continuous uncooled source," *Opt. Lett.* **15**, 507–509.
- Casimir, H. B. G., and D. Polder, 1948, "The influence of retardation on the London-van der Waals forces," *Phys. Rev.* **73**, 360–372.
- Castin, Y., and R. Dum, 1996, "Bose-Einstein condensation in time dependent traps," *Phys. Rev. Lett.* **77**, 5315–5319.
- Castin, Y., K. Mølmer, and J. Dalibard, 1993, "Monte Carlo wave-function method in quantum optics," *J. Opt. Soc. Am. B* **10**, 524–538.
- Chu, S., J. E. Bjorkholm, A. Ashkin, and A. Cable, 1986, "Experimental observation of optically trapped atoms," *Phys. Rev. Lett.* **57**, 314–317.
- Chu, S., L. Hollberg, J. Bjorkholm, A. Cable, and A. Ashkin, 1985, "Three-dimensional viscous confinement and cooling of atoms by resonance radiation pressure," *Phys. Rev. Lett.* **55**, 48–51.
- Clairon, A., C. Salomon, S. Guellati, and W. D. Phillips, 1991, "Ramsey resonance in a Zacharias fountain," *Europhys. Lett.* **16**, 165–170.
- Cline, R. A., J. D. Miller, and D. J. Heinzen, 1993, "Photoassociation spectrum of ultracold Rb atoms," *Phys. Rev. Lett.* **71**, 2204–2207.
- Cline, R. A., J. D. Miller, and D. J. Heinzen, 1994a, "Study of  $\text{Rb}_2$  long-range states by high-resolution photoassociation spectroscopy," *Phys. Rev. Lett.* **73**, 632–635.
- Cline, R. A., J. D. Miller, and D. J. Heinzen, 1994b, "Study of  $\text{Rb}_2$  long-range states by high-resolution photoassociation spectroscopy," *Phys. Rev. Lett.* **73**, 2636(E).
- Cline, R. W., T. J. Greytak, D. Kleppner, 1981, "Nuclear polarization of spin-polarized atomic hydrogen," *Phys. Rev. Lett.* **47**, 1195–1198.
- Cohen-Tannoudji, C., J. Dupont-Roc, and G. Grynberg, 1992, *Atom-Photon Interactions: Basic Processes and Applications* (Wiley, New York).
- Cook, R. J., 1979, "Atomic motion in resonant radiation: An application of Earnshaw's theorem," *Phys. Rev. A* **20**, 224–228.
- Cook, R. J., 1980, "Theory of resonant-radiation pressure," *Phys. Rev. A* **22**, 1078–1098.
- Cornell, E., 1996, "Very cold indeed: The nanokelvin physics of Bose-Einstein condensation," *J. Res. Natl. Inst. Stand. Technol.* **101**, 419–434, and other articles in this special issue on Bose-Einstein Condensation.
- Côte, R., and A. Dalgarno, 1994, "Elastic scattering of two Na atoms," *Phys. Rev. A* **50**, 4827–4835.
- Côté, R., and A. Dalgarno, 1997, "Mechanism for the production of vibrationally excited ultracold molecules of  $^7\text{Li}_2$ ," *Chem. Phys. Lett.* **279**, 50–54.
- Côté, R., A. Dalgarno, and M. J. Jamieson, 1994, "Elastic scattering of two  $^7\text{Li}$  atoms," *Phys. Rev. A* **50**, 399–404.
- Côte, R., A. Dalgarno, Y. Sun, and R. G. Hulet, 1995, "Photoabsorption by ultracold atoms and the scattering length," *Phys. Rev. Lett.* **74**, 3581–3583.
- Côté, R., A. Dalgarno, H. Wang, and W. C. Stwalley, 1998, "Potassium scattering lengths and prospects for Bose-Einstein condensation and sympathetic cooling," *Phys. Rev. A* **57**, R4118–R4121.
- Côté, R., E. J. Heller, and A. Dalgarno, 1996, "Quantum suppression of cold atom collisions," *Phys. Rev. A* **53**, 234–241.
- Crampton, S. B., W. D. Phillips, and D. Kleppner, 1978, "Proposed low temperature hydrogen maser," *Bull. Am. Phys. Soc.* **23**, 86.
- Crampton, S. B., and H. T. M. Wang, 1975, "Duration of hydrogen atom spin-exchange collisions," *Phys. Rev. A* **12**, 1305–1312.
- Dalgarno, A., 1961, "Spin-change cross sections," *Proc. R. Soc. London, Ser. A* **262**, 132–135.
- Dalibard, J., 1988, "Laser cooling of an optically thick gas: The simplest radiation pressure trap?," *Opt. Commun.* **68**, 203–208.
- Dalibard, J., and C. Cohen-Tannoudji, 1985, "Dressed-atom approach to atomic motion in laser light: the dipole force revisited," *J. Opt. Soc. Am. B* **2**, 1707–1720.
- Dalibard, J., and C. Cohen-Tannoudji, 1989, "Laser cooling below the Doppler limit by polarization gradients: Simple theoretical models," *J. Opt. Soc. Am. B* **6**, 2023.
- Dashevskaya, E. I., 1979, "Effect of short-range forces and of twisting on intramultiplet mixing in collision of alkali-metal atoms," *Opt. Spectrosc.* **46**, 236–240.
- Dashevskaya, E. I., A. I. Voronin, and E. E. Nikitin, 1969, "Theory of excitation transfer between alkali atoms. I. Identical partners," *Can. J. Phys.* **47**, 1237–1248.
- Davis, K. B., M.-O. Mewes, M. R. Andrews, N. J. van Druten, D. S. Durfee, D. M. Kurn, and W. Ketterle, 1995, "Bose-Einstein condensation in a gas of sodium atoms," *Phys. Rev. Lett.* **75**, 3969–3973.
- Davis, K. B., M. Mewes, M. A. Joffe, M. R. Andrews, and W. Ketterle, 1995, "Evaporative cooling of sodium atoms," *Phys. Rev. Lett.* **74**, 5202–5205.

- De Goey, L. P. H., H. T. C. Stoof, B. J. Verhaar, and W. Glockle, 1988, "Role of three-body correlations in recombination of spin-polarized atomic hydrogen," *Phys. Rev. B* **38**, 646–658.
- De Goey, L. P. H., T. H. M. Van der Berg, N. Mulders, H. T. C. Stoof, and B. J. Verhaar, 1986, "Three-body recombination in spin-polarized atomic hydrogen," *Phys. Rev. B* **34**, 6183–6191.
- Delves, L. M., 1958, "Effective range expansions of the scattering matrix," *Nucl. Phys.* **8**, 358–373.
- Dodd, R. J., Mark Edwards, C. J. Williams, C. W. Clark, M. J. Holland, P. A. Ruprecht, K. Burnett, 1996, "Role of attractive interactions on Bose-Einstein condensation," *Phys. Rev. A* **54**, 661–664.
- Doery, M. R., E. J. D. Vredengbregt, J. G. C. Tempelaars, H. C. W. Beijerinck, and B. J. Verhaar, 1998, "Long-range diatomic S+P potentials of heavy rare gases," *Phys. Rev. A* **57** (in press).
- Doyle, J. M., B. Friedrich, J. Kim, and D. Patterson, 1995, "Buffer-gas loading of atoms and molecules into a magnetic trap," *Phys. Rev. A* **52**, R2515–R2518.
- Dulieu, O., A. Giusti-Suzor, and F. Masnou-Seeuws, 1991, "Theoretical treatment of the associative ionization reaction between two laser-excited sodium atoms. Direct and indirect processes," *J. Phys. B* **24**, 4391–4408.
- Dulieu, O., and P. S. Julienne, 1995, "Coupled channel bound states calculations for alkali dimers using the Fourier grid method," *J. Chem. Phys.* **103**, 60–66.
- Dulieu, O., P. D. Lett, K. Jones, U. Volz, C. Amiot, and F. Masnou-Seeuws, 1997, "Interpretation of Two-Color Photoassociation Spectroscopy Experiments in a Cold Sodium Sample: Evidence for a  $^1\Pi_u$  Doubly-Excited Autoionizing State," Poster TU172, Abstracts of Contributed Papers, XX, ICPEAC, edited by F. Aumayr, G. Getz, and H. P. Winter (Icpeac, Vienna), vol. II.
- Dulieu, O., S. Magnier, and F. Masnou-Seeuws, 1994, "Doubly-excited states for the  $\text{Na}_2$  molecule: application to the dynamics of the associative ionization reaction," *Z. Phys. D* **32**, 229–240.
- Dulieu, O., J. Weiner, and P. S. Julienne, 1994, "On the accuracy of molecular data in the understanding of ultracold collisions," *Phys. Rev. A* **49**, 607–610.
- Edwards, M., and K. Burnett, 1995, "Numerical solution of the nonlinear Schrodinger equation for small samples of trapped neutral atoms," *Phys. Rev. A* **51**, 1382–1386.
- Esry, B. D., C. H. Greene, J. P. Burke, and J. L. Bohn, 1997, "Hartree-Fock theory for double condensates," *Phys. Rev. Lett.* **78**, 3594–3597.
- Esry, B. D., C. H. Greene, Y. Zhou, and C. D. Lin, 1996, "Role of the scattering length in three-boson dynamics and Bose-Einstein condensation," *J. Phys. B* **29**, L51–L57.
- Faulstich, A., A. Schnetz, M. Sigel, T. Sleator, O. Carnal, V. Balykin, H. Takuma, and J. Mlynik, 1992, "Strong velocity compression of a supersonic atomic beam using moving optical molasses," *Europhys. Lett.* **17**, 393–399.
- Fedichev, P. O., Yu. Kagan, G. V. Shlyapnikov, and J. T. M. Walraven, 1996, "Influence of nearly resonant light on the scattering length in low-temperature atomic gases," *Phys. Rev. Lett.* **77**, 2913–2916.
- Fedichev, P. O., M. W. Reynolds, U. M. Rahmanov, G. V. Shlyapnikov, 1996, "Inelastic decay processes in a gas of spin-polarized triplet helium," *Phys. Rev. A* **53**, 1447–1453.
- Fedichev, P. O., M. W. Reynolds, and G. V. Shlyapnikov, 1996, "Three-body recombination of ultracold atoms to a weakly bound  $s$  level," *Phys. Rev. Lett.* **77**, 2921–2924.
- Feng, P., D. Hoffmann, and T. Walker, 1993, "Comparison of trap-loss collision spectra for  $^{85}\text{Rb}$  and  $^{87}\text{Rb}$ ," *Phys. Rev. A* **47**, R3495–R3498.
- Fioretti, A., D. Comparat, A. Crubellier, O. Dulieu, F. Masnou-Seeuws, and P. Pillet, 1998, " $\text{Cs}_2$  cold molecule formation through photoassociative scheme in a Cs vapor-cell magneto-optical trap," *Phys. Rev. Lett.* **80**, 4402–4405.
- Fioretti, A., J. H. Müller, P. Verkerk, M. Allegrini, E. Arimondo, and P. S. Julienne, 1997, "Direct measurement of fine-structure collisional losses from a Cs magneto optical trap," *Phys. Rev. A* **55**, R3999–R4002.
- Flemming, J., A. M. Tuboy, D. M. B. P. Milori, L. G. Marcassa, S. C. Zilio, and V. S. Bagnato, 1997, "Magneto-Optical Trap for Sodium Atoms Operating on the D1 Line," *Opt. Commun.* **135**, 269–272.
- Freeland, R. S., C. C. Tsai, M. Marinescu, R. A. Cline, J. D. Miller, C. J. Williams, A. Dalgarno, and D. J. Heinzen, 1997, Department of Physics, University of Texas, Austin (unpublished).
- Fried, D. G., T. C. Killian, L. Willmann, D. Landhuis, A. C. Moss, T. J. Greytak, and D. Kleppner, 1998, "Bose-Einstein Condensation of Atomic Hydrogen," *Phys. Rev. Lett.* **81**, 3811–3814.
- Frisch, C. R., 1933, "Experimenteller Nachweis des Einsteinschen Strahlungsruckstosses," *Z. Phys.* **86**, 42–48.
- Gallagher, A., 1991, "Associative ionization in collisions of slowed and trapped sodium," *Phys. Rev. A* **44**, 4249–4259.
- Gallagher, A., and D. E. Pritchard, 1989, "Exoergic collisions of cold  $\text{Na}^*-\text{Na}$ ," *Phys. Rev. Lett.* **63**, 957–960.
- Gao, B., 1997, "Theory of slow-atom collisions," *Phys. Rev. A* **54**, 2022–2039.
- Gardner, J. R., R. A. Cline, J. D. Miller, D. J. Heinzen, H. M. J. M. Boesten, and B. J. Verhaar, 1995, "Collisions of doubly spin-polarized, ultracold  $^{85}\text{Rb}$  atoms," *Phys. Rev. Lett.* **74**, 3764–3767.
- Gaupp, A., P. Kuske, and H. J. Andrä, 1982, "Accurate lifetime measurements of the lowest  $^2P_{1/2}$  states in neutral lithium and sodium," *Phys. Rev. A* **26**, 3351–3359.
- Gensemer, S. D., and P. L. Gould, 1997, "Ultracold collisions observed in real time," *Phys. Rev. Lett.* **80**, 936–939.
- Gensemer, S. D., V. Sanchez-Villicana, K. Y. N. Tan, T. T. Grove, and P. L. Gould, 1997, "Trap-loss collisions of  $^{85}\text{Rb}$  and  $^{87}\text{Rb}$ : Dependence on trap parameters," *Phys. Rev. A* **56**, 4055–4063.
- Ghezali, S., Ph. Laurent, S. N. Lea, and A. Clairon, 1996, "An experimental study of the spin-exchange frequency shift in a laser-cooled cesium fountain frequency standard," *Europhys. Lett.* **36**, 25–30.
- Gibble, K., S. Chang, and R. Legere, 1995, "Direct observation of  $s$ -wave atomic collisions," *Phys. Rev. Lett.* **75**, 2666–2669.
- Gibble, K., and S. Chu, 1992, "Future slow-atom frequency standards," *Metrologia* **29**, 201–212.
- Gibble, K., and S. Chu, 1993, "Laser-cooled Cs frequency standard and a measurement of the frequency shift due to ultracold collisions," *Phys. Rev. Lett.* **70**, 1771–1774.
- Gibble, K., and B. J. Verhaar, 1995, "Eliminating cold-collision frequency shifts," *Phys. Rev. A* **52**, 3370–3373.
- Gordon, J. P., and A. Ashkin, 1980, "Motion of atoms in a radiation trap," *Phys. Rev. A* **21**, 1606–1617.

- Gott, Y. V., M. S. Ioffe, and V. G. Telkovsky, 1962, *Nuclear Fusion* (International Atomic Energy Agency, Vienna), Suppl. Pt. 3, p. 1045.
- Gould, P. L., P. D. Lett, P. S. Julienne, W. D. Phillips, H. R. Thorsheim, and J. Weiner, 1988, "Observation of associative ionization of ultracold laser-trapped sodium atoms," *Phys. Rev. Lett.* **60**, 788–791.
- Gribakin, G. F., and V. V. Flambaum, 1993, "Calculation of the scattering length in atomic collisions using the semiclassical approximation," *Phys. Rev. A* **48**, 546–553.
- Han, D.-J., R. A. Rynar, Ph. Courteille, and D. J. Heinzen, 1997, "Bose-Einstein condensation of large numbers of  $^{87}\text{Rb}$  atoms in a magnetic TOP trap," *Phys. Rev. A* **57**, 958–975.
- Heather, R. W., and P. S. Julienne, 1993, "Theory of laser-induced associative ionization of ultracold Na," *Phys. Rev. A* **47**, 1887–1906.
- Heinzen, D. J., 1995, "Collisions of Ultracold Atoms in Optical Fields," in *Atomic Physics 14*, edited by D. J. Wineland, C. E. Wieman, and S. J. Smith (American Institute of Physics, New York), pp. 369–388.
- Henriet, A., F. Masnou-Seeuws, and O. Dulieu, 1991, "Adiabatic representation for the excited states of the  $\text{Na}_2$  molecule: application to the associative ionization reaction between two excited sodium atoms," *Z. Phys. D* **18**, 287–298.
- Herschbach, D. R., 1966, *Advances in Chemical Physics, Vol X, Molecular Beams*, edited by J. Ross (Wiley Interscience, New York), pp. 319–393.
- Herzberg, G., 1950, *Molecular Spectra and Molecular Structure. I. Spectra of Diatomic Molecules*, Second Ed. (van Nostrand, Princeton).
- Hess, H. F., 1986, "Evaporative cooling of magnetically trapped and compressed spin-polarized hydrogen," *Phys. Rev. B* **34**, 3476–3479.
- Hess, H. F., G. P. Kochanski, J. M. Doyle, T. J. Greytak, and D. Kleppner, 1986, "Spin-polarized hydrogen maser," *Phys. Rev. A* **34**, 1602–1604.
- Hess, H. F., G. P. Kochanski, J. M. Doyle, N. Mashuhara, D. Kleppner, and T. J. Greytak, 1987, "Magnetic trapping of spin-polarized atomic hydrogen," *Phys. Rev. Lett.* **59**, 672–675.
- Hoffmann, D., S. Bali, and T. Walker, 1996, "Trap-depth measurements using ultracold collisions," *Phys. Rev. A* **54**, R1030–R1033.
- Hoffmann, D., P. Feng, and T. Walker, 1994, "Measurements of Rb trap-loss collision spectra," *J. Opt. Soc. Am. B* **11**, 712.
- Hoffmann, D., P. Feng, R. S. Williamson, and T. Walker, 1992, "Excited-state collision of trapped  $^{85}\text{Rb}$  atoms," *Phys. Rev. Lett.* **69**, 753–756.
- Holland, M. J., D. S. Jin, M. L. Chiofalo, and J. Cooper, 1997, "Emergence of interaction effects in Bose-Einstein condensation," *Phys. Rev. Lett.* **78**, 3801–3805.
- Holland, M. J., K.-A. Suominen, and K. Burnett, 1994, "Cold collisions in a laser field: Quantum Monte Carlo treatment of radiative heating," *Phys. Rev. A* **50**, 1513–1530.
- Hoogerland, M., 1993, Ph.D. thesis (Eindhoven University).
- Huang, K., and C. N. Yang, 1957, "Quantum mechanical many-body problem with hard-sphere interactions," *Phys. Rev.* **105**, 767–775.
- Huennekens, J., and A. Gallagher, 1983, "Associative ionization in collisions between two  $\text{Na}(3P)$  atoms," *Phys. Rev. A* **28**, 1276–1287.
- Hurlimann, M. D., W. N. Hardy, A. J. Berlinski, and R. W. Cline, 1986, "Recirculating cryogenic hydrogen maser," *Phys. Rev. A* **34**, 1605–1608.
- Huynh, B., O. Dulieu, and F. Masnou-Seeuws, 1998, "Associative ionization between two laser-excited sodium atoms: Theory compared to experiment," *Phys. Rev. A* **57**, 958–975.
- Inoue, G., J. K. Ku, and D. W. Setser, 1982, "Photoassociative laser induced fluorescence of  $\text{Xe Cl}$ ," *J. Chem. Phys.* **76**, 733–734.
- Inouye, S., M. R. Andrews, J. Stenger, H.-J. Miesner, D. M. Stamper-Kurn, and W. Ketterle, 1998, "Observation of Feshbach Resonances in a Bose-Einstein Condensate," *Nature (London)* **392**, 151–154.
- Jamieson, M. J., A. Dalgarno, J. M. Doyle, 1996, "Scattering lengths for collisions of ground state and metastable state hydrogen atoms," *Mol. Phys.* **87**, 817–826.
- Jessen, P. S., and I. H. Deutsch, 1996, "Optical Lattices," *Adv. At., Mol., Opt. Phys.* **37**, 95–138.
- Jones, K. M., P. S. Julienne, P. D. Lett, W. D. Phillips, E. Tiesinga, and C. J. Williams, 1996, "Measurement of the atomic  $\text{Na}(3P)$  lifetime and of retardation in the interaction between two atoms bound in a molecule," *Europhys. Lett.* **35**, 85–90.
- Jones, K. M., S. Maleki, S. Bize, P. D. Lett, C. J. Williams, H. Richling, H. Knöckel, E. Tiemann, H. Wang, P. L. Gould, and W. C. Stwalley, 1996, "Direct measurement of the ground-state dissociation energy of  $\text{Na}_2$ ," *Phys. Rev. A* **54**, R1006–R1009.
- Jones, K. M., S. Maleki, L. P. Ratliff, and P. D. Lett, 1997, "Two-colour photoassociation spectroscopy of ultracold sodium," *J. Phys. B* **30**, 289–308.
- Jones, R. B., J. H. Schloss, and J. G. Eden, 1993, "Excitation spectra for the photoassociation of  $\text{Kr-F}$  and  $\text{Xe-I}$  collision pairs in the ultraviolet (209–258 nm)," *J. Chem. Phys.* **98**, 4317–4334.
- Julienne, P. S., 1988, "Laser modification of ultracold atomic collision in optical traps," *Phys. Rev. Lett.* **61**, 698–701.
- Julienne, P. S., 1996, "Cold binary atomic collision in a light field," *J. Res. Natl. Inst. Stand. Technol.* **101**, 487–503.
- Julienne, P. S., K. Burnett, Y. B. Band, and W. C. Stwalley, 1998, "Stimulated Raman molecule production in Bose-Einstein condensates," *Phys. Rev. A* **58**, R797–R800.
- Julienne, P. S., and R. Heather, 1991, "Laser modification of ultracold atomic collisions: Theory," *Phys. Rev. Lett.* **67**, 2135–2138.
- Julienne, P. S., and F. H. Mies, 1989, "Collisions of ultracold trapped atoms," *J. Opt. Soc. Am. B* **6**, 2257–2269.
- Julienne, P. S., F. H. Mies, E. Tiesinga, and C. J. Williams, 1997, "Collisional stability of double Bose condensates," *Phys. Rev. Lett.* **78**, 1880–1883.
- Julienne, P. S., A. M. Smith, and K. Burnett, 1993, "Theory of collisions between laser cooled atoms," *Advances in Atomic, Molecular, and Optical Physics* (Academic Press), Vol. 30, pp. 141–198.
- Julienne, P. S., K.-A. Suominen, and Y. Band, 1995, "Complex-potential model of collisions of laser-cooled atoms," *Phys. Rev. A* **49**, 3890–3896.
- Julienne, P. S., and J. Vigué, 1991, "Cold collisions of ground- and excited-state alkali-metal atoms," *Phys. Rev. A* **44**, 4464–4485.
- Julienne, P. S., C. Williams, O. Dulieu, and Y. B. Band, 1994, "Calculations of collisional loss rates of trapped Li atoms," *Laser Phys.* **4**, 1076–1084.

- Kagan, Yu., B. V. Svistunov, and G. V. Shlyapnikov, 1985, "Effect of Bose-Einstein condensation on inelastic processes in gases," *Pis'ma Zh. Eksp. Teor. Fiz.* **42**, 169–172 (*JETP Lett.* **42**, 209–212).
- Kasevich, M. A., E. Riis, S. Chu, and R. G. DeVoe, 1989, "Rf spectroscopy in an atomic fountain," *Phys. Rev. Lett.* **63**, 612–615.
- Katori, H., H. Kunugita, and T. Ido, 1995, "Quantum statistical effect on ionizing collisions of ultracold metastable Kr isotopes," *Phys. Rev. A* **52**, R4324–R4327.
- Katori, H., and F. Shimizu, 1994, "Laser-Induced Ionizing Collisions of Ultracold Krypton Gas in the  $1s_5$  Metastable State," *Phys. Rev. Lett.* **73**, 2555–2558.
- Kawanaka, J., K. Shimizu, H. Takuma, and F. Shimizu, 1993, "Quadratic collisional loss rate of a  $^7\text{Li}$  trap," *Phys. Rev. A* **48**, R883–R885.
- Kazantsev, A. P., G. I. Surdutovich, D. O. Chudesnikov, and V. P. Yakovlev, 1989, "Scattering, Velocity Bunching, and Self-Localization of Atoms in a Light Field," *J. Opt. Soc. Am. B* **6**, 2130–2139.
- Ketterle, W., K. B. Davis, M. A. Joffe, A. Martin, and D. Pritchard, 1993, "High densities of cold atoms in a dark spontaneous-force optical trap," *Phys. Rev. Lett.* **70**, 2253–2256.
- Ketterle, W., and H.-J. Miesner, 1997, "Coherence properties of Bose condensates and atom lasers," *Phys. Rev. A* **56**, 3291–3293.
- Ketterle, W., and N. J. Van Druten, 1996, "Evaporative cooling of trapped atoms," *Adv. At., Mol., Opt. Phys.* **37**, 181–236.
- King, G. W., and J. H. Van Vleck, 1939, "Dipole-Dipole Resonance Forces," *Phys. Rev.* **55**, 1165–1172.
- Kleppner, D., H. C. Berg, S. B. Crampton, N. F. Ramsey, R. C. Vessot, H. E. Peters, and J. Vanier, 1965, "Hydrogen-maser principles and techniques," *Phys. Rev.* **138**, A972–A983.
- Koelman, J. M. V. A., S. B. Crampton, H. T. C. Stoof, O. J. Luiten, and B. J. Verhaar, 1988, "Spin-exchange frequency shifts in cryogenic and room-temperature hydrogen masers," *Phys. Rev. A* **38**, 3535–3547.
- Koelman, J. M. V. A., H. T. C. Stoof, B. J. Verhaar, and J. T. M. Walraven, 1987, "Spin polarized deuterium in magnetic traps," *Phys. Rev. Lett.* **59**, 676–679.
- Koelman, J. M. V. A., H. T. C. Stoof, B. J. Verhaar, and J. T. M. Walraven, 1988, "Lifetime of magnetically trapped ultracold atomic deuterium gas," *Phys. Rev. B* **38**, 9319–9322.
- Kokkelmans, S. J. J. M. F., H. M. J. M. Boesten, and B. J. Verhaar, 1997, "Role of collisions in creation of overlapping Bose condensates," *Phys. Rev. A* **55**, R1589–R1592.
- Kokkelmans, S. J. J. M. F., B. J. Verhaar, K. Gibble, and D. J. Heinzen, 1997, "Predictions for laser-cooled Rb clocks," *Phys. Rev. A* **56**, R4389–R4392.
- Krauss, M., and W. J. Stevens, 1990, "Effective core potentials and accurate energy curves for  $\text{Cs}_2$  and other alkali diatomics," *Chem. Phys.* **93**, 4236–4242.
- Kunugita, H., T. Ido, and F. Shimizu, 1997, "Ionizing collision rate of metastable rare-gas atoms in an optical lattice," *Phys. Rev. Lett.* **79**, 621–624.
- Kuyatt, C. E., 1967, *Electron Optics Lectures* (unpublished, but available from the author at NIST).
- Legendijk, A., I. F. Silvera, and B. J. Verhaar, 1986, "Spin-exchange and dipolar relaxation rates in atomic hydrogen: Lifetimes in magnetic traps," *Phys. Rev. B* **33**, 626–628.
- Lai, W. K., K.-A. Suominen, B. M. Garraway, and S. Stenholm, 1993, "Dissipation effects on wave packets in level crossings: A comparison between two numerical approaches," *Phys. Rev. A* **47**, 4779–4785.
- Laloë, F., Ed., 1980, *Spin polarized quantum systems*, Supplement to *J. Phys. (Paris)*, Colloque C7.
- Lawall, J., C. Orzel, and S. L. Rolston, 1998, "Suppression and enhancement of collisions in optical lattices," *Phys. Rev. Lett.* **80**, 480–483.
- Lee, T. D., and C. N. Yang, 1958, "Low-temperature behavior of dilute Bose system of hard spheres. I. Equilibrium properties," *Phys. Rev.* **112**, 1419–1429.
- Leo, P., E. Tiesinga, P. S. Julienne, D. K. Walter, S. Kadlecek, and T. G. Walter, 1998, "Elastic and inelastic collisions of cold spin-polarized  $^{133}\text{Cs}$  atoms," *Phys. Rev. Lett.* **81**, 1389–1392.
- Leonhardt, D., and J. Weiner, 1995, "Direct two-color photo-associative ionization in a rubidium magneto-optic trap," *Phys. Rev. A* **52**, R4332–R4335.
- Leonhardt, D., and J. Weiner, 1996, "Direct two-color photo-associative ionization in a rubidium magneto-optic trap," *Phys. Rev. A* **53**, 2904(E).
- LeRoy, R. J., and R. B. Bernstein, 1970, "Dissociation energy and long-range potential of diatomic molecules from vibrational spacings of higher levels," *J. Chem. Phys.* **52**, 3869–3879.
- Lett, P. D., K. Helmerson, W. D. Phillips, L. P. Ratliff, S. L. Rolston, and M. E. Wagshul, 1993, "Spectroscopy of  $\text{Na}_2$  by photoassociation of laser-cooled Na," *Phys. Rev. Lett.* **71**, 2200–2203.
- Lett, P. D., P. S. Jessen, W. D. Phillips, S. L. Rolston, C. I. Westbrook, and P. L. Gould, 1991, "Laser modification of ultracold collisions: Experiment," *Phys. Rev. Lett.* **67**, 2139–2142.
- Lett, P. D., P. S. Julienne, and W. D. Phillips, 1996, "Photoassociative spectroscopy of laser cooled atoms," *Annu. Rev. Phys. Chem.* **46**, 423–452.
- Lett, P. D., K. Mølmer, S. D. Gensemer, K. Y. N. Tan, A. Kumarakrishnan, C. D. Wallace, and P. L. Gould, 1995, "Hyperfine structure modifications of collisional losses from light-force atom traps," *J. Phys. B* **28**, 65–81.
- Lett, P. D., R. N. Watts, C. I. Westbrook, W. D. Phillips, P. L. Gould, and H. J. Metcalf, 1988, "Observation of Atoms, Laser-Cooled Below the Doppler Limit," *Phys. Rev. Lett.* **61**, 169–172.
- Lovelace, R. V. E., C. Mehanian, T. J. Tommila, and D. M. Lee, 1985, "Magnetic confinement of a neutral gas," *Nature (London)* **318**, 30–36.
- Lu, Z. T., K. L. Corwin, M. J. Renn, M. H. Anderson, E. A. Cornell, and C. E. Wieman, 1996, "Low-velocity intense source of atoms from a magneto-optical trap," *Phys. Rev. Lett.* **77**, 3331–3334.
- Maan, A. C., H. T. C. Stoof, and B. J. Verhaar, 1990, "Cryogenic H maser in a strong B field," *Phys. Rev. A* **41**, 2614–2620.
- Magnier, S., Ph. Millié, O. Dulieu, F. Masnou-Seeuws, 1993, "Potential curves for the ground and excited states for the  $\text{Na}_2$  molecule up to the  $(3s+5p)$  dissociation limit: Results of two different effective potential calculations," *J. Chem. Phys.* **98**, 7113–7125.
- Marcassa, L., V. Bagnato, Y. Wang, C. Tsao, J. Weiner, O. Dulieu, Y. B. Band, and P. S. Julienne, 1993, "Collisional loss

- rate in a magneto-optical trap for sodium atoms: Light-intensity dependence,” *Phys. Rev. A* **47**, R4563–R4566.
- Marcassa, L., K. Helmerson, A. M. Tuboy, D. M. B. P. Milori, S. R. Muniz, J. Flemming, S. C. Zilio, and V. S. Bagnato, 1996, “Collisional loss rate of sodium atoms in a magneto-optical trap operating on the D1 line,” *J. Phys. B* **29**, 3051–3057.
- Marcassa, L., R. Horowicz, S. Zilio, V. Bagnato, and J. Weiner, 1995, “Intensity dependence of optical suppression in photoassociative ionization collisions in a sodium magneto-optic trap,” *Phys. Rev. A* **52**, R913–R916.
- Marcassa, L., S. Muniz, E. de Queiroz, S. Zilio, V. Bagnato, J. Weiner, P. S. Julienne, and K.-A. Suominen, 1994, “Optical suppression of photoassociative ionization in a magneto-optical trap,” *Phys. Rev. Lett.* **73**, 1911–1914.
- Marcassa, L., S. R. Muniz, and J. Flemming, 1997, “Optical catalysis in a Na-vapor cell MOT,” *Braz. J. Phys.* **27**, 238–242.
- Mastwijk, H. C., J. W. Thomsen, P. van der Straten, and A. Niehaus, 1998, “Optical collisions of cold, metastable helium atoms,” *Phys. Rev. Lett.* **80**, 5516–5519.
- Masuhara, N., J. M. Doyle, J. C. Sandberg, D. Kleppner, and T. J. Greytak, 1988, “Evaporative cooling of spin-polarized atomic hydrogen,” *Phys. Rev. Lett.* **61**, 935–938.
- McAlexander, W. I., E. R. I. Abraham, and R. G. Hulet, 1996, “Radiative lifetime of the  $2P$  state of lithium,” *Phys. Rev. A* **54**, R5–R8.
- McAlexander, W. I., E. R. I. Abraham, N. W. M. Ritchie, C. J. Williams, H. T. C. Stoof, and R. G. Hulet, 1995, “Precise atomic radiative lifetime via photoassociative spectroscopy of ultracold lithium,” *Phys. Rev. A* **51**, R871–R874.
- McLone, R. R., and E. A. Power, 1964, “On the interaction between two identical neutral dipole systems, one in an excited state and the other in the ground state,” *Mathematika* **11**, 91–94.
- Meath, W. J., 1968, “Retarded interaction energies between like atoms in different energy states,” *J. Chem. Phys.* **48**, 227–235.
- Metcalf, H., and P. van der Straten, 1994, “Cooling and trapping of neutral atoms,” *Phys. Rep.* **244**, 203–286.
- Mewes, M.-O., M. R. Andrews, D. M. Kurn, D. S. Durfee, C. G. Townsend, and W. Ketterle, 1997, “Output coupler for Bose-Einstein condensed atoms,” *Phys. Rev. Lett.* **78**, 582–585.
- Mewes, M.-O., M. R. Andrews, N. J. van Druten, D. M. Kurn, D. S. Durfee, and W. Ketterle, 1996, “Bose-Einstein condensation in a tightly confining dc magnetic trap,” *Phys. Rev. Lett.* **77**, 416–419.
- Mies, F. H., 1973a, “Molecular theory of atomic collisions: Fine-structure transitions,” *Phys. Rev. A* **7**, 942–957.
- Mies, F. H., 1973b, “Molecular theory of atomic collisions: Calculated cross sections for  $H^+ + F(^2P)$ ,” *Phys. Rev. A* **7**, 957–967.
- Mies, F. H., C. J. Williams, P. S. Julienne, and M. Krauss, 1996, “Estimating bounds on collisional relaxation rates of spin-polarized  $^{87}\text{Rb}$  atoms at ultracold temperatures,” *J. Res. Natl. Inst. Stand. Technol.* **101**, 521–535.
- Migdall, A. L., J. V. Prodan, W. D. Phillips, T. H. Bergman, and H. J. Metcalf, 1985, “First observation of magnetically trapped neutral atoms,” *Phys. Rev. Lett.* **54**, 2596–2599.
- Miller, J. D., R. A. Cline, and D. J. Heinzen, 1993a, “Far-off-resonance optical trapping of atoms,” *Phys. Rev. A* **47**, R4567–R4570.
- Miller, J. D., R. A. Cline, and D. J. Heinzen, 1993b, “Photo-association spectrum of ultracold Rb atoms,” *Phys. Rev. Lett.* **71**, 2204–2207.
- Moerdijk, A. J., H. M. J. M. Boesten, and B. J. Verhaar, 1996, “Decay of trapped ultracold alkali atoms by recombination,” *Phys. Rev. A* **53**, 916–920.
- Moerdijk, A. J., W. C. Stwalley, R. G. Hulet, and B. J. Verhaar, 1994, “Negative scattering length of ultracold  $^7\text{Li}$  Gas,” *Phys. Rev. Lett.* **72**, 40–43.
- Moerdijk, A. J., and B. J. Verhaar, 1994, “Prospects for Bose-Einstein condensation in atomic  $^7\text{Li}$  and  $^{23}\text{Na}$ ,” *Phys. Rev. Lett.* **73**, 518–521.
- Moerdijk, A. J., and B. J. Verhaar, 1995, “Laser cooling and the highest bound states of the Na diatom system,” *Phys. Rev. A* **51**, R4333–R4436.
- Moerdijk, A. J., and B. J. Verhaar, 1996, “Collisional two- and three-body decay rates of dilute quantum gases at ultralow temperatures,” *Phys. Rev. A* **53**, R19–R22.
- Moerdijk, A. J., B. J. Verhaar, and A. Axelsson, 1995, “Resonances in ultracold collisions of  $^6\text{Li}$ ,  $^7\text{Li}$ , and  $^{23}\text{Na}$ ,” *Phys. Rev. A* **51**, 4852–4861.
- Moerdijk, A. J., B. J. Verhaar, and T. M. Nagtegaal, 1996, “Collisions of dressed ground-state atoms,” *Phys. Rev. A* **53**, 4343–4351.
- Moi, L., 1984, “Application of a very long cavity laser to atom slowing down and optical pumping,” *Opt. Commun.* **50**, 349–352.
- Molenaar, P. A., P. van der Straten, and H. G. M. Heidemann, 1996, “Long-range predissociation in two-color photoassociation of ultracold Na atoms,” *Phys. Rev. Lett.* **77**, 1460–1463.
- Monroe, C., 1992, Ph.D. Dissertation (University of Colorado).
- Monroe, C. R., E. A. Cornell, C. A. Sackett, C. J. Myatt, and C. E. Wieman, 1993, “Measurement of Cs-Cs elastic scattering at  $T=30\ \mu\text{K}$ ,” *Phys. Rev. Lett.* **70**, 414–417.
- Monroe, C., W. Swann, H. Robinson, and C. Wieman, 1990, “Very cold trapped atoms in a vapor cell,” *Phys. Rev. Lett.* **65**, 1571–1574.
- Morinaga, M., M. Yasuda, T. Kishimoto, and F. Shimizu, 1996, “Holographic manipulation of a cold atomic beam,” *Phys. Rev. Lett.* **77**, 802–805.
- Mott, N. F., and H. S. W. Massey, 1965, *The Theory of Atomic Collisions*, Third Edition (Clarendon, Oxford).
- Mourachko, I., D. Comparat, F. de Tomasi, A. Fioretti, P. Nosbaum, V. M. Akulin, and P. Pillet, 1998, “Many-body effects in a frozen Rydberg gas,” *Phys. Rev. Lett.* **80**, 253–256.
- Movre, M., and G. Pichler, 1977, “Resonance interaction and self-broadening of alkali resonance lines I. Adiabatic potential curves,” *J. Phys. B* **10**, 2631–2638.
- Muniz, S. R., L. G. Marcassa, R. Napolitano, G. D. Telles, J. Weiner, S. C. Zilio, and V. S. Bagnato, 1997, “Optical suppression of hyperfine-changing collisions in a sample of ultracold sodium atoms,” *Phys. Rev. A* **55**, 4407–4411.
- Myatt, C. J., E. A. Burt, R. W. Ghrist, E. A. Cornell, and C. E. Wieman, 1997, “Production of two overlapping Bose-Einstein condensates by sympathetic cooling,” *Phys. Rev. Lett.* **78**, 586–589.
- Myatt, C. J., N. R. Newbury, R. W. Ghrist, S. Loutzenhiser, and C. E. Wieman, 1996, “Multiply loaded magneto-optical trap,” *Opt. Lett.* **21**, 290–292.
- Napolitano, R., J. Weiner, and P. S. Julienne, 1997, “Theory of optical suppression of ultracold-collision rates by polarized light,” *Phys. Rev. A* **55**, 1191–1207.

- Napolitano, R., J. Weiner, C. J. Williams, and P. S. Julienne, 1994, "Line shapes of high resolution photoassociation spectra of optically cooled atoms," *Phys. Rev. Lett.* **73**, 1352–1355.
- Nellessen, J., J. Werner, and W. Ertmer, 1990, "Magneto-optical compression of a monoenergetic sodium atomic beam," *Opt. Commun.* **78**, 300–308.
- Newbury, N. R., C. J. Myatt, and C. E. Wieman, 1995, "s-wave elastic collisions between cold ground state  $^{87}\text{Rb}$  atoms," *Phys. Rev. A* **51**, R2680–R2683.
- Orzel, C., S. D. Bergeson, S. Kulin, and S. L. Rolston, 1998, "Time-resolved studies of ultra-cold ionizing collisions," *Phys. Rev. Lett.* **80**, 5093–5096.
- Peters, M. G., D. Hoffmann, J. D. Tobiason, and T. Walker, 1994, "Laser-induced ultracold  $\text{Rb}(5S_{1/2}) + \text{Rb}(5P_{1/2})$  collisions," *Phys. Rev. A* **50**, R906–R909.
- Phillips, W. D., J. V. Prodan, and H. J. Metcalf, 1985, "Laser cooling and electromagnetic trapping of neutral atoms," *J. Opt. Soc. Am. B* **2**, 1751–1767.
- Pierce, J. R., 1954, *Theory and Design of Electron Beams*, 2nd ed. (Van Nostrand, Princeton, NJ).
- Pillet, P., A. Crubellier, A. Bleton, O. Dulieu, P. Nosbaum, I. Mourachko, and F. Masnou-Seeuws, 1997, "Photoassociation in a gas of cold alkali atoms: I. Perturbative quantum approach," *J. Phys. B* **30**, 2801–2820.
- Prentiss, M., A. Cable, J. Bjorkholm, S. Chu, E. Raab, and D. Pritchard, 1988, "Atomic-density-dependent losses in an optical trap," *Opt. Lett.* **13**, 452–454.
- Pritchard, D. E., 1983, "Cooling neutral atoms in a magnetic trap for precision spectroscopy," *Phys. Rev. Lett.* **51**, 1336–1339.
- Pritchard, D. E., 1986, in *Electron and Atomic Collisions*, edited by D. C. Lorents, W. E. Meyerhof, and J. R. Petersen (North Holland, Amsterdam), pp. 593–604.
- Pritchard, D. E., E. L. Raab, V. Bagnato, C. E. Wieman, and R. N. Watts, 1986, "Light traps using spontaneous forces," *Phys. Rev. Lett.* **57**, 310–313.
- Prodan, J. V., W. D. Phillips, and H. J. Metcalf, 1982, "Laser production of a very slow monoenergetic atomic beam," *Phys. Rev. Lett.* **49**, 1149.
- Raab, E., M. Prentiss, A. Cable, S. Chu, and D. E. Pritchard, 1987, "Trapping of neutral sodium atoms with radiation pressure," *Phys. Rev. Lett.* **59**, 2631–2634.
- Rafac, R. J., C. E. Tanner, A. E. Livingston, K. W. Kukla, H. G. Berry, and C. A. Kurtz, 1994, "Precision lifetime measurements of the  $6p\ ^2P_{1/2,3/2}$  states in atomic cesium," *Phys. Rev. A* **50**, R1976.
- Ratliff, L. P., M. E. Wagshul, P. D. Lett, S. L. Rolston, and W. D. Phillips, 1994, "Photoassociative spectroscopy of  $1_g$ ,  $0_u^+$ , and  $0_g^-$  states of  $\text{Na}_2$ ," *J. Chem. Phys.* **101**, 2638–2641.
- Riis, E., D. S. Weiss, K. A. Moler, and S. Chu, 1990, "Atom funnel for the production of a slow, high-density atomic beam," *Phys. Rev. Lett.* **64**, 1658–1661.
- Ritchie, N. W. M., E. R. I. Abraham, and R. G. Hulet, 1994, "Trap loss collisions of  $^7\text{Li}$ : The Role of Trap Depth," *Laser Phys.* **4**, 1066–1075.
- Ritchie, N. W. M., E. R. I. Abraham, Y. Y. Xiao, C. C. Bradley, R. G. Hulet, and P. S. Julienne, 1995, "Trap-loss collisions of ultracold lithium atoms," *Phys. Rev. A* **51**, R890–R893.
- Rolston, S., 1997, NIST, private communication.
- Sackett, C. A., C. C. Bradley, and R. G. Hulet, 1997, "Optimization of evaporative cooling," *Phys. Rev. A* **55**, 3797–3801.
- Sanchez-Villicana, V., S. D. Gensemer, and P. L. Gould, 1996, "Observation of flux enhancement in collisions between ultracold atoms," *Phys. Rev. A* **54**, R3730–R3733.
- Sanchez-Villicana, V., S. D. Gensemer, K. Y. N. Tan, A. Kumarakrishnan, T. P. Dinneen, W. Süptitz, and P. L. Gould, 1995, "Suppression of ultracold ground-state hyperfine-changing collisions with laser light," *Phys. Rev. Lett.* **74**, 4619–4622.
- Santos, M. S., P. Nussenzeig, L. G. Marcassa, K. Helmerson, J. Flemming, S. C. Zilio, and V. S. Bagnato, 1995, "Simultaneous trapping of two different atomic species in a vapor-cell magneto-optical trap," *Phys. Rev. Lett.* **52**, R4340–R4343.
- Santos, M., P. Nussenzeig, S. Zilio, and V. S. Bagnato, 1996, "Intensity Dependence of the Collisional Loss Rate for Potassium Atoms in a Vapor Cell," preprint, IFSC, Universidade de São Paulo, São Carlos, SP.
- Scheingrager, H., and C. R. Vidal, 1977, "Discrete and continuous Franck Condon factors of the  $\text{Mg}_2\ A^1\Sigma_u^+ - X^1\Sigma_g^+$  system and their  $J$  dependence," *J. Chem. Phys.* **66**, 3694–3704.
- Sesko, D., T. Walker, C. Monroe, A. Gallagher, and C. Wieman, 1989, "Collisional losses from a light-force trap," *Phys. Rev. Lett.* **63**, 961–964.
- Sesko, D. W., T. G. Walker, and C. Wieman, 1991, "Behavior of neutral atoms in a spontaneous force trap," *J. Opt. Soc. Am. B* **8**, 946–958.
- Shaffer, J. P., W. Chalupczak, and N. P. Bigelow, 1997, "Photoassociative spectroscopy of a laser cooled binary mixture," *Conference on Quantum Electronics and Laser Science, '97*, Baltimore, MD, OSA Technical Digest Series **12**, 85.
- Shang, S-Q, Z. T. Lu, and S. J. Freedman, 1994, "Comparison of the cold-collision losses for laser-trapped sodium in different ground-state hyperfine sublevels," *Phys. Rev. A* **50**, R4449.
- Sheehy, B., S.-Q. Shang, R. Watts, S. Hatamian, and H. Metcalf, 1989, "Diode-laser deceleration and collimation of a rubidium beam," *J. Opt. Soc. Am. B* **6**, 2165–2170.
- Shlyapnikov, G. V., J. T. M. Walraven, U. M. Rahmanov, and M. W. Reynolds, 1994, "Decay kinetics and Bose condensation in a gas of spin-polarized triplet helium," *Phys. Rev. Lett.* **73**, 3247–3250.
- Silvera, I. F., and J. T. M. Walraven, 1980, "Stabilization of atomic hydrogen at low temperature," *Phys. Rev. Lett.* **44**, 164–168.
- Silvera, I. F., and J. T. M. Walraven, 1986, "Spin-polarized atomic H," in *Progress in Low Temperature Physics*, edited by D. F. Brewer (Elsevier, Amsterdam), Vol. X, pp. 139–370.
- Smith, A. M., K. Burnett, and P. S. Julienne, 1992, "Semiclassical theory of collision-induced loss from optical traps," *Phys. Rev. A* **46**, 4091–4099.
- Soding, J., D. Guery-Odelin, P. Desbiolles, G. Ferrari, M. Ben Dahan, and J. Dalibard, 1998, "Giant spin relaxation of an ultracold cesium gas," *Phys. Rev. Lett.* **80**, 1869–1872.
- Solts, R., A. Ben-Reuven, and P. S. Julienne, 1995, "Optical collisions in ultracold atom traps: Two-photon distorted-wave theory," *Phys. Rev. A* **52**, 4029–4042.
- Sprink, R., R. J. T. M. Walraven, G. H. Yperen, and I. F. Silvera, 1982, "State-dependent recombination and suppressed nuclear relaxation in atomic hydrogen," *Phys. Rev. Lett.* **49**, 153–156.

- Steane, A., M. M. Chowdhury, and C. J. Foot, 1992, "Radiation force in the magneto-optical trap," *J. Opt. Soc. Am. B* **9**, 2142–2158.
- Stenholm, S., 1986, "The semiclassical theory of laser cooling," *Rev. Mod. Phys.* **58**, 699–739.
- Stoof, H. T. C., M. Bijlsma, and M. Houbiers, 1996, "Theory of interacting quantum gases," *J. Res. Natl. Inst. Stand. Technol.* **101**, 443–457.
- Stoof, H. T. C., A. M. L. Janssen, J. M. V. A. Koelman, and B. J. Verhaar, 1989, "Decay of spin-polarized atomic hydrogen in the presence of a Bose condensate," *Phys. Rev. A* **39**, 3157–3169.
- Stoof, H. T. C., J. M. V. A. Koelman, and B. J. Verhaar, 1988, "Spin-exchange and dipole relaxation rates in atomic hydrogen: rigorous and simplified calculations," *Phys. Rev. B* **38**, 4688–4697.
- Stwalley, W. C., 1970, "The dissociation energy of the hydrogen molecule using long-range forces," *Chem. Phys. Lett.* **6**, 241–244.
- Stwalley, W. C., and L. Nosanow, 1976, "Possible new quantum systems," *Phys. Rev. Lett.* **36**, 910–913.
- Stwalley, W. C., Y.-H. Uang, and G. Pichler, 1978, "Pure long-range molecules," *Phys. Rev. Lett.* **41**, 1164–1166.
- Sukenik, C. I., D. Hoffmann, S. Bali, and T. Walker, 1998, "Low saturation intensities in two-photon ultracold collisions," *Phys. Rev. Lett.* **81**, 782–785.
- Suominen, K.-A., 1996, "Theories for cold atomic collisions in light fields," *J. Phys. B* **29**, 5981–6007.
- Suominen, K.-A., Y. B. Band, I. Tuvi, K. Burnett, and P. S. Julienne, 1998, "Quantum and semiclassical calculations of cold collisions in light fields," *Phys. Rev. A* **55**.
- Suominen, K.-A., K. Burnett, and P. S. Julienne, 1996, "Role of off-resonant excitation in cold collisions in a strong laser field," *Phys. Rev. A* **53**, R1220–R1223.
- Suominen, K.-A., K. Burnett, P. S. Julienne, M. Walhout, U. Sterr, C. Orzel, M. Hoogerland, and S. L. Rolston, 1996, "Ultracold collisions and optical shielding in metastable xenon," *Phys. Rev. A* **53**, 1658–1689.
- Suominen, K.-A., M. J. Holland, K. Burnett, and P. S. Julienne, 1994, "Excited-state survival probabilities for cold collisions in a weak laser field," *Phys. Rev. A* **49**, 3897–3902.
- Suominen, K.-A., M. J. Holland, K. Burnett, and P. Julienne, 1995, "Optical shielding of cold collisions," *Phys. Rev. A* **51**, 1446–1457.
- Suominen, K.-A., E. Tiesinga, and P. S. Julienne, 1998, "Nonadiabatic dynamics in evaporative cooling of trapped atoms by a radio frequency field," *Phys. Rev. A* **58**, 3983–3992.
- Swanson, T. B., N. J. Silva, S. K. Mayer, J. J. Maki, and D. H. McIntyre, 1996, "Rubidium atomic funnel," *J. Opt. Soc. Am. B* **13**, 1833–1836.
- Tellinghuisen, J., 1985, in *Photodissociation and Photoionization*, edited by K. P. Lawley, *Advances in Chemical Physics LX* (Wiley, New York), pp. 299–369.
- Thorsheim, H. R., Y. Wang, and J. Weiner, 1990, "Cold collisions in an atomic beam," *Phys. Rev. A* **41**, 2873–2876.
- Thorsheim, H. R., J. Weiner, and P. S. Julienne, 1987, "Laser-induced photoassociation of ultracold sodium atoms," *Phys. Rev. Lett.* **58**, 2420–2423.
- Tiesinga, E., S. B. Crampton, B. J. Verhaar, and H. T. C. Stoof, 1993, "Collisional frequency shifts and line broadening in the cryogenic deuterium maser," *Phys. Rev. A* **47**, 4342–4347.
- Tiesinga, E., S. J. M. Kuppens, B. J. Verhaar, and H. T. C. Stoof, 1991, "Collisions between cold ground state Na atoms," *Phys. Rev. A* **43**, R5188–R5191.
- Tiesinga, E., A. J. Moerdijk, B. J. Verhaar, and H. T. C. Stoof, 1992, "Conditions for Bose-Einstein condensation in magnetically trapped atomic cesium," *Phys. Rev. A* **46**, R1167–R1170.
- Tiesinga, E., H. T. C. Stoof, and B. J. Verhaar, 1990, "Spin-exchange frequency shift of the cryogenic deuterium maser," *Physica B* **165**, 19–20.
- Tiesinga, E., B. J. Verhaar, and H. T. C. Stoof, 1993, "Threshold and resonance phenomena in ultracold ground-state collisions," *Phys. Rev. A* **47**, 4114–4122.
- Tiesinga, E., B. J. Verhaar, H. T. C. Stoof, and D. van Bragt, 1992, "Spin-exchange frequency-shift in a cesium atomic fountain," *Phys. Rev. A* **45**, 2671–2674.
- Tiesinga, E., C. J. Williams, and P. S. Julienne, 1998 (unpublished).
- Tiesinga, E., C. J. Williams, and P. S. Julienne, 1998, "Photoassociative spectroscopy of highly excited vibrational levels of alkali dimers: Green's function approach for eigenvalue solvers," *Phys. Rev. A* **57**, 4257–4267.
- Tiesinga, E., C. J. Williams, P. S. Julienne, K. M. Jones, P. D. Lett, and W. D. Phillips, 1996, "A Spectroscopic Determination of Scattering Lengths for Sodium Atom Collisions," *J. Res. Natl. Inst. Stand. Technol.* **101**, 505–520.
- Townsend, C., W. Ketterle, and S. Stringari, 1997, "Bose-Einstein condensation," *Phys. World* **10**, 29–34.
- Trost, J., C. Eltschka, and H. Friedrich, 1998, "Quantization in molecular potentials," *J. Phys. B* **31**, 361–374.
- Tsai, C. C., R. S. Freeland, J. M. Vogels, H. M. J. M. Boesten, B. J. Verhaar, and D. J. Heinzen, 1997, "Two-color photoassociation spectroscopy of ground state  $Rb_2$ ," *Phys. Rev. Lett.* **79**, 1245–1248.
- Tsao, C.-C., 1996, Ph.D. thesis (University of Maryland).
- Tsao, C.-C., R. Napolitano, Y. Wang, and J. Weiner, 1995, "Ultracold photoassociative ionization collisions in an atomic beam: Optical field intensity and polarization dependence of the rate constant," *Phys. Rev. A* **51**, R18–R21.
- Tsao, C.-C., Y. Wang, R. Napolitano, and J. Weiner, 1998, "Anisotropy of optical suppression in photoassociative ionization collisions within a slow, collimated sodium atom beam," *Eur. Phys. J. D* **4**, 139–144.
- Tsao, C.-C., Y. Wang, J. Weiner, and V. S. Bagnato, 1996, "Optical collimation and compression of a thermal atomic beam," *J. Appl. Phys.* **80**, 8–14.
- Uang, Y.-H., and W. C. Stwalley, 1980, "Close-coupling calculations of spin-polarized hydrogen-deuterium collisions," *Phys. Rev. Lett.* **45**, 627–630.
- Ungar, P. J., D. S. Weiss, E. Riis, and S. Chu, 1989, "Optical molasses and multilevel atoms: Theory," *J. Opt. Soc. Am. B* **6**, 2058–2071.
- van Roijen, R., J. J. Berkhout, S. Jaakkola, and J. T. M. Walraven, 1988, "Experiments with atomic hydrogen in a magnetic trapping field," *Phys. Rev. Lett.* **61**, 931–934.
- Vardi, A., D. Abrashkevich, E. Frishman, and M. Shapiro, 1997, "Theory of radiative recombination with strong laser pulses and the formation of ultracold molecules via stimulated photo-recombination of cold atoms," *J. Chem. Phys.* **107**, 6166–6174.
- Verhaar, B. J., K. Gibble, and S. Chu, 1993, "Cold-collision properties derived from frequency shifts in a Cs fountain," *Phys. Rev. A* **48**, R3429–R3432.

- Verhaar, B. J., J. M. V. A. Koelman, H. T. C. Stoof, O. J. Luiten, and S. B. Crampton, 1987, "Hyperfine contribution to spin-exchange frequency shifts in the hydrogen maser," *Phys. Rev. A* **35**, 3825–3831.
- Vigué, J., 1986, "Possibility of applying laser-cooling techniques to the observation of collective quantum effects," *Phys. Rev. A* **34**, 4476–4479.
- Vogels, J. M., C. C. Tsai, R. S. Freeland, S. J. J. M. F. Kokkelmans, B. J. Verhaar, and D. J. Heinzen, 1997, "Prediction of Feshbach resonances in collisions of ultracold rubidium atoms," *Phys. Rev. A* **56**, R1067–R1070.
- Wagshul, M. E., K. Helmerson, P. D. Lett, S. L. Rolston, W. D. Phillips, R. Heather, and P. S. Julienne, 1993, "Hyperfine effects on associative ionization of ultracold sodium," *Phys. Rev. Lett.* **70**, 2074–2077.
- Walhout, M., U. Sterr, C. Orzel, M. Hoogerland, and S. L. Rolston, 1995, "Optical control of ultracold collisions in metastable xenon," *Phys. Rev. Lett.* **74**, 506–509.
- Walker, T., and P. Feng, 1994, "Measurements of collisions between laser-cooled atoms," *Adv. At., Mol., Opt. Phys.* **34**, 125–170.
- Walker, T., and D. R. Pritchard, 1994, "Effects of hyperfine structure on alkali trap-loss collisions," *Laser Phys.* **4**, 1085–1092.
- Walker, T., D. Sesko, and C. Wieman, 1990, "Collective behavior of optically trapped neutral atoms," *Phys. Rev. Lett.* **64**, 408–411.
- Wallace, C., T. Dinneen, K. Tan, T. Grove, and P. Gould, 1992, "Isotopic difference in trap loss collisions of laser cooled rubidium atoms," *Phys. Rev. Lett.* **69**, 897–900.
- Wallace, C., V. Sanchez-Villicana, T. P. Dinneen, and P. L. Gould, 1995, "Suppression of trap loss collisions at low temperature," *Phys. Rev. Lett.* **74**, 1087–1090.
- Walraven, J. T. M., 1984, "Atomic hydrogen at sub-Kelvin temperatures," in *Atomic Physics*, edited by R. S. Dyck, Jr., and E. N. Fortson (World Scientific, Singapore), Vol. 9, pp. 187–211.
- Walsworth, R. L., I. F. Silvera, H. P. Gottfried, C. C. Agosta, R. F. C. Vessot, and E. M. Mattison, 1986, "Hydrogen maser at temperatures below 1 K," *Phys. Rev. A* **34**, 2550–2553.
- Wang, H., P. L. Gould, and W. C. Stwalley, 1996a, "Photoassociative spectroscopy of ultracold  $^{39}\text{K}$  atoms in a high-density vapor-cell magneto-optical trap," *Phys. Rev. A* **53**, R1216–R1219.
- Wang, H., P. L. Gould, and W. C. Stwalley, 1996b, "Photoassociative spectroscopy of pure long-range molecules," *Z. Phys. D* **36**, 317–323.
- Wang, H., P. L. Gould, and W. C. Stwalley, 1997, "Long-range interaction of the  $^{39}\text{K}(4s)+^{39}\text{K}(4p)$  asymptote by photoassociative spectroscopy. I: The  $0_g^-$  pure long-range state and the long-range potential constants," *J. Chem. Phys.* **106**, 7899–7912.
- Wang, H., P. L. Gould, and W. C. Stwalley, 1998, "Fine structure predissociation of ultracold photoassociated  $^{39}\text{K}_2$  molecules observed by fragmentation spectroscopy," *Phys. Rev. Lett.* **80**, 476–479.
- Wang, H., J. Li, X. T. Wang, C. J. Williams, P. L. Gould, and W. C. Stwalley, 1997, "Precise determination of the dipole matrix element and radiative lifetime of the  $^{39}\text{K} 4p$  state by photoassociative spectroscopy," *Phys. Rev. A* **55**, R1569–R1572.
- Wang, H., and W. C. Stwalley, 1998, "Ultracold photoassociative spectroscopy of heteronuclear alkali-metal diatomic molecules," *J. Chem. Phys.* **108**, 5767–5771.
- Wang, H., X. T. Wang, P. L. Gould, and W. C. Stwalley, 1997, "Optical-optical double resonance photoassociative spectroscopy of ultracold  $^{39}\text{K}$  atoms near highly excited asymptotes," *Phys. Rev. Lett.* **78**, 4173–4176.
- Wang, M-X., J. Keller, J. Boulmer, and J. Weiner, 1986, "Strong velocity dependence of the atomic alignment effect in  $\text{Na}(3p)+\text{Na}(3p)$  associative ionization," *Phys. Rev. A* **34**, 4497–4500.
- Wang, M-X., J. Keller, J. Boulmer, and J. Weiner, 1987, "Spin-selected velocity dependence of the associative ionization cross section in  $\text{Na}(3p)+\text{Na}(3p)$  collisions over the collision energy range from 2.4 to 290 meV," *Phys. Rev. A* **35**, 934–937.
- Wang, X., H. Wang, P. L. Gould, W. C. Stwalley, E. Tiesinga, and P. S. Julienne, 1998, "Observation of the pure long range  $1_u$  state of an alkali-metal dimer in photoassociation spectroscopy," *Phys. Rev. A* **57**, 4600–4603.
- Wang, Y., and J. Weiner, 1990, "Velocity-selected atomic-beam collisions in the energy range from 300 to 5 K," *Phys. Rev. A* **42**, 675–677.
- Weiner, J., 1989, "Experiments in cold and ultracold collisions," *J. Opt. Soc. Am. B* **6**, 2270–2278.
- Weiner, J., 1995, "Advances in Ultracold Collisions: Experimentation and Theory," in *Advances in Atomic, Molecular and Optical Physics*, edited by D. Bates and B. Bederson (Academic, Boston), Vol. 35, pp. 45–78.
- Weiner, J., F. Masnou-Seeuws, and A. Giusti-Suzor, 1989, "Associative Ionization: Experiments, Potentials, and Dynamics," in *Advances in Atomic, Molecular and Optical Physics*, edited by D. Bates and B. Bederson (Academic Press, Boston), Vol. 26, pp. 209–296.
- Wigner, E. P., 1948, "On the behavior of cross sections near thresholds," *Phys. Rev.* **73**, 1002–1009.
- Williams, C. J., and P. S. Julienne, 1993, "Mass effects in the theoretical determination of nuclear spin relaxation rates for atomic hydrogen and deuterium," *Phys. Rev. A* **47**, 1524–1527.
- Williams, C. J., and P. S. Julienne, 1994, "Molecular hyperfine structure in the photoassociation spectroscopy of laser cooled atoms," *J. Chem. Phys.* **101**, 2634–2637.
- Williams, C. J., E. Tiesinga, and P. S. Julienne, 1996, "Hyperfine structure of the  $\text{Na}_2 0_g^-$  long-range molecular state," *Phys. Rev. A* **53**, R1939–R1942.
- Williamson, R. S., and T. Walker, 1995, "Magneto-optical trapping and ultracold collisions of potassium atoms," *J. Opt. Soc. Am. B* **12**, 1393–1397.
- Wineland, D. J., and W. M. Itano, 1979, "Laser cooling of atoms," *Phys. Rev. A* **20**, 1521–1540.
- Yu, J., J. Djemaa, P. Nosbaum, and P. Pillet, 1994, "Funnel with orientated Cs atoms," *Opt. Commun.* **112**, 136–140.
- Yurovsky, V. A., and A. Ben-Reuven, 1997, "Incomplete optical shielding in cold atom traps: three-dimensional Landau-Zener theory," *Phys. Rev. A* **55**, 3772–3779.
- Zilio, S. C., L. Marcassa, S. Muniz, R. Horowicz, V. Bagnato, R. Napolitano, J. Weiner, and P. S. Julienne, 1996, "Polarization dependence of optical suppression in photoassociative ionization collisions in a sodium magneto-optic trap," *Phys. Rev. Lett.* **76**, 2033–2036.